Fibre Optic Distributed Temperature Sensors Applications & Temperature Modelling in Intelligent Wells Environments

Fajhan Hilal Hamad Almutairi

A thesis submitted for the degree of Doctor of Philosophy
Institute of Petroleum Engineering, Heriot-Watt University
Edinburgh, United Kingdom

May 2007

Thesis Abstract

The rapid industry move toward implementing the concept of intelligent fields (I-fields) relies heavily on the optimum use of the components that provide intelligence to the conventional field operations. Downhole monitoring and control using intelligent wells are important part of I-fields along with the automation and organizational work-processes. This later automation and control depends on the interpretation of the monitored downhole data.

Fibre optic sensors introduction to the oil and gas E&P industry provided operators with a non-intrusive, highly reliable, cost-effective sensors and huge amount of downhole data to be interpreted. The most common application of fibre optic sensors is the distributed temperature sensor (DTS). It has been used primarily for detection of unwanted fluids (water and gas) because of their thermal properties, which are significantly different from oil. A second important application area is flow assurance in monitoring the hydrate and wax formation temperatures. Recently, inflow profiling using DTS data to eliminate uncertainties in well parameters such as permeability and pressure has received attention from many researchers.

The first part of this work was two field case studies to show the importance of having suitable downhole data to achieve effective operation of downhole Inflow Control Valves (ICVs). The viability of a novel application of DTS data to detect scale deposition was explored to develop guidelines for when its detection is possible.

A new approach of modelling intelligent well flowing fluid temperature using a steady state energy balance model is proposed. The model takes into account the producing zone inflow profile and the mixing temperatures of different inflows. The study concludes that incorporation of the inflow profile into the calculation of the flowing fluid temperature is necessary since the assumption of a single point of inflow (usually used in conventional nodal analysis) can over-estimate the flowing fluid temperature; resulting in an inaccurate matching to DTS data. The requirements for detection of water influx in intelligent wells are also studied. Recommendations to expand some of the concepts outlined in the thesis are also proposed.

Dedication

First and foremost I want to dedicate this work to my beloved wife Nassimah Alabduljaleel, whom without her love, support and patience in living away from me throughout my study time in Edinburgh I would not be able to finish this work. This work, as hard as it was, can not match the difficulty and challenge she faced in raising our two daughters alone. I also would like to dedicate this work to my lovely daughters Hala and Ghala, whom the desire to be with again inspired me to work harder to finish this work and consoled me in times of difficulty and hardship during the study.

This work is also dedicated to my dear parents for all their prayers, support, love and education; I hope I am making them proud.

I also would like to dedicate this work and knowledge to my beloved country Kuwait.

Acknowledgements

In The Name of Allah, Most Gracious, Most Merciful

Praise be to Allah, the Sustainer of the worlds, the one who blessed me with the spirit and energy to carry out this research, and taught me what I did not know. Peace and blessings be upon the Prophet Mohammad, his family and all his companions. I pray that God accept this work and that it is counted in my good deeds.

The following thesis, while an individual work, benefited from the insights and direction of several people. First, my supervisor, Dr. David Davies, exemplifies the high quality scholarship to which I aspire. In addition, he provided timely and instructive comments and evaluation at every stage of the thesis process, allowing me to complete this project on schedule. Next, I wish to thank Kuwait Institute for Scientific Research for the financial support and the sponsorship of my study. The members of the "Added Value of Intelligent Wells Systems" Joint Industry Project also provided insights that guided and challenged my thinking, substantially improving the finished product. I would also like to acknowledge Dr. Eric MacKay for his assistance and guidance.

In addition to the technical and academic assistance above, I received equally important assistance from the support staff at the Institute of Petroleum Engineering at Heriot-Watt University. Mr. Alan Brown and Andrew Kidd provided an outstanding computer support throughout my study. Mrs. Claire MacMillan, the librarian, and all the secretarial and support staff in IPE. I would also like to acknowledge Mrs. Morag Patten from the Student Welfare Office in the University for her help.

Without the companionship of my colleagues and friends at the office, the time spent doing this work would have been much difficult, therefore I would like to acknowledge Mr. Faisal Alkhelaiwi, Mr. George Aggrey, Dr. Salem Elmsallati and Dr. Farhad Ebadi for their help and friendship throughout my study time.

Finally, and most deeply, I thank wife, my children and all my family members, support.

ACADEMIC REGISTRY
Research Thesis Submission

Name:	Fajhan Hilal Hamad Almutairi		
School/PGI:	Institute of Petroleum Engineering		
Version: *(i.e. First, Resubmission, Final)*	Final	Degree Sought:	PhD

Declaration

In accordance with the appropriate regulations I hereby submit my thesis and I declare that:

1) the thesis embodies the results of my own work and has been composed by myself
2) where appropriate, I have made acknowledgement of the work of others and have made reference to work carried out in collaboration with other persons
3) the thesis is the correct version of the thesis for submission*.
4) my thesis for the award referred to, deposited in the Heriot-Watt University Library, should be made available for loan or photocopying, subject to such conditions as the Librarian may require
5) I understand that as a student of the University I am required to abide by the Regulations of the University and to conform to its discipline.

* *Please note that it is the responsibility of the candidate to ensure that the correct version of the thesis is submitted.*

Signature of Candidate:		Date:	04-06-2007

Submission

Submitted By *(name in capitals)*:	FAJHAN ALMUTAIRI
Signature of Individual Submitting:	
Date Submitted:	04-06-2007

For Completion in Academic Registry

Received in the Academic Registry by *(name in capitals)*:	L BOAG.		
1.1 Method of Submission *(Handed in to Academic Registry; posted through internal/external mail)*:	Handed into Academic Registry		
Signature:	L Boag	Date:	4/6/07

Table of Contents

List of Tables

List of Figures

Nomenclature

GOR = Gas-Oil Ratio

PLT = Production Logging Tool

DTS = Distributed Temperature Sensor

DPS = Distributed Pressure Sensors

IGIP = Initial Gas in Place

WGR = Water Gas Ratio

THP = Tubing Head Pressure

BHP = Bottom Hole Pressure

NWM = Near Wellbore Modelling

SSD = Sliding Sleeve Door

ICV = Inflow Control Valve

I-Well = Intelligent Well

I-Completion = Intelligent Completion

OPEX = Operating Expenditure

CAPEX = Capital Expenditure

WC = Water Cut

BLPD = Barrels of Liquid Per Day

GOC = Gas-Oil Contact

DOL = Dual Opposed Lateral

NPV = Net Present Value

ESP = Electric Submersible Pump

OFDR = Optical Frequency Domain Reflection

OTDR = Optical Time Domain Reflection

JTE = Joule-Thompson effect

GPP = Geothermal Pivot Point

SAGD = Steam Assisted Gravity Drained

HPHT = High Pressure – High Temperature

BHCT = Bottom Hole Circulating Temperature

α = Thermal diffusivity, ft^2/s

γ_g = Gas volume fraction

γ_L = Liquid volume fraction

γ_o= Specific Gravity of Oil

$\overline{C}_p$ = Average heat capacity for the two-phase mixture

T_∞ = Temperature of the fluid sufficiently far from the surface of the tubing (e.g. T_{ci}), °F

A_s = Surface Area, ft^2

C_p = specific heat at constant pressure of fluid, Btu/lb.°F

g = acceleration due to gravity, 32.17 ft/s^2

g_c = Conversion factor, 32.17 (lbm.ft)/(lbf.s^2)

g_G = geothermal gradient, °F/ft

h = Convection heat transfer coefficient, Btu/(hr.ft^2.°F)

H = Fluid Enthalpy, Btu

h = reservoir thickness, ft

h_a = Convection Heat Transfer Coefficient in the Annulus, Btu/(hr.ft^2.°F)

h_{nc} = Natural Convection Heat Transfer Coefficient in Casing Annulus, Btu/(hr.ft^2.°F)

h_r = Radiation Heat Transfer Coefficient, Btu/(hr.ft^2.°F)

h_t = Convection Heat Transfer Coefficient in the Tubing, Btu/(hr.ft^2.°F)

h_t = Tubing Convection Heat Transfer Coefficient, Btu/(hr.ft^2.°F)

J = Mechanical Equivalent of heat, 778 ft.lb/Btu

k = Permeability, mD

k_e = thermal conductivity of earth, Btu/day.ft^2.°F

k_{cas} = Casing Thermal Conductivity, Btu/(hr.ft.°F)

k_{ins} = Insulation Thermal Conductivity, Btu/(hr.ft.°F)

k_{scale} = Scale Layer Thermal Conductivity, Btu/(hr.ft.°F)

k_t = Tubing Thermal Conductivity, Btu/(hr.ft.°F)

L = Tubing Length, ft

N_{GZ} = Dimensionless Graetz Number

N_{RA} = Dimensionless Ramey's Number

O = "on the order of"

P_r = Reservoir Pressure, psi

P_w = Wellbore Pressure, psi

Q = Volumetric Flow Rate, STB/Day

r_{ci} = Casing Inside Radius, ft

r_{co} = Casing outside radius, ft

r_{co} = outside radius of casing, ft

r_e = Reservoir Radius, ft

r_{ins} = Insulation Radius, ft

r_{si} = Scale Layer inside Radius, ft

r_{ti} = inside radius of tubing, ft

r_{ti} = Inside Tubing Radius, ft

r_{to} = Outside Tubing Radius, ft

r_{wb} = wellbore radius, ft

S = Skin Factor, Dimensionless

t = time from the start of injection/production, days

T_{co}= Casing Temperature, °F

T_{ei} = formation temperature at initial condition, °F

T_{ei} = Undisturbed formation (geothermal) temperature, °F

T_{eibh} = Static formation temperature at the bottom hole, °F

T_i = Temperature at pipe intake, °F

T_m = Mixture temperature, °F

T_o = Surface temperature of injected fluid, °F

T_s = Tubing Surface Temperature, °F

$T_{sG} = T_{cs}$ = Surface geothermal temperature, °F

T_{wb}= Wellbore Temperature, °F

u = Darcy velocity vector,

U = Overall Heat Transfer Coefficient, Btu/day.ft^2.°F

v = fluid velocity inside the tubing, ft/s

w = fluid injection mass rate, lb/hr

x = distance from bottom of tubing

Z = Gas compressibility factor

Z = measured well depth from surface, ft

β = Thermal expansion Coefficient

θ = Wellbore inclination from the horizontal, degrees

μ = Viscosity, cp

μ_{JT} = Joule-Thompson Coefficient, °F/psi

Chapter 1 Introduction

The development and optimisation of oil and gas fields' production strategies relies heavily on the gathering and the interpretation of well and field production data, such as zonal flow rates, bottom-hole pressures, water cut, gas-oil ratios (GOR), etc. The production logging tool (PLT) has been historically the primary source of such data. In addition, the number of permanent, downhole pressure/temperature conventional quartz and thermocouple gauges has increased over the last 10-15 years. Recently, the industry's move toward more complex wells, such as intelligent, subsea and multilateral wells in difficult environments, has rendered the practice of frequent PLT logs as impractical and costly. The accuracy and reliability of conventional pressure and temperature gauges in harsh production environments usually associated with I-Wells deployments (e.g. subsea, high pressure and high temperature reservoirs, high rate gas wells) led to questions being asked about the reliability of the data they deliver for making critical production optimisation decisions. Any requirement for calibration and maintenance will prove extremely costly in a subsea installation.

The successful application in the telecommunication industry of fibre optic technology and the resulting low cost, large scale production of components led to the use of optic fibres as sensing devices in oil and gas wells. Their minimal size, resistance to interference, and the provision of non-intrusive, sensing devices that are both reliable and maintenance free encouraged this development. Fibre optic sensors can be installed to gather data at specific points or they can gather distributed data along the length of the well using a single fibre optic cable. Many wells have been completed with distributed temperature sensors (DTS) in recent years. By contrast, distributed pressure sensors (DPS) are not yet fully developed and commercialized for oil and gas wells.

The optimal use of intelligent and/or complex wells, such as multilateral wells, to increase the production cannot be achieved without the measurements of downhole data to allow for quick and informed decision making to optimise the production strategy, one of the most promising and attractive applications of DTS is flow profiling. The other major areas for DTS data interpretation are flow assurance and water/gas influx detection. Interpretation of temperature data requires an in-depth understanding of the heat transfer phenomenon in the wellbore, an area that was pioneered in the 1960s by Ramey in his classic paper on wellbore heat transmission [1.1]. This area received little attention in subsequent years, but has now been brought back to life with the increasing deployment of DTS systems and multipoint or single point fibre optic temperature sensors. This increase in utilization of fibre optic sensors lead to an increasing demand that new ways are found to use the gathered DTS data for optimising the production strategy.

This study looks at two examples of field cases where downhole flow control is required to control and optimise the production operation. The drivers behind the application of downhole flow control in these field studies were different. They will be used to demonstrate the value that can be derived from the presence of temperature data in intelligent well and complex wells developments. The first case is an economically marginal, stacked sands gas reservoir that can only be developed as a commercially attractive prospect through accelerating the production. The difficulty is that government regulations do not allow commingled production of the various sands. Downhole flow control and measurements has the potential to meet the government's audit concerns when depleting the reserves. Intelligent wells, as well as other conventional completion strategies, are investigated to accelerate production. The second field case is a thin oil column reservoir where the impact of problems such as

early and rapid gas breakthrough and water coning needs to be minimized to increase the well oil production rate and the ultimate recovery from the field.

The use of temperature data in flow profiling and anomaly detection, such as water and gas breakthrough, has been long established [1.2, 1.3, 1.4, 1.5]. Other applications, such as monitoring water flood projects [1.6] and flow assurance [1.7, 1.8] have also been demonstrated.

The objective of this thesis is to investigate the effect of the intelligent completion components and well design on the produced fluid's temperature profile. In addition, a new application of DTS data in the area of flow assurance will be presented. The thesis chapters are summarised as follows:

The benefits from using intelligent well controls and complex wells are illustrated in **Chapters 2 & 3.** Chapter 2 shows how an intelligent well can convert an economically marginal, stacked gas sands prospect into an attractive business proposal by accelerating production through commingling and managing unwanted water production. Chapter 3 is a case where water - and gas - breakthrough needs to be controlled in a thin oil column reservoir. Three typical well locations presenting different problems have been studied. The study shows that intelligent and other complex wells designs such as multilateral wells can increase the oil production from a particular well. The value of these new technologies will be greatest when implemented alongside conventional reservoir engineering practices, such as the proper selection of the standoff distance from fluid contacts within a thin oil column and choice of the optimum length for the horizontal section. Since the studies presented in Chapter 2 and 3 are simulation studies it was assumed that knowledge of downhole conditions and inflows were known. Parameters that are essential to optimise the wells production in practice will be presented at the end of Chapter 3, which will lead to the investigation of the application of fibre optic temperature sensors in downhole data gathering for the detection of water and gas breakthrough.

Chapter 4 reviews the principles of operation and the physics behind fibre optic technology. Attention is paid to the backscattering phenomenon and the different properties of the Rayleigh, Brillouin and Raman backscattered spectra, which are used to infer the different data required from the system such as temperature (Raman Stokes and Anti-stokes) and strain and temperature (Brillouin). The chapter also provides a comprehensive review of the published literature, describing the various applications for

fibre optic temperature sensors in the oil and gas industry. The latest fibre optic interrogation techniques being applied in the oil and gas industry will also be highlighted.

The most important application examined is flow profiling. This is based on matching the DTS data with the temperature profile predicted by a physics based, temperature model (widely available as part of the nodal analysis well performance prediction programs). Anomaly detection using the Joule-Thompson coefficient is also reviewed, as is the usage of downhole temperature data in flow assurance such as managing wax and hydrate inhibition treatments.

Chapter 5 is a review of the existing wellbore temperature prediction models used in the petroleum industry literature. These models provide the basis of most of the available DTS downhole data interpretation methodologies. This chapter shows that most of the current temperature prediction models originate from the principles laid down in Ramey's paper [1.1]. They employ an energy, mass and momentum balance in the wellbore; but have different modifications to his approach and have revised some of his assumptions. These models were derived for conventional wells were production is either through the tubing or the tubing and the annulus. This is not the case for either intelligent or multilateral wells.

A careful examination of the temperature prediction models has been completed because they form the basis of flow profile analysis using DTS data - if the temperature model is wrong, parameters derived from the DTS data will also be wrong; potentially resulting in a less than optimum production strategy.

Chapter 5 concludes with examination of the modelling of the intelligent wells and identifies their major differences, from a flow behaviour point of view, compared to conventional wells. The chapter shows that an intelligent well's modelling complexity arises from the zonal isolation it provides, the requirements for extra packers and for valves to connect flow in the annulus to fluid flow in the tubing. Intelligent wells can be visualized as providing a series of different wells within the main wellbore. Different flow regimes and conditions for each zone can exist. This affects the heat transfer phenomenon in each zone and, in turn, affects the overall fluid temperature in the tubing. The identification of those differences and the impact of this additional complexity is important when examining the applicability of the existing temperature models for predicting the temperature behaviour in intelligent wells.

Chapter 6 presents a new flow assurance application of DTS data by examining the problem of scale deposition. Using the downhole flow control capability of intelligent wells to manage scale deposition through delaying and minimizing water production and through targeted treatment has been discussed by Kavel et. al. [1.9]. **Chapter 6** focus on studying the possibility of using the DTS to detect scale deposition within the production tubing in a conventional well by applying existing temperature models with modification of the overall heat transfer coefficient of the tubing. The low conductivity of Calcium Carbonate ($CaCO_3$) and Barium Sulphate ($BaSO_4$) scales cause them to act as an insulator placed inside the tubing causing the temperature of the fluid within the tubing to increase, as there is a reduced heat loss rate to the formation. The temperature increase within the tubing is dependant on many factors that can be categorized into two main categories: the production factors (total production flow rate and water cut) and the well design factors (tubing dimensions, well length, presence of scale, etc.). This chapter also provides guidelines on where the scale deposition is detectable through DTS and presents an algorithm that can be used to infer the thickness of scale deposition layer. Its use will allow early identification of scaling problems, while the gathered data can assist the engineer in minimizing the problem and recommending a fit-for-purpose treatment.

Chapter 7 modifies the solution of an existing temperature model [1.10, 1.11] that predicts the temperature in the tubing and the annulus so that it can be used in an intelligent well environment. The main modifications of the temperature prediction formula are in the initial and boundary conditions required for finding a solution for the annulus temperature. This modification is important as it will affect the mixing temperature at the valves. The mixing temperature represents the initial condition for solving the differential equation for the tubing temperature after each valve. An accurate estimation of the mixing temperature is important for accurately estimating the overall well temperature profile.

Another important parameter that is investigated is the zonal inflow. Most existing models assume a single inflow point (usually at the bottom of the zone). Some zones in intelligent wells will be fully perforated and the inflow profile will not normally be uniform across the zone. This will yield different convection heat coefficients along the entire zone. The study investigates whether variation of the liquid production rate in a single-phase oil well can be detected in the temperature data and how water production will affect the temperature profile under varying production conditions. In addition, the

temperature profile along the tubing and annulus, along with the impact of the water production on the ICV mixing temperature has been studied.

Chapter 8 summarizes the conclusions of this study from the above chapters. Recommendations for future work and research opportunities in the heat transfer and production wells temperature modelling area are also presented in this chapter.

1.1 References:

1.1. H.J. Ramey, J., *Wellbore Heat Transmission.* Journal of Petroleum Technology, 1962(April 1962): SPE96 p. 427-435.

1.2. Yoshioka, K., et al. *Detection of Water or Gas Entries in Horizontal Wells From Temperature Profiles*. Paper SPE100209 presented at SPE Europec/EAGE Conference and Exhibition, Vienna, Austria, 12-15 June 2006, Society of Petroleum Engineers.

1.3. Brown, G. *Monitoring Multilayered Reservoir Pressures and Gas/Oil Ratio Changes Over Time Using Permanently Installed Distributed Temperature Measurements*. Paper SPE101886 presented at 2006 SPE Annual Technical Conference and Exhibition, San Antonio, Texas, U.S.A., 24-27 September 2006, Society of Petroleum Engineers.

1.4. Dawkrajai, P., et al. *Detection of Water or Gas Entries in Horizontal Wells From Temperature Profiles*. Paper SPE100050 presented at 2006 SPE/DOE Symposium on Improved Oil Recovery, Tulsa, Oklahoma, U.S.A., 22-26 April 2006, Society of Petroleum Engineers.

1.5. Yoshioka, K., et al. *Interpretation of Temperature and Pressure Profiles Measured in Multilateral Wells Equipped with Intelligent Completions*. Paper SPE94097 presented at SPE Europec/EAGE Annual Conference, Madrid, Spain, 13-16 June 2005, Society of Petroleum Engineers.

1.6. Element, D.J., S.G. Goodyear, and A.J. Jayasekera. *The Use Of Distributed Well Temperature Measurements In Waterflood Management.* Paper presented at IEA Collaborative Project on Enhanced Oil Recovery 23rd International Workshop and Symposium, Caracas, Venezuela, September 2002,

1.7. Ratulowski, J., et al. *Flow Assurance and Subsea Productivity: Closing the Loop with Connectivity and Measurements*. Paper SPE90244 presented at 2004 SPE Annual Technical Conference and Exhibition, Houston, Texas, U.S.A., 26–29 September 2004, Society of Petroleum Engineers.

1.8. Kragas, T.K., B.A. Williams, and G.A. Myers. *The Optic Oil Field: Deployment and Application of Permanent In-well Fibre Optic Sensing Systems for Production and Reservoir Monitoring*. Paper SPE71529 presented at 2001 SPE Annual Technical Conference and Exhibition, New Orleans, Louisiana, U.S.A., 30 September–3 October 2001, Society of Petroleum Engineers.

1.9. Kavle, V., et al. *Impact of Intelligent Wells on Oilfield Scale Management.* Paper SPE100112 presented at SPE Europec/EAGE Annual Conference and Exhibition, Vienna, Austria, 12–15 June 2006, Society of Petroleum Engineers.

1.10. Hasan, A.R. and C.S. Kabir, *Fluid Flow and Heat Transfer in Wellbores*: Published by Society of Petroleum Engineering in 2002.

1.11. Hasan, A.R. and C.S. Kabir, *A Mechanistic Model for Computing Fluid Temperature Profiles in Gas-Lift Wells.* SPE Production & Facilities, 1996: SPE26098 p. 179-185.

Chapter 2 Redefining the Economics of Marginal Stacked Sands Reservoirs Using Intelligent Wells

2.1 Objective and Motivation:

Chapters 2 and 3 presents two case studies that illustrate the benefits of the intelligent completions and identifies the important parameters required by operators to effectively optimise the oil and gas production. The important parameters will be listed in a table at the end of Chapter 3.

2.2 Introduction:

An intelligent completion maybe defined as "a completion system capable of collecting, transmitting, and analyzing wellbore production, reservoir, and completion-integrity data, then enabling remote action to enhance reservoir control and well-production performance." [2.1]. Therefore, a major benefit of the intelligent completions is that they eliminate the need for conventional wireline or workover intervention by allowing immediate intervention rather than waiting for weeks or months to perform the conventional intervention. An important benefit from intelligent completions "is that they can increase the oil recovery through better management of reservoir via the

availability of real time, down-hole information from the producing zones" [2.2]. Other important benefit of intelligent wells is the reduction of production personnel and health and safety concerns to the personnel.

Intelligent wells are ideally suited for wells producing from or injecting into layer-cake type reservoirs or in long horizontal wells with a significant contrast in the rock properties. A greater value from zonal control will be provided by intelligent completions will add to the well for greater variations in the reservoir properties of the segments along the well, such as the location of any fluid contacts, the aquifer strength, the ratio of the gas to oil volumes (the term *m* in the material balance equation) and rock properties [2.3]. This reference shows the ability of intelligent wells to manage geological uncertainty associated with the field development.

The C field study involved modelling and applying intelligent completion in a single well model sector of a large, stacked pay offshore gas field. An intelligent completion will be used to demonstrate the advantage of commingled flow from the three, gas-bearing sands. Government regulations prohibit commingling if zonal control is not provided. However, these sands are economically marginal on a stand-alone basis, hence commingling of the zonal flow from this well is essential.

Producing the stacked sands simultaneously accelerates production, hence increasing the value of the produced gas. Also, the well production remains above the economic limit for a longer period. In addition, the intelligent completion provides the facility to monitor and optimise production, which will aid in increasing the ultimate recovery from the field.

The focus of this study relates to well location B (Figure 2-1) on the flank of the reservoir. This flank location was chosen to illustrate the possible advantage of the intelligent well to handle increased water production from a well located near the water aquifer. Location A was used to compare the intelligent completion with other conventional completion strategies.

The main objectives of the study can be summarized as follows:

- Compare the intelligent completion to alternative completion strategies to maximize economic benefit.
- Simulation of an intelligent completion to commingle flow from the three gas sands to accelerate production.

- Investigate the role of intelligent completion to control water production in a gas reservoir.
- Optimise choking policy to maximise monetary value of the produced gas.
- Identify the parameters required for optimisation of the well production policy.

2.3 Field Description:

The C field is an offshore gas field consisting of three stacked sands containing gas of similar properties. Pressure support is provided by an active aquifer while commingling the three sands without zonal control is prohibited by government regulations. The upper and middle sands have a permeability of approximately 600 mD, while the lower sand has an average permeability of 55 mD. The upper sands have a similar average value for the porosity (23%) that is higher than the lower sand's average porosity of 15%. The base case assumes producing each sand sequentially until abandonment conditions are reached; starting from the bottom reservoir and ending with the top sand. The total Initial Gas In Place (IGIP) is 101.9 Bscf, with each sand containing almost equal gas volumes. The overall field (model) pressure is 3,199 psia. Table 2-1 contains a summary of the sands and their properties.

Table 2-1. Sands and Field Properties

Sand	IGIP (Bscf)	Max. Gas Leg Thickness (ft)	Layer Pressure (psia)	Avg. Horizontal Permeability (mD)	Aquifer/GIP (volume Ratio)	Average Porosity (%)
Upper Sand	32.8	197	2,894	660	20.8	23%
Middle Sand	32.9	65	3,322	600	2.89	23%
Lower Sand	36.2	190	3,405	50	3.14	15%
Total	101.9	-	-	-	8.74	-

The constraints and conditions that the field operates under are:

- Water Gas Ratio (WGR) = 100 STB/MMscf
- Minimum Production Rate = 3 MMscf/day
- Tubing Head Pressure (THP) Limit = 1100 psia
- Bottom Hole Pressure (BHP) Limit = 1300 psia

2.3.1 Model & Software Description:

The C field simulation model, is a fine grid, Frontsim model, which has been converted to Eclipse™ 100 model, was provided by BP. The model size was 42x225x30 grid blocks. Figure 2-1 shows the two well locations studied for the I-Well evaluation. An aquifer volume was included within the volume of each sand. Intelligent well completion modelling was performed using GeoQuest's Schedule suite [2.4]. This suite automatically split the well into an optimum number of segments. This new approach to intelligent completion modelling was used in this study, to minimize, time-consuming, manual modelling since the Schedule suite allows the user to specify the ICV location, the packer location, the tubing and casing properties.

The alternative techniques available within Eclipse™ 100 is to use the WELSEGS and COMPSEGS keywords or the "Semi-Automated" Near Wellbore Modelling (NWM) suite [2.4], which segments the wellbore, leaving the user to mirror the wellbore segmentation to create the annular segments and add extra small segments to simulate the ICVs in the model.

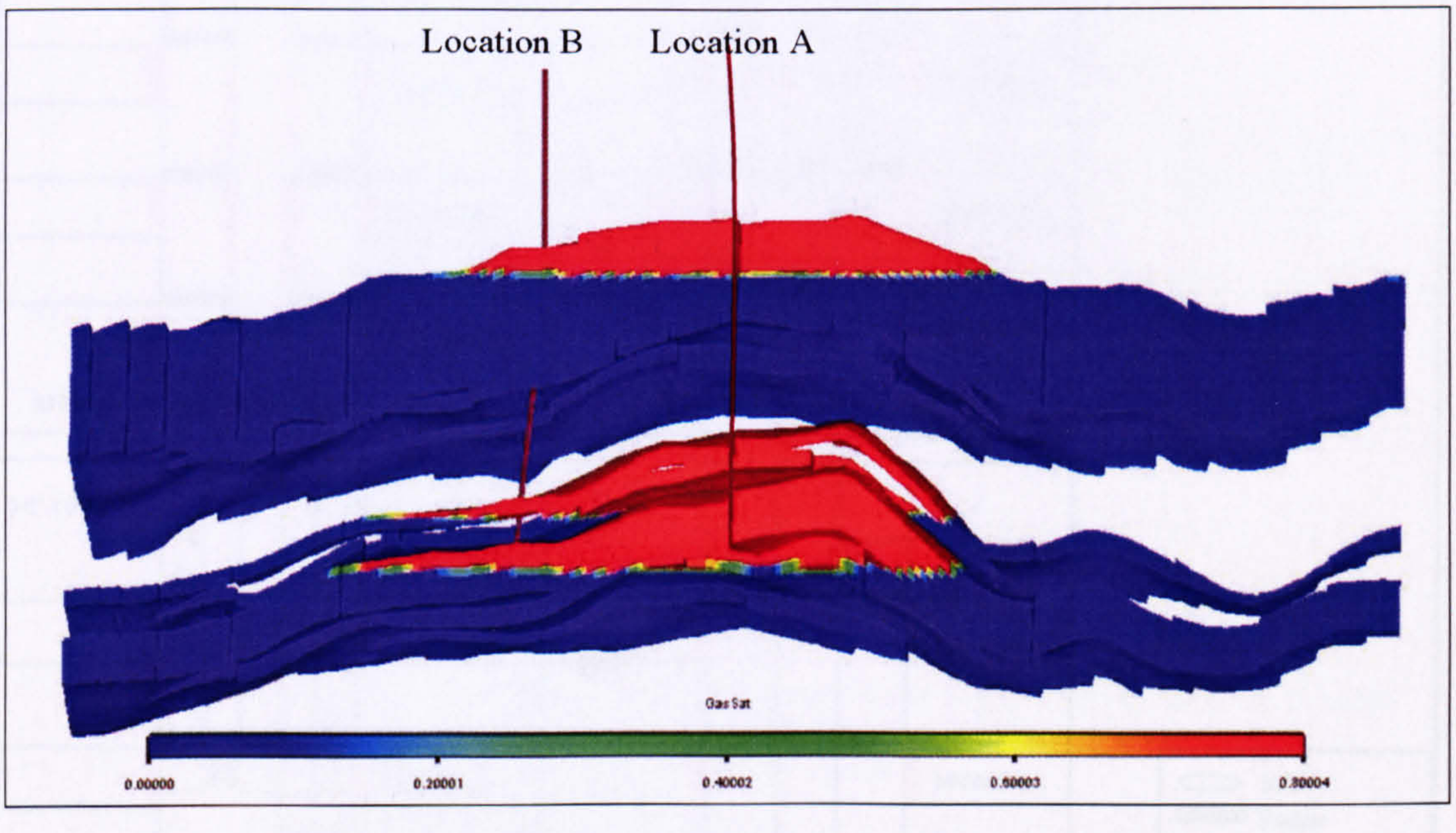

Figure 2-1. Model with Well Located on the flank

2.4 Comparison with Other Conventional Completion Strategies:

Before any decision can be made to complete any well with intelligent completions any alternative conventional completion strategies need to be investigated to build the case for using the more expensive I-completion equipments and to justify the risks associated with their installation.

The main objective of this study is to transform the economically marginal sands to a viable development through production acceleration. Therefore all the completions designs were chosen so that they presented different options to accelerate the production. However, they are unable to control the zonal water production, which can only be achieved using intelligent completion. Water control is discussed in detail later in this chapter. The potential for water production was minimized by moving the well location to a crestal position at the centre of the field.

The available completion options simulated in Location A of the field (crestal location) are (Figure 2-2):

1. Single Tubing Completion
2. Dual Completion with sliding sleeve
3. Dual Completion with Annular flow
4. Intelligent Well

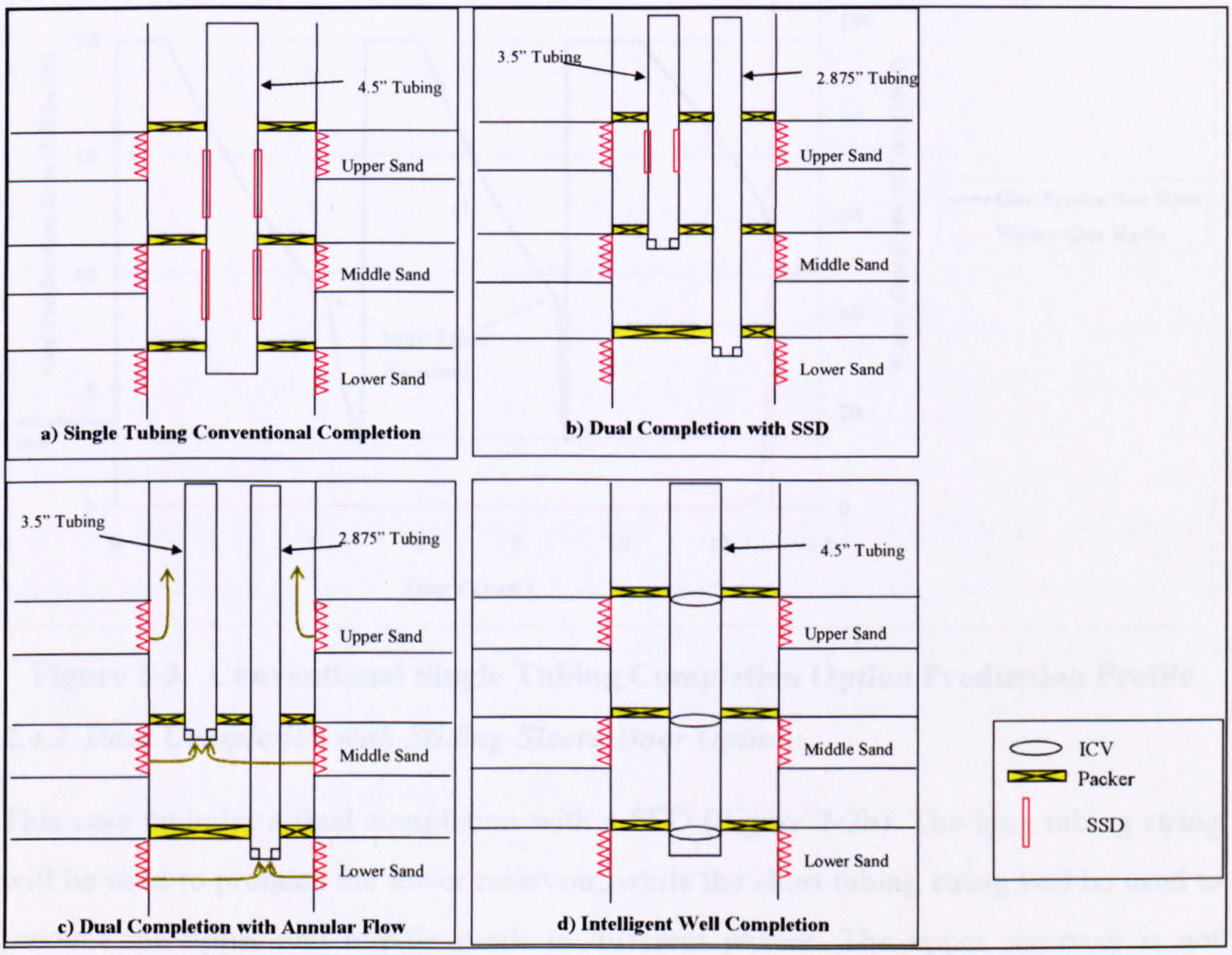

Figure 2-2. Completion Options Schematics

2.4.1 Single Tubing Completion [sequential production]

The single tubing completion option uses the strategy of depleting the sands sequentially (one sand at a time) using a Sliding Sleeve Door (SSD). The lower reservoir is produced first, followed by the middle one and finally the upper one. This bottom-up sequence is typically used in gas fields. Once the bottom reservoir reaches the assigned limits, it is plugged back through a wireline job and the middle zone is produced. The maximum production plateau for this case is 20 MMscf/d, since each reservoir is produced individually.

The simulation model used Eclipse keywords ACTIONW that activates the SSD when the sand reach any of the constraints and the WECON keyword to terminate the production of the field when an economical constraint is reached. Figure 2-3 shows the production profile of the base case of sequential production.

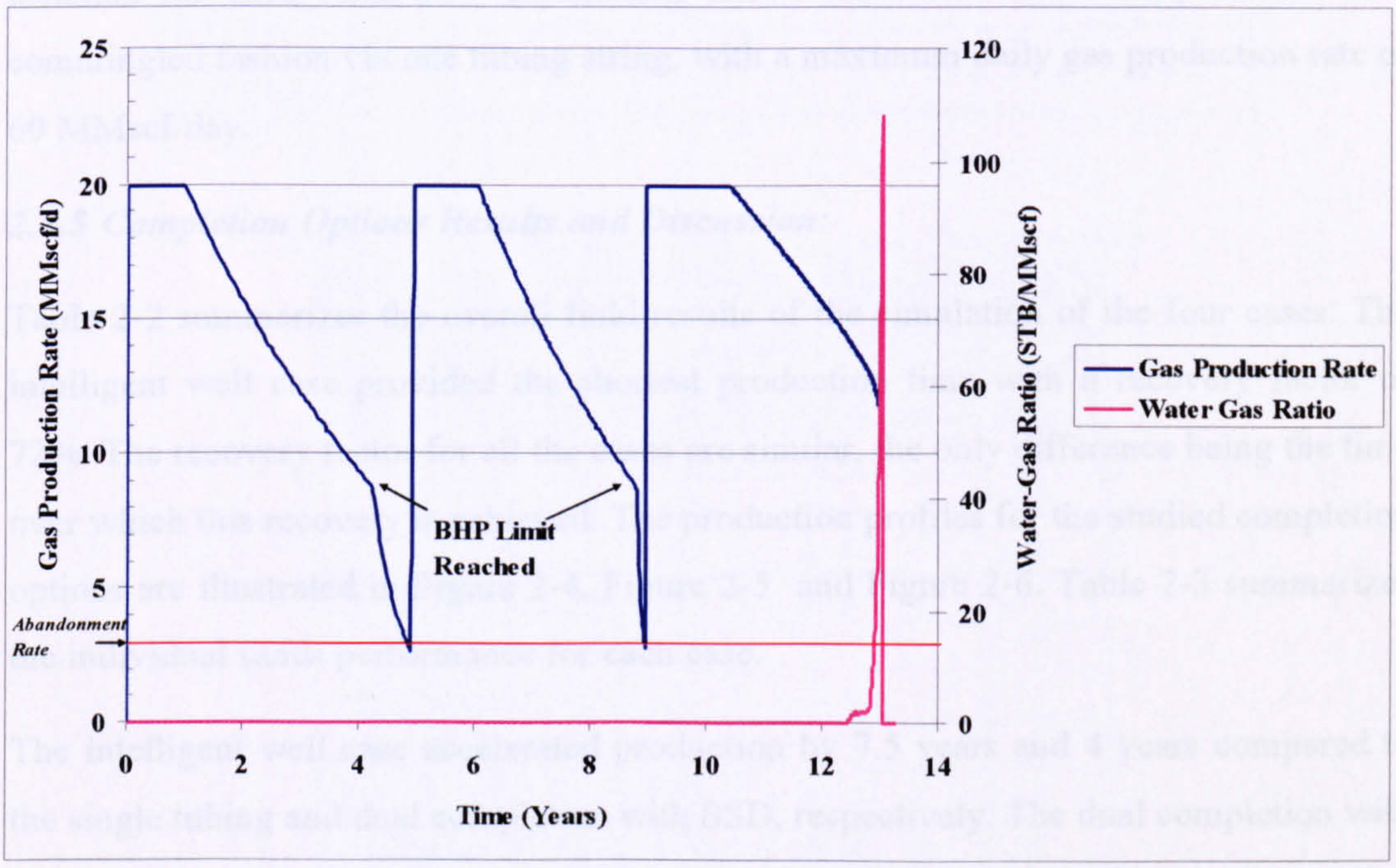

Figure 2-3. Conventional Single Tubing Completion Option Production Profile

2.4.2 Dual Completion with Sliding Sleeve Door Option:

This case includes a dual completion with a SSD (Figure 2-2b). The long tubing string will be used to produce the lower reservoir, while the short tubing string will be used to produce the upper and middle sands in different phases. The upper reservoir is not produced until the middle and lower reservoirs together reach the assigned limitation. After that, the middle reservoir is closed and the upper reservoir is opened. Therefore, a

maximum production plateau of 40 MMscf/d will be obtained since the lower and middle sands are produced together at the same time from different tubing strings.

2.4.3 Dual Completion with Annular Flow Option:

This case includes dual completion with annular flow in which the three sands are produced at the same time. The middle and lower sands are produced from different tubing stings whereas the upper reservoir is produced via the annulus. The maximum production plateau of 60 MMscf/day is expected with 20 MMscf/day from each reservoir. This case is expected to have a shorter production period compared to the previous two cases due to the acceleration of production.

2.4.4 Intelligent well Option

Three ICVs and down-hole sensors are used in this smart well case with one ICV being installed for each sand. ICV installation allows the reservoirs to be produced in a commingled fashion via one tubing string, with a maximum daily gas production rate of 60 MMscf/day.

2.4.5 Completion Options Results and Discussion:

Table 2-2 summarizes the overall field results of the simulation of the four cases. The intelligent well case provided the shortest production time with a recovery factor of 72%. The recovery factor for all the cases are similar, the only difference being the time over which this recovery is achieved. The production profiles for the studied completion options are illustrated in Figure 2-4, Figure 2-5 and Figure 2-6. Table 2-3 summarizes the individual sands performance for each case.

The intelligent well case accelerated production by 7.5 years and 4 years compared to the single tubing and dual completion with SSD, respectively. The dual completion with annular flow achieves the same recovery factor in a similar period of production to that of the intelligent wells, but carries with it many associated risks, such as:

1. Corrosion of the casing.
2. Erosion
3. Pressured gas in the annulus
4. Regulations: Local legal framework for well production

Therefore, the intelligent well completion option provides the most attractive option to accelerate the production, in addition to the controlling ability that the ICV provide. The benefits of water control will be discussed in the next section.

Table 2-2. Summary of Field Results for Alternative Conventional Completions

Completion Option	Recovery Factor	Total Production (Bscf)	Total Production Period (years)	Plateau rate (MMscf/d)
Single Tubing	0.72	73.2	13.03	20.00
Dual completion with sliding sleeve	0.73	74.9	9.15	40.00
Dual completion with annulus flow	0.72	73.4	5.50	60.00
Intelligent Well	0.72	73.7	5.33	60.00

Table 2-3. Completion Options Zones Performance

Completion Option	Zone	Gas Produced (Bscf)	Recovery Factor
Single Tubing	US	26.3	0.80
	MS	22.4	0.68
	LS	24.6	0.68
Dual completion with sliding sleeve	US	26.3	0.80
	MS	22.7	0.69
	LS	26.0	0.72
Dual completion with annulus flow	US	26.3	0.80
	MS	22.4	0.68
	LS	24.7	0.68
Intelligent Well	US	26.3	0.80
	MS	22.6	0.69
	LS	24.9	0.69

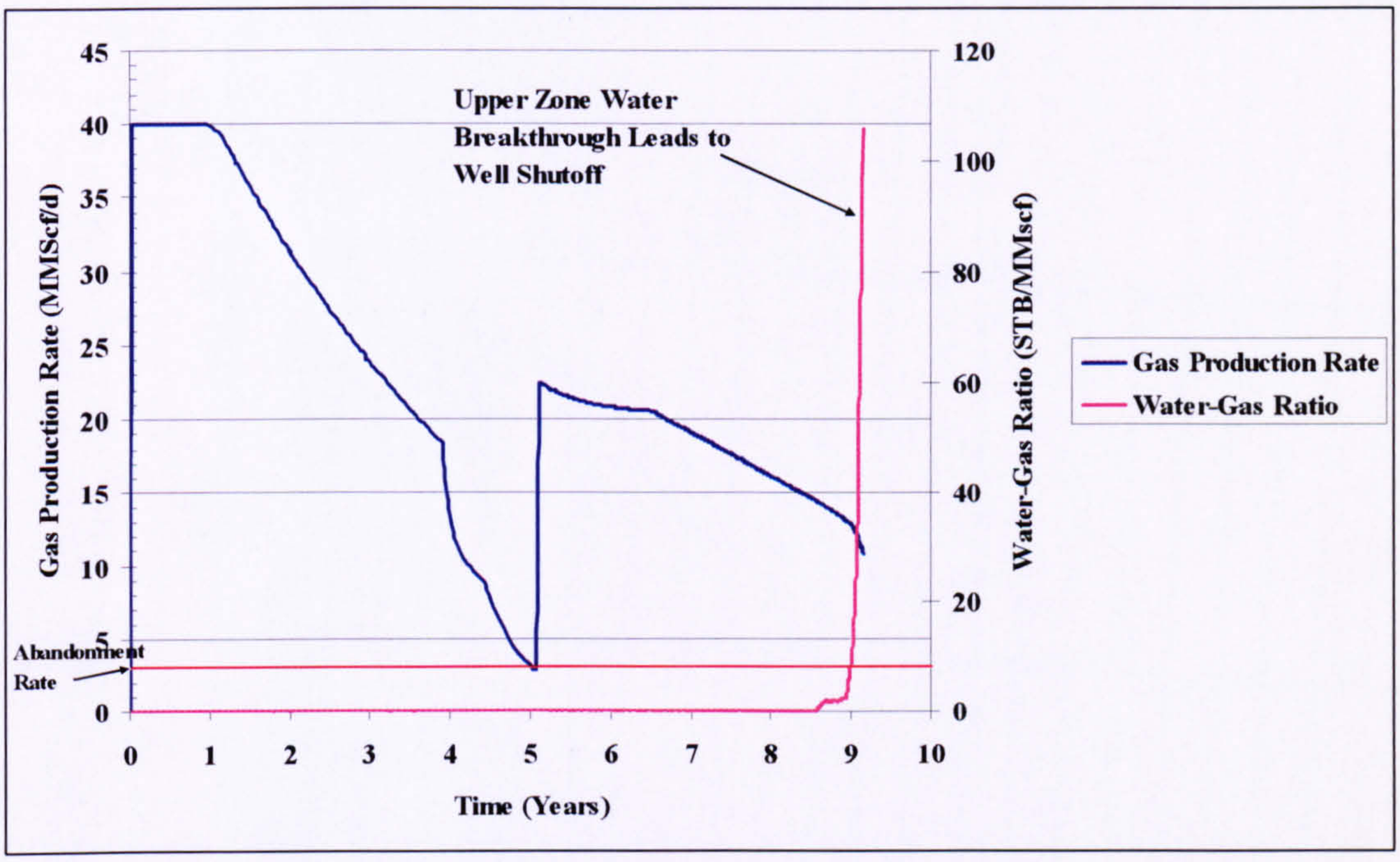

Figure 2-4. Dual Compltion with SSD Production Profile

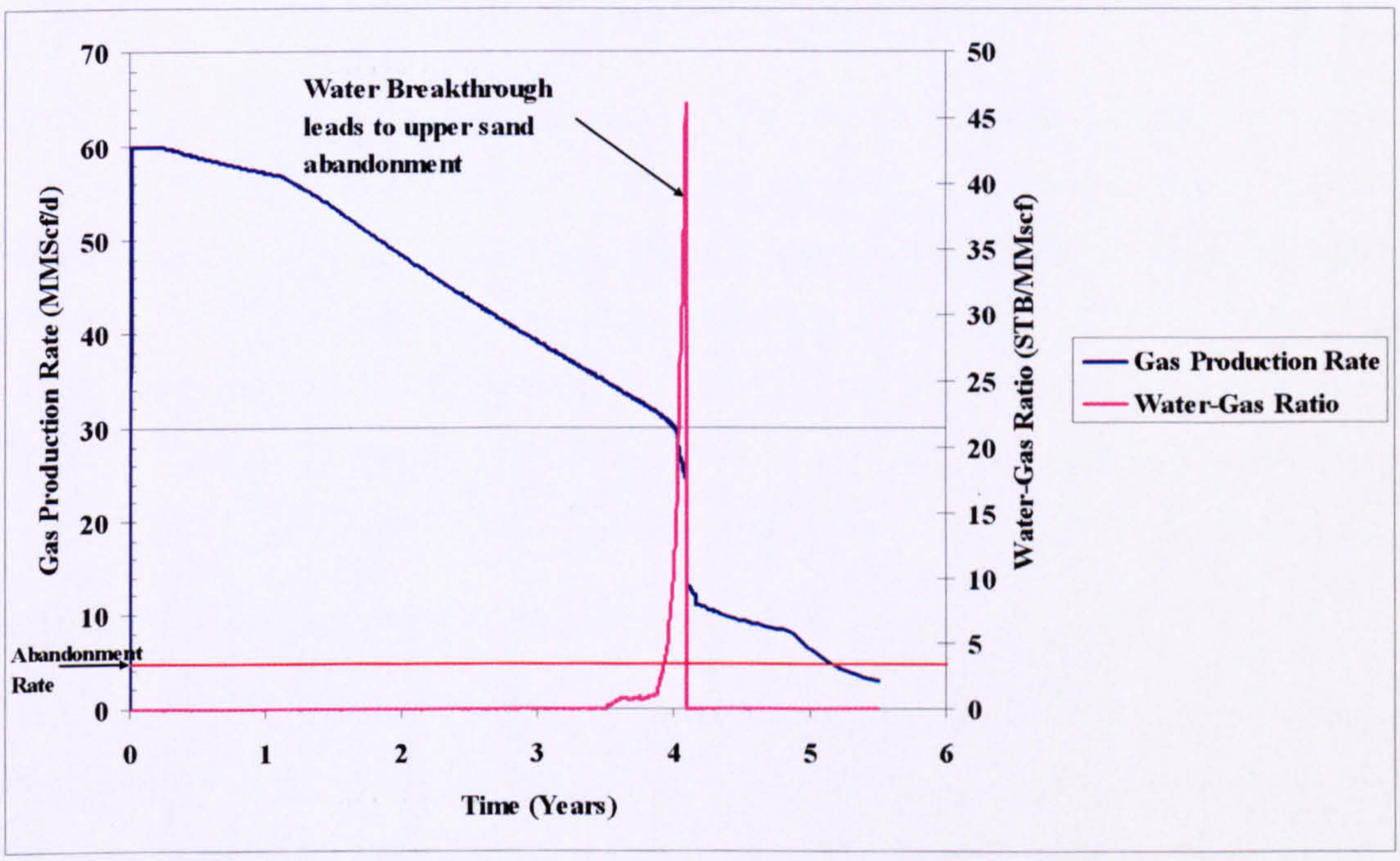

Figure 2-5. Dual Completion with Annular Flow Production Profile

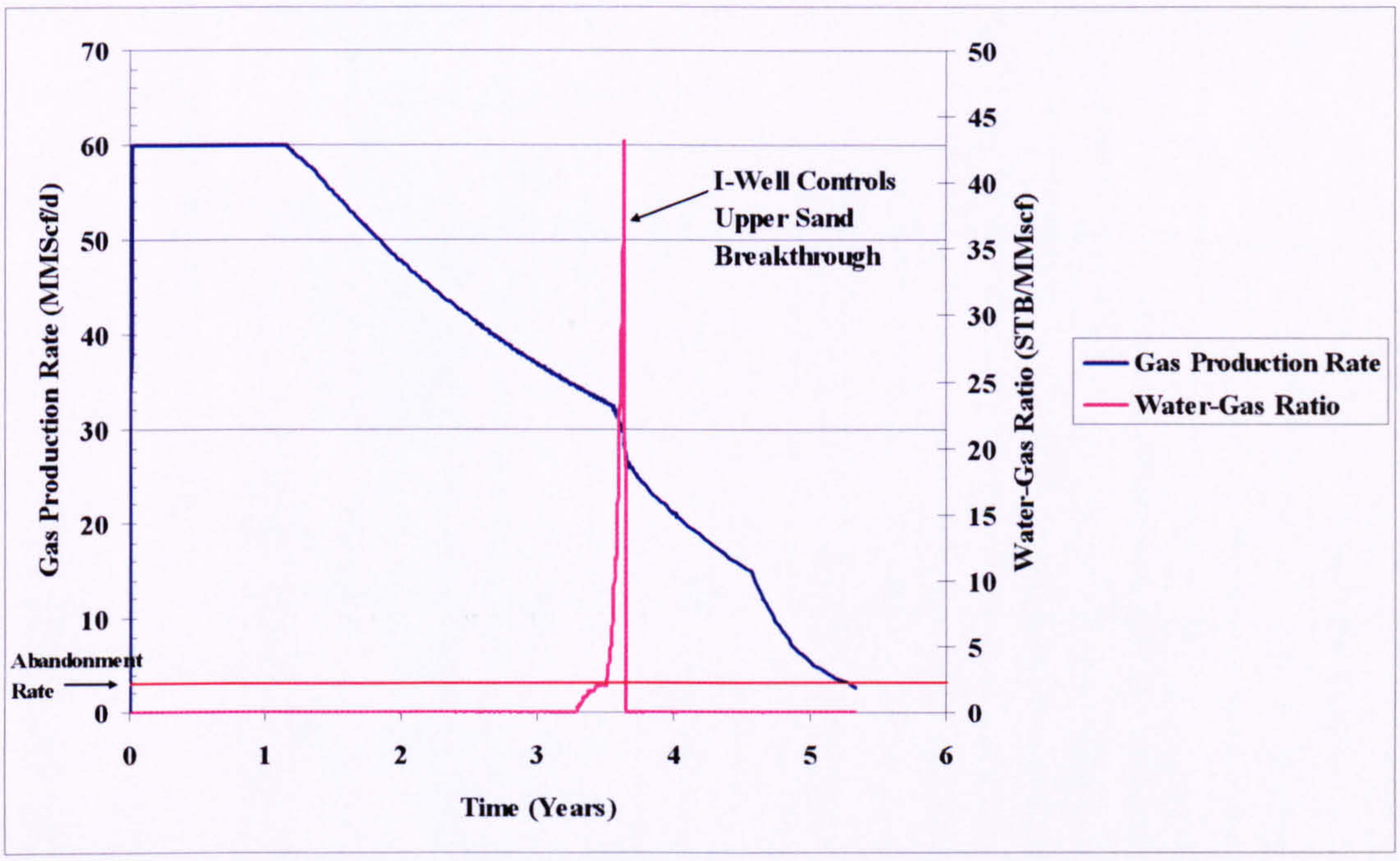

Figure 2-6. Intelligent Well Completion Production Profile

2.5 Water Control Benefit of Intelligent Well Completion:

The previous section has shown that the I-completion option can accelerate production. An important function of the intelligent completion is the ability to control the flow from an isolated zone. This controlling ability is particularly important when the well is producing an unwanted fluid such as water that could reduce the well performance. This part of the study investigates the effect of water control on the accelerated production provided by the intelligent completion and the benefit of controlling such water production in increasing the value of the development.

2.5.1 Base Case Modifications and Analysis:

Well location A, producing from the crestal portion of the field, showed water production from the upper gas sand only after the production rate decreased below its plateau value (Figure 2-3). This is because the well was located at the centre of the field and away from the water zone (location A in Figure 2-1). To demonstrate the effect of water control, the well was moved to location B on the flank of the field to encourage water production.

Figure 2-7 shows production profile for the single tubing conventional completion option (Base Case). The lower and upper sands was shut-in after approximately 2 years and less than one year respectively due to the WGR reaching its maximum allowable

limit. By contrast, the middle sand was shut-in after 3.6 years of production when the production rate reached its abandonment value.

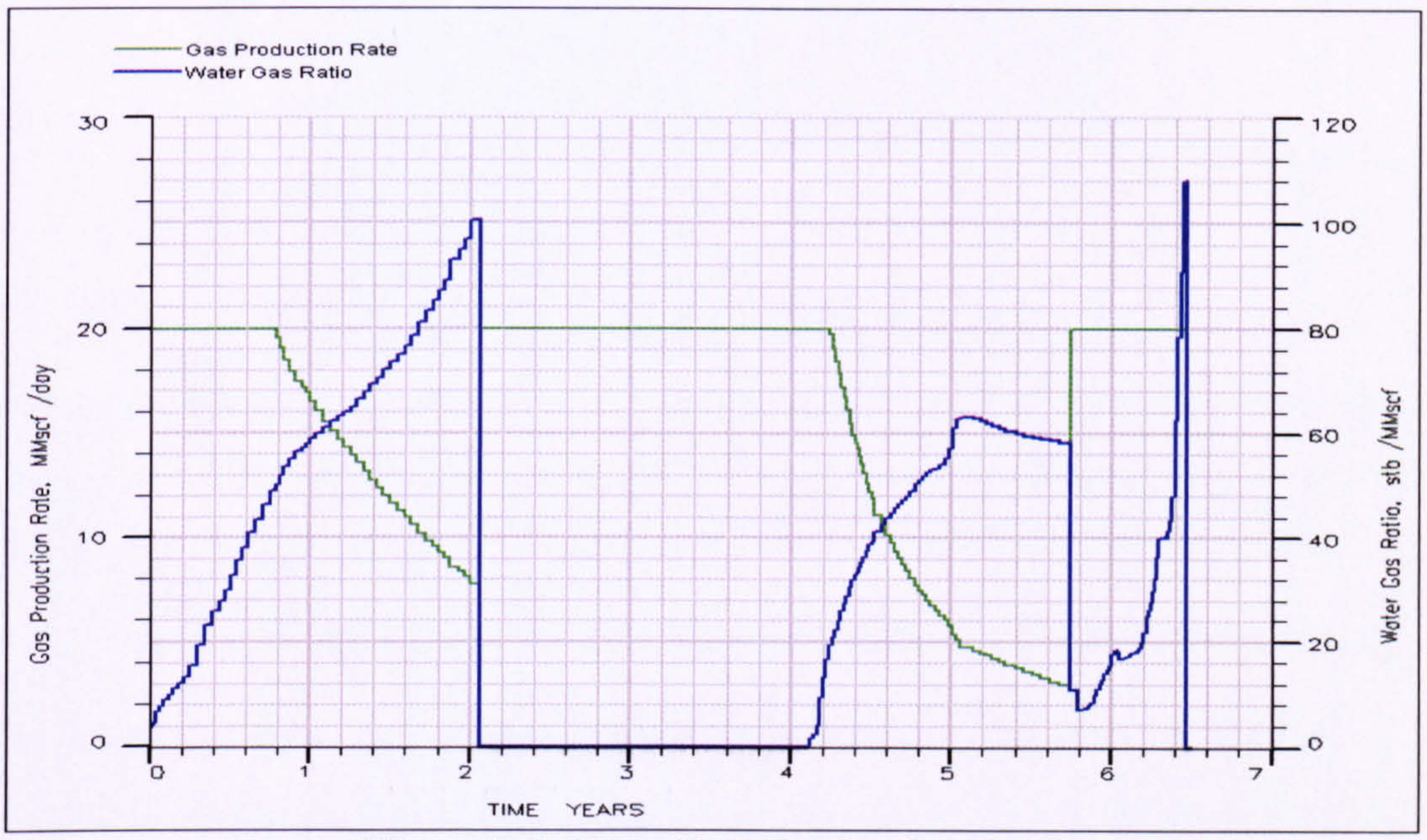

Figure 2-7. Base Case Production Profile

The sand pressure development is illustrated in Figure 2-8 while Table 2-4 shows the sands' production performance. Rapid and early water breakthrough in the upper sand results in a low recovery of 16%. The Lower sand also suffers from a relatively low recovery (32%) due to the water breakthrough, while the middle sand provided the best recovery (61%). The overall recovery factor for the field is 36% is significantly lower than that achieved when the well was positioned in location A, away from the water zone.

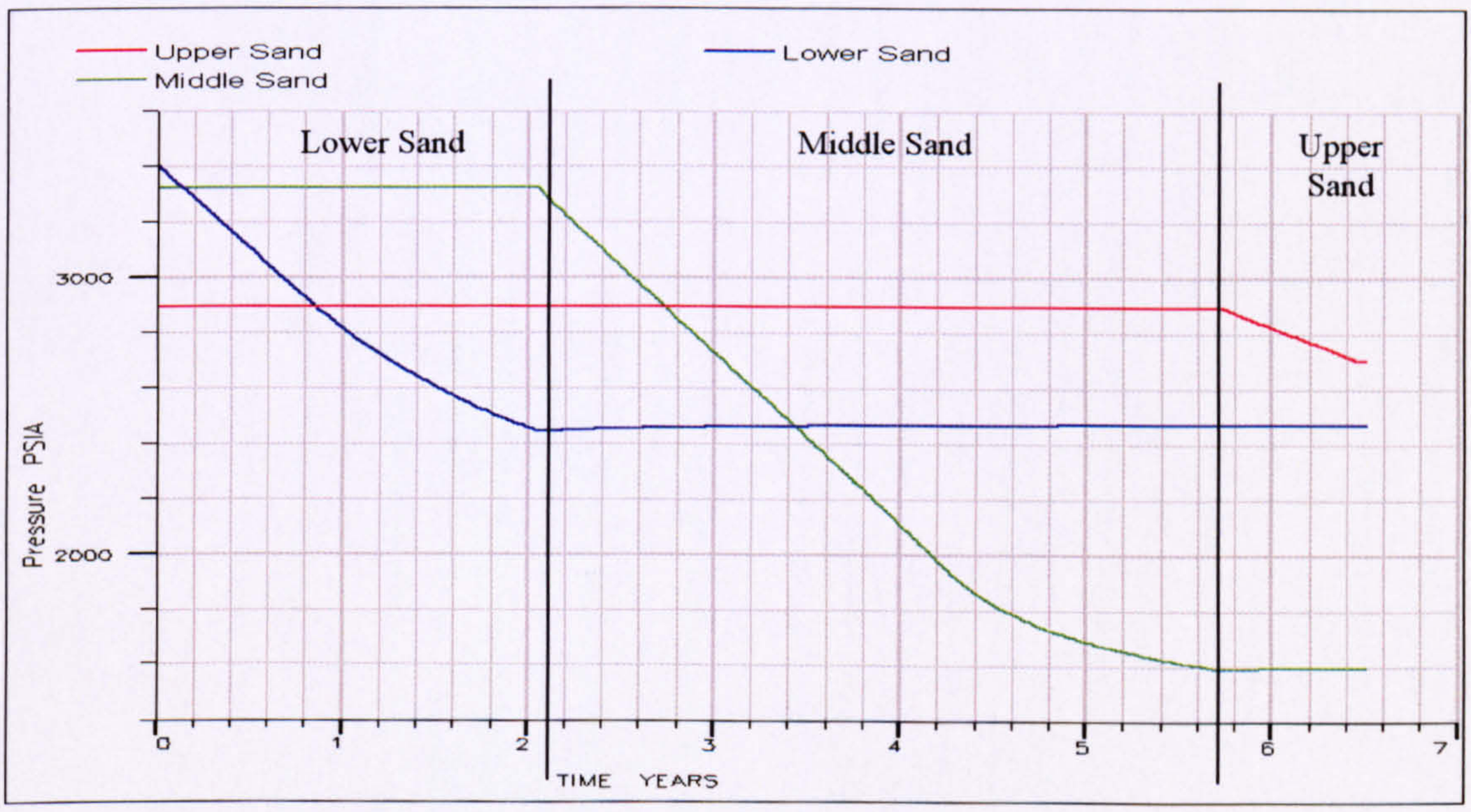

Figure 2-8. Pressure Development of the Gas Sands during Production

Table 2-4. Base Case Gas Recovery

Zone	IGIP (Bscf)	Total Gas Produced (Bscf)	Base Case Recovery Factor
Upper Sand	32.8	5.3	16.1%
Middle Sand	32.9	20.0	60.8%
Lower Sand	36.2	11.7	32.2%
Total	101.9	37.0	36.3%

The study objective will now be to evaluate how to increase the recovery factor for the individual sands using an intelligent completion to obtain the maximum field economic value.

2.5.2 Extended Plateau Case – an alternative conventional case production strategy:

An alternative base case scenario, which may increase the value of the gas, is to accelerate production by producing each sand sequentially until it can no longer sustain the plateau rate of 20 MMscf/day. The sands are then opened sequentially once none of the sands can produce at the plateau rate and produced until they reach one of the abandonment conditions.

Figure 2-9 illustrates the resulting production profile and compares it to the base case. Figure 2-10 illustrates the production acceleration (and increased value) achieved. Only minor differences in recovery were predicted between the two cases.

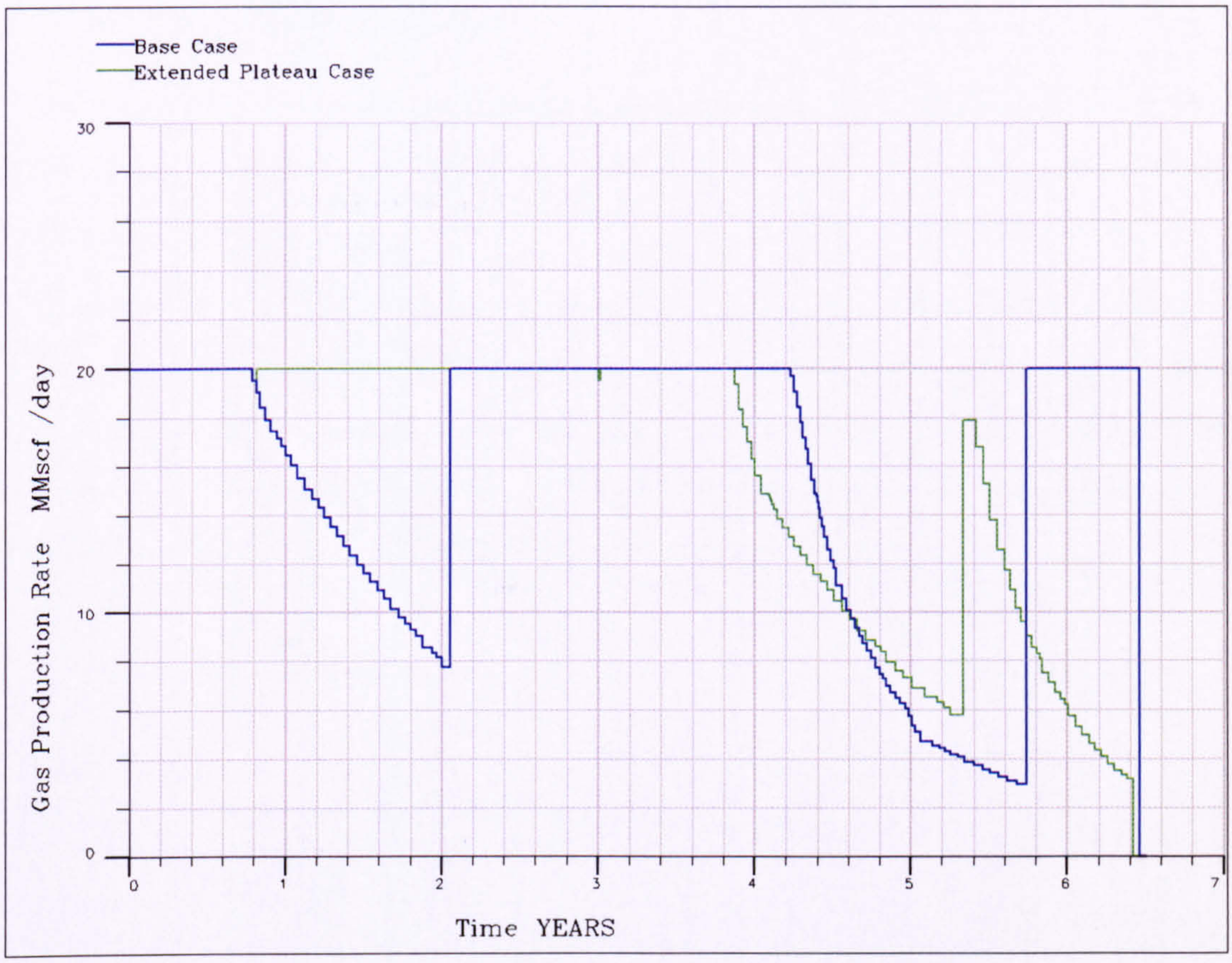

Figure 2-9. Production Profile for the Sequential Production Base Case and the Extended Plateau Case

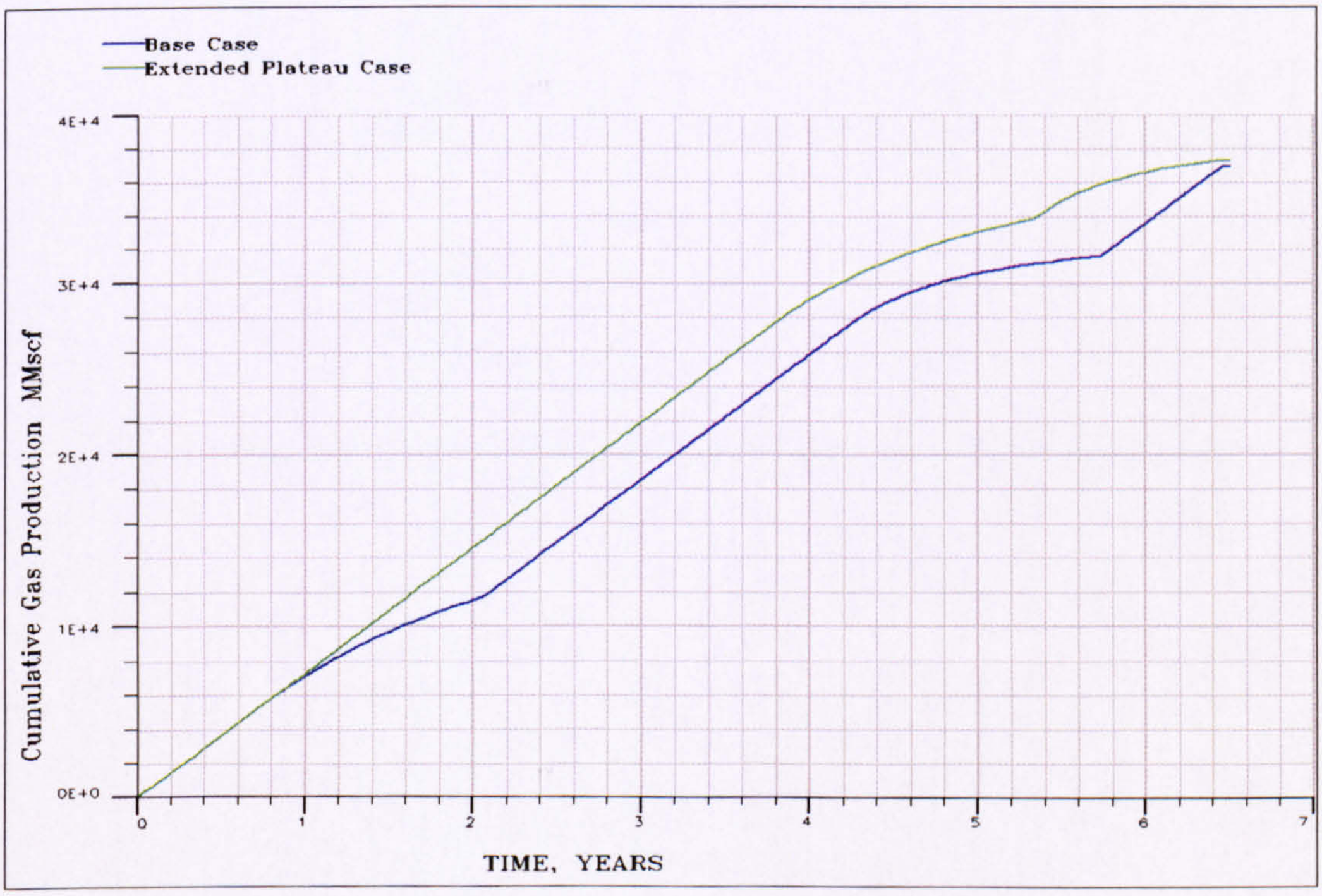

Figure 2-10. Cumulative Gas Production for the Single Tubing Sequntial Production Base Case and the Extended Plateau Case

2.5.3 Intelligent Well (I-Well) Case:

Commingling flow from the well allows a production rate up to 60 MMscf/day. A 4.5-in. tubing is sufficient to produce this 60 MMscf/day. The tubing is also suitable as the production rate decline.

The control strategy is based on continuously controlling the water by choking the ICV from early in the well life. The I-Well case provided 3.2% increase in the overall field recovery. The major increase was in the upper sand which had the lowest recovery in the base case. The high plateau rate could only be sustained for 54 days (Figure 2-11 and Figure 2-12).

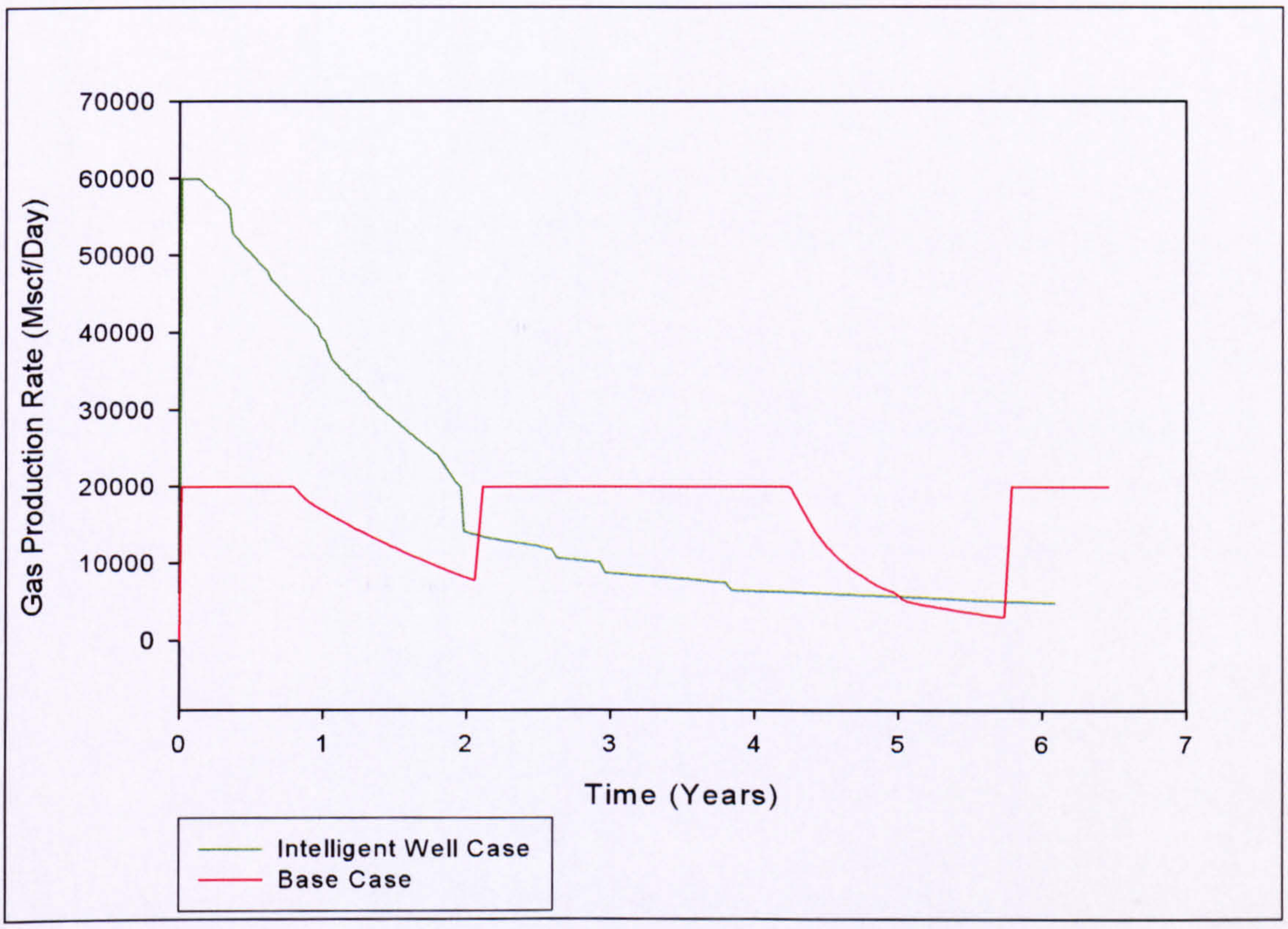

Figure 2-11. Production Profile Comparison Between IW and Base Cases

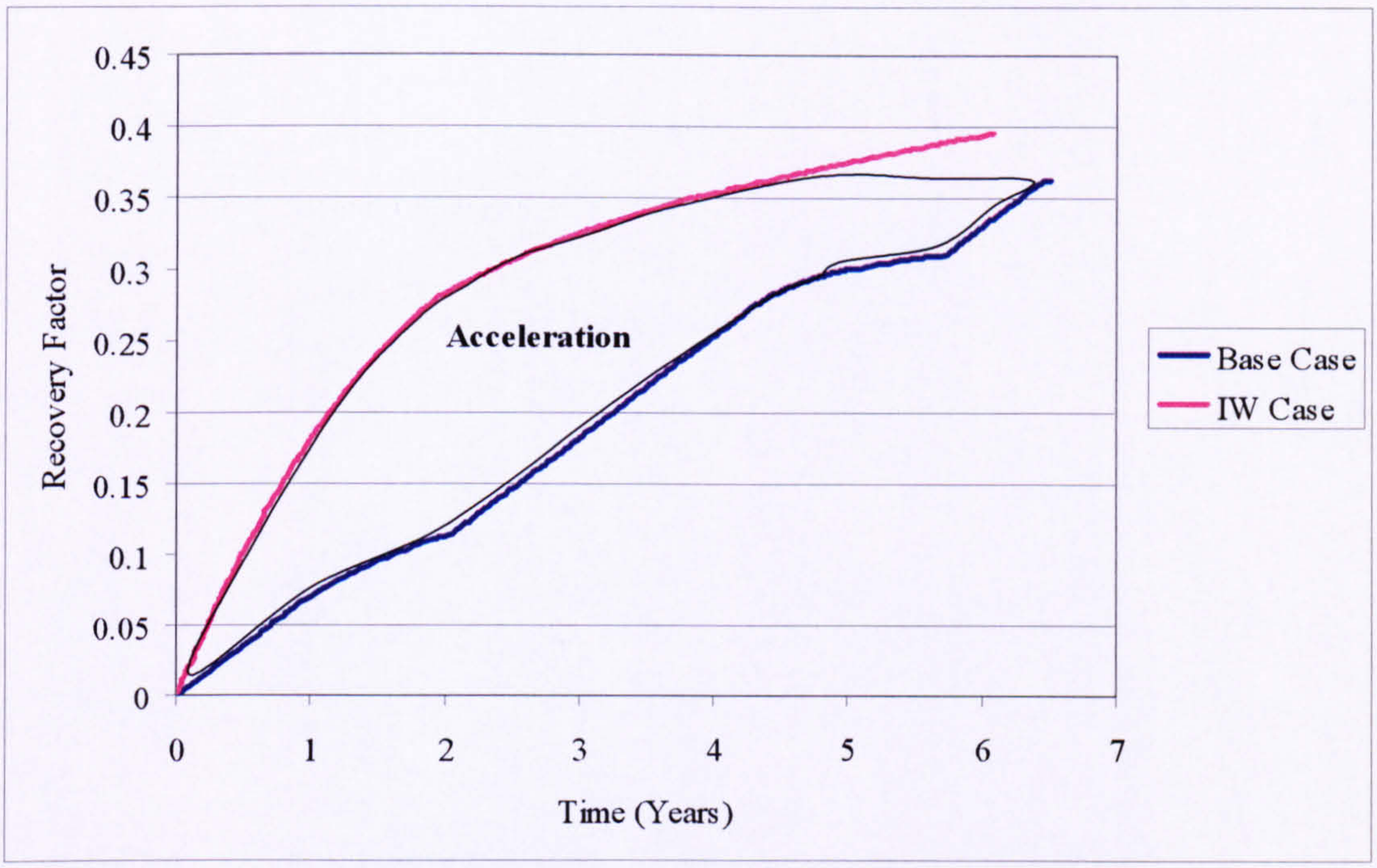

Figure 2-12. IW Gas Recovery Factor Profile

The acceleration effect is best illustrated by plotting the annual gas recovery for the I-Well over time and by discounting the annual gas production. A discount rate of 8% has been chosen to highlight the generated value (Figure 2-13 and Table 2-5). The difference between the total discounted gas production for the two cases is 20.8% in favour of the IW case.

Table 2-5. Annual Reserve Recovery

	Base Case	I-Well Case	I-Well – Base Case Recovery
Year	**Recovery**	**Recovery**	
1	7.0%	18.1%	**11.1%**
2	11.3%	28.3%	**17.0%**
3	18.2%	32.5%	**14.3%**
4	25.4%	35.3%	**9.9%**
5	30.1%	37.5%	**7.4%**
6	33.0%	39.4%	**6.4%**
6.5	36.3%	39.5%	**3.2%**

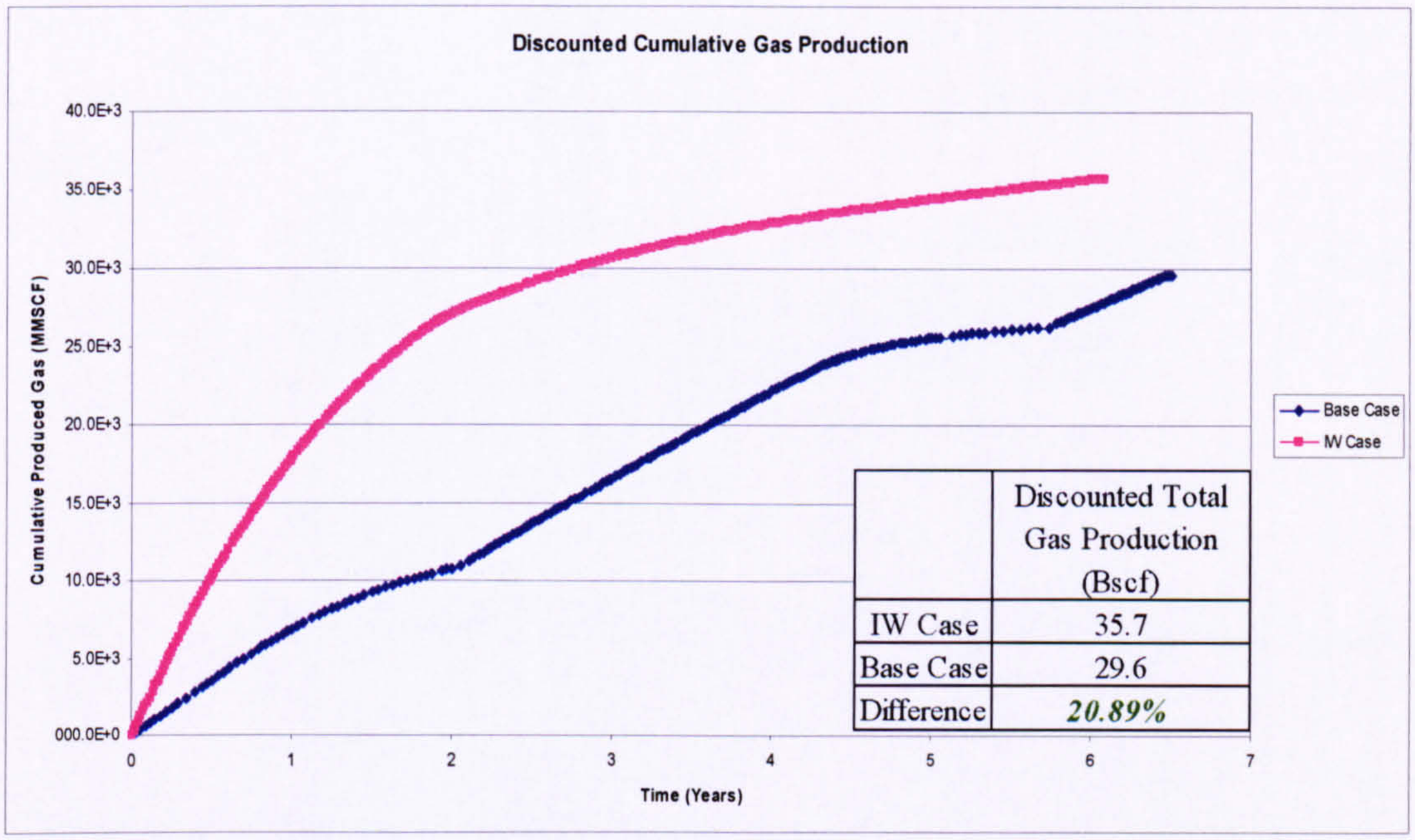

Figure 2-13. Discounted Cumulative Gas Production

The I-well completion allowed a greater volume of water to be produced throughout the well's lifetime. Figure 2-14 shows the water gas ratio for the two cases. It can be seen that the WGR limit was the constraint leading to the abandonment of the I-well.

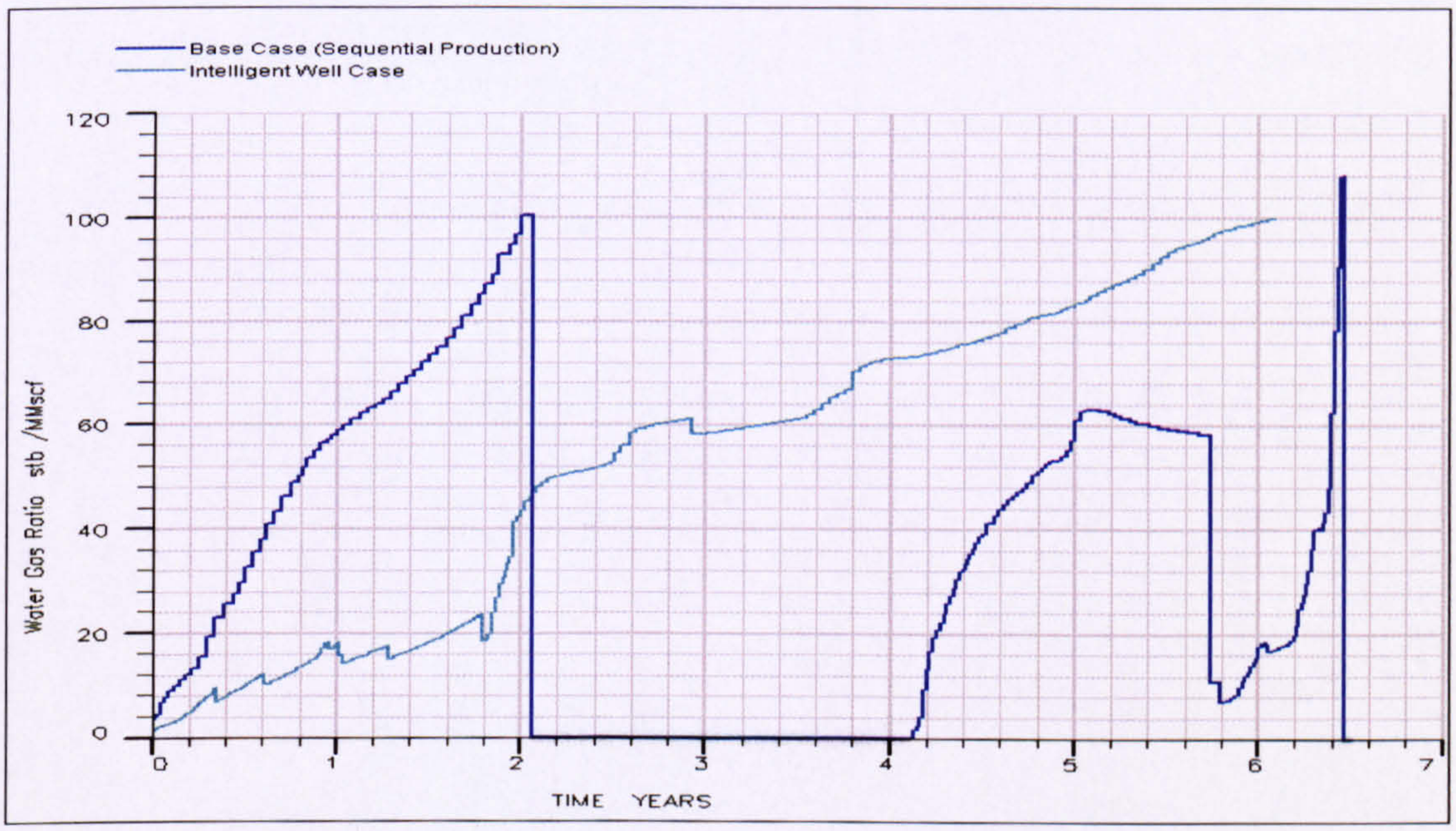

Figure 2-14. Water Gas Ratio Comparison between the I-Well and the Base Case

2.5.4 Sands Performance:

The gas recovery for the upper zone increased significantly to 28.8% from the base case recovery of 16.1%. The middle and lower sands experienced a slight decrease in the gas

recovery. This is due to the well being abandoned because of the high WGR caused by the increase in production from the upper zone. Table 2-6 shows the gas recovery for each zone.

Table 2-6. I-Well and Base Case Gas Recovery

Zone	I-Well	Base Case	Difference
Upper Sand	28.82%	16.14%	+12.68%
Middle Sand	58.66%	60.85%	-2.20%
Lower Sand	31.86%	32.24%	-0.39%
Total	39.53%	36.30%	+3.23%

2.5.5 I-Well Rate Sensitivity Analysis:

Figure 2-11 showed that the production rate of 60 MMscf/d could not be sustained. The results for a reduced plateau rates (40 and 50 MMscf/d) are reported in Figure 2-15 to Figure 2-17.

Figure 2-15 shows that 40 MMscf/d provides the longest plateau period (455 days), the 50 MMscf/d rate plateau period is 191 days while the 60 MMscf/d rate plateau period was 49 days. Figure 2-16 shows the total gas production for each of the production rates, these figures being discounted at 8%/annum in Figure 2-17. The plateau rate of 60 MMscf/d provides the best acceleration, while the 40 MMscf/d rate provides the best ultimate recovery.

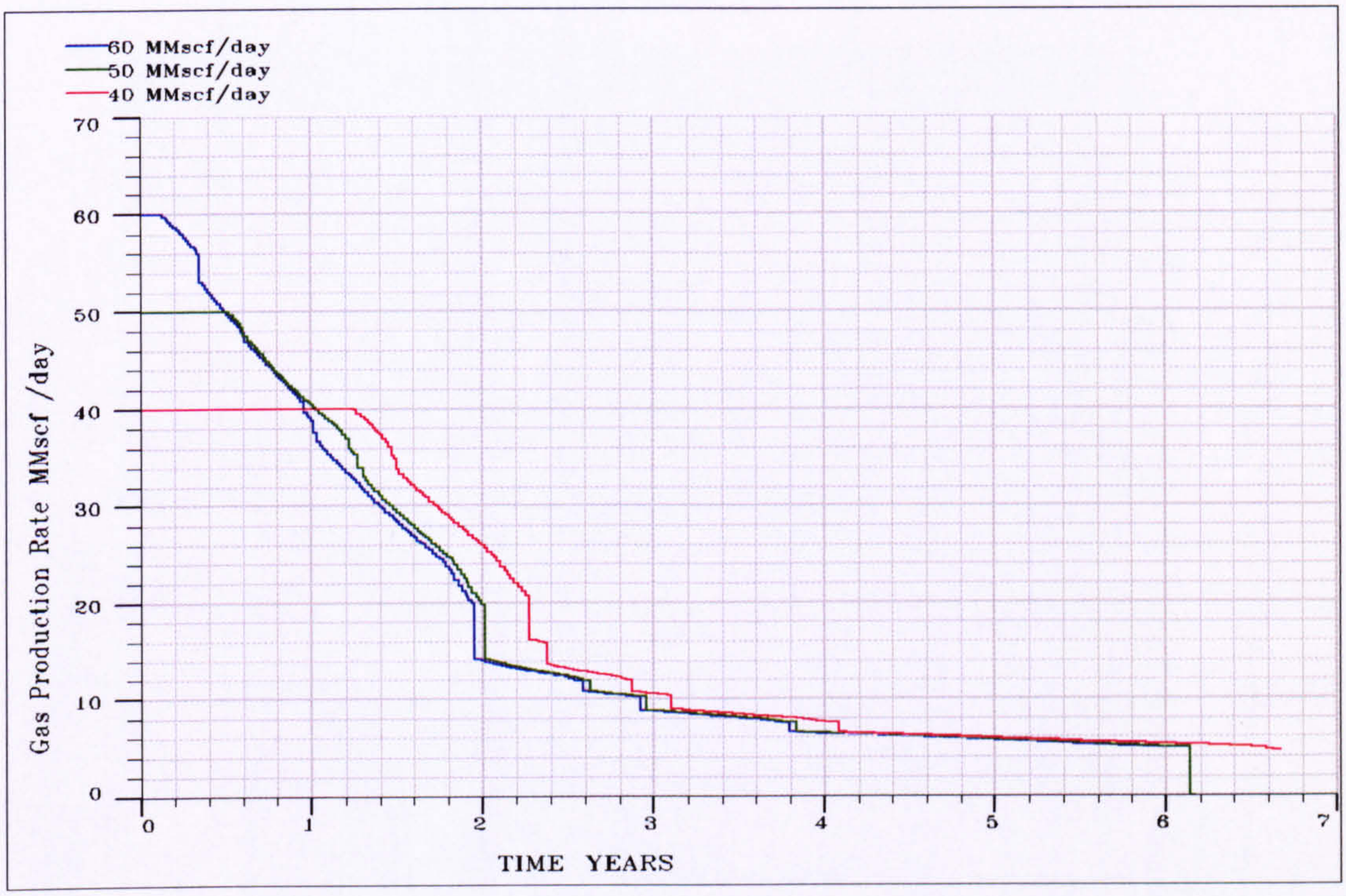

Figure 2-15. Rate Sensitivity Analysis to the I-Well Case

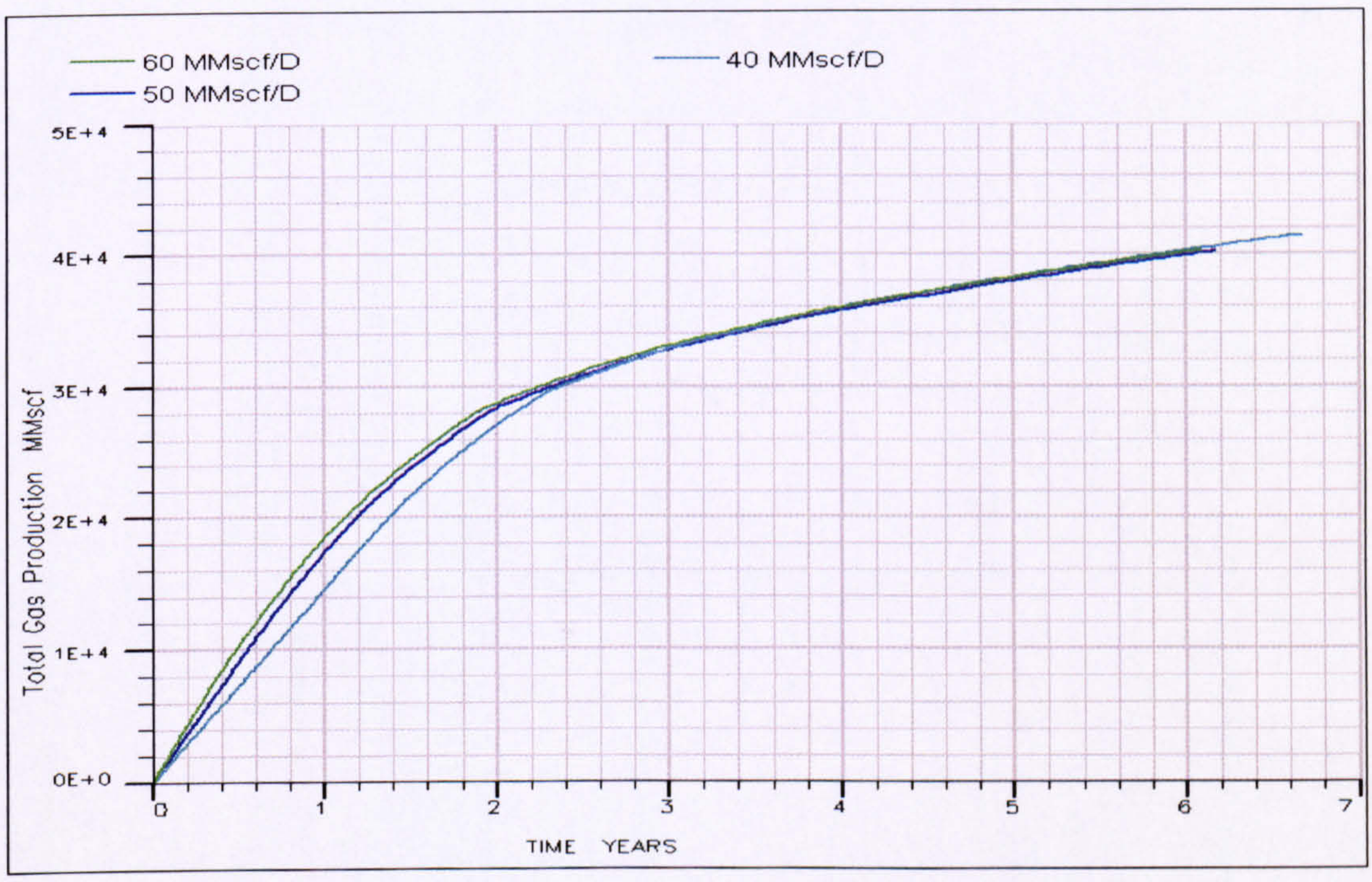

Figure 2-16. Total Gas Production for Rate Sensitivity

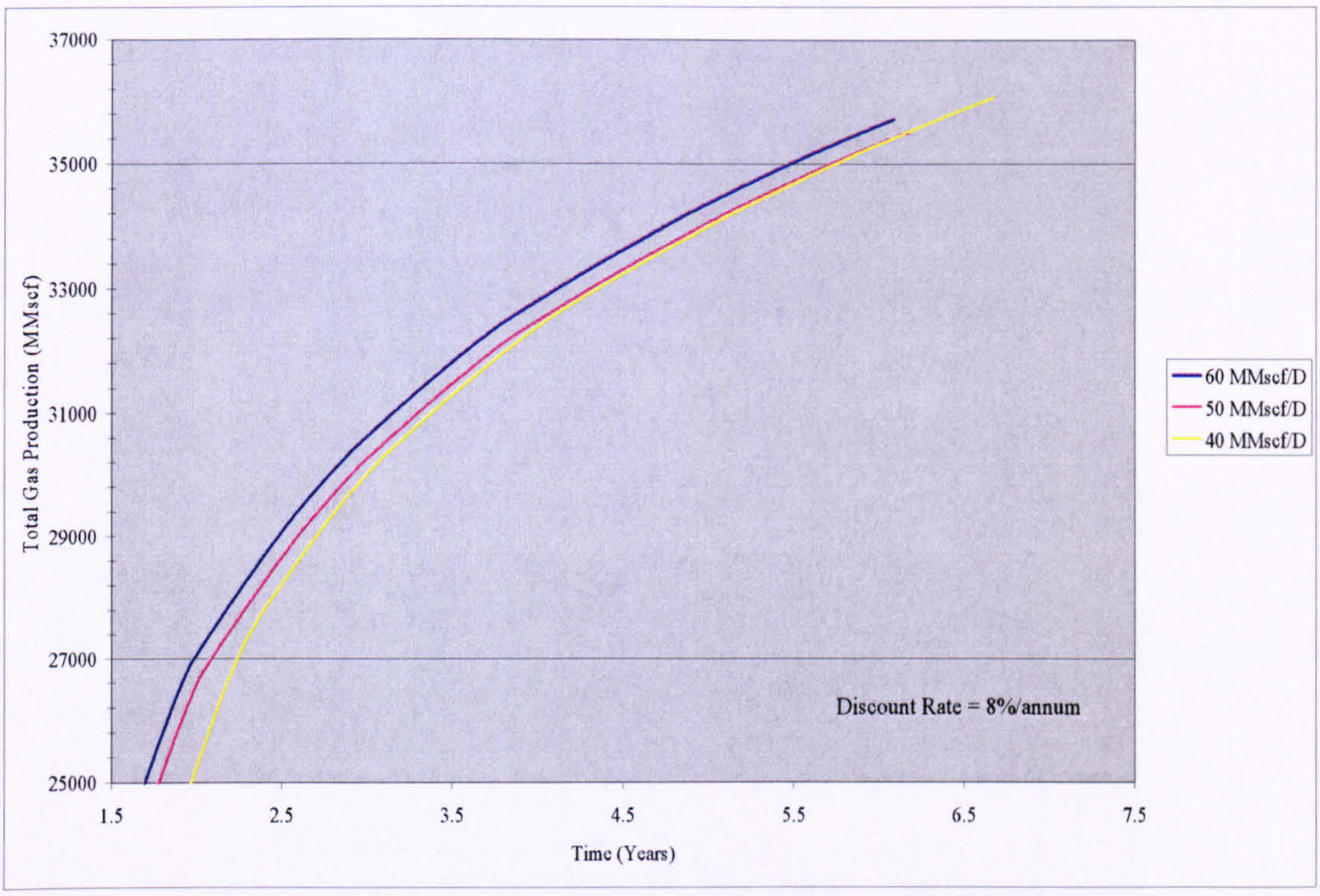

Figure 2-17. Discounted Total Gas Production for Various Production Rates

2.5.6 I-Well Tubing Head Pressure Sensitivity:

Lowering the THP limit by 50% to 550 psia extended the Plateau Rate to 127 days from 49 days and increased the recovery by 2.78% (1.1 Bscf) (Figure 2-18).

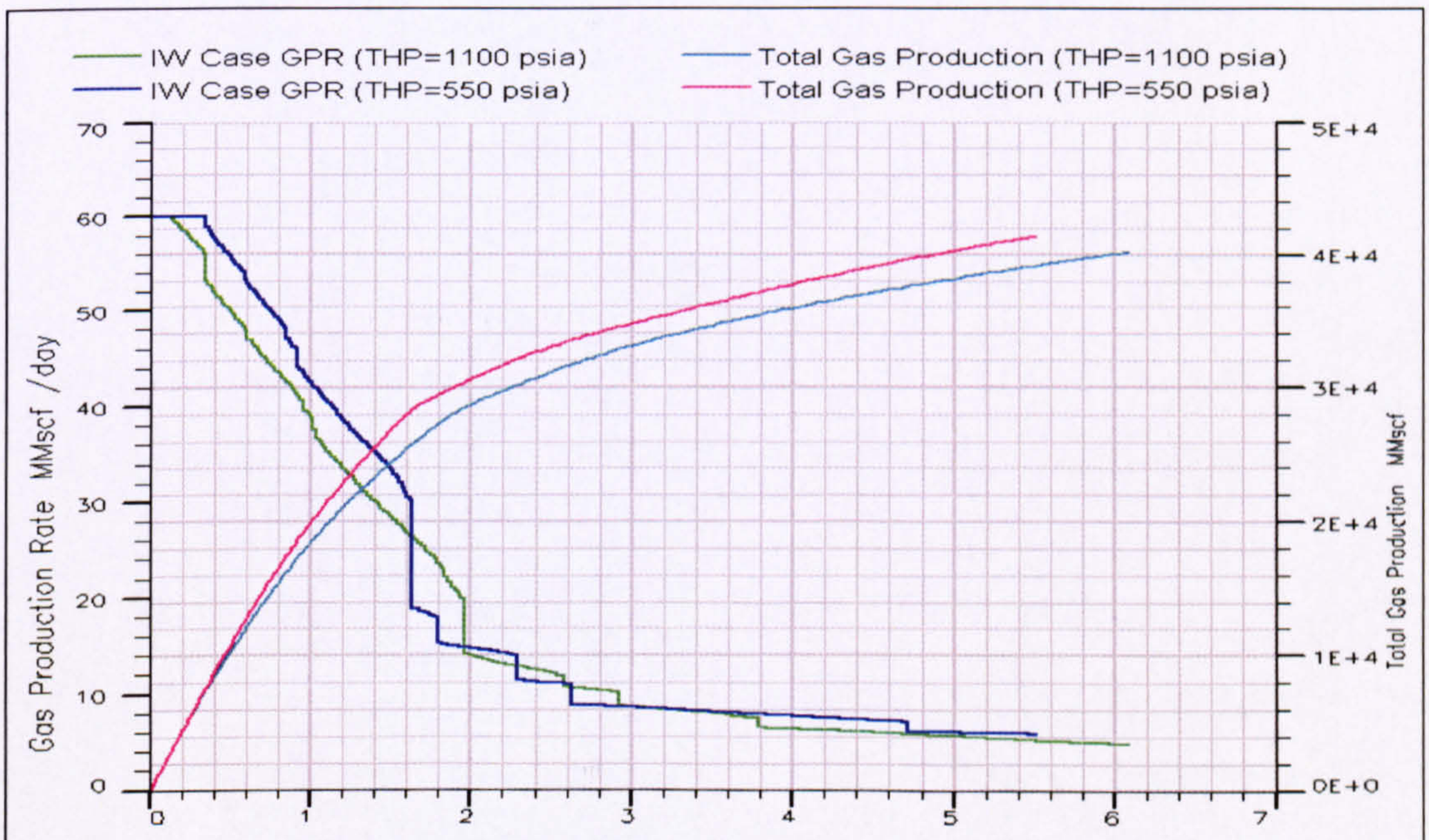

Figure 2-18. Production Profile and Total Gas Production for THP Sensitivity

2.5.7 Impact of the Choking Strategy:

Gas is lost due to the restriction of flow using the ICV when implementing early water control. An alternative choking strategy based on producing the well at a high WGR and near to the production constraint of 100 STB/MMscf was implemented. ICV choking control will now start at a high WGR value. Figure 2-19 shows how the WGR and the optimum choking ICV flow area size are related to one another when implementing this strategy.

This strategy assumes that a simple ICV with only two fixed sizes, the initial position and the choking position that is chosen once the WGR condition is reached, has been installed. A fixed, two position ICV is cheaper to install than a multi-position or infinitely variable valves, but is less flexible.

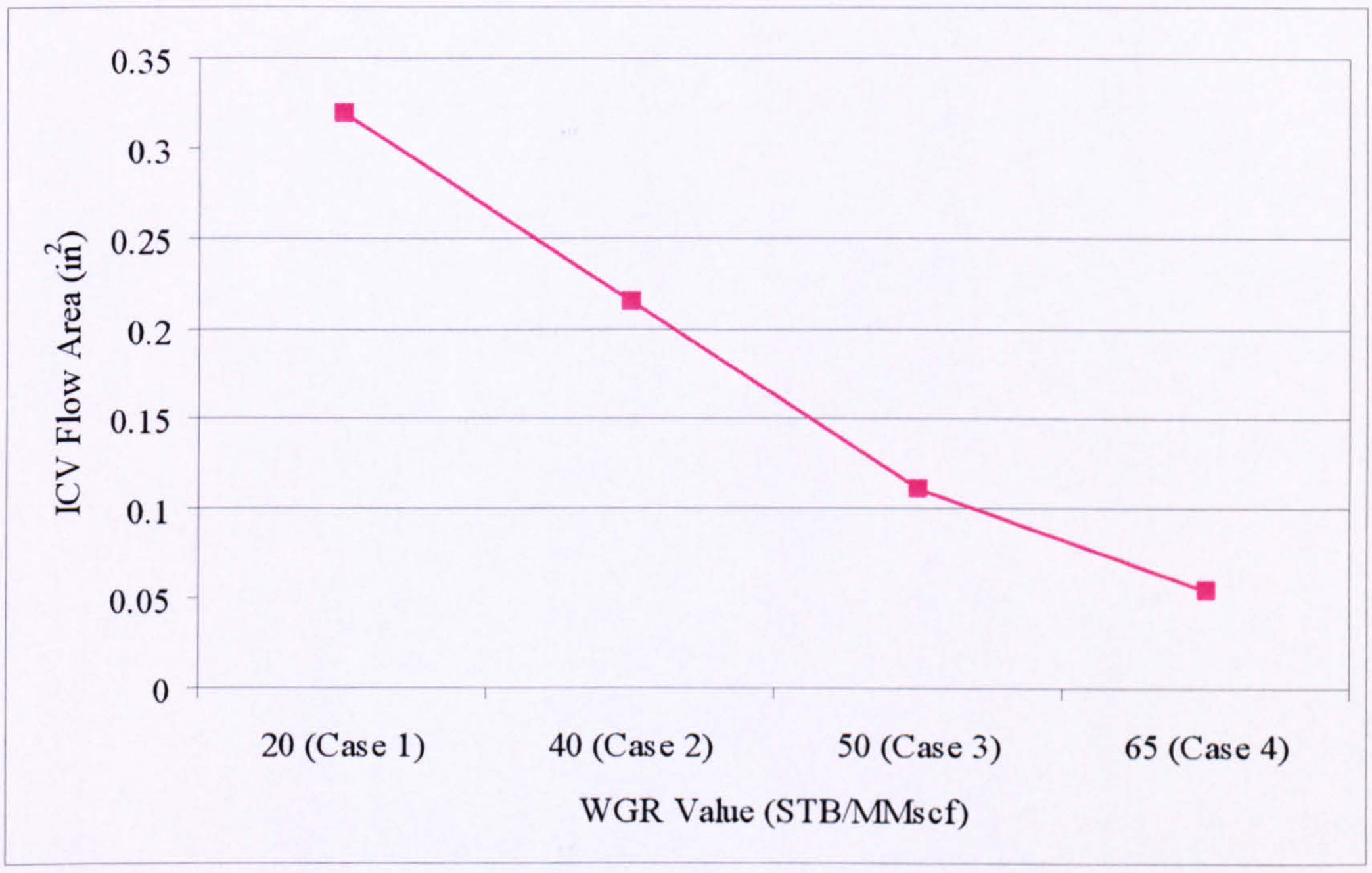

Figure 2-19. Alternative Choking Strategies using a Two Position ICV

2.5.8 An Alternative Choking Strategy:

Figure 2-20, shows that choking strategy 4 (WGR value = 65 STB/MMscf) provides the greatest total gas production and well life. Figure 2-21 shows the water gas ratio trend for each of the four cases. It is not a surprise to see that Choking strategy 4 provide the longest period of production with the initial ICV flow area. Table 2-7 compares the gas recovery for the Base case, IW case, choking strategy 4 case. Choking strategy 4 provides an increased recovery compared to the IW and Base cases by 0.8% and 4%,

respectively. Choking strategy 4 case achieved reasonable sand performance of the upper sand, though somewhat less than when employing continuous choking. The middle sand achieved the greatest recovery of all cases while the recovery factor for the lower sand showed a small decrease (1.5%, Table 2-7).

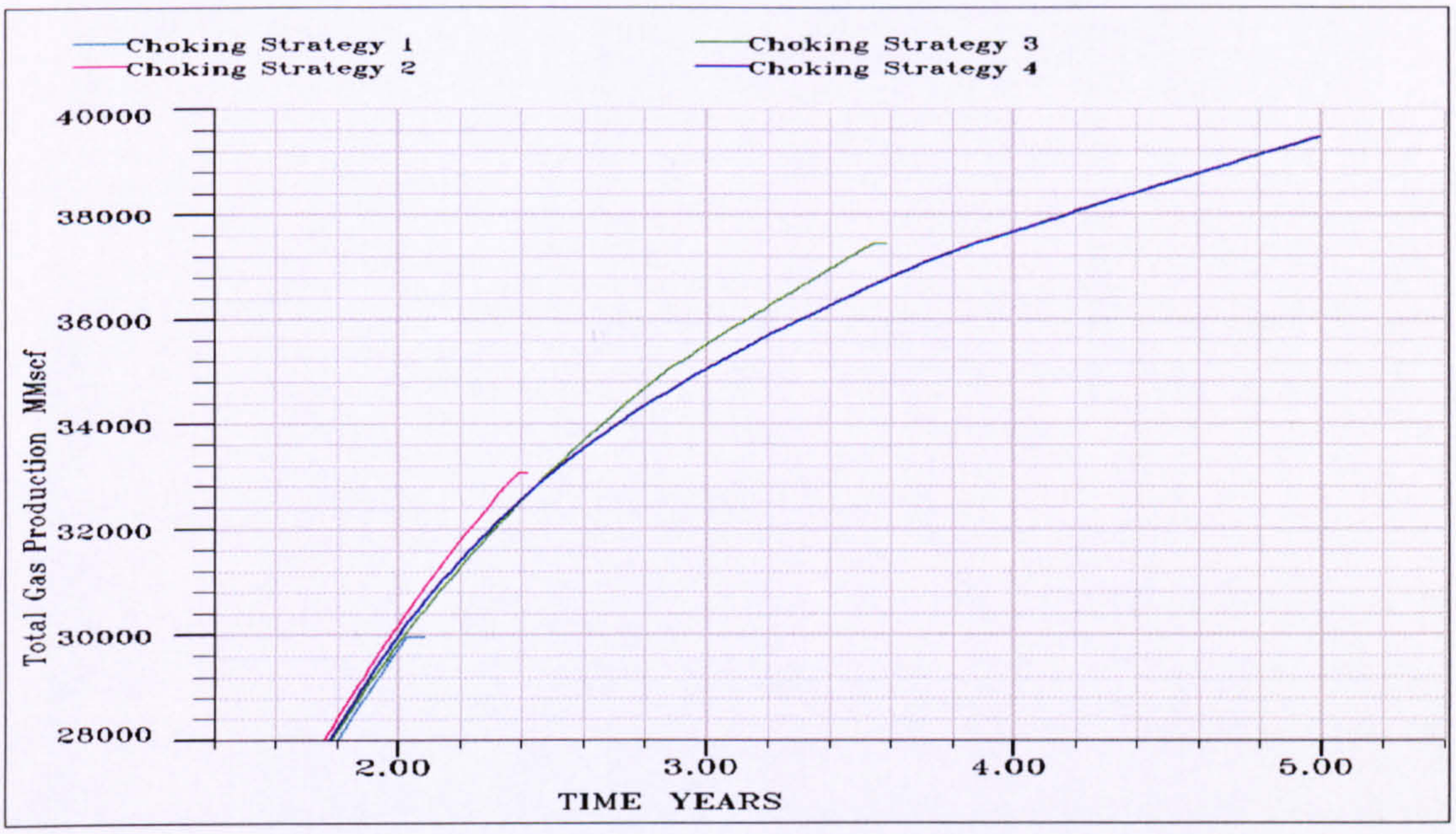

Figure 2-20. End of Well Life Total Gas Production for Alternative Choking Strategy

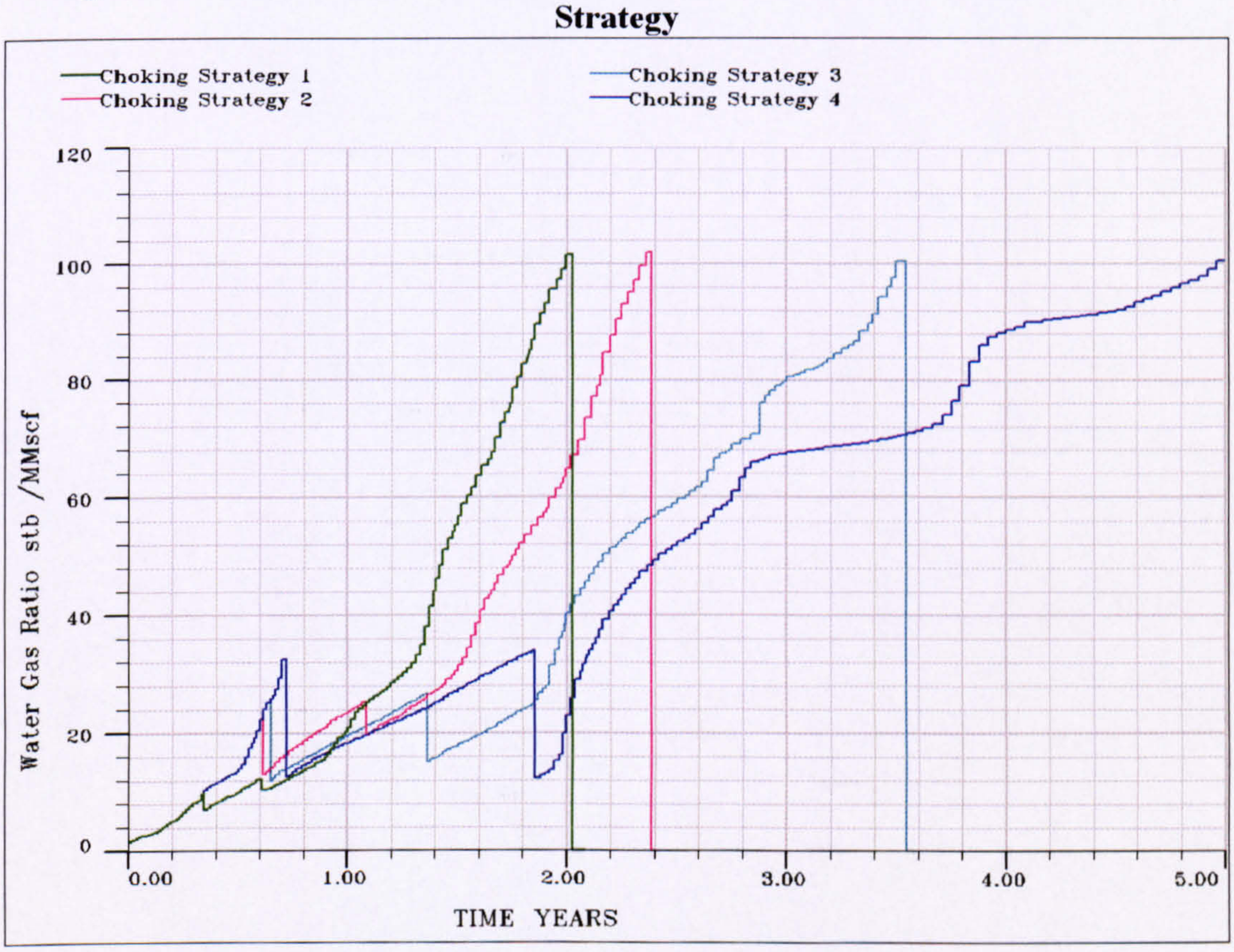

Figure 2-21. Water Gas Ratio for Cases of Alternative Choking Strategy

Table 2-7. Sands Gas Recovery

Zone	Base Case Recovery	IW (Continuous Water Control) Recovery	Choking Strategy 4 (Delayed Control) Recovery	Difference between Base and Choking Strategy 4 Cases
US	16.14%	28.82%	26.48%	+10.35%
MS	60.85%	58.66%	64.62%	+3.77%
LS	32.24%	31.86%	30.76%	-1.49%
Total	36.30%	39.53%	40.31%	+3.99%

2.5.9 An Extension of the Alternative Choking Strategy

Increasing the ICV flexibility to a multi-position valve allows for the Choking Strategy 4 be extended to control the designated WGR value from 65 STB/MMscf to 75 and later 85 STB/MMscf WGR. This will be called Choking Strategy 5. Figure 2-22 shows the benefit of more flexibility in water control later in well life (after 1.5 years) can achieve a higher total gas production in a shorter time.

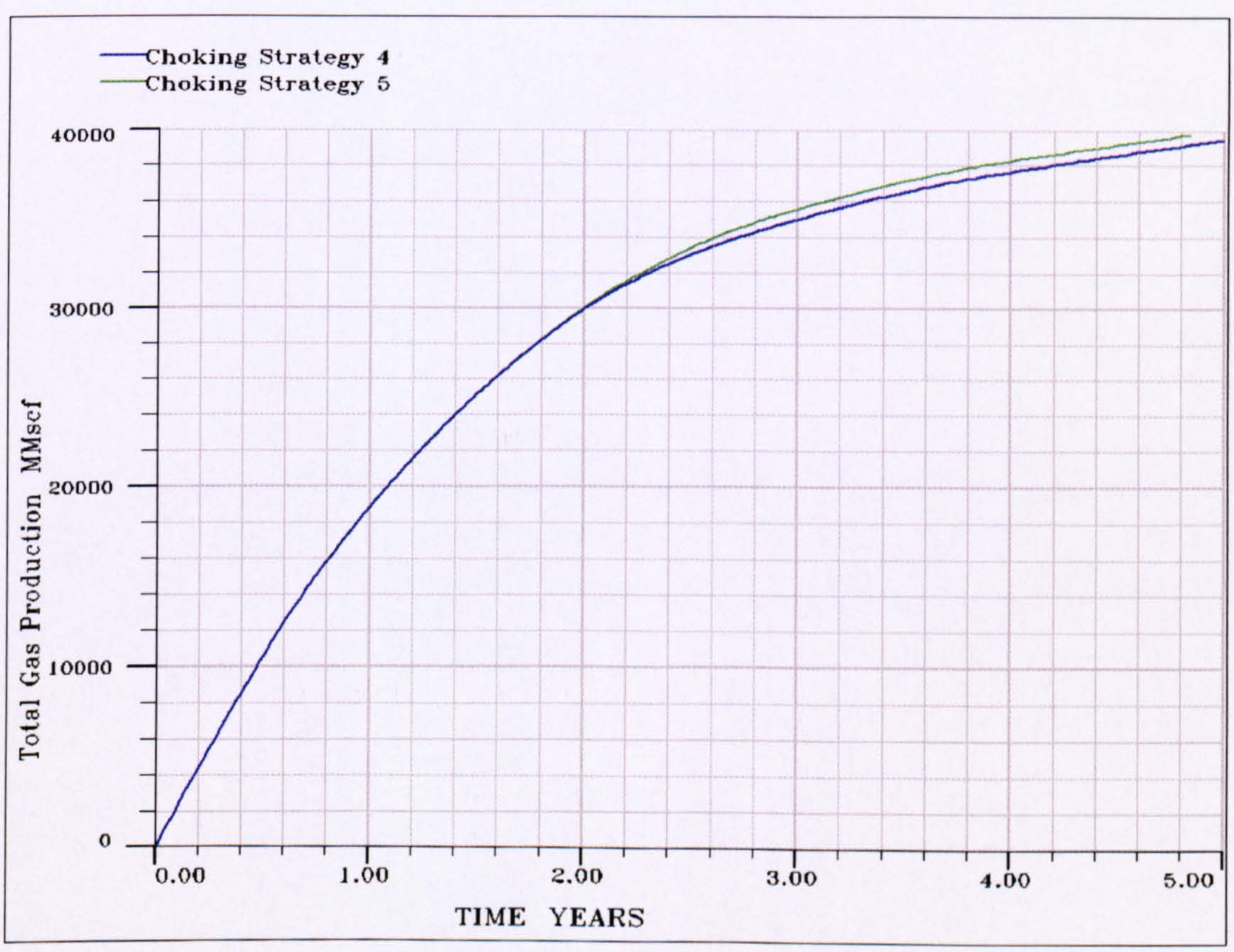

Figure 2-22. Total Gas Production for Choking Strategy Cases 4 and 5

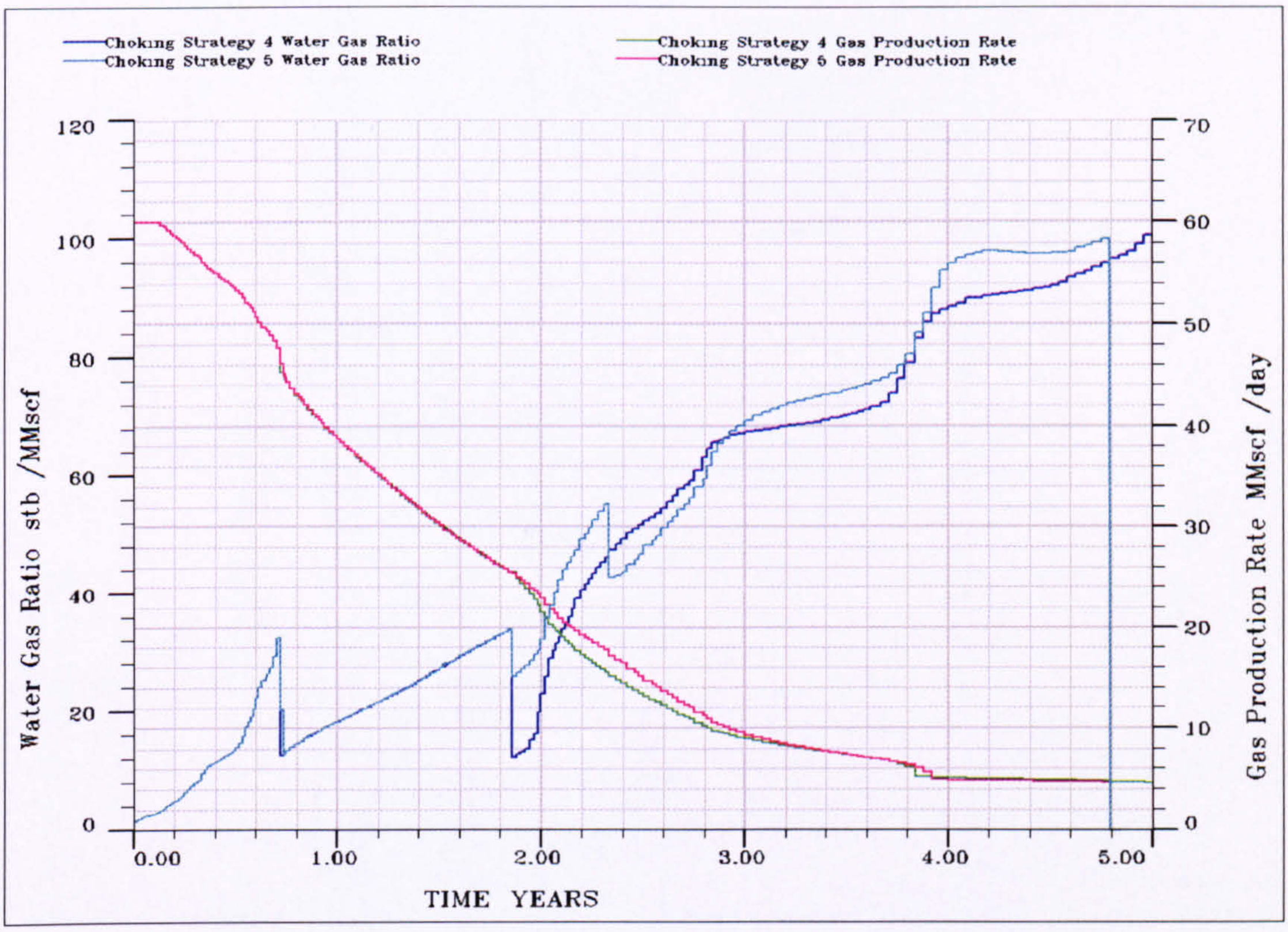

Figure 2-23. Production Profile for Cases 4 and 5 of Alternative Choking Strategy

2.5.10 Economic Impact of I-Well:

Table 2-8 shows the discounted total gas production for different completion scenarios that were analyzed for the well located on the flank of Field C. The discounted total gas production indicates the economical benefits of the different options. The intelligent well case provided an additional 5 Bscf of gas compared to the two scenarios of the conventional completions. The additional gas produced was a result of the water control strategy implemented.

Even though the extended plateau conventional base case (Figure 2-9) produced an extra 1 billion scf of gas, this might not reflect if economical analysis of OPEX and CAPEX is included, as this scenario will require 6 interventions to operate the SSDs over 6 years to carry out such a scenario.

Table 2-8. Discounted Total Gas Production for the flank well location with different Completion Techniques

Case	Discounted Total Gas Production (Bscf)
Base Case (Conventional Well with Sequential Production	29.6
Base Case (Extended Plateau Scenario)	30.6
I-Well Case (Choking Strategy 5)	35.9

2.6 Conclusions:

1. Intelligent well completions are capable of accelerating production from gas fields where commingling is not allowed with conventional completions.

2. Intelligent well completions can manage unwanted fluid production through non-optimum well placement. Thus, a higher ultimate recovery can be achieved with an intelligent well completion because of the ability to control water production when the well was located at the flanks of the reservoirs. An intelligent well located at the crest of the reservoir did not increase the recovery but accelerated the production.

3. Delayed water control can provide good results when compared to early and continuous water control

4. Upon developing the intelligent well design an optimization investigating of the sensitivity of the reservoir to different plateau rate.

5. Lowering THP pressure can provide high recoveries and acceleration but the cost and practicality of installing a pressure boosting facility needs to be investigated.

6. Intelligent completion proves the more attractive option when comparing with other alternative conventional completion designs.

2.7 References:

2.1. Robinson, M., *Intelligent Well Completions.* Journal of Petroleum Technology, 2003(August 2003): p.

2.2. Yu, S., D.R. Davies, and D.W.Sherrard. *The Modelling of Advanced "Intelligent" Well – An Application.* Paper SPE62950 presented at 2000 SPE Annual Technical Conference and Exhibition, Dallas, Texas, U.S.A., 1–4 October 2000, Society of Petroleum Engineers.

2.3. Glandt, C.A. *Reservoir Aspects of Smart Wells.* Paper SPE81107 presented at SPE Latin American and Caribbean Petroleum Engineering Conference, Port-of-Spain, Trinidad, West Indies, 27-30 April 2003, Society of Petroleum Engineers.

2.4. Schlumberger, Geoquest Eclipe 100 Reservoir Simulator Manual 2005A. 2005.

Chapter 3 Enhancing Production from Thin Oil Column Reservoirs Using Intelligent Well Completions and Multilateral Wells

3.1 Objectives and Motivation

Intelligent wells are defined as wells with the ability to install, operate and monitor and control completions without the need for conventional interventions [3.1]. This chapter's objective is to examine the benefits of using downhole control to improve the production from a more difficult reservoir environment than that studied in Chapter 2. It assumes that a constant and clear knowledge of the flow conditions, fluid cuts are available to control the production from the well using the ICVs at all times. One motivation behind this work is to highlight the importance of the monitoring to achieve the benefit of the downhole flow control.

3.2 Introduction

Thin oil column reservoirs, where the pay is sandwiched between an aquifer and a gas cap with a thickness of the order of tens of feet, are common throughout the world [3.2]. Reservoirs are considered to have an "Ultra-Thin" oil column when the thickness is less than 20ft [3.3]. These reservoirs can still contain substantial volumes of hydrocarbons-

in-place despite their small pay thickness. Developing such reservoirs (i.e. turning Oil-In-Place into reserves) presents many technical challenges to the field development planners. One important issue is water coning and gas cusping - problems that have a detrimental effect on the ultimate oil recovery, and hence the project economics. Recent studies [3.2, 3.3, 3.4] have shown that developing this type of reservoir using horizontal wells have many benefits:

1. The well geometry will drain a larger volume of the reservoir.
2. The horizontal well's reduced drawdown will:
    a. Minimize coning and cusping [3.2, 3.3].
    b. Alleviate any sand problems.

Employment of intelligent completions in horizontal wells for developing thin oil column reservoirs has already produced many benefits. Experience in the Mahogany gas field [3.5] showed that distributed temperature measurements eliminated the need for production logs and provided a continuous indication of the lateral length that was actually contributing to the flow. Such information allows determination of the producing well's efficiency; while also providing the justification for any stimulation job required to maximize production.

A second example of intelligent completions installed in a horizontal well producing from thin oil column in a compartmentalized reservoir from the Iron Duke Field [3.6]. This well was forecast to produce an extra 38% cumulative oil compared to a conventional well by managing production from the five production zones, all of which had different reservoir characteristics.

3.3 Reservoir and Well Models:

The operator made available a real, full field reservoir simulation model of a thin oil column reservoir, from which two sector models were extracted:

1. Sector A is on the flank of the field where the main production problem is excessive production of water. Two of the study wells (A1 and A2) were from sector A.
2. Sector B is a more central location where the overlaying gas cap causes early well gas production. Well B1 was selected from a location immediately under the gas cap.

The base case well design called for all three example wells to have their horizontal section placed in the middle of the oil column. Local grid refinement around the well bore increased the modelling accuracy when water and gas was being produced into the horizontal wellbore. The well's open-hole, horizontal completion's inflow performance was fully modelled using the Eclipse^{TM} [3.7] reservoir simulator's multi-segment well modelling option. The size of the well segment was the same size as the reservoir grid block. The vertical lift performance was input as a Vertical Lift Performance (VLP) table. All wells were produced under the same constraints of:

1. Maximum Gas Oil Ratio (GOR) of 10,000 scf/STB.
2. Maximum Water Cut (WC) of 95%.
3. Minimum Flowing Bottom Hole Pressure (BHP) of 1,000 psi.

The reservoir properties of all three wells are summarized in Table 3-1 while Figure 3-1 shows the A2 well's reservoir grid. The worst case coning / cusping scenario was chosen by assuming a vertical to horizontal permeability ratio of unity. Well A2 has an additional problem compared to well A1 due to the presence of a high gas-production streak in the mid-section of the well.

Table 3-1. The Base Case Well Properties

Well	Horizontal Section Length (ft)	Oil Column Thickness (ft)	Average Permeability (mD)	Reservoir Pressure (psi)	Porosity (%)	Target Liquid Production Rate (BLPD)
A1	3,843	79	204	2,329	21.61	2,000
A2	3,408	64	191	2,324	28.92	3,000
B1	1,863	61	142	2,400	23.98	1,000

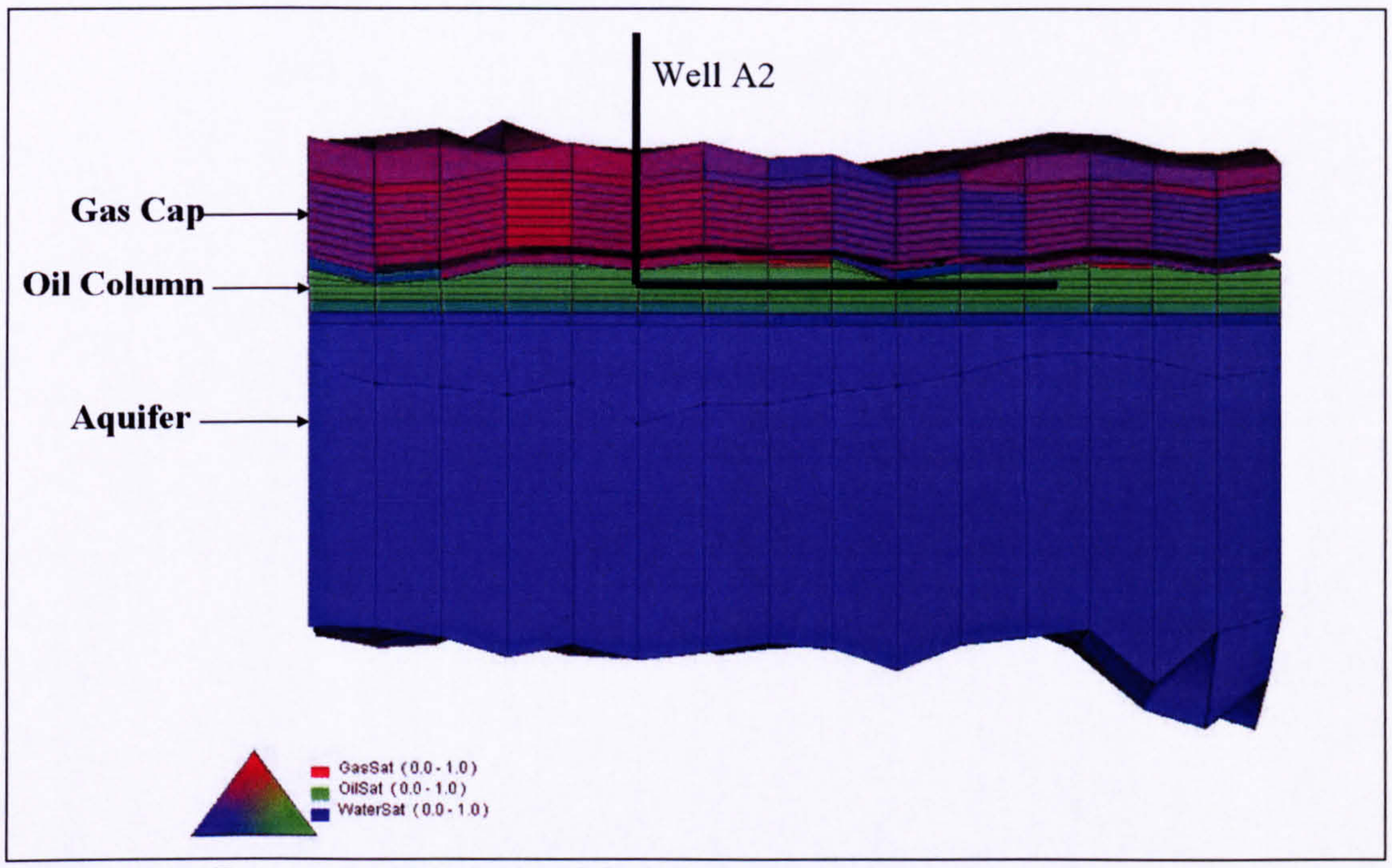

Figure 3-1. Reservoir Simulation Model of a Thin Oil Column Reservoir for Well A2

Both the A1 (Figure 3-2) and A2 (Figure 3-3) wells produced for the complete production period (10 years) without being affected by the production constraints. By contrast, well B1 reached the GOR constraint after only 2.5 years of production (Figure 3-4). The well life could be extended by lowering the well target rate to 500 BLPD, however the well would then no longer have satisfied the economic criteria at this lower production rate.

The above horizontal well performance is a vast improvement over that observed with a conventional vertical or deviated well design - a vertical equivalent of the A1 well did not produce any oil as the local gas zone broke through immediately, while a vertical B1 well fared somewhat better, managing 21 days production before gas cusped into the well.

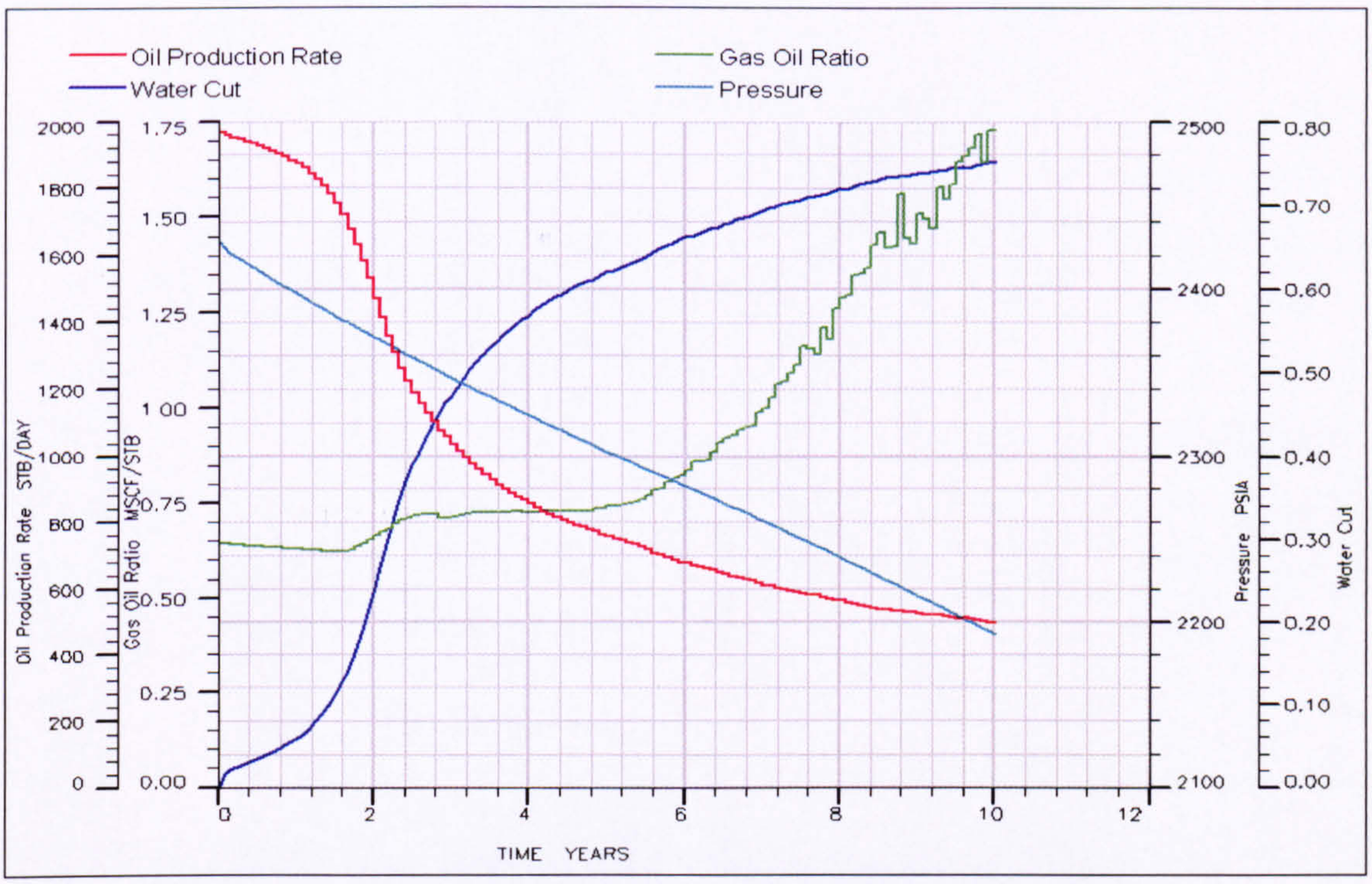

Figure 3-2. Well A1 Open-Hole Completion Production Profile

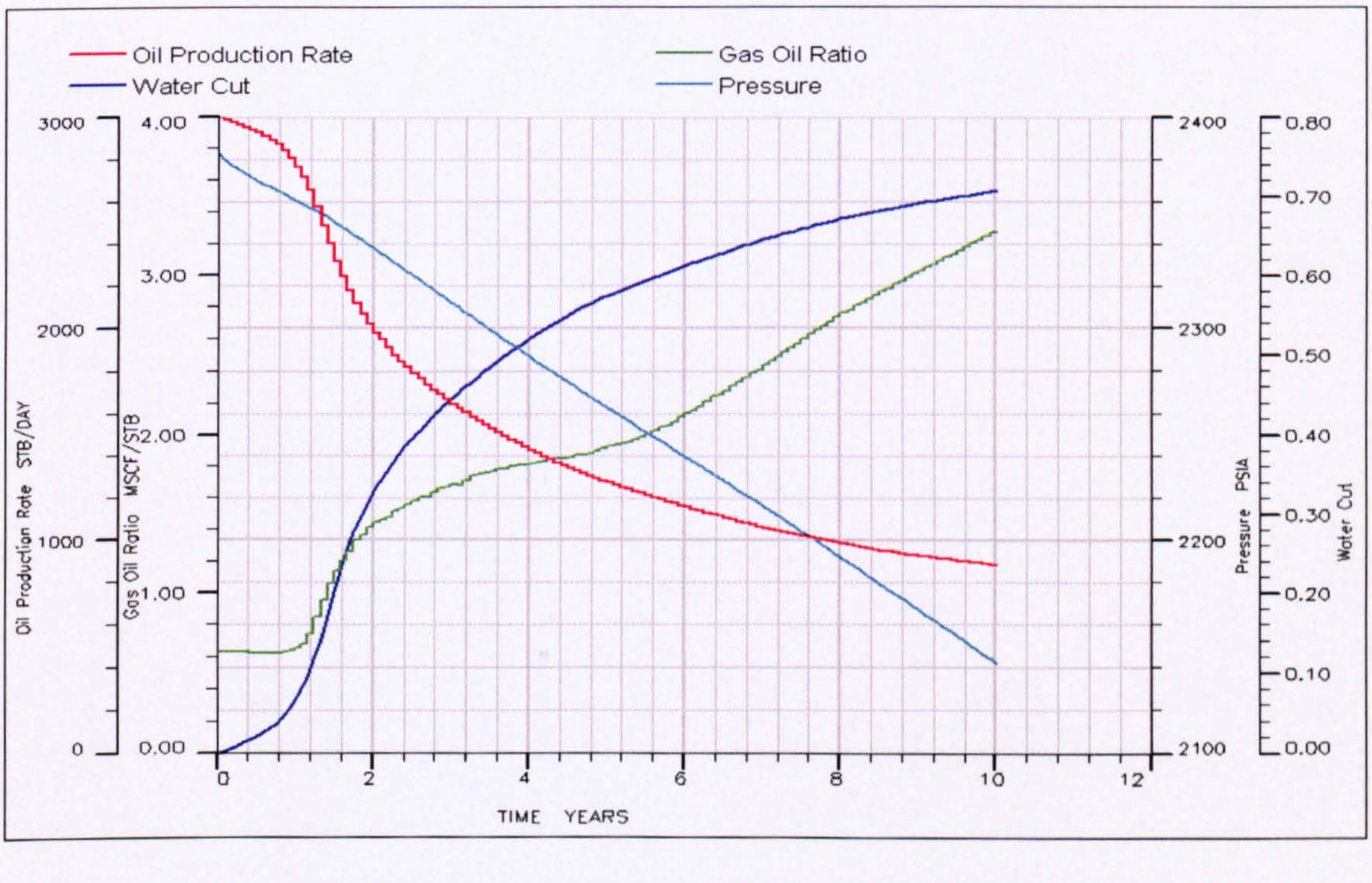

Figure 3-3. Well A2 Open-Hole Completion Production Profile

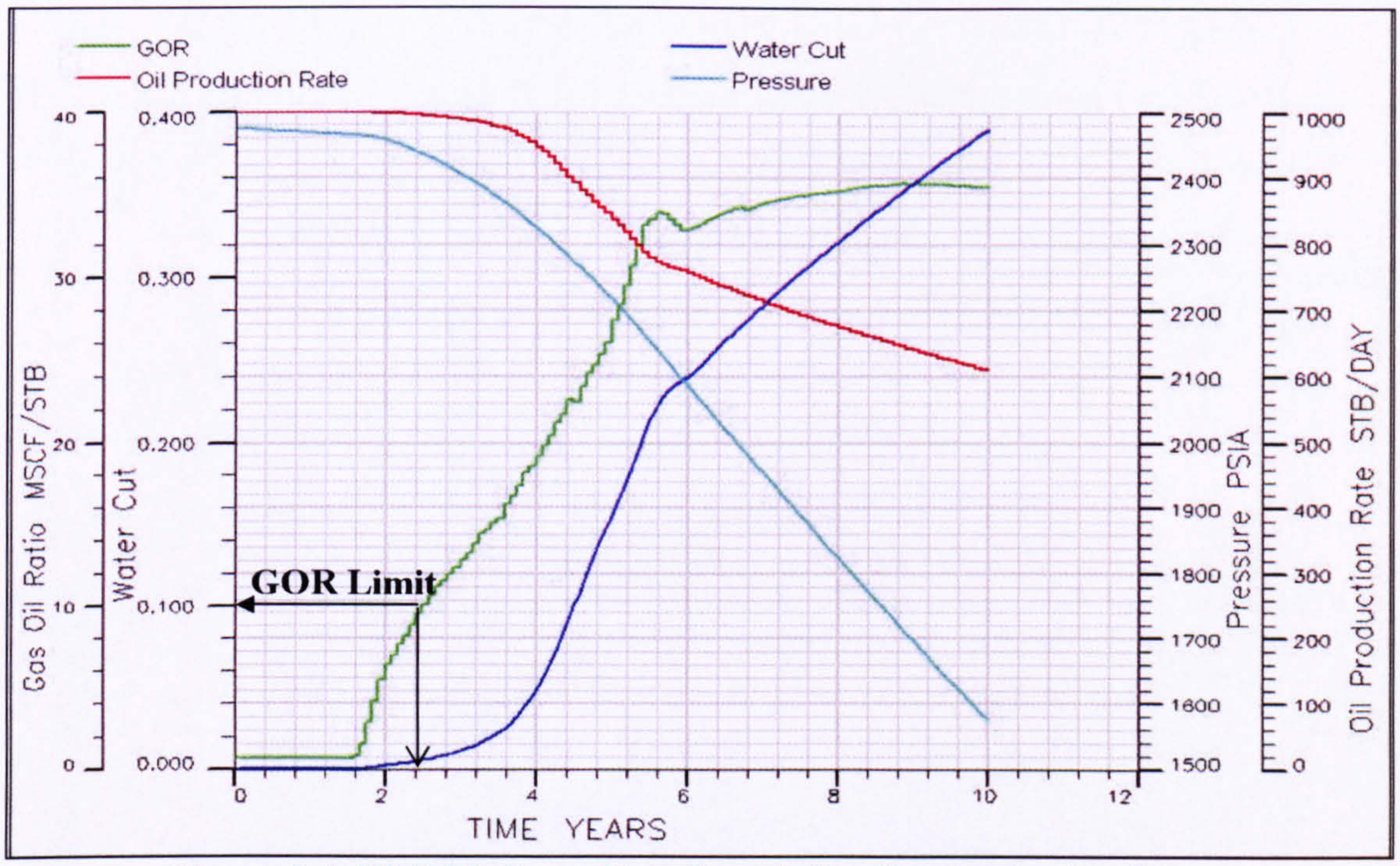

Figure 3-4. Well B1 Open-Hole Completion Production Profile

3.4 Scope and Studied Cases:

The objective of this study is to investigate the impact of utilizing the downhole inflow control valves (ICVs) on the performance of these horizontal wells and to quantify any increase in recovery achieved by controlling the production from various sections of the horizontal well. The following factors controlling the intelligent well performance were investigated:

1. ICV arrangement within the wellbore.
2. Reservoir permeability distribution.
3. ICV choking policies.
4. Well-Standoff from the oil-water contact.

The benefit of using intelligent wells was evaluated by comparing the following cases:

a) **Conventional Case:** An Openhole Completion (Figure 3-5a)

b) **Base Case:** Intelligent well (I-Well) completion without ICV control. The ICV remains fully open at all times with a flow diameter similar to or greater than the tubing area (Figure 3-5b).

c) **I-Well Case:** I-Well completion with ICV Control (Figure 3-5c).

d) **Multilateral Well Case**

The Base Case captures the effect on the oil recovery of an ICV-style completion with its increased pressure drop along the wellbore. Previous studies [3.8] showed that the installation of such a completion (tubing, valves, etc) compared to a conventional openhole completion may effect the well's recovery either positively or negatively.

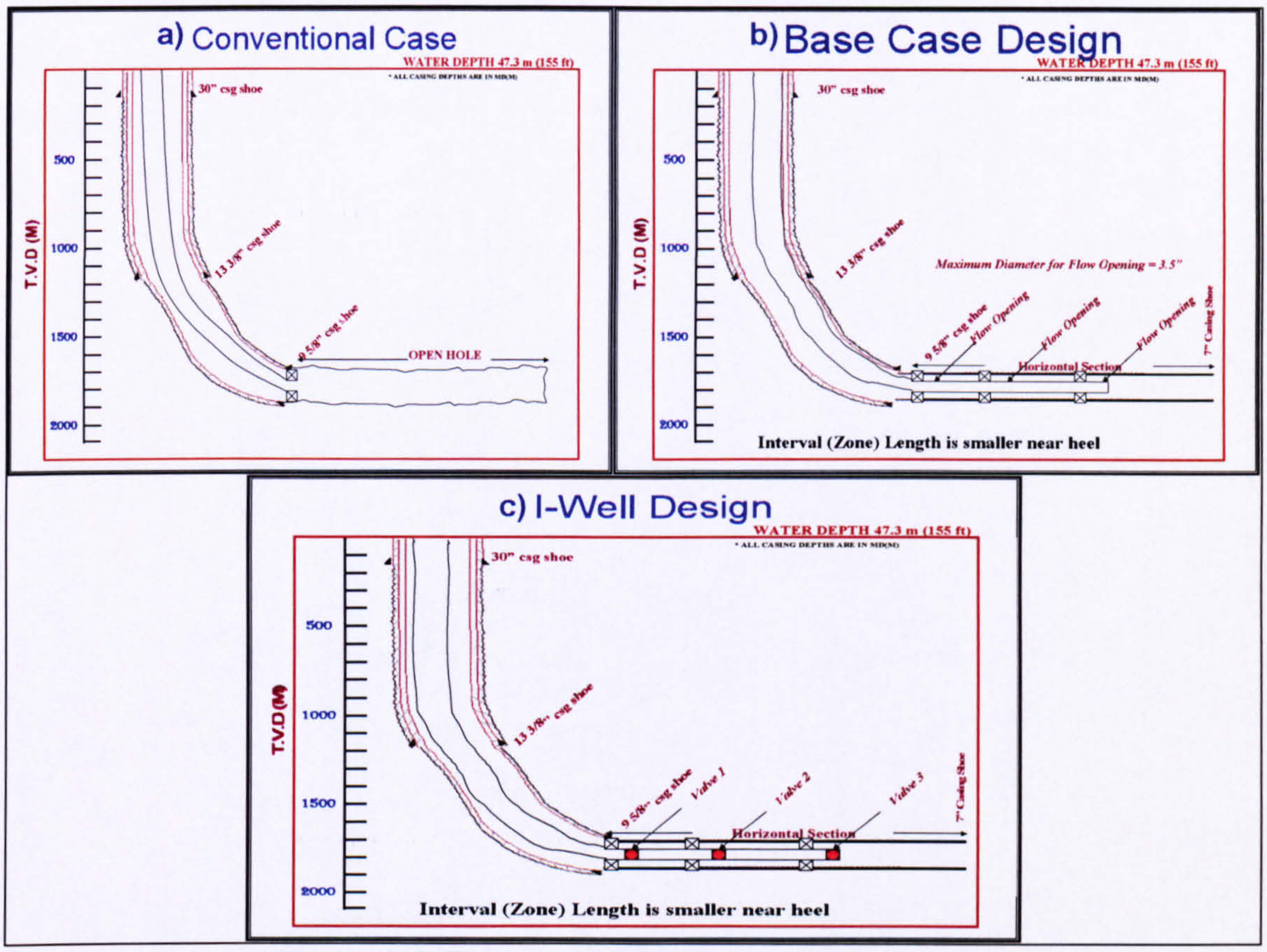

Figure 3-5. Horizontal Well Cases Schematics

3.4.1 Intelligent Well Design:

The intelligent wells were completed with a 3.5" tubing inside a 7" casing. The well was divided into three production interval with the smallest interval near the toe and progressively larger intervals toward the heel (Figure 3-5c). This arrangement is designed to deliver the greatest control near the heel of the well. This is required since the largest drawdown, and hence the greatest coning potential, will occur at the heel.

The intelligent completion was modelled with a 10 position ICV (Table 3-2) using the multi-segment well option of the Eclipse^{TM} reservoir simulator [3.7].

Table 3-2. ICV Positions

Position	0	1	2	3	4	5	6	7	8	9	10
Equivalent pipe flow area (in^2)	0	0.055	0.11	0.215	0.319	0.472	0.626	0.856	1.163	1.776	8.073

3.5 Well A1:

The well production was not affected by any of the constraints during the 10 year production period studied. The conventional (openhole) completion shows an exponential increase in the water cut (Figure 3-2). A water control strategy of continuous choking of that region of the completion that produces water was developed. This strategy required monitoring of the WC at both the well and the ICV level (Figure 3-6).

The opening of the ICV was reduced by one step when the well's, or any of the ICV's, WC values exceeded the current limit. The resulting improved tubing performance due to the consequent reduction in water production leads to an increased oil production rate (Table 3-3).

Table 3-3. A1 I-Well Results

Case	Total Oil Production (10^3 STB)	Increase in Production Compared to Conventional Case
I-Well	3,613	+ 2.3%
Base Case	3,572	+ 1.2%
Conventional Case	3,533	-

The effect of the ICV control policy can be observed on the well's WC profile after 2 years (Figure 3-7 and Figure 3-8). There is a high water production from the heel and the toe for the first two years of producing well's life. The ICV action slowly stabilizes the water production from all the zones for the third and later years.

The I-well control no longer achieves the greatest oil recovery if the well is produced at a higher target flow rates (Table 3-4). This comes about because "excessive" choking while attempting to control water production; the well's production then being constrained by the BHP limit reduces the well inflow performance.

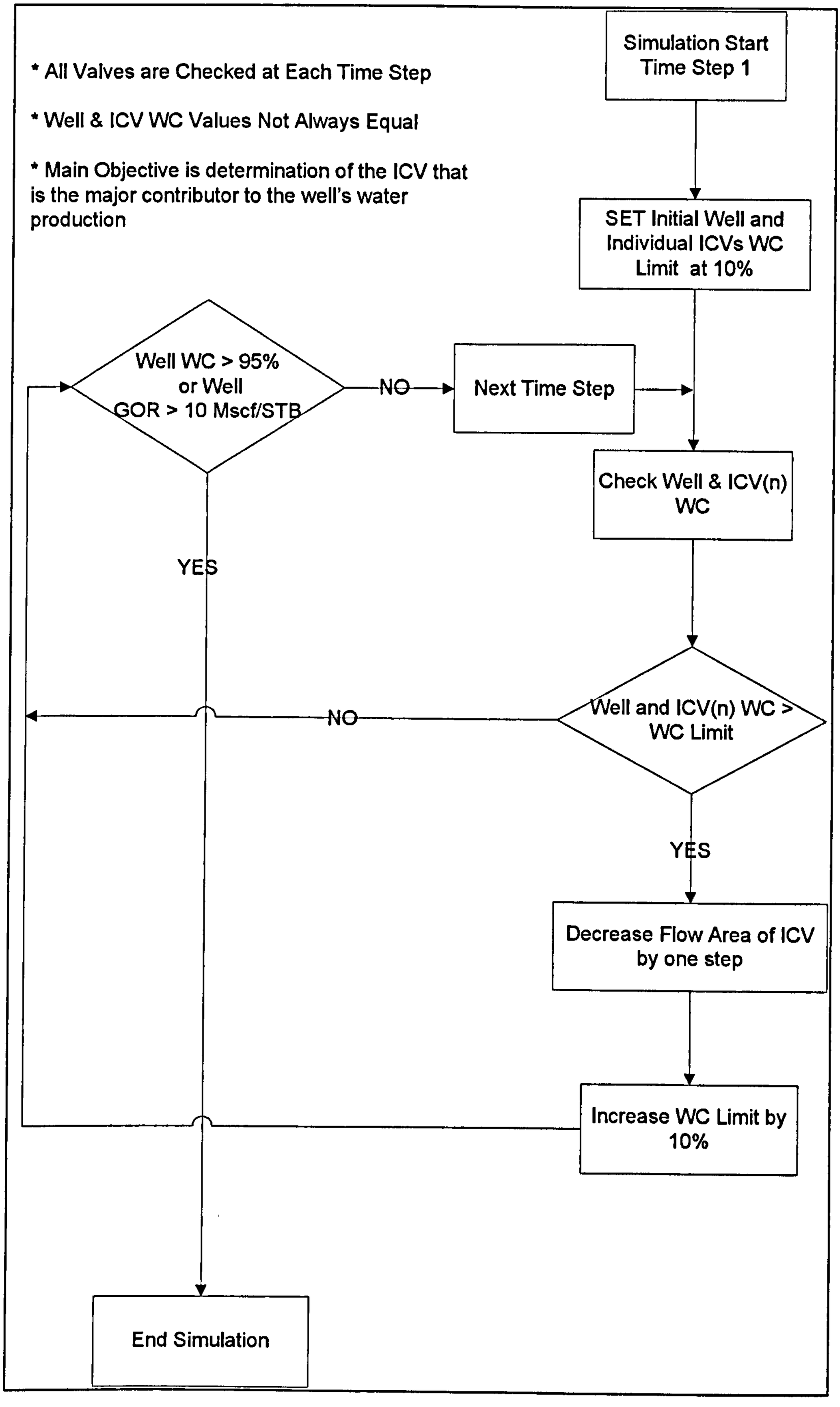

Figure 3-6. Well A1 Choking Strategy Flow Chart (WC Control)

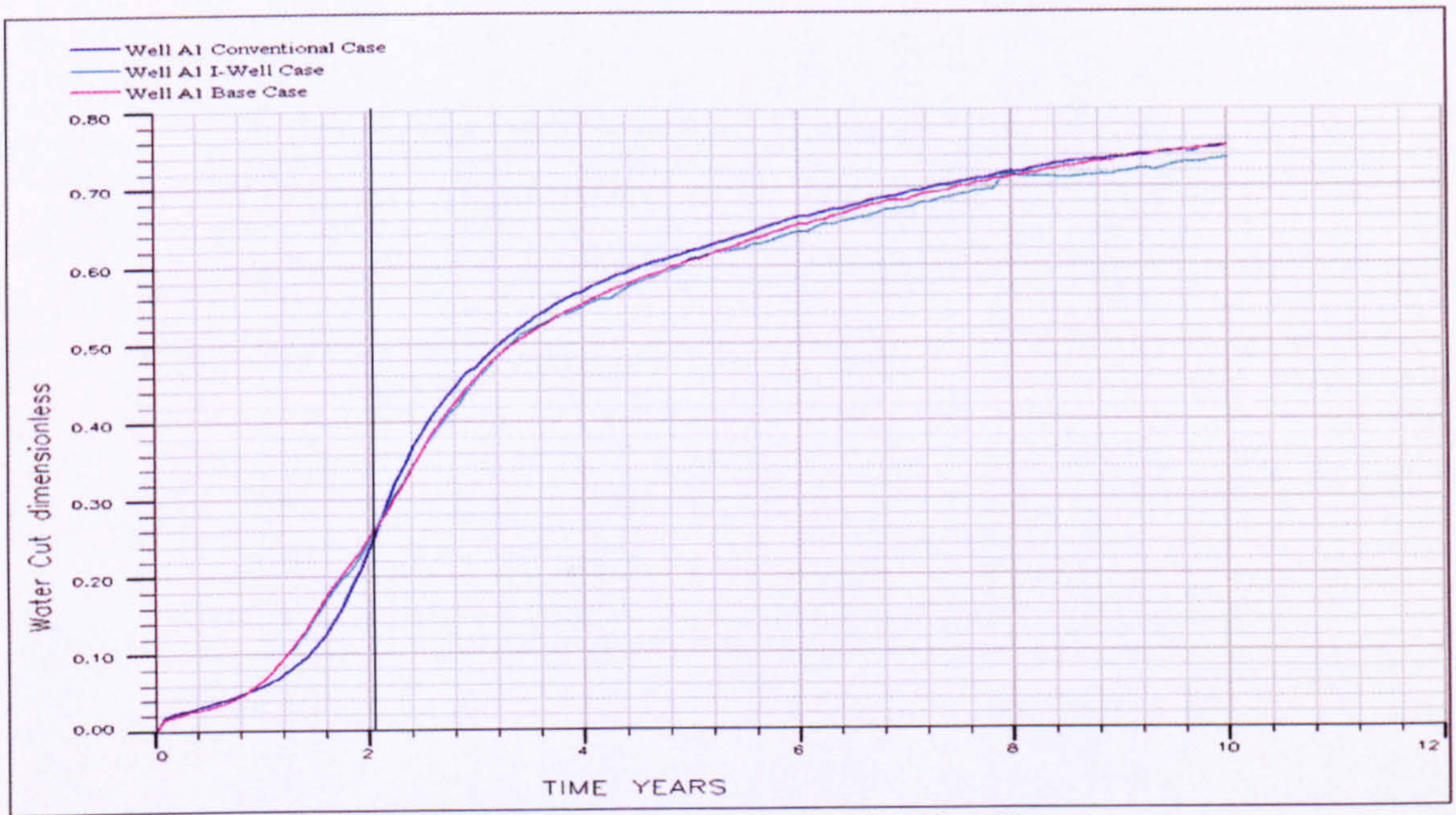

Figure 3-7. A1 I-Well Water Cut Profile

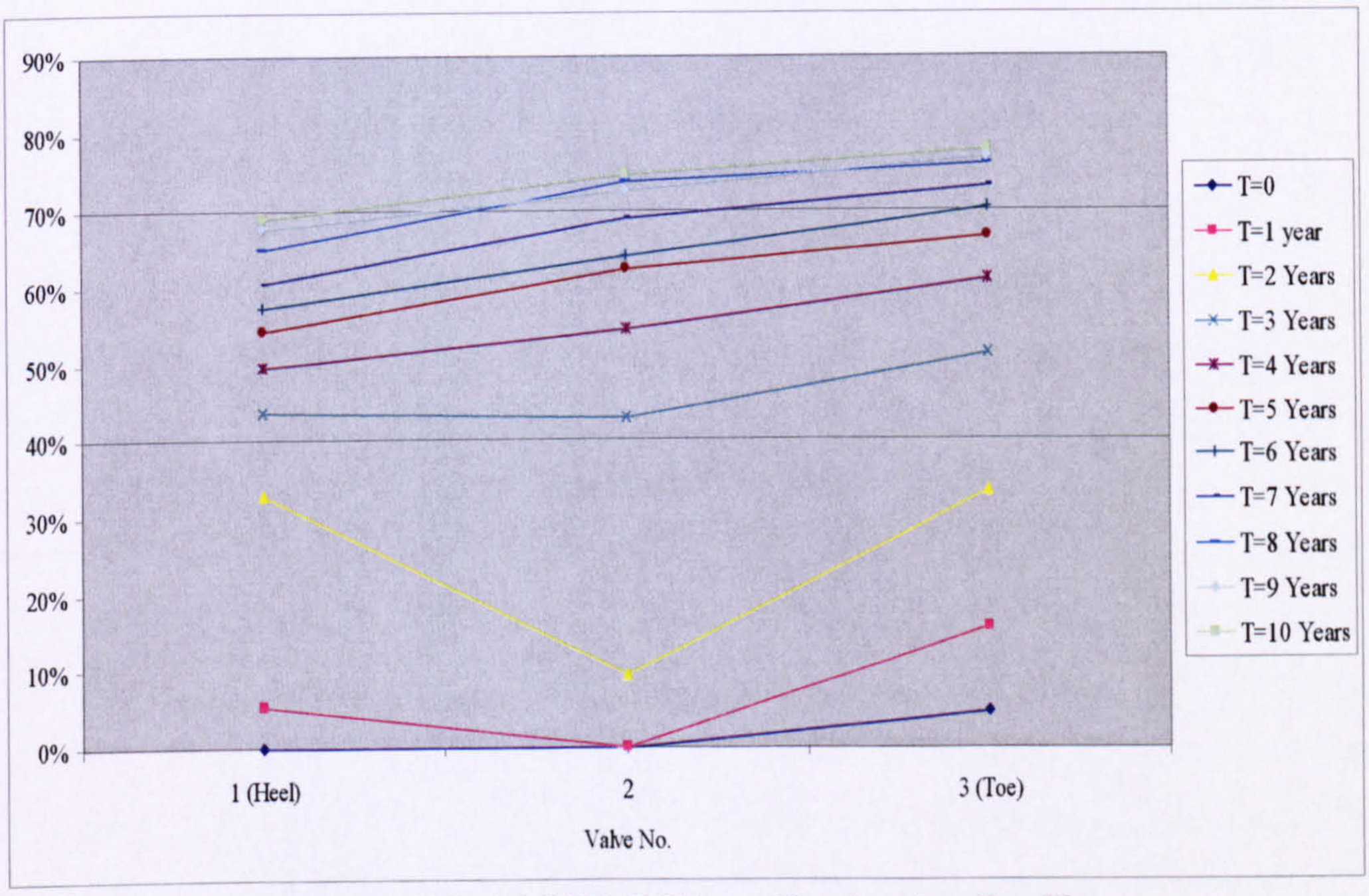

Figure 3-8. A1 I-Well Water Production Profile

Table 3-4. Well A1 Production Rate Sensitivity

Maximum Liquid Production Rate (STB/D)	Case	Total Oil Production (10^3 STB)	Increase in Production Compared to Conventional Case
2,000	Conventional Case	3,533	-
	Base Case	3,572	+ 1.1%
	I-Well	3,613	+ 2.3%
4,000	Conventional Case	4,358	-
	Base Case	4,555	+ 4.5%
	I-Well	4,484	+ 2.9%
6,000	Conventional Case	4,936	-
	Base Case	5,237	+ 6.1%
	I-Well	4,661	- 5.6%
9,000	Conventional Case	5,086	-
	Base Case	5,441	+ 7.0%
	I-Well	4,711	- 7.4%

3.5.1 Effect of I-Well Control on Drawdown Profile:

The use of ICVs to control the inflow from a horizontal well has long been promoted as a means to maintain the well inflow profile by encouraging flow from the "lower drawdown" part of the well (normally found at the well's toe). Conventional wells similar to A1 are normally produced at a flow rate that provides the maximum total oil recovery for the forecast field life. Production at higher flow rates will cause a decrease in the well life, decreasing the field's economical viability. The initial, liquid production rates used in this study (Table 3-1) causes a relatively uniform drawdown profile to develop along the wellbore. Obtaining a uniform pressure drawdown profile is easily achieved for single-phase production, where the control strategy can be focused on balancing production from the different completion zones, rather than controlling the influx of undesirable fluids (gas or water).

The ability of the A1 I-well to provide a uniform drawdown from the heel to the toe was tested by increasing the flow rate to 10,000 BLPD using the previously described water control strategy. The resulting drawdown profile along the wellbore (Figure 3-9) shows that the difference in drawdown between the heel and the toe is higher (29 psi) for the I-Well case than for the base case (9 psi). This came about because the control strategy was based on controlling the water production at the well and valve level. The toe of the well is the first region to show an increased water flow rate (Figure 3-10). Maintaining the target liquid production rate requires an increased drawdown to compensate for the

lost production from the toe of the well once the ICV acts to choke the toe zone. I.e. controlling the well by a target liquid rate will result in a higher drawdown for the last choked zone. This action may maintain the liquid rate, but will simultaneously be promoting a non-uniform pressure drawdown profile.

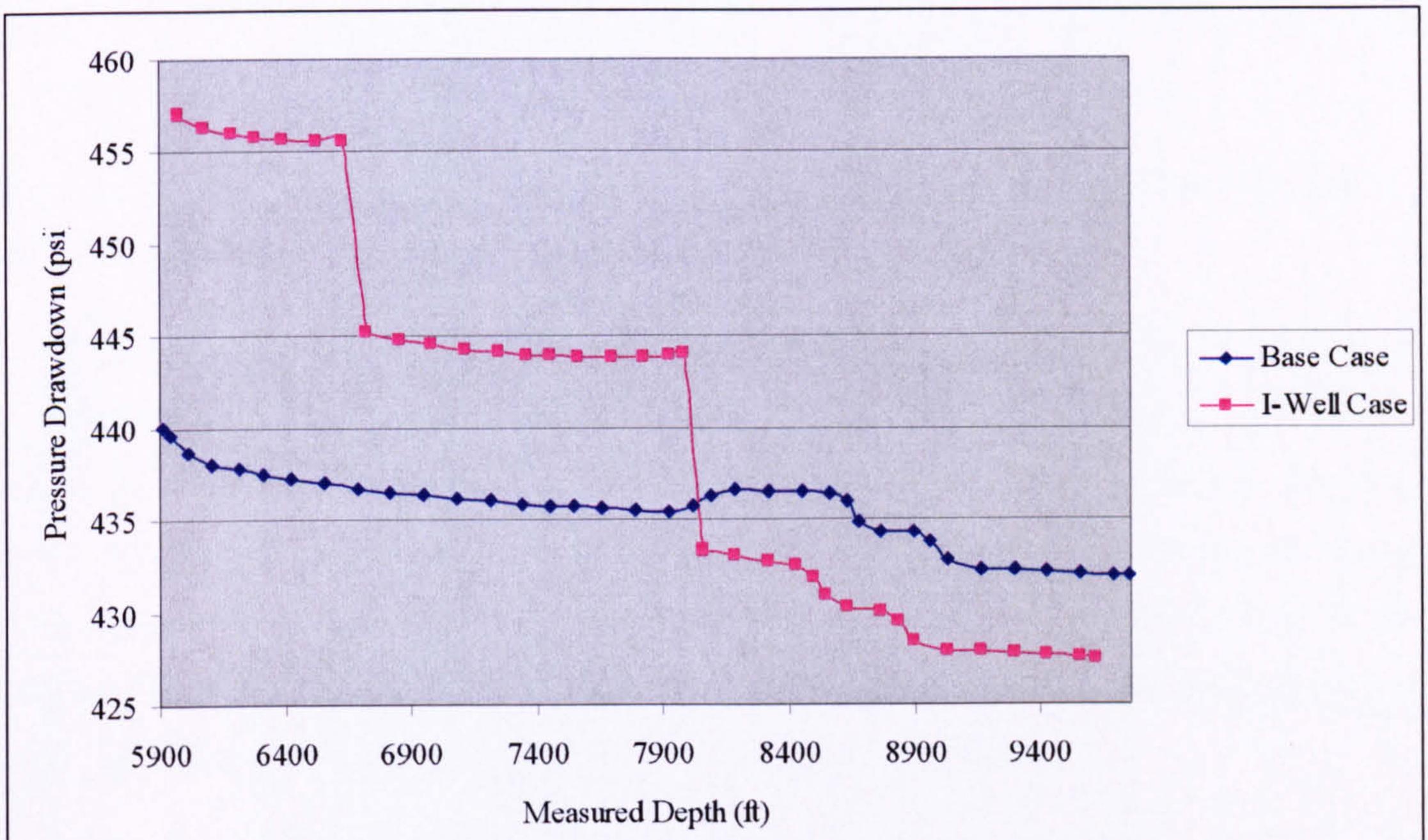

Figure 3-9. Well A1 Base Case vs. I-Well Case (Q=10,000 BLPD) Drawdown Profile

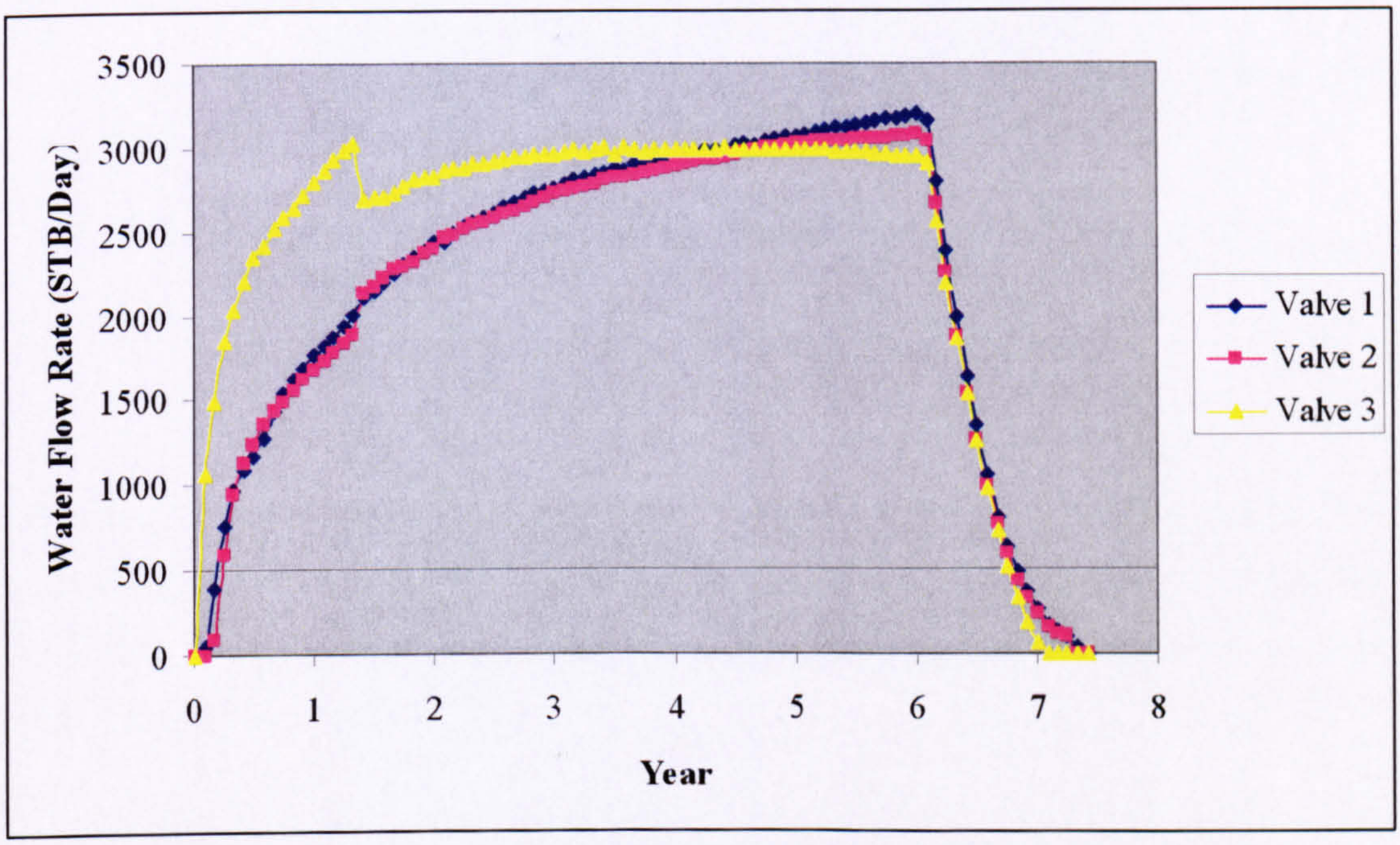

Figure 3-10. A1 I-Well (q=10,000 BLPD) Valves Water Flow Rate

There was a 4% increase in the total oil production over the 10 year period despite the drawdown profile across the well being less uniform for the I-Well case. The algorithm (Figure 3-6) successfully equalized and controlled the water production from each zone.

The optimum ICV control strategy is case specific. Continuous choking was applicable in this case because the homogeneous permeability profile and the exponentially increasing breakthrough of water in all sections of the wellbore (Figure 3-2 and Figure 3-3). An alternative strategy that is widely used in field operations is to always keep at least one ICV fully open and use the other ICVs to adjust the pressure balance along the wellbore while managing the total well target rate with a wellhead choke.

3.5.2 Impact of Horizontal Well Design considerations on the A1 Well Multilateral Well Design:

Multilateral wells were first conceived in the 1920s, though drilling of the world's first multilateral well in Russia had to wait until 1953 [3.9]. High drilling costs prevented the idea from maturing at that time. The advances in drilling technology in the last 20 years have allowed the cost-effective construction of complex wells. Multilateral and long horizontal wells have found widespread application, with some 5,000 wells/year being drilled. These wells have proved capable of economically developing marginal reservoirs against a background of high oil demand and oil prices.

Multilateral wells have proved to be beneficial in many field situations [3.10, 3.11]:

1. Fewer wells are required for field development.
2. Reduced environmental impact (reduced well numbers, less drill cuttings and mud disposal).
3. Increased well exposure to the reservoir (drainage area).
4. Greater flowing bottom hole pressure for a given liquid rate.
5. Accelerated hydrocarbon production.

The base case horizontal well design for the A1 well was re-visited to ensure an optimum design. Parameters that affect production from thin oil column reservoirs are the standoff from the fluid contacts, the length of the horizontal section and the diameter of the completion [3.12].

Well A1 was originally placed in the middle of the 79 ft (average) oil column. The column thickens to around 90 ft near the heel where a localized gas zone, separated from the main gas cap by a permeability barrier, is present. A sensitivity study on the well stand-off showed that placing the well at the top of the oil column, a few feet below this permeability barrier results in a 30% increase in the total oil production

compared to the base case due to reduced water production. Inflow profile analysis showed that the toe section of the horizontal section produced water immediately after the well was placed on production. Water production from the remainder of the completion did not occur until after one year's production. A reduced horizontal section length of 1,500 ft delivered an additional 2.6% oil production (Figure 3-11).

The above considerations form the platform for the three, multilateral A1 well designs that were tested (Figure 3-12). Optimizing the multilateral well type, location within the field and trajectory is a time consuming process due to the many possible choices of the number of laterals, their arrangements as well as their trajectories. The Dual Opposed Lateral (DOL) design (Figure 3-13) with a total lateral length of 6,221 ft produced the highest total oil production of all the A1 well designs considered.

Yeten et. al. suggested the application of genetic algorithms to generate an optimum design for non-conventional wells [3.13]. Testing of further options could well have further increased the oil production for the A1 Well.

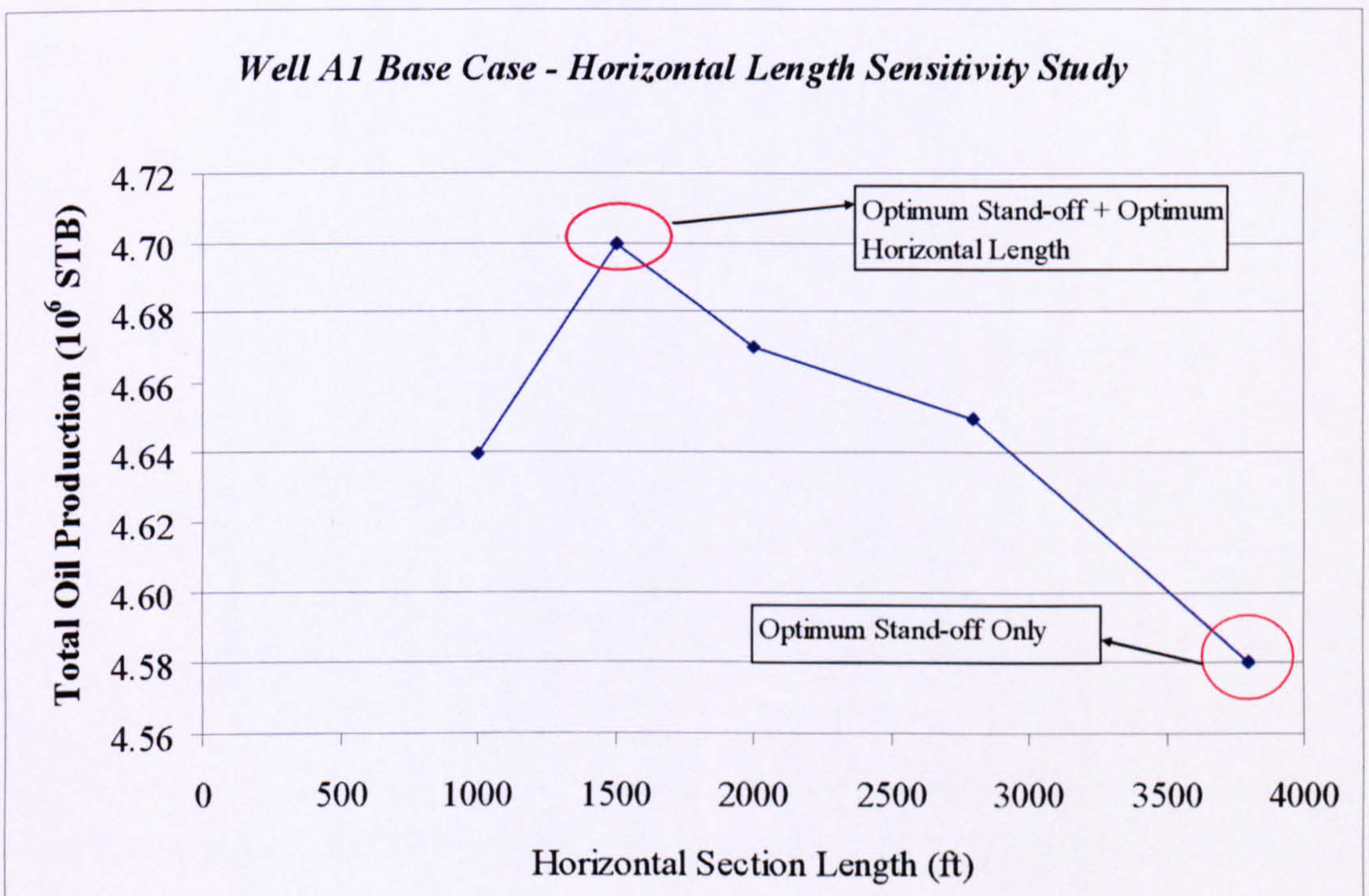

Figure 3-11. The Optimum Horizontal Length for Well A1 is 1500 ft

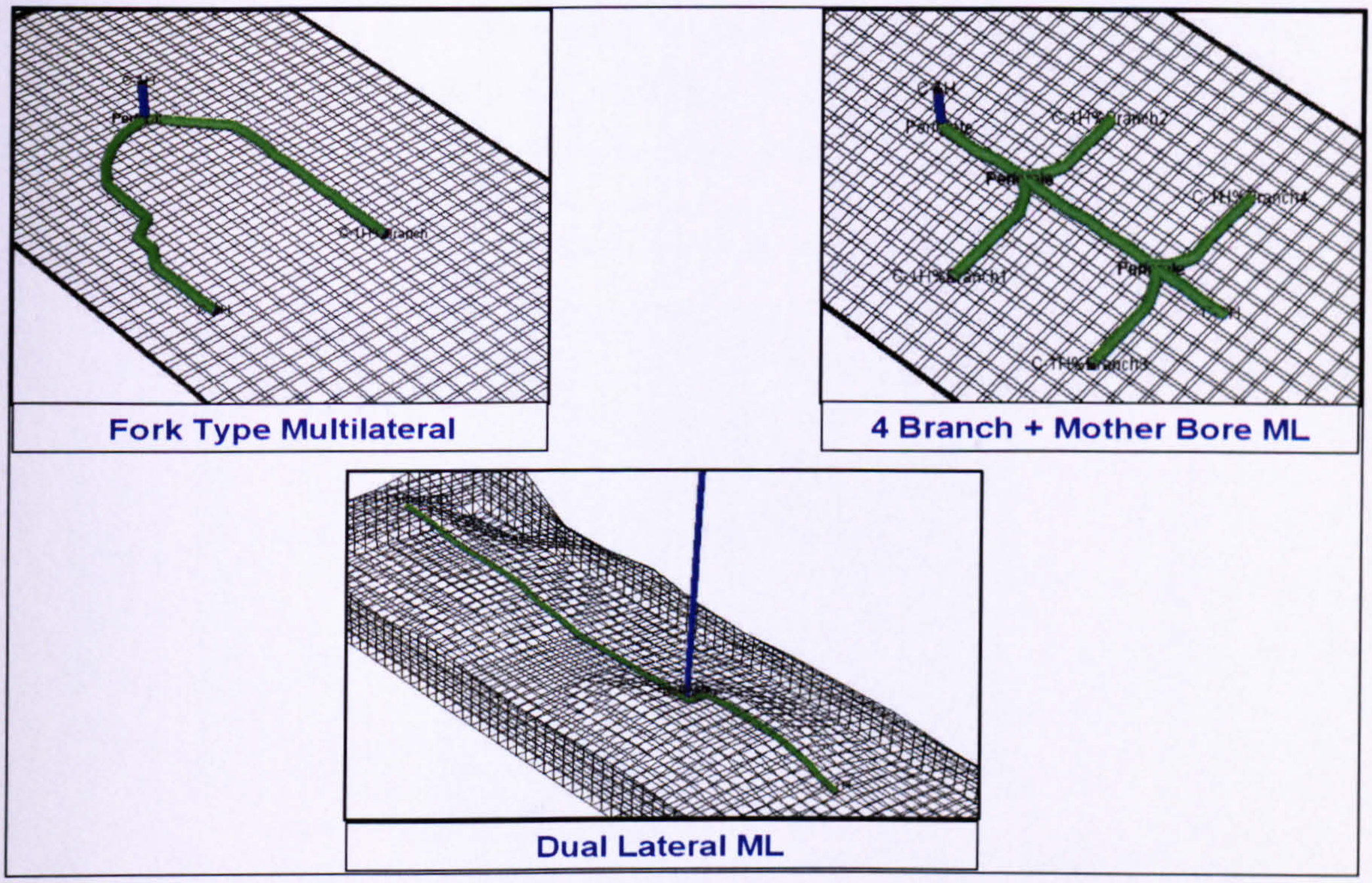

Figure 3-12. Well A1 Multilateral Well Designs Tested

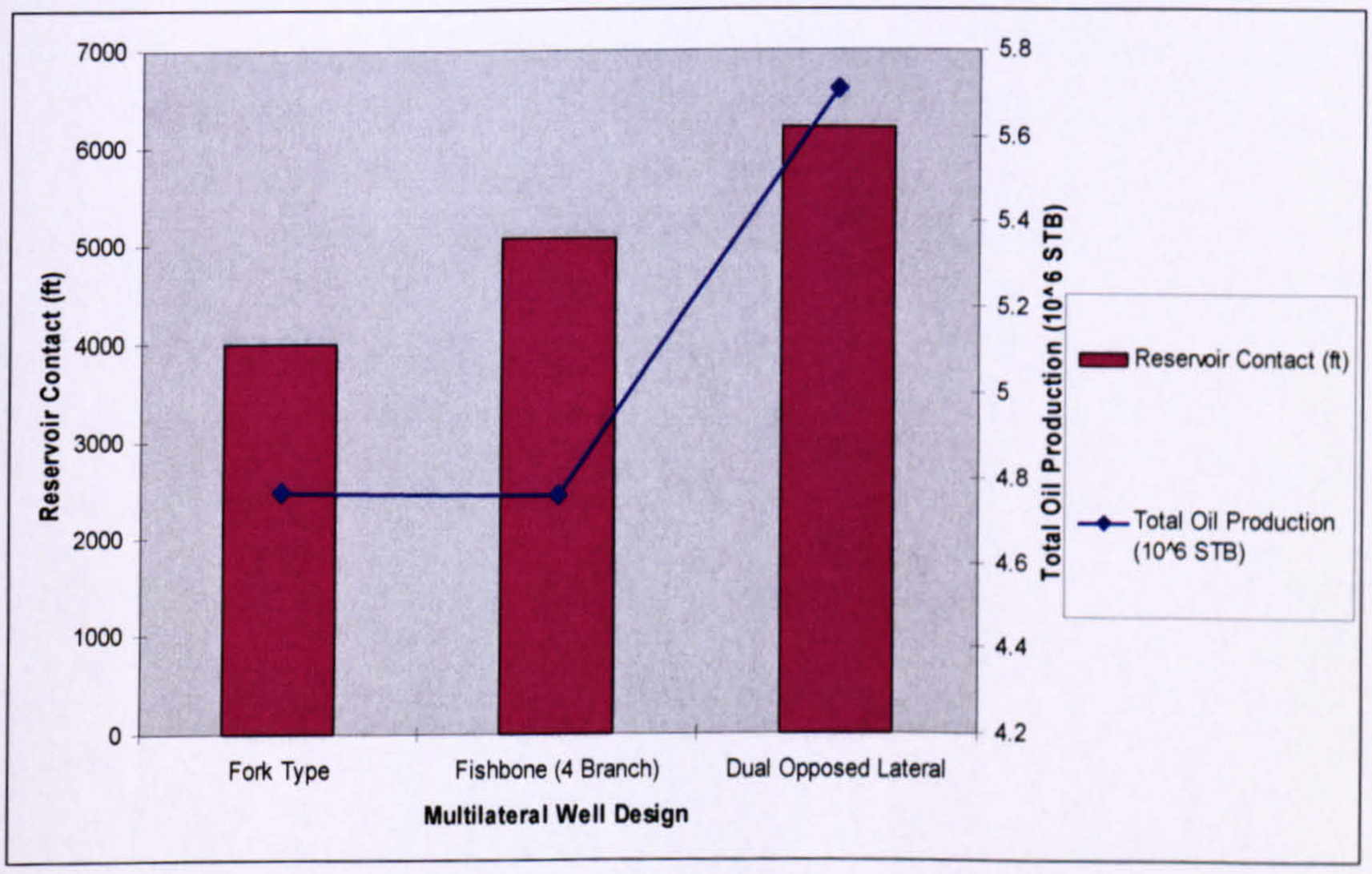

Figure 3-13. Total Oil Production for Various Well A1 Multilateral Designs

3.5.3 Well A1 Multilateral Production Rate Sensitivity:

The A1 well with the DOL design required a smaller drawdown than the horizontal single lateral well when delivering the target production rate. The multilateral A1 well thus experienced delayed and less extensive water production (Figure 3-14). This provided the opportunity to increase the target rate, not only accelerating the production

but also increasing the total oil produced (Figure 3-15). The benefit of the advanced well design is best illustrated by examining the economic value of production acceleration using the economic assumptions summarised in Table 3-5.

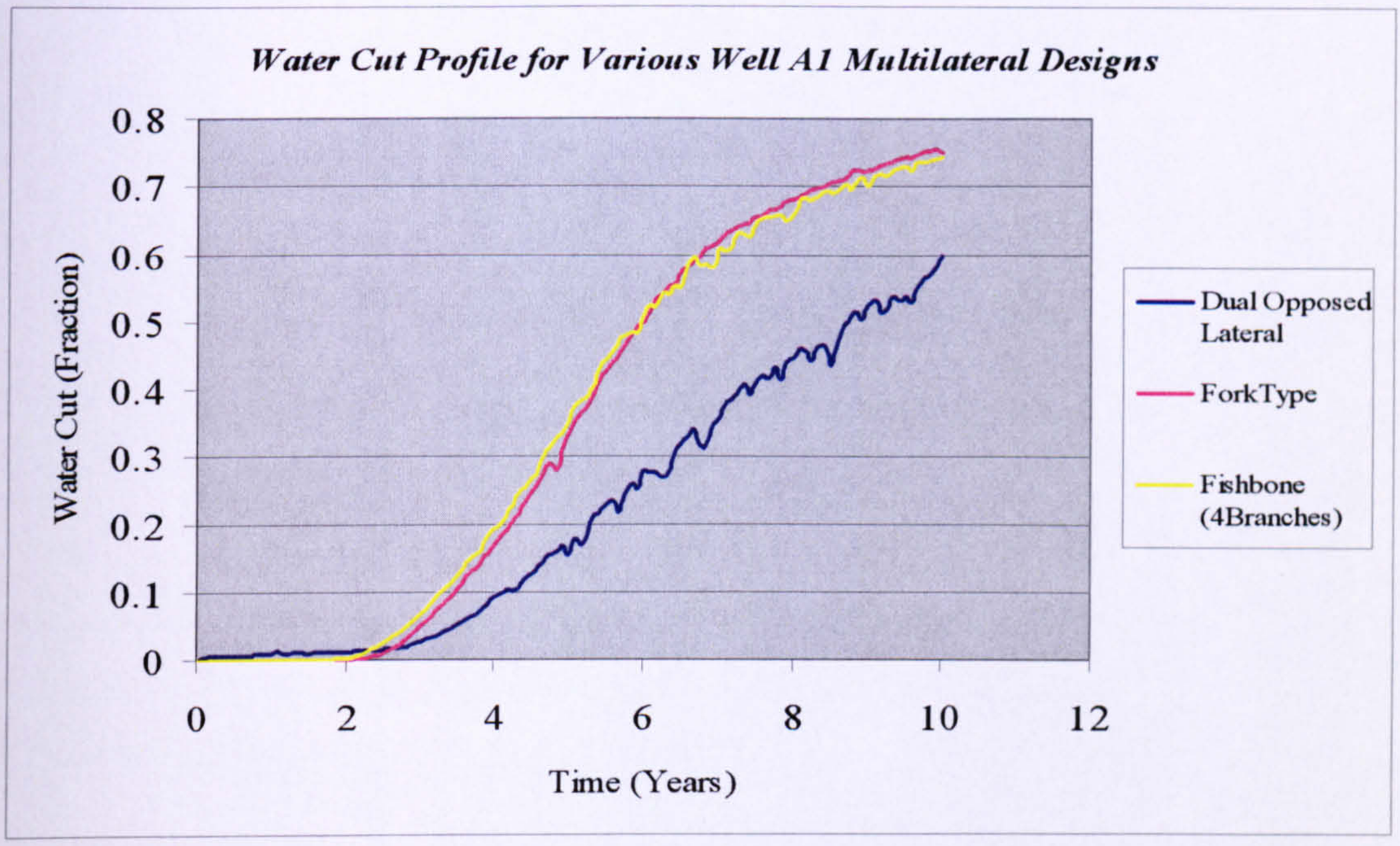

Figure 3-14. Water Cut Profile for Various Well A1 Multilateral Designs

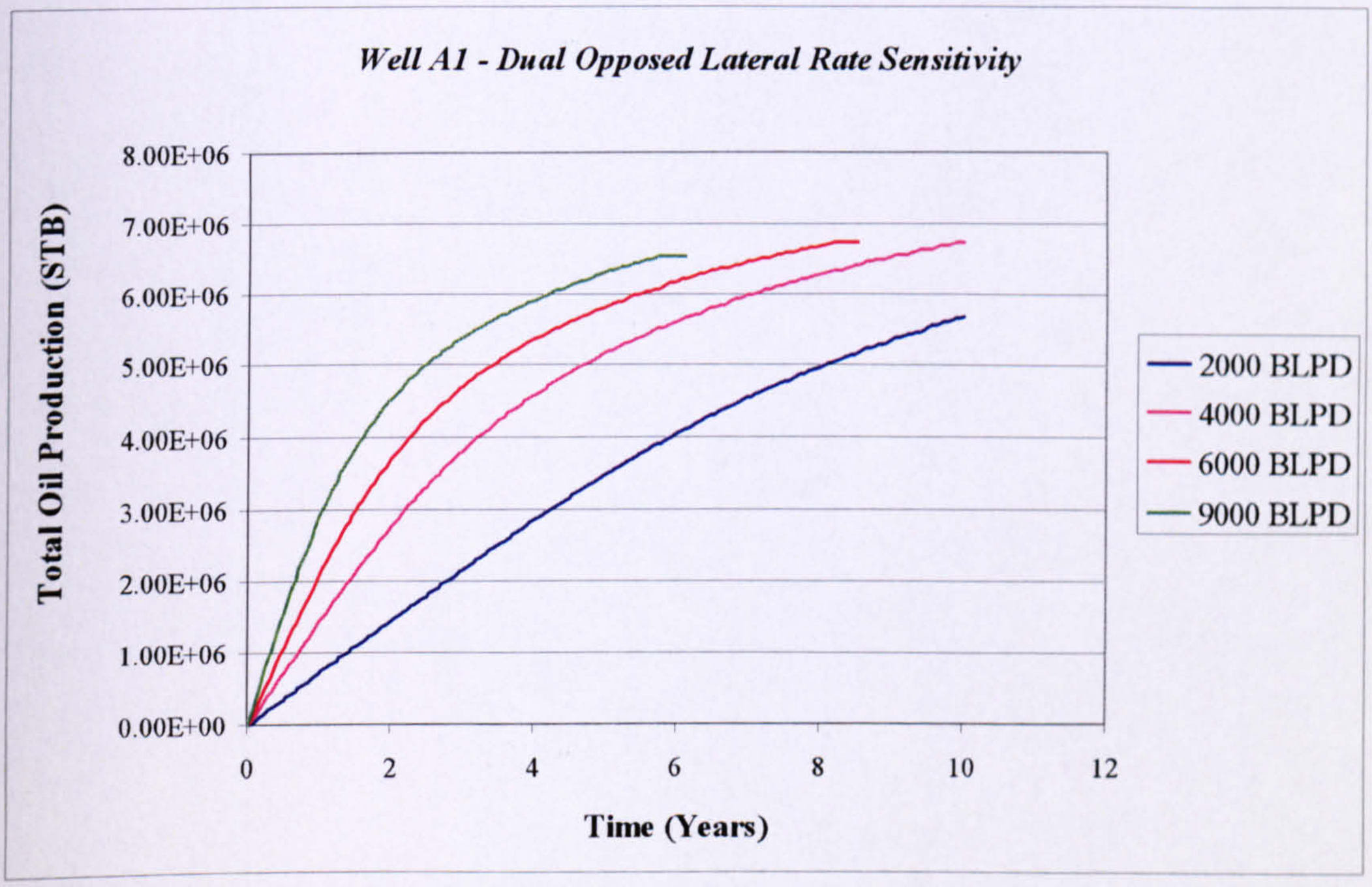

Figure 3-15. Sensitivity Total Oil Production to the A1 Well's Production Rate

Table 3-5. Economic Evaluation Assumptions

Parameter	Value
Inflation Rate	3%
Discount Rate	10%
Oil Price($/bbl)	18.00
Gas Price (US $2003 / 10^3cf)	0.00
OPEX	
Lifting Costs (US $/bbl)	0.50
Oil Processing Costs (US $/bbl)	1.70
Water Processing Costs (US $/bbl)	0.25
Gas Processing Costs (US $/$10^3$cf)	0.5
CAPEX	
CAPEX - Initial Well Costs (US $)	$4*10^6$
Multilateral CAPEX	+ 15%
I-Well CAPEX	+ 30%

Table 3-6 shows that an increased value of US$ $10x10^6$ resulted from the DOL multilateral well design; while tripling the rate from 2,000 BLPD to 6,000 BLPD delivered a further US$ $27.5x10^6$. Further increases in the production rate were not successful due to excessive pressure depletion of the reservoir pressure (Figure 3-16).

Table 3-6. NPV calculations for Well A1 Multilateral Well Rate Sensitivity

Well Design	Total Oil Production (10^6 STB)	Total Oil Production Discounted @10%/yr (10^6 STB)	NPV (US 10^6)
Base Case (Middle of Oil Column)	3.53	2.57	40.5
Optimised Horizontal Well (2,000 BLPD)	4.70	3.37	55.9
Dual Opposed Lateral (2,000 BLPD)	5.71	3.90	66.2
Dual Opposed Lateral (4,000 BLPD)	6.76	5.09	81.7
Dual Opposed Lateral (6,000 BLPD)	6.76	5.46	83.6
Dual Opposed Lateral (9,000 BLPD)	6.55	5.64	82.7

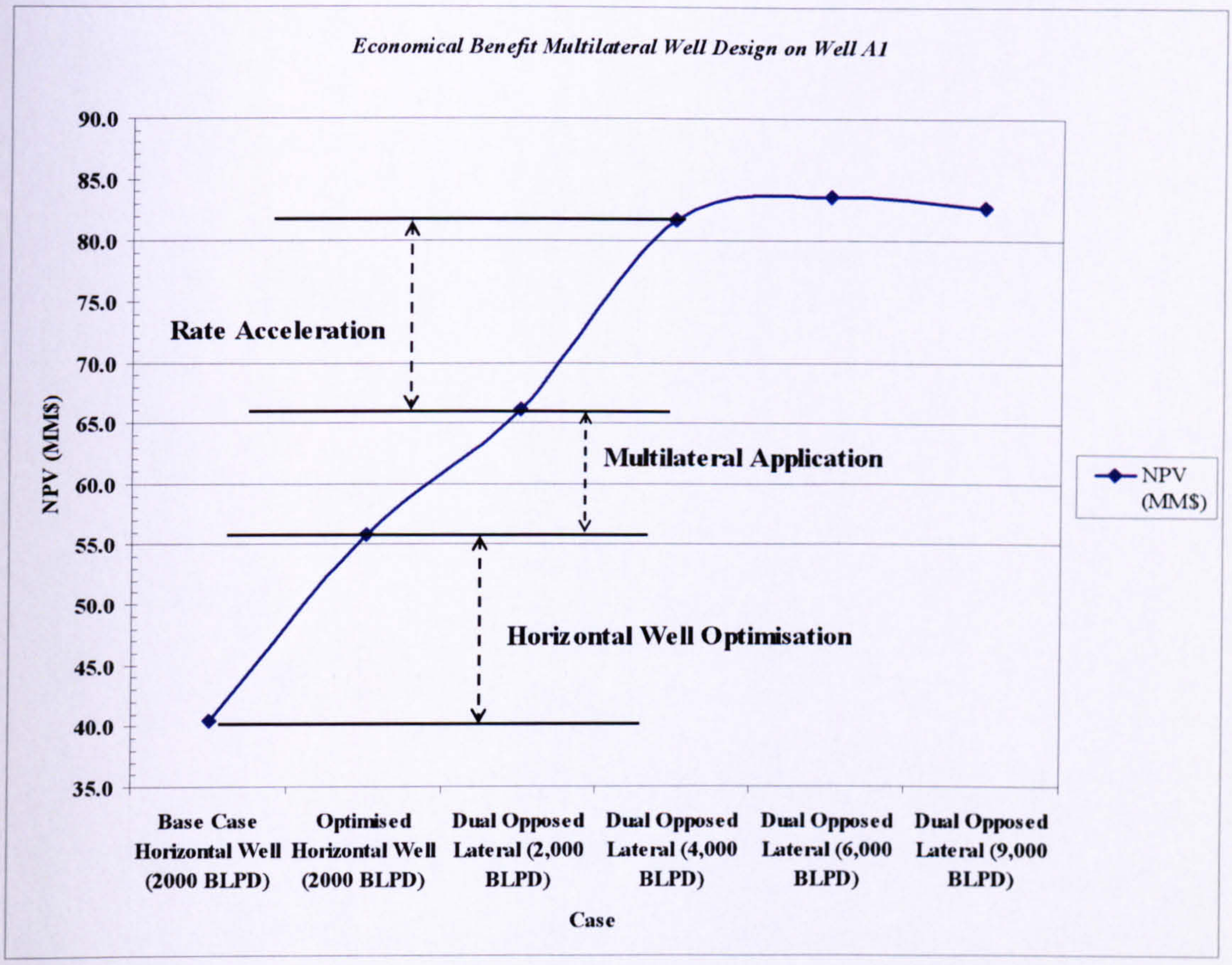

Figure 3-16. Economic Analysis for Well A1 Horizontal and Multilateral Options

3.6 Well A2:

The simultaneous increase in both the WC and GOR in this well presents a more difficult challenge for the development of an ICV choking policy. The choking strategy chosen was GOR management - the ICV being closed by one position when the valve GOR increases beyond a designated limit.

Figure 3-17 shows the GOR profile for well A2. The ICV control actions can clearly be seen by the reductions in the produced gas. An increase of 1.9% in the oil recovery was achieved along with a decrease of 2.9% in the water production. An increase of the target liquid production rate greater than the 3,000 BLPD used here results in a decrease in the total oil production.

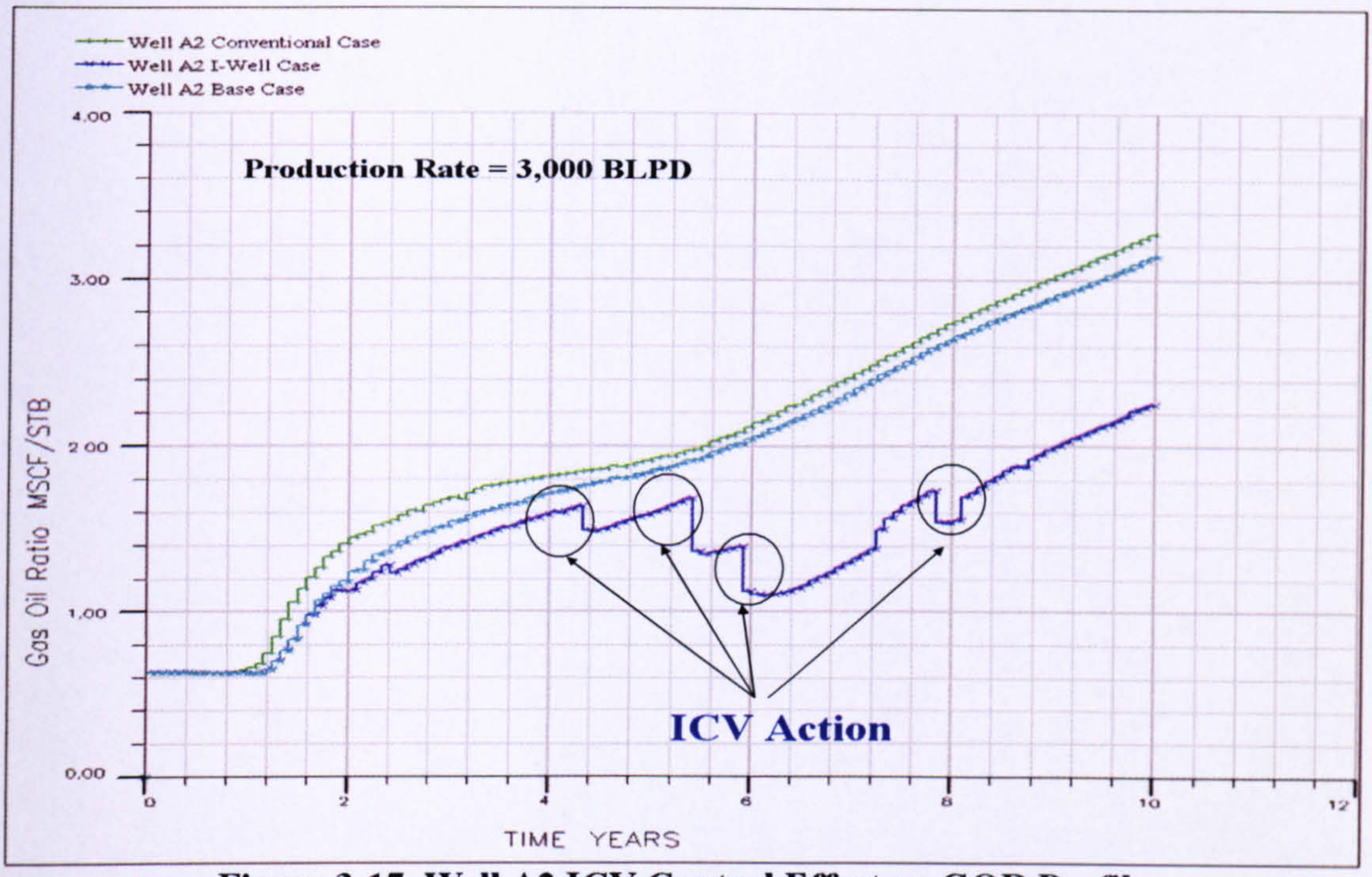

Figure 3-17. Well A2 ICV Control Effect on GOR Profile

3.6.1 Presence of High Permeability Zone:

Close analysis of the well inflow profile shows a high gas production interval in the mid-section of the well (controlled by valve No. 2). The high permeability streak had little effect on the base case well's production (Table 3-7). However, in general the need to control gas production from high permeability streaks is a significant source of value generation when installing I-Wells [3.6]. Such high permeability streaks can often be detected during drilling operations.

Table 3-7. High Gas Production Feature Effect on Well A2 Production

Total Oil Production	I-Well Case (10^3 STB)	Base Case (10^3 STB)	Conventional Case (10^3 STB)
With High Permeability streak	5,757	5,631	5,573
Without High Permeability streak	5,723	5,616	5,568
Difference	- 0.59%	- 0.26%	- 0.08%

3.6.2 ICV Placement Sensitivity:

The standard ICV placement philosophy used in this study is a geometric arrangement of the ICVs. The impact of reversing this strategy and the use of equal zone lengths has been investigated (See Figure 3-18 for a schematic completion diagrams). Table 3-8 shows that the inverse arrangement has a very slightly reduced recovery.

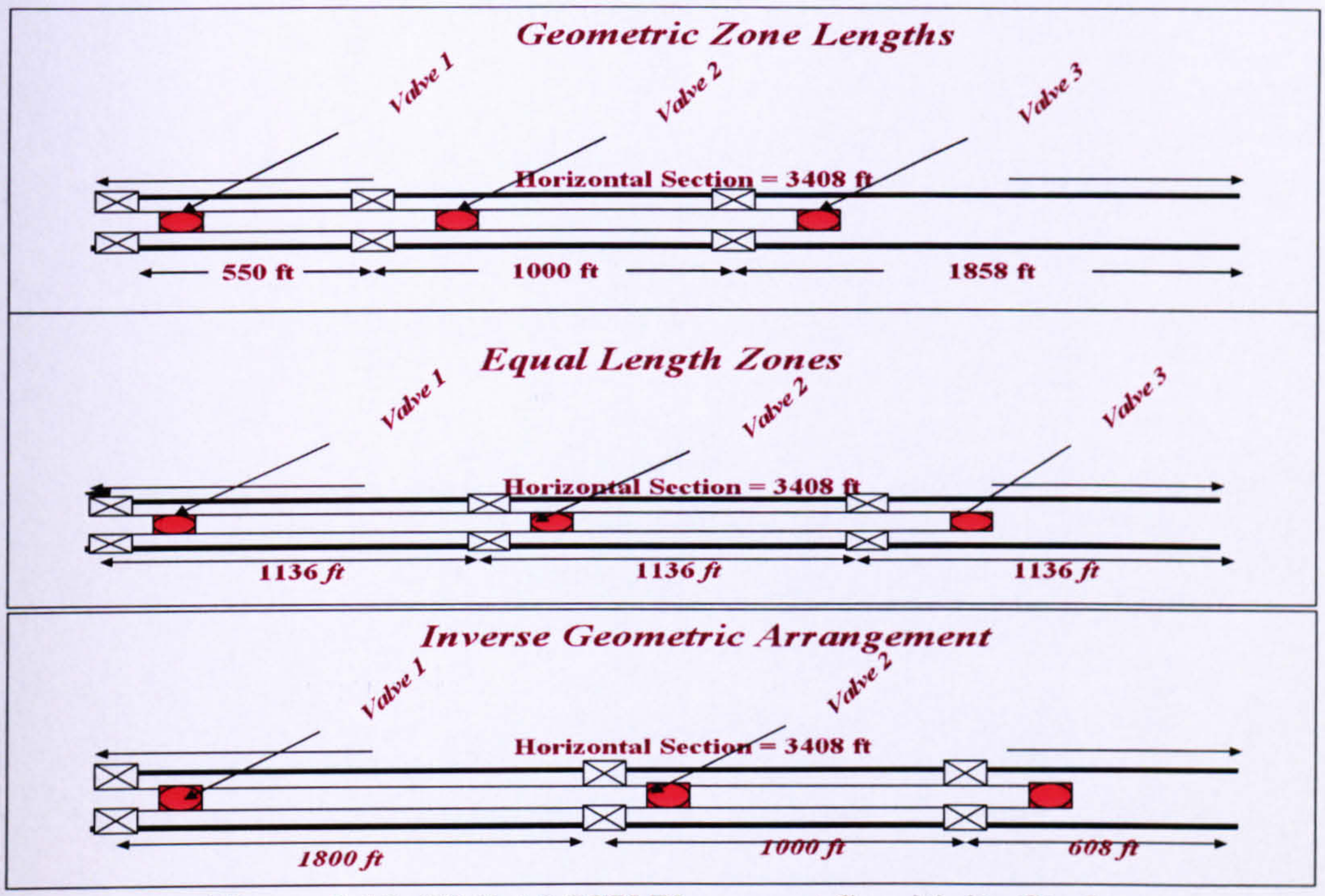

Figure 3-18. Well A2 ICV Placement Sensitivity Study

Table 3-8. Well A2 ICV Placement Sensitivity Study

	Total Oil Production (10^6 STB)		
ICV Placement	No Control	Control	Increase
Inverse Geometric	5.589	5.568	- 0.38%
Equal	5.622	5.697	+ 1.33%
Geometric	5.616	5.723	+ 1.90%

Table 3-8 shows that the equal zone arrangement provides the highest oil recovery for the "no control" case. The geometric arrangement delivers the greatest oil recovery when ICV control is available. The small differences in the results are attributed to the relatively homogeneous nature of the permeability distribution along the wellbore. However, they do highlight the need to investigate the appropriate zonal length selection when designing an I-well completion.

3.6.3 Water Control vs. Gas Control

GOR control was used to obtain the above results when managing A2 well's production. This well produces both water and gas at high rates, hence it was decided to evaluate whether changing the control strategy to water control could have an effect on the recovery. Two water control strategies were tested:

1. Use both well and valve water cut as a trigger to progressively choking the valve.

2. Progressive choking of the valve based on increase of water cut at the valve level.

The above water control strategies were tested on the *Equal ICV Arrangement* configuration. The best results were obtained with water control being implemented at both the well and the ICV level (reflecting the decreased tubing outflow performance with increasing water cut). However, GOR control provided better results than water control (Table 3-9).

Table 3-9. Water Control vs. GOR Control Effect on Total Oil Production

Well A2 (ICV Equal Arrangement)	Total Oil Production (10^6 STB)	Increase in Total Oil Production Compared to Base Case
Base Case (No Control)	5.622	
I-Well GOR Control	5.697	+1.33%
I-Well Water Control (Case 1)	5.598	-0.42%
I-Well Water Control (Case 2)	5.378	-4.33%

Analysis of the water cut profiles (Figure 3-19) shows that there was limited control on the water production while the GOR fluctuated (Figure 3-20). ICVs proved to be incapable of controlling the water production. The choking action increases the drawdown, resulting in an increased water production. Further, the well productivity index to gas is higher than that for water. The GOR reacted faster than the WC to the ICV choking due to gas's lower viscosity. These factors all lead to a reduced oil recovery.

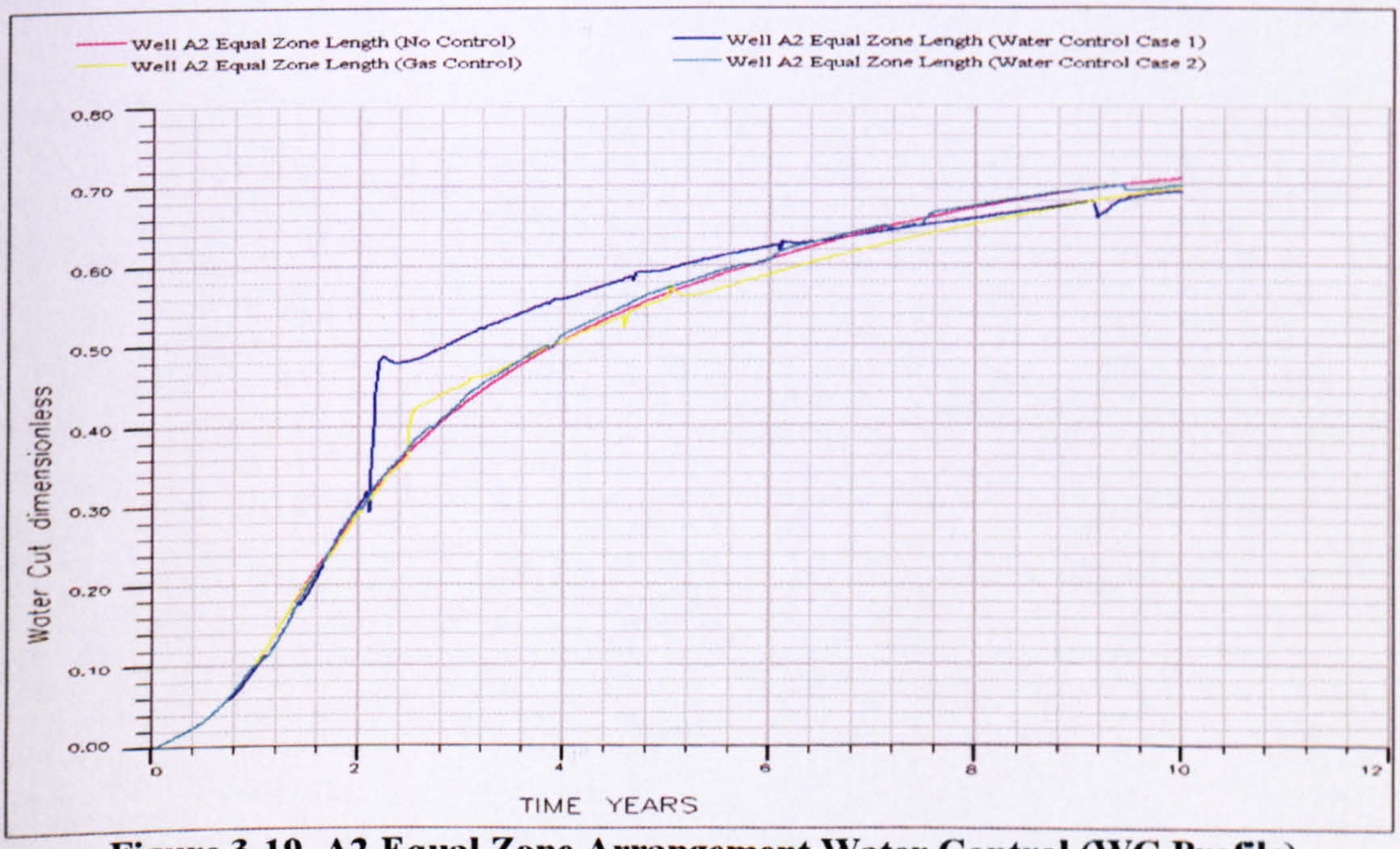

Figure 3-19. A2 Equal Zone Arrangement Water Control (WC Profile)

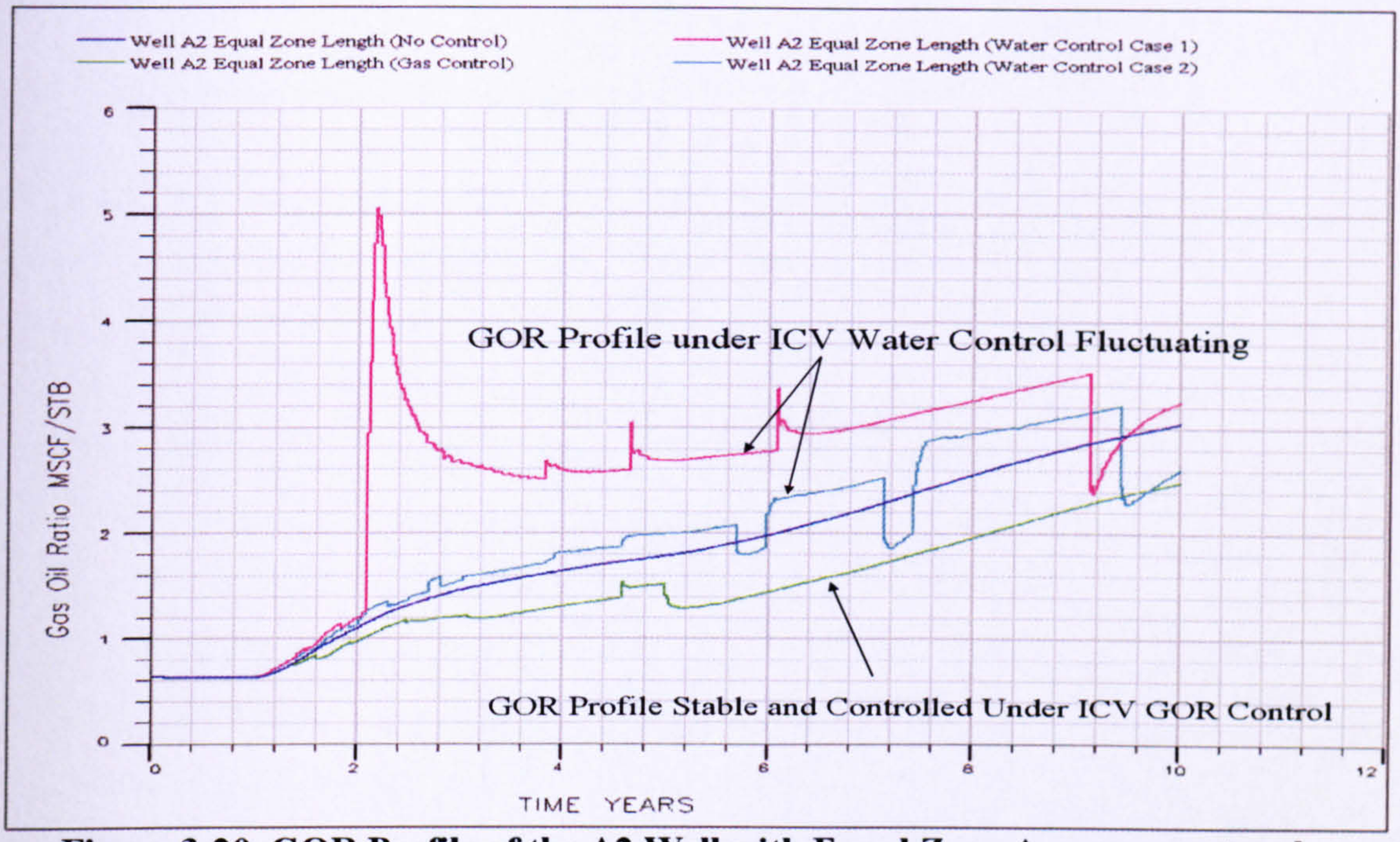

Figure 3-20. GOR Profile of the A2 Well with Equal Zone Arrangement and Water Control Choking Strategy

Delaying rather than controlling the water production provides a more efficient method to increase the oil recovery in this situation as illustrated by analysis of the importance of the well standoff showed. Changing the horizontal standoff from the middle to the top 15% of the oil column (10 ft below the GOC) delayed the water production by almost a year (Figure 3-21). This change in well placement resulted in a 4% increase in the total oil production from the previous ICV control case. This highlights that ICVs cannot (completely) compensate for incorrect well design or placement.

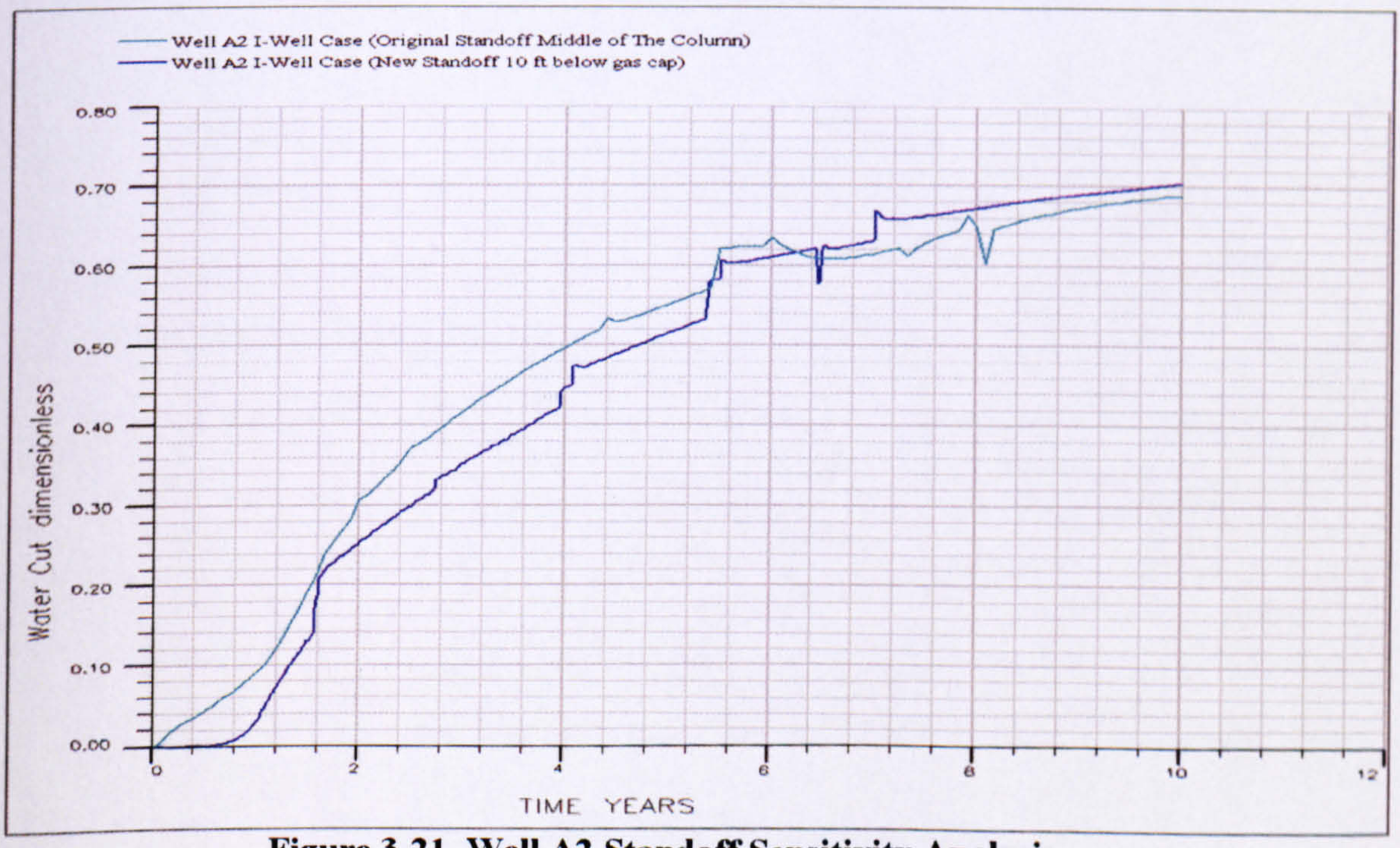

Figure 3-21. Well A2 Standoff Sensitivity Analysis

3.6.4 Well A2 Multilateral Studies:

Installation of an I-completion to replace the original A2 well open-hole showed a small (+1.5%) increase in oil production. However, it presented the most difficult fluid management challenge of the three wells due to the simultaneous gas and water production. It was hoped that the multilateral well would show an improvement by distributing the well's target production rate of 3,000 BLPD between the two laterals. Two multilateral well designs were considered, a fork design with two laterals and the DOL design which had been so successful for Well A1. The total length for the laterals was the same as the base case horizontal well (≈ 3,300 ft). The fork design proved to be the optimum (Table 3-10), with a 7.5% increase in the discounted total oil production compared to the horizontal well case.

Table 3-10. Well A2 Total Oil Production Study

Case	Total Oil Production (10^6 STB)	Total Oil Production Discounted @ 10% (10^6 STB)	Comparison with Base Case
Base Case Horizontal Well (Middle of oil Column)	5.62	4.00	-
Horizontal I-Well (Middle of Oil Column)	5.72	4.06	+ 1.5%
Fork Type Multilateral	6.03	4.30	+ 7.5%

All the horizontal well cases (with and without control) found that an oil rate of 3,000 BLPD could not be achieved due to the immediate water breakthrough caused by the higher drawdown (Figure 3-22). It was hoped that the multilateral well would be able to decrease the drawdown and delay the water and gas breakthrough. The increased production from the multilateral was due to its ability to maintain the target rate of 3,000 BLPD for 10 months.

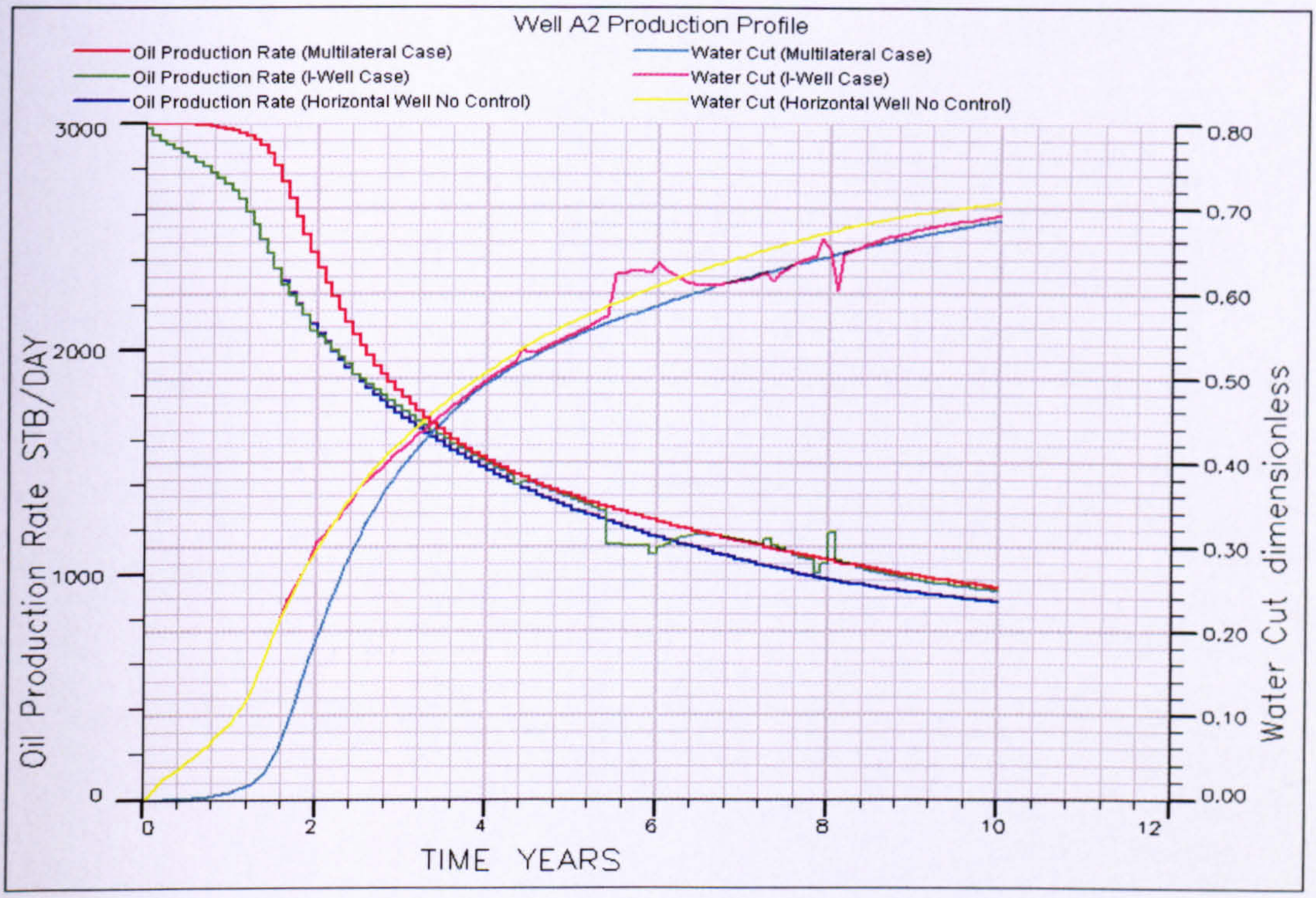

Figure 3-22. Well A2 Multilateral Production Profile

3.6.5 Well A2 Multilateral Well Rate Sensitivity:

One of the arguments for using multilateral well is the ability to provide an opportunity for an increased production rate by redistribution of the drawdown required to obtain a certain flow rate on the laterals.

Table 3-11 shows the total oil production for the completion options studied for Well A2. The advantage of the multilateral style completion becomes smaller as the rate and drawdown increases. The intelligent completion was unsuccessful at 9,000 BLPD because the choking algorithm designed to manage a rapid increase in water production resulted in continuous and rapid choking of the intelligent wells. The decreasing benefit of the multilateral well could possibly have been countered by increasing the reservoir exposure (e.g. by increasing number of laterals).

Table 3-11. Well A2 Multilateral Completion Rate Sensitivity

Discounted Total Oil Production (10^6 STB)				
Rate (BLPD)	Base Case Horizontal Well	I-Well	Multilateral	Multilateral compared to Base Case
3,000	4.00	4.06	4.30	+ 7.5%
6,000	5.98	6.12	6.21	+ 3.9%
9,000	7.51	6.85	7.61	+ 1.3%

3.6.6 Impact of Conventional Reservoir Engineering on Multilateral wells:

The role of conventional reservoir engineering studies on the placement of intelligent or complex wells is illustrated by the A2 well. Table 3-12 shows that the choice of the optimum standoff (10 feet below the gas cap) increases the total oil produced by 4.3%; while changing the A2 well's orientation (Figure 3-23) so that the laterals are pointing away from the gas cap decreases the oil production by 4.6%. The early water breakthrough due to the unfavourable well orientation caused a decrease in the early as well as the total oil production (Figure 3-24). These "conventional" considerations need to be considered when designing an optimum I-completion.

Table 3-12. Effect of Stand-off on Well A2 Multilateral Well

Lateral Stand-off	Discounted Total Oil Production (10^6 STB)	Lateral Orientation	Discounted Total Oil Production (10^6 STB)
Middle of the Oil Column	4.30	Laterals Point Towards Gas Cap	4.30
10 ft below GOC	4.49	Laterals Point Away from Gas Cap	4.10
Difference	+ 4.4%	Difference	- 4.6%

The careful selection of the well placement leading to extra value generation is clearly exemplified by the B1 multilateral well studied in the next section.

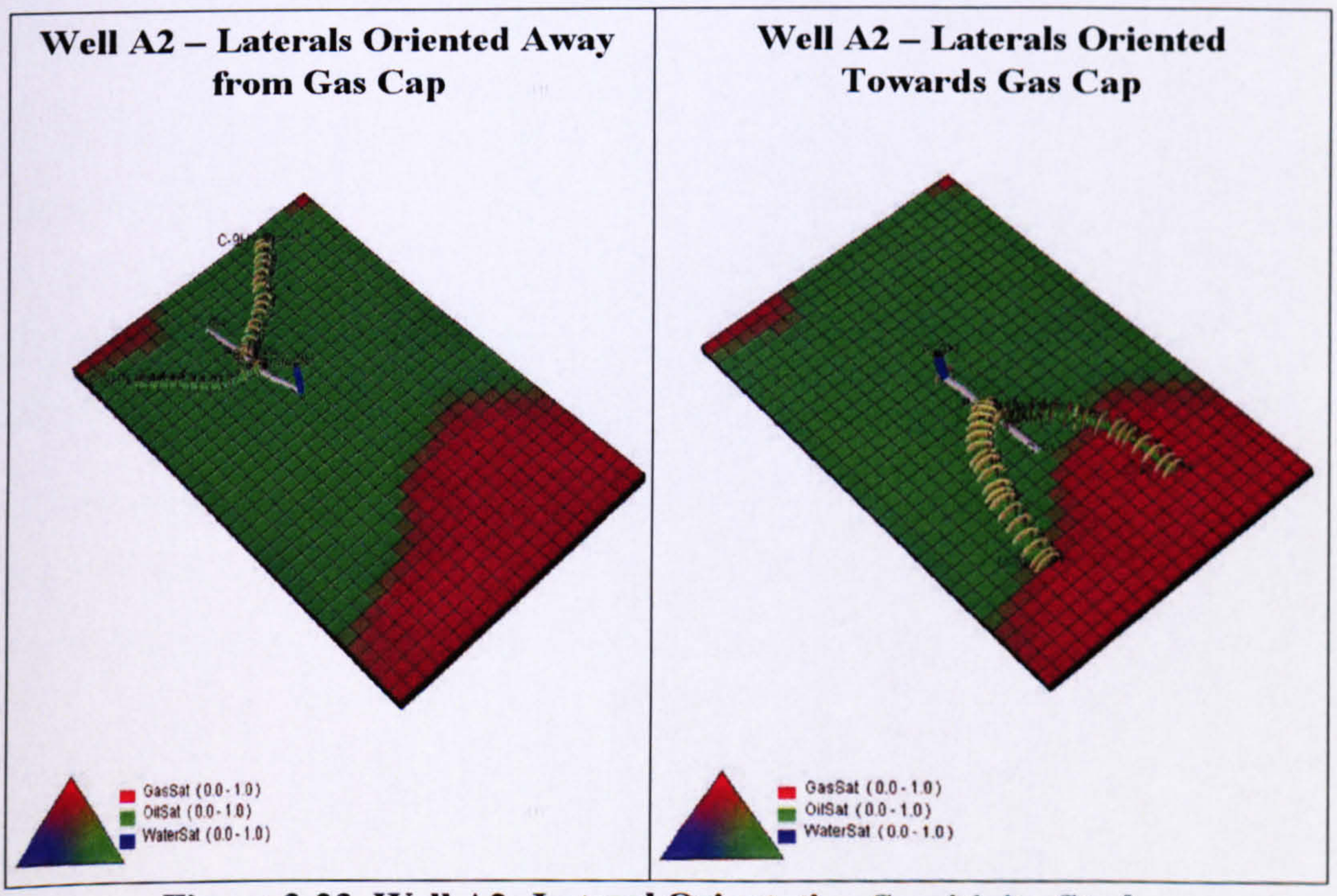

Figure 3-23. Well A2: Lateral Orientation Sensitivity Study

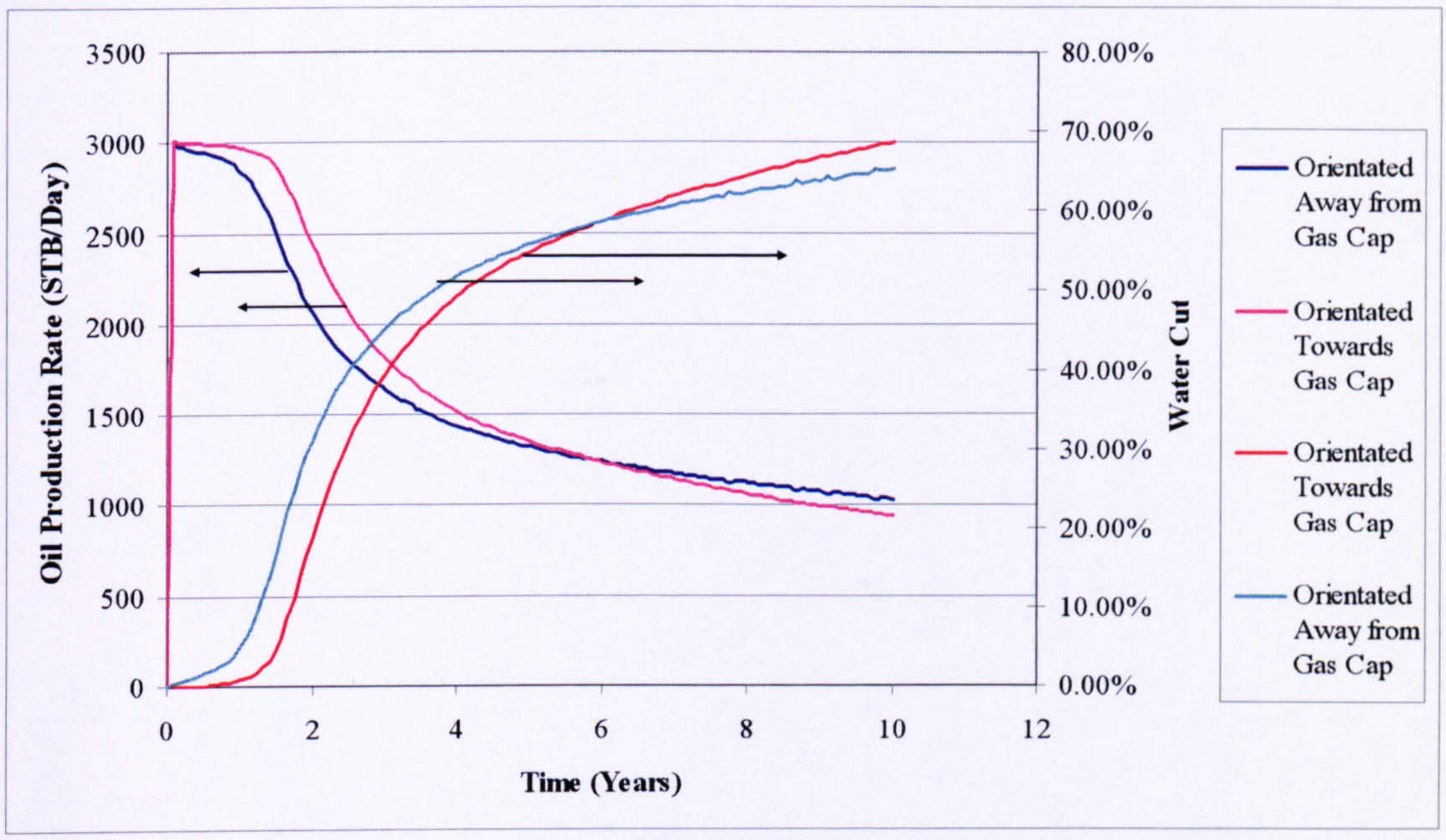

Figure 3-24. Well A2 Orientation Study: Oil Production and Water Cut Profile

3.7 Well B1:

This well is located immediately under the field's gas cap. It experiences rapid gas breakthrough, limiting the well life to only 2.5 years. The B1 well is different from the previous two wells since they had been able to produce throughout the 10 year study period without reaching any of the production constraints. (I.e. the only opportunities for ICV control of the A1 and A2 wells was related to the improved tubing performance by control of unwanted fluids.)

The B1 well thus potentially provides a good showcase of the benefit of using the intelligent completion to efficiently control the gas production and extend the well life. The logical ICV control strategy is to control the GOR since water production is minimal (less than 2% after 2.5 years). The well target liquid production rate is 1,000 BLPD, this low value having been chosen in order to help minimize the GOR increase.

Aggressive choking of the ICV (Figure 3-25) reduced the gas production to such an extent that the well life is extended by 4 years with an increased total oil production (discounted at 8%) of 69% (Table 3-13).

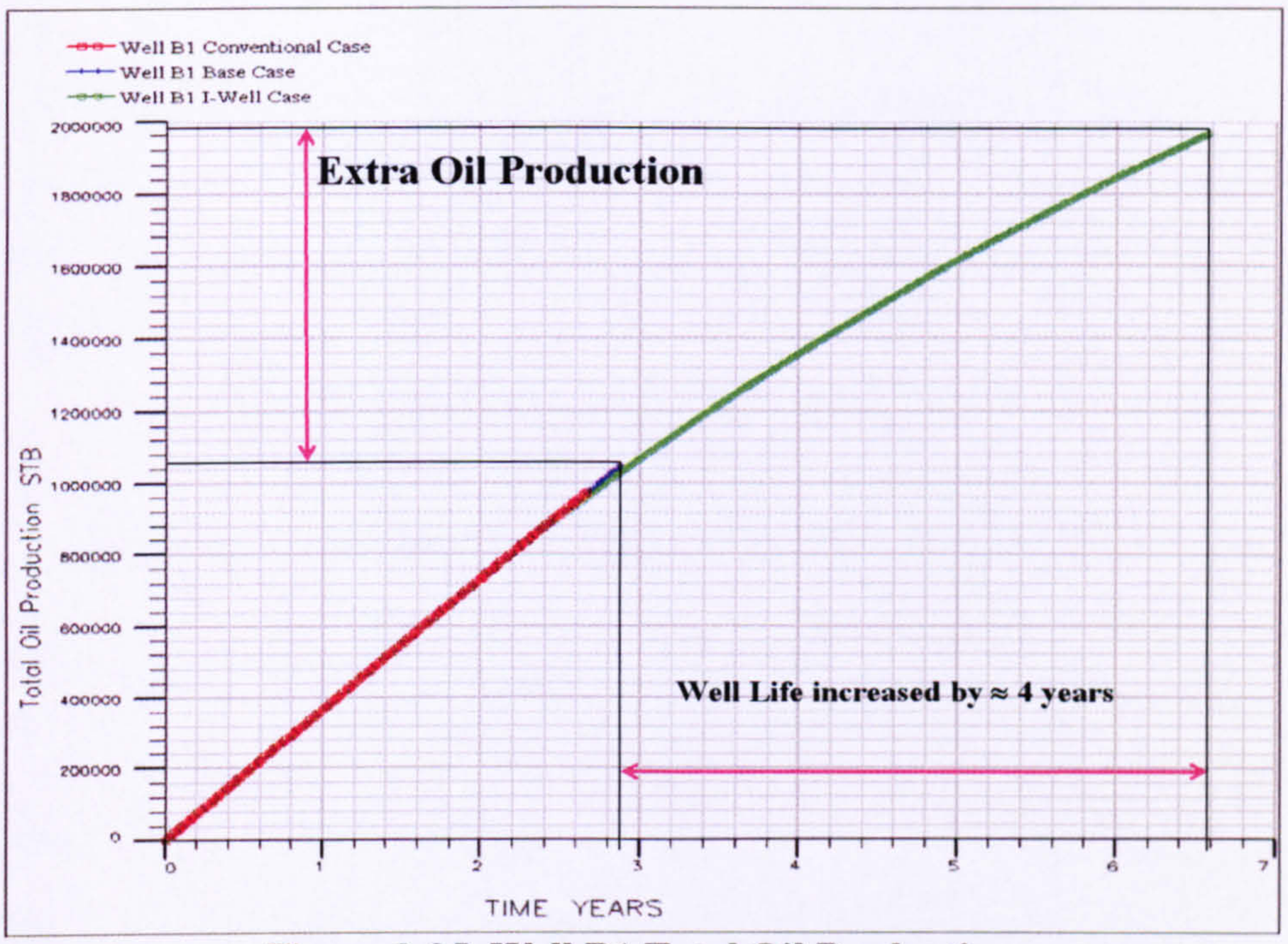

Figure 3-25. Well B1 Total Oil Production

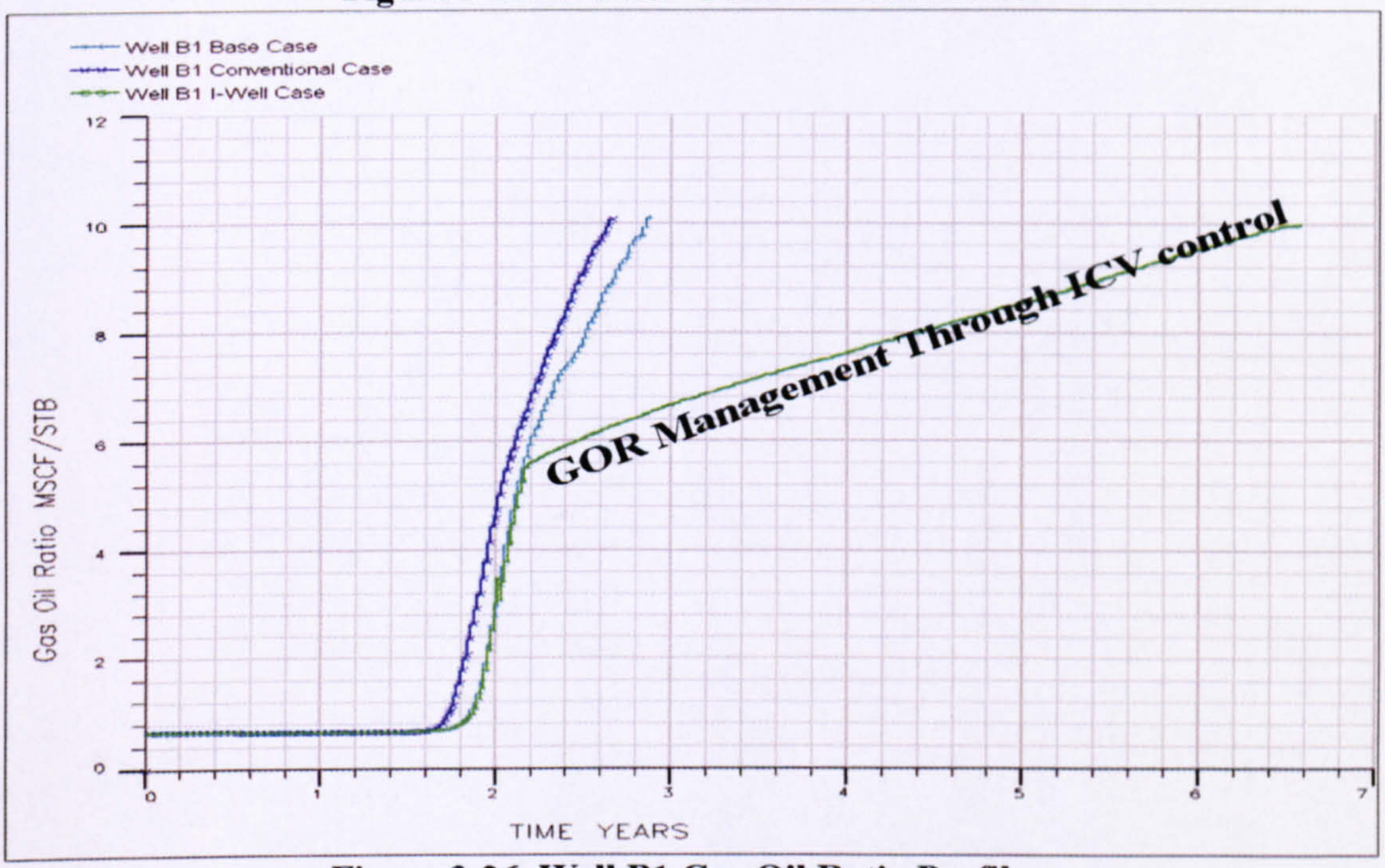

Figure 3-26. Well B1 Gas Oil Ratio Profiles

Table 3-13. Well B1 Discounted Total Oil Production

Cases	Discounted Total Oil Production (10^6 STB)
I-Well Case	1.585
Base Case	0.940
Conventional Case	0.878
Difference Between I-Well & Base Case	+69%

ICV control allows the target liquid production rate to be increased up to 6,000 BLPD (Table 3-14). This brings a large, potential impact on project economics (increased recovery per well combined with production acceleration). This option was not available with the open-hole conventional completion since it is essential to have the means to control the gas production downhole.

Table 3-14. Well B1 I-Well Rate Sensitivity

Target Liquid Production Rate (BLPD)	Increase in Well Life (Years)	Extra Oil Production (10^6 STB)
1,000	4.00	0.995
2,000	5.10	1.524
4,000	5.30	1.697
6,000	5.40	1.765

3.7.1 Importance of Well Stand-off

The initially chosen position of the horizontal section was in the middle of the column, similar to wells A1 & A2. The minimal water production indicates that lowering the well position towards the oil-water contact could be beneficial by further reducing the gas-coning tendency.

Table 3-15. Well B1 Standoff Sensitivity

Well Placement	Discounted Oil Production (10^6 STB)	Increase Compared to Base Case
Base Case (Middle of Oil Column)	1.585	-
Bottom 10% of the Column (1000 BLPD + No Control)	3.301	+108%
Bottom 10% of the Column (2000 BLPD + Control)	4.501	+184%

Lowering the well to the bottom 10% of the oil column and producing at 1,000 BLPD increased the life of the well to 10 years without gas breakthrough (Figure 3-27). The water cut at the end of the well life was only 18% despite the well being positioned near the aquifer. This result prompted the evaluation of an increase in the liquid production rate to accelerate the production further. A production rate of 2,000 BLPD coupled with I-well control of the increased gas production yielded a 184% increase in the discounted total oil production (Table 3-15). Figure 3-28 illustrates the ICV actions required to control the increase in the gas production in the period between 3.5 and 7 years to ensure that the well's producing life is extended to the full study period of 10 years.

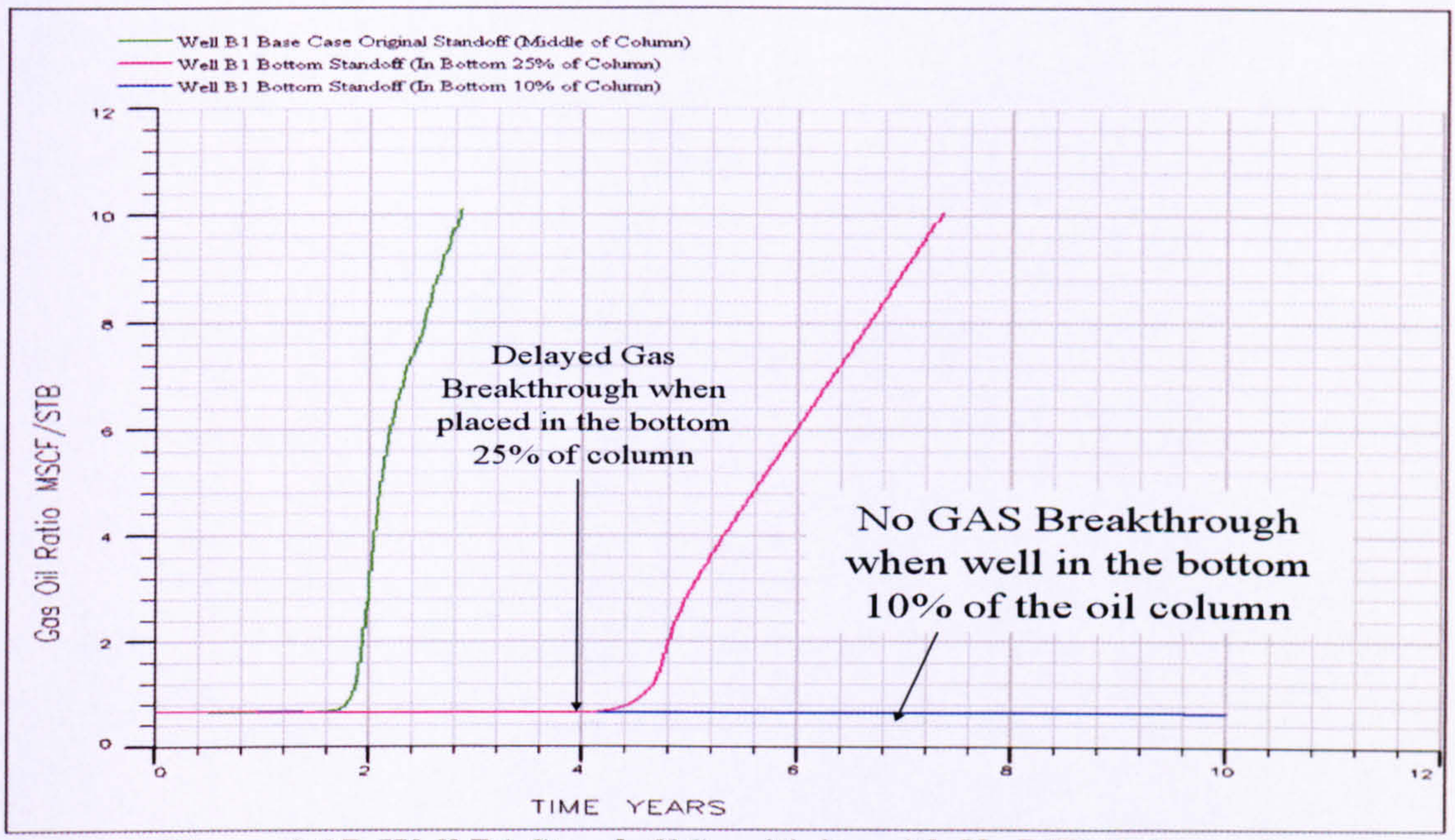

Figure 3-27. Well B1 Standoff Sensitivity with No I-Well Control

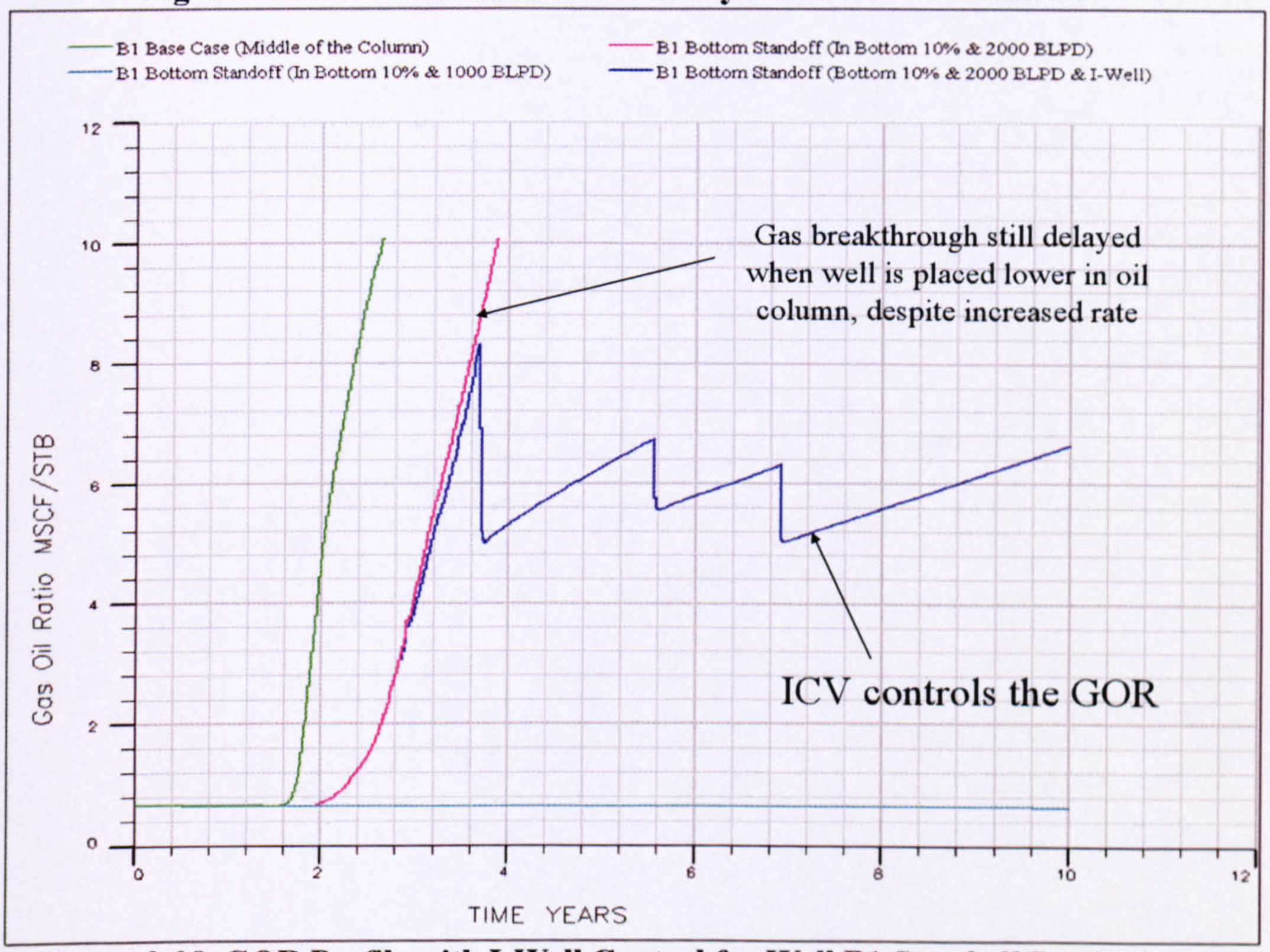

Figure 3-28. GOR Profile with I-Well Control for Well B1 Standoff Sensitivity Study

3.7.2 Can I-Wells Manage Permeability Variation and Uncertainty?

One of advantages of I-well completions is their ability to manage the unpredictable nature of the reservoir's geological features. This is illustrated by the presence of higher permeability gas producing conduit in A2 well. The permeability is almost

homogeneous along the wellbore in the cases studied so far (Figure 3-29). Several permeability distributions along the completion interval were introduced into well B1 to assess the robustness of the chosen choking strategy to a limited amount of geological uncertainty (See below and Figure 3-30).

1. **Toe-Centric:** Low permeability at the heel, gradually increasing toward the toe.
2. **Convex:** Low at the heel and toe, with an increased permeability in the middle section.
3. **Heel-Centric:** High at the heel, gradually decreasing towards the toe.
4. **Base Case:** constant permeability along the wellbore.

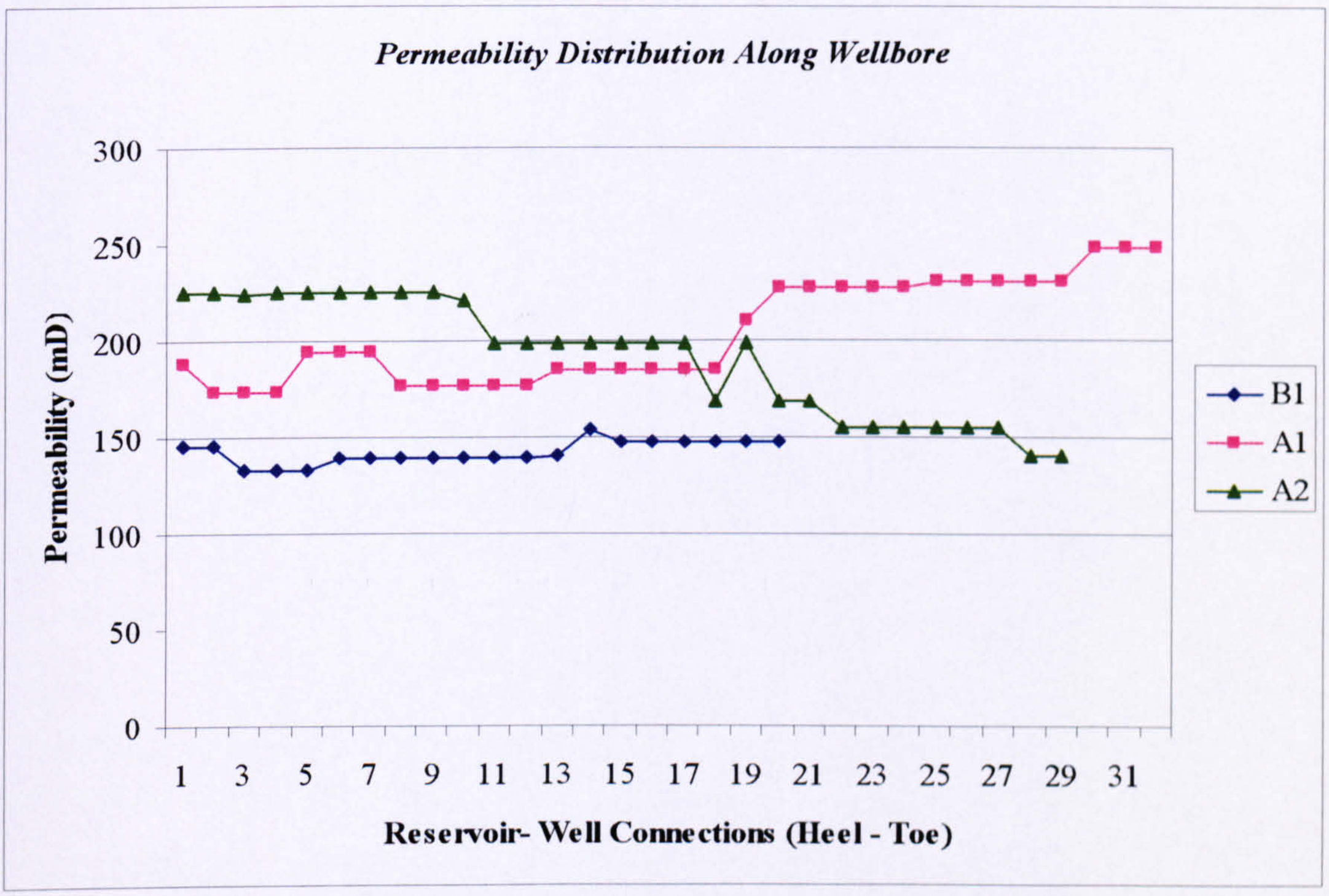

Figure 3-29. Well's Original Permeability Distribution

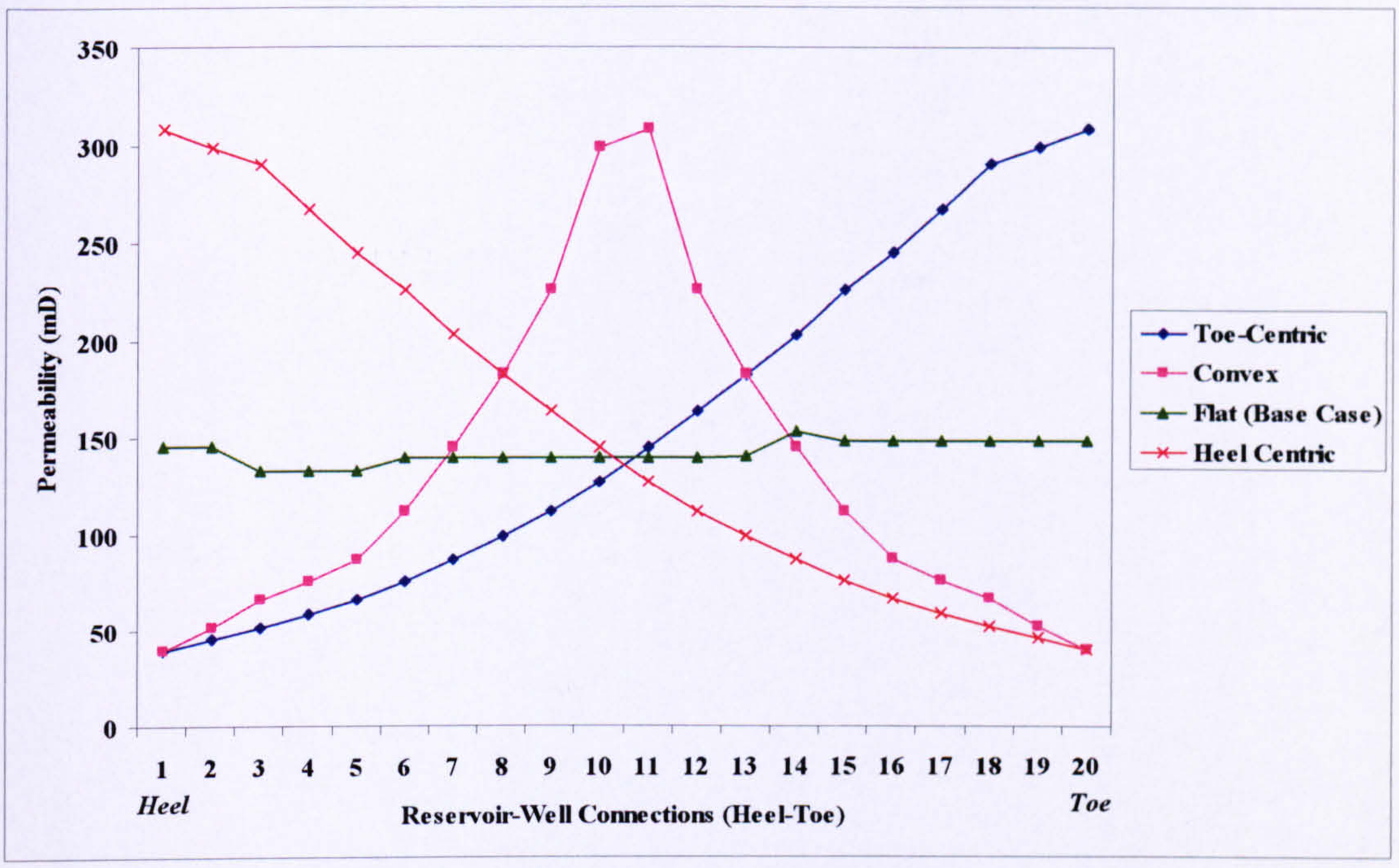

Figure 3-30. Well B1 Near Wellbore Permeability Distribution Sensitivity Study

The permeability range was based on the range of the upscaled values of the geological model of the reservoir that had been used in the reservoir simulation model. It varied from a minimum of 40 to a maximum of 308 mD. The choking strategy and the geometric arrangement of the ICVs was not been changed. Only minor differences in the total oil recovered form the well were observed for these scenarios, though significant differences in the GOR profiles were recorded during the period between 15 and 24 months (Figure 3-31). The heel-centric distribution had the earliest gas breakthrough (12 months) due to the combination of both a high reservoir permeability and a higher drawdown at the heel. The gas break-through was delayed until 18 months for the constant permeability distribution, while the other permeability distributions showed gas break-through at about 15 months.

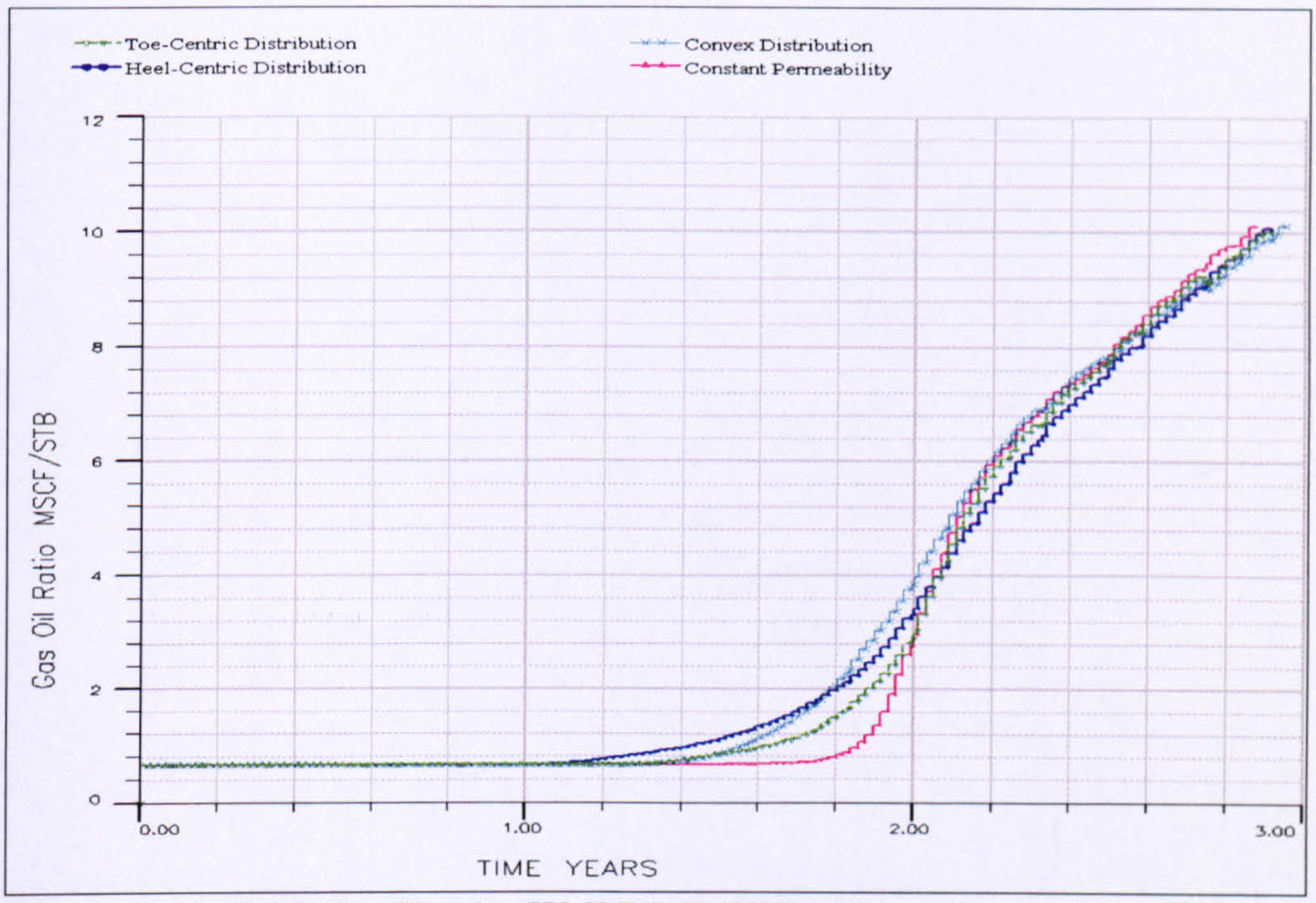

Figure 3-31. GOR Profiles for Well B1 (I-Well without Control) for Various Permeability Distributions

The relatively small permeability variation, as expected, did not affect the robustness of the choking strategy (Table 10). I-Well control of the toe-centric permeability distribution provided a slightly higher total oil production (having the low permeability at the heel as an extra restriction delayed the gas breakthrough, while the higher permeability at the toe counter-balanced the lower drawdown).

Table 3-16. Total Oil Production for Well B1 with Various Permeability Distribution

	I-Well Case	Base Case	
Permeability Distribution	Total Oil Production (10^6 STB)	Total Oil Production (10^6 STB)	Difference
Toe-Centric	1.982	1.062	+87%
Heel-Centric	1.972	1.062	+86%
Flat	1.967	1.048	+88%
Convex	1.943	1.076	+81%

This investigation confirms the importance of proper well placement to increase the potential value of the intelligent completion to enhance production.

3.7.3 Well B1 Multilateral Studies:

The B1 horizontal well has shown the greatest increase in value creation on installation of an intelligent well. This was due to the base case horizontal well showing such a rapid gas production increase that the well ceased production after 2.5 years (Figure 3-4). The intelligent completion controlled the gas production, increasing the well life and the total oil production. The optimum I-completion design required lowering the single lateral standoff from the GOC to the bottom 10% of the oil column and implementing a progressive choking of the produced gas. The well life increased from 2.5 to 10 years and the target production rate could be doubled from 1,000 to 2,000 BLPD. A multilateral completion will now be evaluated to see if it can further increase the well productivity.

3.7.4 Lateral Separation and Interference

Interference between the laterals will be an important issue for the B1 well as it combines homogeneous reservoir permeability with rapid gas breakthrough. A dual, fishbone multilateral well (Figure 3-32) with a 106 ft separation between the two lateral entries was placed in the middle of the oil column. The same reservoir exposure as the horizontal well (2,178 ft) was chosen. Gas broke through in both laterals at almost the same time after 2 years production. An increasing lateral separation further delayed the gas breakthrough, but the subsequent rate of increase of the GOR remained the same (Figure 3-33). The delayed gas breakthrough allowed production to continue for an extra 12 months, increasing the total oil production by 31% (Figure 3-34). A separation of 435 ft was chosen as a practical option for this study. The increasing separation between the laterals has resulted in a reduction in their mutual interference, an increase in the drainage area and an improved recovery through an increase in the sweep efficiency.

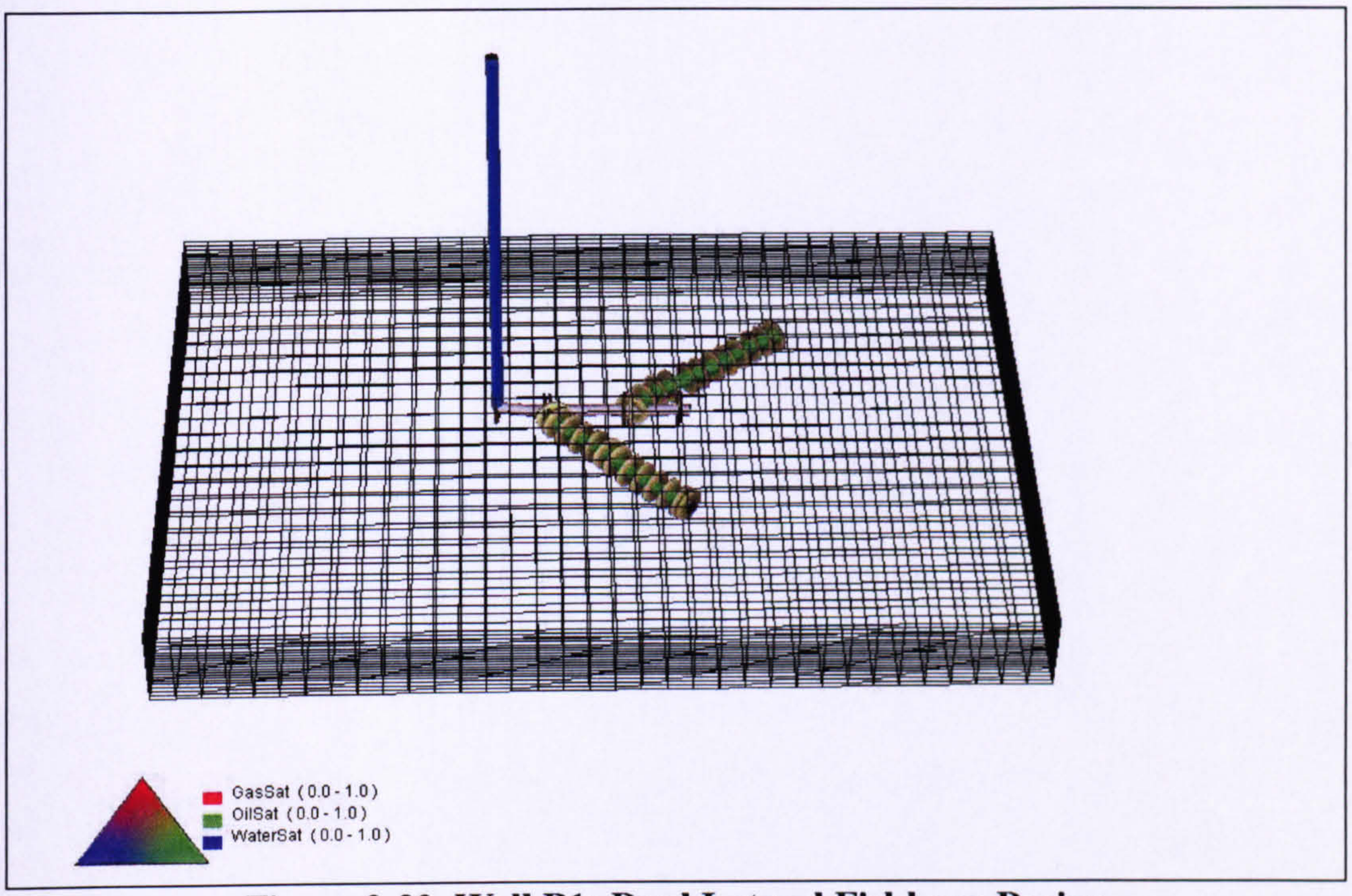

Figure 3-32. Well B1: Dual Lateral Fishbone Design

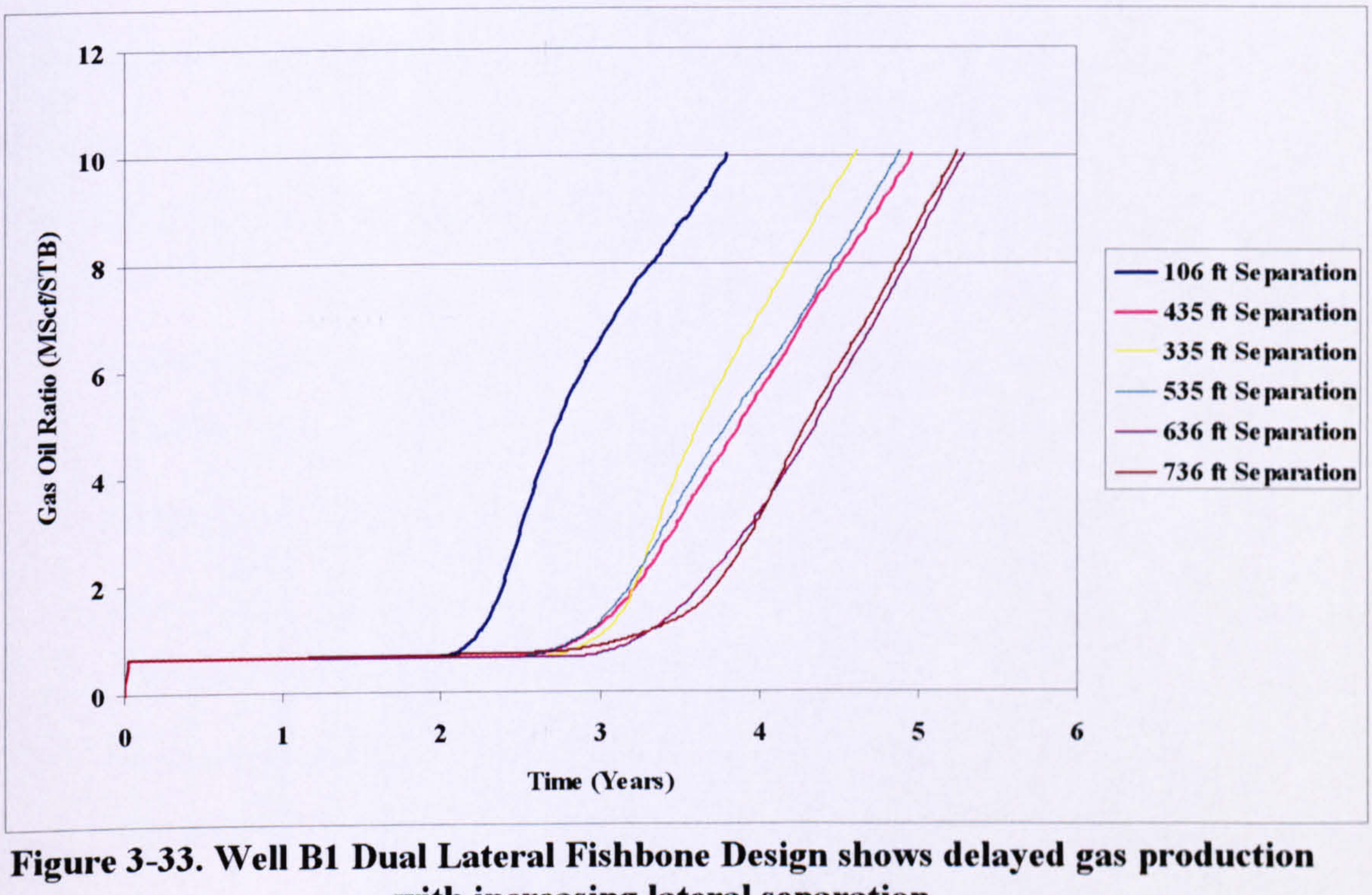

Figure 3-33. Well B1 Dual Lateral Fishbone Design shows delayed gas production with increasing lateral separation

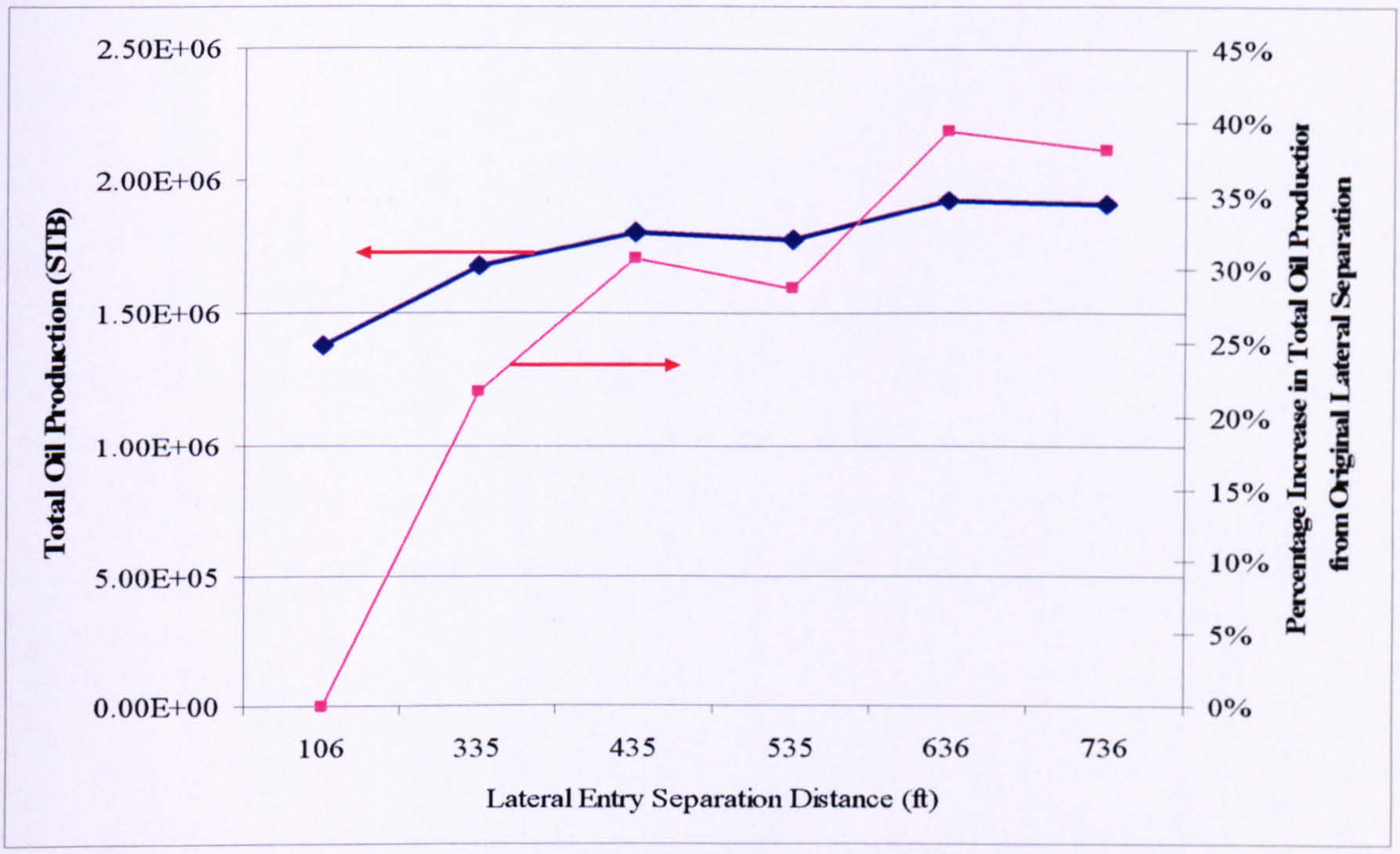

Figure 3-34. Well B1 Dual Fishbone Lateral: Total Oil Production for Various Lateral Separations

3.7.5 Maximizing the Value of the B1 Multilateral Well

Well B1 is a good candidate for demonstrating the benefit of integrating Multilaterals and I-Completion technologies. A four lateral, fishbone design I-completion was designed based on the following considerations:

1. Locating all the laterals in the bottom 10% of the oil column to delay the gas breakthrough.
2. Employing a Lateral Separation of 435 ft.
3. Increasing the reservoir exposure from 2,178 ft to 3,824 ft using three laterals of fishbone design and the motherbore (Figure 3-35).
4. Installing 4 ICVs in the motherbore, one to control the inflow from each lateral and one to manage the flow from the toe of the motherbore.
5. Increasing the target liquid production rate from 1,000 to 3,000 BLPD.

The impact of all these changes was to increase the well life from 3.6 to 10 years, mainly due to the GOR control provided by the ICVs. This well life extension was achieved despite the increase in the well's target production rate (Figure 3-36). The total oil production increased by an extra 127 % compared to the Original Base Case

Horizontal Well located in the middle of the oil column and produced at 1,000BLPD (Table 3-17).

An I-completion is not required when the well target production rate is 1,000 BLPD since the drawdown is now so low that the gas breakthrough does not occur within the 10 year well lifetime considered here. An I-completion has to have something to control before it can deliver value. The I-completion's benefit is clearer for the 2,000 and 3,000 BLPD cases since selective gas breakthrough along the length of the completion can be controlled by the ICV. The above production performance of these horizontal wells is already a vast improvement over that observed with a conventional vertical or deviated well design.

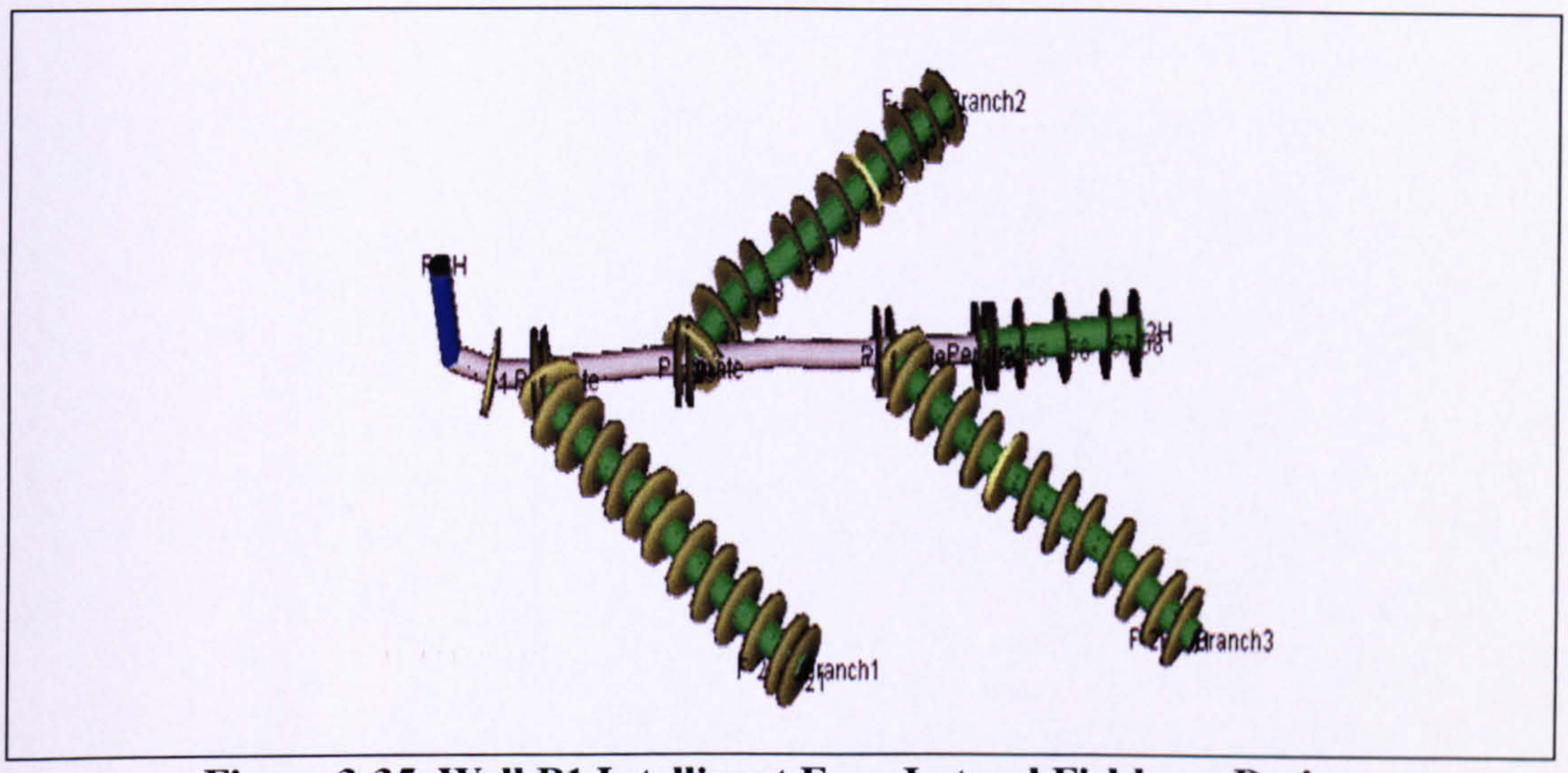

Figure 3-35. Well B1 Intelligent Four Lateral Fishbone Design

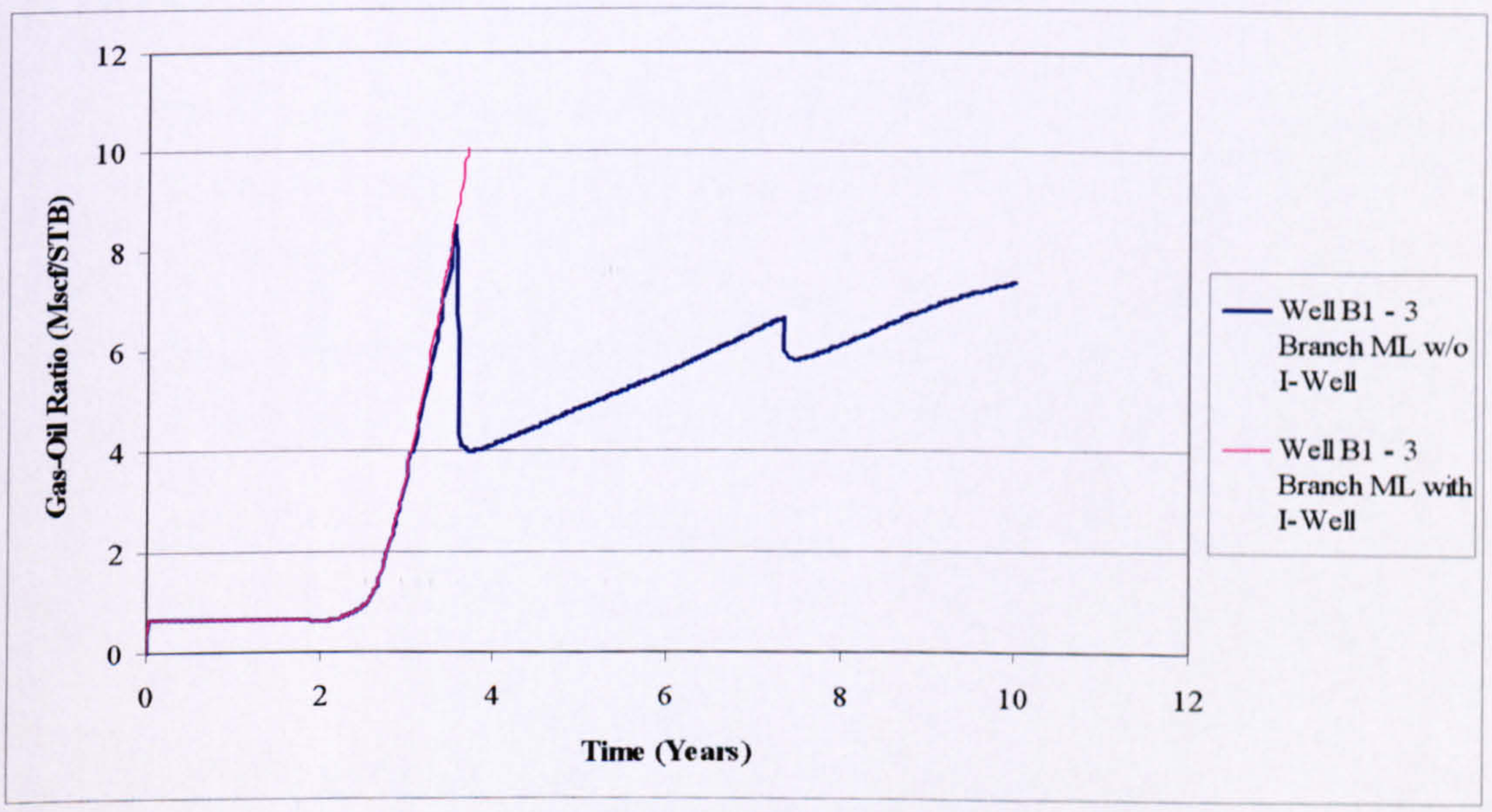

Figure 3-36. Well B1: Multilateral I-Completion controls the GOR

Table 3-17. GOR control provided by I-well when producing the B1 ML Well with an increased target production rate

Case	Total Oil Production Discounted @ 10% (10^6 STB)		
Liquid Production Rate (BLPD)	1,000	2,000	3,000
Base Case Horizontal Well in Middle of Oil Column	0.97	0.38	0.23
Base Case Horizontal Well (Optimum Standoff)	1.07	1.06	0.82
Impact of Standoff Point Optimisation	*+ 10 %*	*+ 179 %*	*+ 257 %*
Intelligent Horizontal Well (Optimum Standoff)	1.07	1.59	1.69
Impact of I-Completion on Optimum Horizontal Well	*0 %*	*+ 50 %*	*+ 106 %*
3 Branch Multilateral Without ICV Control	1.12	1.76	1.54
3 Branch Multilateral With ICV Control	1.12	1.98	2.2
Impact of I-Completion on Multilateral Well	*0 %*	*+ 13 %*	*+ 43 %*
Impact of 3 Branch Multilateral well With ICV Control compared to Original Base Case Well @ 1,000 BLPD	*+ 15 %*	*+ 104 %*	*+ 127 %*

3.8 Conclusions:

1. Three example horizontal wells taken from differing locations in a real, thin oil-column reservoir model showed a better performance than a vertical well installed at an equivalent position.

2. Intelligent completions provide an effective tool for managing production from thin oil columns reservoirs, thus increasing the total oil production per well.

3. Maximum value was derived from the proactive control strategy of ***delaying*** rather than the reactive strategy of ***controlling*** the breakthrough of unwanted fluids.

4. Emphasis should be placed on controlling the gas if the well experiences simultaneous gas and water break through of equal severity.

5. Control at both the well and ICV level proves an effective methodology of controlling unwanted fluids in a well.

6. Knowledge of the (relative) activities (size and connectivity) of the gas cap and aquifer are important in determining the optimum wellbore placement. Correct well positioning is required to maximize the value from the I-Well installation.

7. Advanced well construction (Multilateral well designs & I-Completions) should always be used in conjunction with good reservoir engineering practices. They are not a replacement for them.

8. A Multilateral well was shown to be an even better development option for thin oil column reservoirs, particularly those with a homogeneous permeability and equal vertical and horizontal permeability.

9. The optimum placement of laterals within the oil column, their separation and their orientation are all determined by the reservoir permeability, fluid properties and the strengths of the gas cap and the aquifer. The impact of these properties was illustrated for three typical reservoir scenarios from a real field model.

10. The combination of multilateral and I-completion technologies yields value when the reservoir can support a greater production rate and the ICVs are able to control excessive, unwanted fluid production created by the increased drawdown.

11. Conventional simulation studies are a good tool to determine the applicability of multilateral wells to a particular reservoir. They are inadequate to determine the optimum multilateral well design due to the many possible, multilateral well design options.

3.9 Discussion

This chapter has illustrated how an I-completion can enhance the production from difficult reservoir environments through their ability to control the production of unwanted fluid. The use of downhole flow control valves depends on knowledge of the produced fluid's production rates and the downhole production conditions. The full value of downhole control can only be achieved with reliable, accurate downhole monitoring and the detection of unwanted fluid entry at various locations along the length of the well.

Chapter 2 and chapter 3 used simulation studies to provide the data on downhole flow conditions and the production rates of the different fluid phases. In practice, the only way to get such data are either by a PLT light well intervention or by deploying downhole gauges, to measure the temperature and pressure and multiphase flow meters. Table 3-18 illustrates the important parameters, based on Chapter 2 & 3 case studies, that the operators of the studied fields would require for the effective optimisation of the ICV actions to maximize the hydrocarbon production.

Table 3-18. Parameters Required for Effective Optimisation of ICVs

Case Study	Objective	Required Data
Chapter 2: Stacked Gas Sands (C-Field)	Production Acceleration through Commingling	Zonal Production Rate
	Water Control	Water Cut Water Production Zone
Chapter 3: Thin Oil Column (A & B Field Sectors)	Water and Gas Control	Water Cut GOR

DTS is becoming one of the most frequently deployed sensor in production wells. To reap the full benefit from its measurements it is important to understand the underlying heat transfer phenomena that control the DTS measurements. This understanding will allow better interpretation of the DTS data in intelligent wells. The cost of an intelligent completion is considerably higher than that of a conventional completion. Hence, establishing what can and what can not be detected using DTS data is important for fit-for-purpose I-Well design. Hence, Chapters 4 will review the existing application of DTS and other fibre optic temperature sensors while Chapter 5 will review the published temperature prediction models. Chapter 6 will examine the use of DTS in the area of flow assurance by modelling the effect of scale deposition on the temperature profile inside the tubing and how this effect can be detected on the DTS profiles. Chapter 7 attempts to incorporate the intelligent well completion equipment in existing temperature models and their effect on temperature profiles in wellbores.

3.10 References

3.1. Yu, S., D.R. Davies, and D.W.Sherrard. *The Modelling of Advanced "Intelligent" Well – An Application.* Paper SPE62950 presented at 2000 SPE Annual Technical Conference and Exhibition, Dallas, Texas, U.S.A., 1–4 October 2000, Society of Petroleum Engineers.

3.2. Jansen, J.D., et al. *Smart Well Solutions for Thin Oil Rims: Inflow Switching and the Smart Stinger Completion.* Paper SPE77942 presented at SPE Asia Pacific Oil and Gas Conference and Exhibition, Melbourne, Australia, 8-10 October 2002, Society of Petroleum Engineers.

3.3. Vo, D.T., et al. *Reservoir Management for Ultra-Thin Oil Columns Under Gas-Cap and Water Support: Attaka Field Examples.* Paper SPE68675 presented at SPE Asia Pacific Oil and Gas Conference and Exhibition, Jakarta, Indonesia, 17–19 April 2001, Society of Petroleum Engineers.

3.4. Bayley-Haynes, E. and E. Shen. *Thin Oil Rim Development in the Amherstia/Immortelle Fields, Offshore Trinidad.* Paper SPE81088 presented at SPE Latin American and Caribbean Petroleum Engineering Conference, Port-of-Spain, Trinidad, West Indies, 27-30 April 2003, Society of Petroleum Engineers.

3.5. Mackow, M.H., et al. *Finding New Limits with Horizontal Wells in a Thin Oil Column in the Mahogany Gas Field, Offshore Trinidad.* Paper SPE81090 presented at SPE Latin American and Caribbean Petroleum Engineering Conference Port-of-Spain, Trinidad, West Indies, 27-30 April 2003, Society of Petroleum Engineers.

3.6. Glandt, C.A. *Reservoir Aspects of Smart Wells.* Paper SPE81107 presented at SPE Latin American and Caribbean Petroleum Engineering Conference, Port-of-Spain, Trinidad, West Indies, 27-30 April 2003, Society of Petroleum Engineers.

3.7. Schlumberger, Geoquest Eclipe 100 Reservoir Simulator Manual 2005A. 2005.

3.8. Elmsallati, S.M., D.R. Davies, and S.M. Erliandsen. *A Case Study of Value Generation with Intelligent Well Technology in a High Productivity, Thin Oil Rim Reservoir.* Paper SPE94995 presented at 14th SPE Middle East Oil & Gas

Show and Conference, Bahrain, 12-15 March 2005, Society of Petroleum Engineers.

3.9. Chambers, M.R. *Making Multilateral Well Cost Effective.* Paper SPE51244 presented at 22nd Annual International Conference and Exhibition, Lagos, Nigeria, 5-7 August 1998, Society of Petroleum Engineers.

3.10. Yildiz, T. *Multilateral Horizontal Well Productivity.* Paper SPE94223 presented at SPE Europec/EAGE Annual Conference, Madrid, Spain, 13-16 June 2005, Society of Petroleum Engineers.

3.11. Owodunni, A., T. Travis, and G. Dunk. *The Use of Multilateral Technology to Arrest Production Decline in a West-Texas Gas Field.* Paper SPE84029 presented at 2003 SPE Annual Technical Conference and Exhibition, Denver, Colorado, U.S.A., 5-8 October 2003, Society of Petroleum Engineers.

3.12. Joshi, S.D., *Horizontal Well Technology*: Published by PennWell Books in 1991. 552 Pages.

3.13. Yeten, B., L.J. Durlofsky, and K. Aziz, *Optimization of Nonconventional Well Type, Location, and Trajectory.* SPE Journal, 2003: SPE86880 p. 200-210.

Chapter 4 Fibre Optic Distributed Temperature Sensors Theory and Applications

4.1 Introduction:

Temperature measurements in oil and gas wells were introduced in the late 1930's, signalling the introduction of production logging [4.1]. The initial drive for temperature logging was to locate the presence of hydrocarbons. However it was soon discovered that the differences between thermal properties of hydrocarbons and water are small in the absence of flow; thus the location of hydrocarbon can not be determined from temperature data alone. It can, however, be used to detect anomalies; both in the structure of the well (e.g. a leak in a tubing or casing) and in the fluid production from the well. Temperature log interpretation has become an important tool for well production optimisation. This was recognised with the integration of temperature logging into the production logging tool (PLT)

Thermocouples and other types of electrical gauges were initially used for temperature measurement. Temperature sensing took a big step forward with the use of optical fibre distributed temperature sensors in oil and gas wells. This became possible with the advances in the technology and the mass production of optical fibres e.g. fibre optic temperature measurement has been commercially available for steam flood wells, where operating temperature reaches up to 280 °C, since the early 1990s [4.2]. The initial application in steam injection projects is being extended to include many different oil and gas production environments. Early fibre optic temperature measurement used point sensors at a particular location. This has now been extended with fibre optic distributed temperature sensors (DTS) technology.

This chapter discusses fibre optic sensing technology and compares it to the conventional temperature logging. The different configurations and installation practices used for DTS system deployment in oil and gas wells are also covered. As discussed, the temperature changes measured in oil and gas wells are small; hence thermal measurement accuracy and resolution play an important role in the accurate interpretation of the measured temperature data. Examples of different applications will be discussed to illustrate the utilization of such data in well production optimisation.

Fibre optic temperature sensors are the most recently developed technology for temperature measurement. Two types of electrically based sensor technologies were employed prior to the development of fibre optics:

1. RTD (Resistive temperature detectors)
2. Thermocouples

The RTD operating principle relies on changes of the electrical resistance of a metal as a function of temperature. By contrast, a thermocouple is based on the generation of a low voltage signal that is a function of temperature from a junction of two metals at different temperature.

Fibre optic sensors come in two types. Single point temperature sensor, which has a Bragg grating etched into the fibre at the measurement point and continuous or distributed temperature sensor (DTS) technology. The latter provides a temperature data log along the length of the well at a spatial resolution of one meter. DTS opens the opportunity to monitor the performance of the complete production interval and the integrity of the well continuously. Examples of temperature anomalies that can be detected by such sensors are [4.3]:

1. Cross flow between adjacent sets of perforations
2. Water breakthrough from a nearby water injector
3. Flow behind the casing.
4. Localised heating around an ESP.
5. Identification of the location of water or gas breakthrough point.
6. Variance in permeability.
7. Estimation of the zone contribution to the flow rate in a multi-zone completion.

Advantages of fibre optic technology over electrical based measurements [4.2] are:

1. Real-time measurements (though an electrical temperature gauge could also be permanently installed in the well)
2. Solid state downhole sensor (no moving parts).
3. No downhole electronics.
4. Little or no impact on the well operations.

In addition, DTS provides:

1. Continuous measurement profile along the complete well length.
2. Reduced operational down-time compared to conventional logging techniques.

4.2 Distributed Temperature Sensors vs. Production Logging Tools:

Practical and economical considerations also favour the use of a DTS system. For example, DTS allows measurement to be available even when the platform configuration restricts access to the wellheads during drilling operations. Further, running a PLT log will result in a loss of production during the time required to rig-up the logging equipment as well as the need to reduce the production rate when logging a high rate wells. This will have an economic impact due to deferred production, while the measured data (e.g. for zone production allocation) may not be fully representative of the normal, producing conditions. Other advantages include increasing safety that arises from the avoidance of mechanical interventions in the wells. The DTS surveillance cost thus increases the Capital content of the well (CAPEX) while reducing the Operating Costs (OPEX) [4.4].

Data frequency and measurement point location are important factors when analysing DTS and PLT data or when making a comparison between the two types of data. DTS and PLT results may show a different temperature profile for the flowing well if the DTS is installed outside the tubing, i.e. in the casing/tubing annulus. The PLT is in direct contact with the hot produced fluids in the tubing; while the cooler fluids in the annulus will influence the DTS measurement. By contrast, there will be a fairly good agreement between the two tools when the well is shut-in [4.5]. The periodic clamping of the fibre against the tubing causes additional anomalies that can occur in a DTS measurement. The fibre will be in direct contact with the warmer tubing at the clamp position; the increased thermal contact provided by the clamp leading to a higher temperature being recorded at that point. The cable will register a cooler temperature between the clamps as a layer of cooler annulus fluid will now surround the fibre since it will be positioned at a location some distance from the tubing.

4.3 Fibre Optic Technology & Measurement Techniques:

The idea of fibre optic communication goes back to 1880 when Alexander Graham Bell reported the transmission of speech using a light beam. In fact, the "photophone" was actually proposed four years earlier than the telephone. Speech transmission over a distance of 200 m was achieved by modulating sunlight with diaphragm. Lack of a suitable light source meant that the use of light in communication did not gain momentum until the 1960s when the laser was invented [4.6].

An optical fibre is a thin strand of glass with a diameter similar to that of a human hair. It contains two concentric glass layers with slightly different refractive indices (N.B. the refractive index of a material is the ratio of the phase velocity of electromagnetic radiation in the material compared to the velocity in a vacuum [4.7]). The inner region, known as the fibre core, has a lower refractive index than the outer region, or the cladding (see Figure 4-1). A plastic coating for protection usually surrounds the glass fibre. Further protective layers are normally included to provide additional protection during installation and operation.

Fibre optic sensors have the following advantages over conventional sensors:

1. Free from electromagnetic interference.
2. Immune to environments of high voltage, high electrical noise and relatively high temperatures.

3. Multiple sensors devices that sense different physical parameters can be deployed with a single fibre.
4. Distributed sensing capability
5. Small size and light weight
6. Large bandwidth and a high sensitivity

4.3.1 Fibre Optic Losses

Optical losses in a fibre are attributed to several factors, the most important ones being [4.8]:

1. Material Absorption
2. Scattering Effects (Light Losses)
3. Interface inhomogeneities (both impurities and geometry imperfections)
4. Radiation from bends

Material Absorption:

Material absorption is due to the molecules of the material the fibre is constructed from. (Fibres can be constructed from either glass or plastic). Careful choice of the base material can be used to overcome these absorptions. Two sources of material absorptions are:

a) *Impurity Ions:* Metallic ions (iron, cobalt, copper and chromium) and the Hydroxyl (OH^-) ion from water are the primary source of material impurities in a glass fibre. Losses due to the metallic ions can be reduced to below 1 dB/km through refining of the glass mixture during optic fibre manufacturing to an impurity level below 1 ppb. The effect of water vapour in glass can be minimized by drying the glass in chlorine gas to leach out the level of water vapour to such a low level that the hydroxyl-ion concentration is reduced to below 1 ppb.

b) *Hydrogen Effects (Hydrogen Darkening):* Exposure of the fibre to hydrogen gas can result in the production of hydroxyl ions (with their corresponding losses) or by interaction with the glass by diffusion of the gas through the fibre (which also produces losses). The solution to this problem is to eliminate all hydrogen-

producing sources from contacting the fibre or to add an outer coating to the fibre that is impermeable to hydrogen.

Scattering Losses:

Scattering losses occur when a light wave interacts with a fibre particle in a way that removes energy in the direction of the propagating wave and transfers it to other directions

a) *Rayleigh scattering (Linear Scattering):* results from light interacting with inhomogeneities that are much smaller than the wavelength of the light.

b) *Mie Scattering (Linear Scattering):* is caused by inhomogeneities that are of comparable size to the wavelength.

c) *Brillouin Scattering (Non-Linear):* is a modulation of the light by the thermal energy in the material. The incident photon undergoes a non-linear interaction to produce a low frequency vibrational energy ("phonons") in the glass as well as scattered light ("photons")

d) *Raman Scattering (Non-Linear):* this non-linear interaction produces a high-frequency phonon and a scattered photon, instead of the low-frequency phonon associated with Brillouin scattering.

Interface Inhomogeneities:

These inhomogeneities are caused by either impurities trapped at the core-cladding interface or by geometric changes in the shape and/or size of the core due to the (normal) fibre manufacturing tolerance. Single mode fibres are more susceptible to such losses. This is due to the smaller diameter of the fibre, thus a defect of a given size represents larger portions of the fibre diameter compared to the greater diameter of a multimode fibre.

Macrobending and Microbending Losses:

These losses are due to both large bends in the cable and fibre (Macrobends) and to small-scale bends in the core-cladding interface (microbends). Again, single mode fibres are more prone to this kind of loss. Careful design and installation procedures can minimize this type of loss.

4.3.2 Fibre Optic Cables Types:

Two basic types of fibre optic cable are available, single mode and multi-mode. The primary difference between these is the thickness of the fibre core. The fibre thickness affects the number of modes of light that can be transmitted through the fibre (Figure 4-1). Distributed temperature sensing systems usually use multi-mode fibres [4.9].

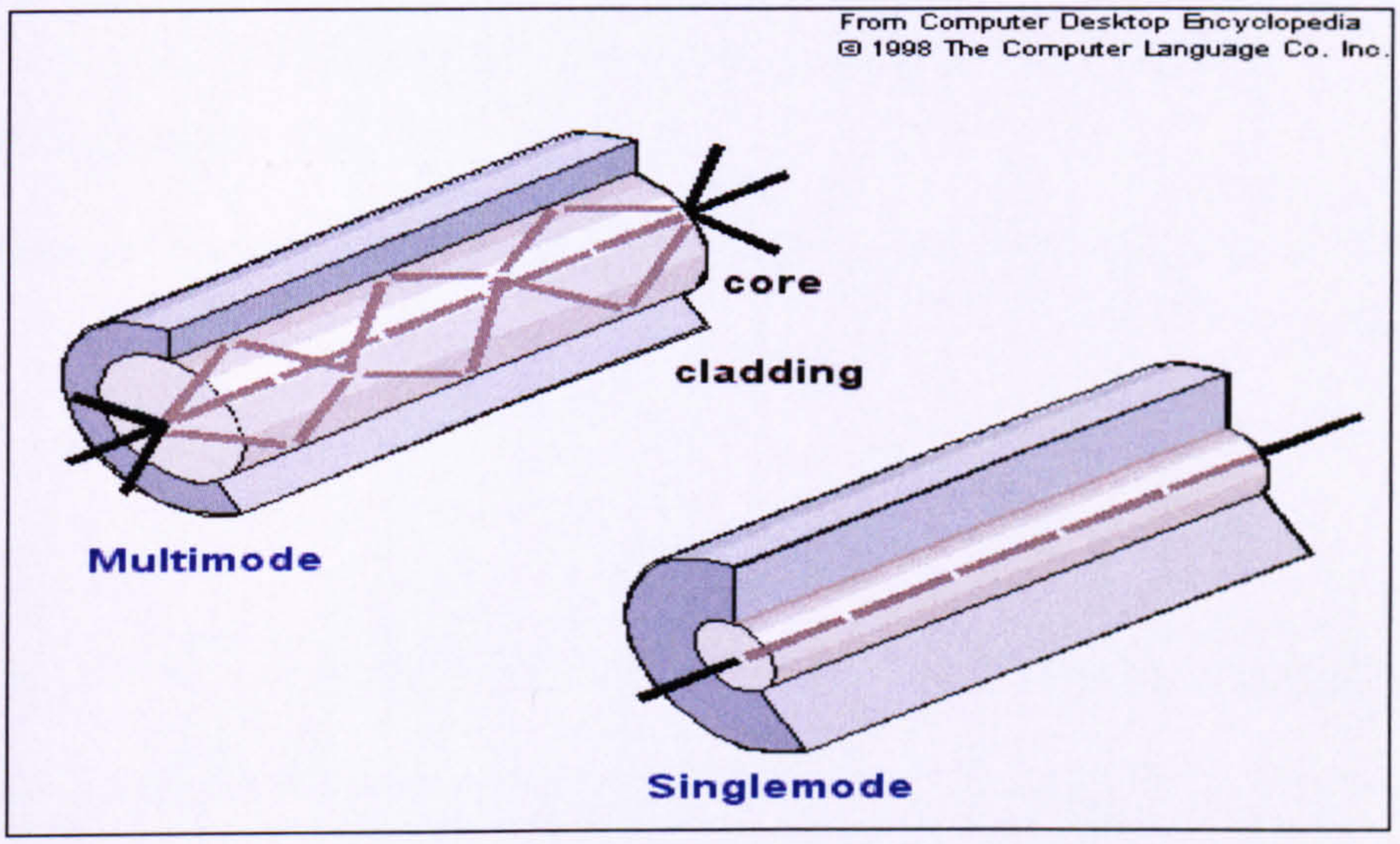

Figure 4-1. Single Mode vs. Multi-Mode Optical Fibres

The thicker core in multimode optical fibres allows the rays of light to travel along several different pathways through the fibre. The light rays are reflected both at the core and at the cladding interface. These different light pathways are referred to as the spatial modes. The small diameter core of a single mode fibre allows only one path for the light rays to travel through the fibre. Single mode fibre may have lower attenuation (loss of intensity) compared to multimode fibres [4.10]. Single mode fibres can achieve a measurement range of 30 km, but with reduced resolution due to the low level of scattering compared to the multimode fibres which limited to 15 km length but with higher resolution [4.11].

The higher losses experienced in the multimode fibre is countered by a thicker core, which allows the transmission of larger laser beam power along the fibre. This ability to transmit a larger power laser beam provide a larger threshold available for nonlinear light scattering which is essential for magnifying the signal [4.12]. This is particularly advantageous for DTS measurements because they depend on backscattered light. The greater input power results in a stronger backscattered signal, even though only a tiny proportion of the input laser signals are actually used for making the measurements.

The DTS measurement along the length of the fibre relies on the backscattered light reflected back from many points along the cable length. Backscattering is an inherent property of the fibre, being based on the interaction of the laser light with the molecular structure of the fibre [4.3]. Commercial DTS equipment employs an industrial laser to launch a ten nanosecond burst of light down the optic fibre [4.13]. The speed of light is known and is assumed constant. Hence the time delay between sending the light signal and detecting the reflected signal indicates the position along the fibre at which the backscattering occurred [4.3].

The distance of the backscatter point along the fibre may be calculated from [4.14]:

$$x = \frac{v_g t}{2} = \frac{c}{2n} t \qquad \text{Equation 4.1}$$

Where,

x = Distance along the fibre (from the source to the backscattering point)

t = Backscatter detection time (the time between the generation of the very short laser pulse and the detection of the backscatter signal)

n = the refractive index of the medium

c = the speed of light in a vacuum

v_g = the group velocity within the fibre (the velocity with which the variations in the shape of the wave's amplitude (known as the modulation) propagate through space)

The spectrum of the backscattered light is measured for each meter of the fibre length by using the time sampling technique described above. Generation of a continuous log of the spectra obtained from various points along the fibre can then be translated into a continuous temperature measurement along the fibre length. This is achieved by computing the ratio of the Raman Stokes bands (which are non-temperature sensitive) to the temperature sensitive, Raman Anti-Stokes bands (Figure 4-2). This ratio between the two bands is directly proportional to the temperature of the point along the fibre length from which the measurements were made [4.15].

The absolute temperature can now be calculated by comparing the above ratio to that measured in a second, similar (or reference) fibre at a known temperature [4.15]:

$$\frac{1}{Temp} = \frac{1}{T_{ref}} - \frac{\ln\left(\left(TTS/NTS\right)_x \left(TTS/NTS\right)_c\right)}{Sens} \qquad \text{Equation 4.2}$$

Where,

Temp = calculated temperature, K

T_{ref} = reference-coil temperature, K

Sens = temperature sensitivity factor

$\left(TTS/NTS\right)_x$ = Raman anti-Stokes/Raman Stokes ratio at the point of interest along the fibre

$\left(TTS/NTS\right)_c$ = Raman anti-Stokes/Raman Stokes ratio in the reference coil.

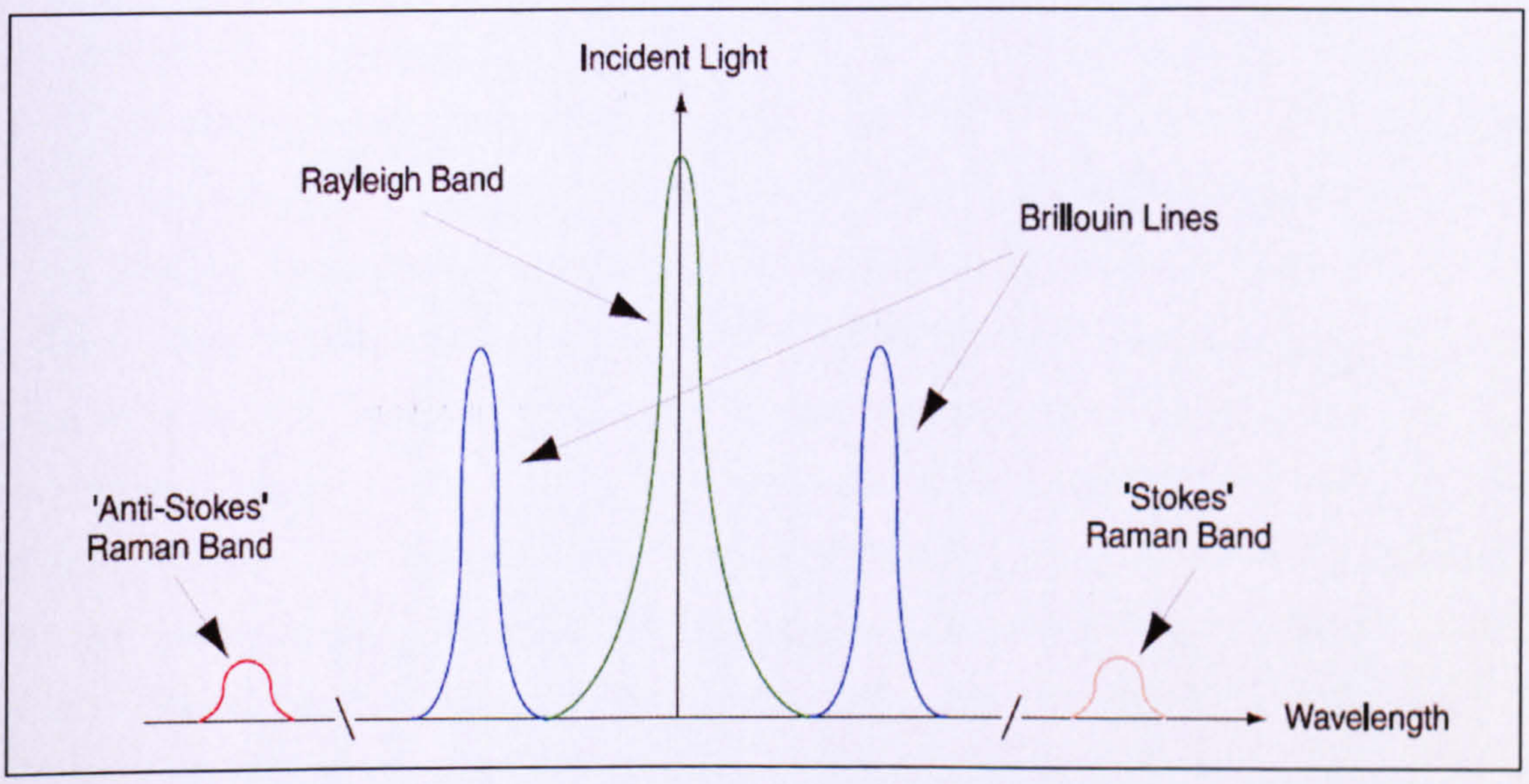

Figure 4-2. Spectra of Backscattered Light from a Point along an Optical Fibre Showing Brillouin and Raman Stokes Reflection Bands [4.15]

The main advantage of using Raman scattering as the measurement technique is its capability of self-calibration, in the case of double-ended installation of the fibre, and its low sensitivity to interference from other parameters, such as pressure and strain variation along the fibre (though this might also be considered a disadvantage if strain and pressure measurements are also desired!). An additional disadvantage of using the Raman backscattered signal that is the very weak return signal, being some 30 dB lower than the Rayleigh backscattered signal [4.14].

N.B. Rayleigh scattering (Figure 4-2) is the dominant light loss mechanism that reduces the intensity of the incident laser signal as it travels along the fibre. It results from the

non-ideal, physical properties of the fibre, such as impurities that are difficult, or sometimes, impossible to eradicate [4.6, 4.16].

Measurement acquisition time can range between a few seconds to several hours. A longer acquisition time increases the accuracy and the resolution of the resulting temperature log. A resolution of 0.1 °C at a typical measurement interval of 1.0165 m (usually shortened to 1m) is typically required for reservoir surveillance purposes since wellbore temperature changes of only few degrees centigrade have to be interpreted. DTS can achieve this resolution to a maximum fibre length of 12 km. The resolution will decrease with further increases in the fibre length. For example, a longer measurement interval of 10 m is required to achieve a similar accuracy with fibre lengths of up to 30 km [4.15].

A recent development is the application of Brillouin Optical Time Domain Reflectometry. Brillouin reflections (Figure 4-2) are caused by an interaction between the light waves and the naturally occurring, sound waves that travel within the fibre [4.17]. Such thermally generated, acoustic waves exist in all media above absolute zero (0 °K) [4.14]. Measurement and analysis of spontaneous Brillouin scattering allows the optical fibre to act simultaneously as a temperature and a strain sensor (Raman scattering is not sensitive to strain). Raman spectra were initially favoured for temperature measurement due to the relatively wide frequency separation of the Rayleigh and Raman Spectra. This larger separation simplified the technical challenge for the measurement equipment. Recent technological advances in the production of narrow band, laser light sources at commercially attractive prices and of low-loss, narrowband optical filters have made it possible for the Brillouin scattering signal to be successfully differentiated from the Rayleigh scattering signal [4.14].

The emergence of optical frequency domain reflection (OFDR) Raman scattering based DTS measurement systems is expected to increase the market for DTS since inexpensive, semi-conductor laser diodes and other electronic components for signal averaging can be employed in the signal generation and measurement equipment. This occurs because a continuously operating laser can now be employed rather than the pulsed laser source required by Raman scattering. This type of equipment has been successfully deployed in civil engineering projects e.g. long tunnels and tall buildings, where continuous monitoring of the tunnel condition is required [4.18]. A recent pilot project Brunei installed Raman OFDR based DTS systems on 8 wells along with pressure - temperature fibre optic pressure gauges [4.19].

4.3.3 Fibre Bragg Grating Sensors:

Fibre optic Bragg grating based temperature sensors are employed when higher resolution measurements are required. Higher resolution are usually required for anomaly detection such as water and gas breakthrough detection and other short term events that is important for well flow assurance.

A Bragg grating sensor is a short length of optical fibre that filters out a particular wavelength. Periodically spaced zones in the fibre core are altered to have a slightly higher refractive index than that of the core. This structure selectively reflects a very narrow range of wavelengths, while allowing the other wavelengths to be transmitted. Figure 4-3 illustrate the principle of fibre Bragg grating.

Bragg grating sensors are deployed as part of the production string and they are full-bore. Pressure/Temperature Bragg grating sensors can also be part of the multiphase fibre optic flow meter [4.20]. Since the etched gratings on the fibre are the measuring components of the sensor, careful installation practices is required to avoid damaging the gratings, in highly deviated wells, centralizers are used to avoid contact between the gauges and the casing walls [4.21].

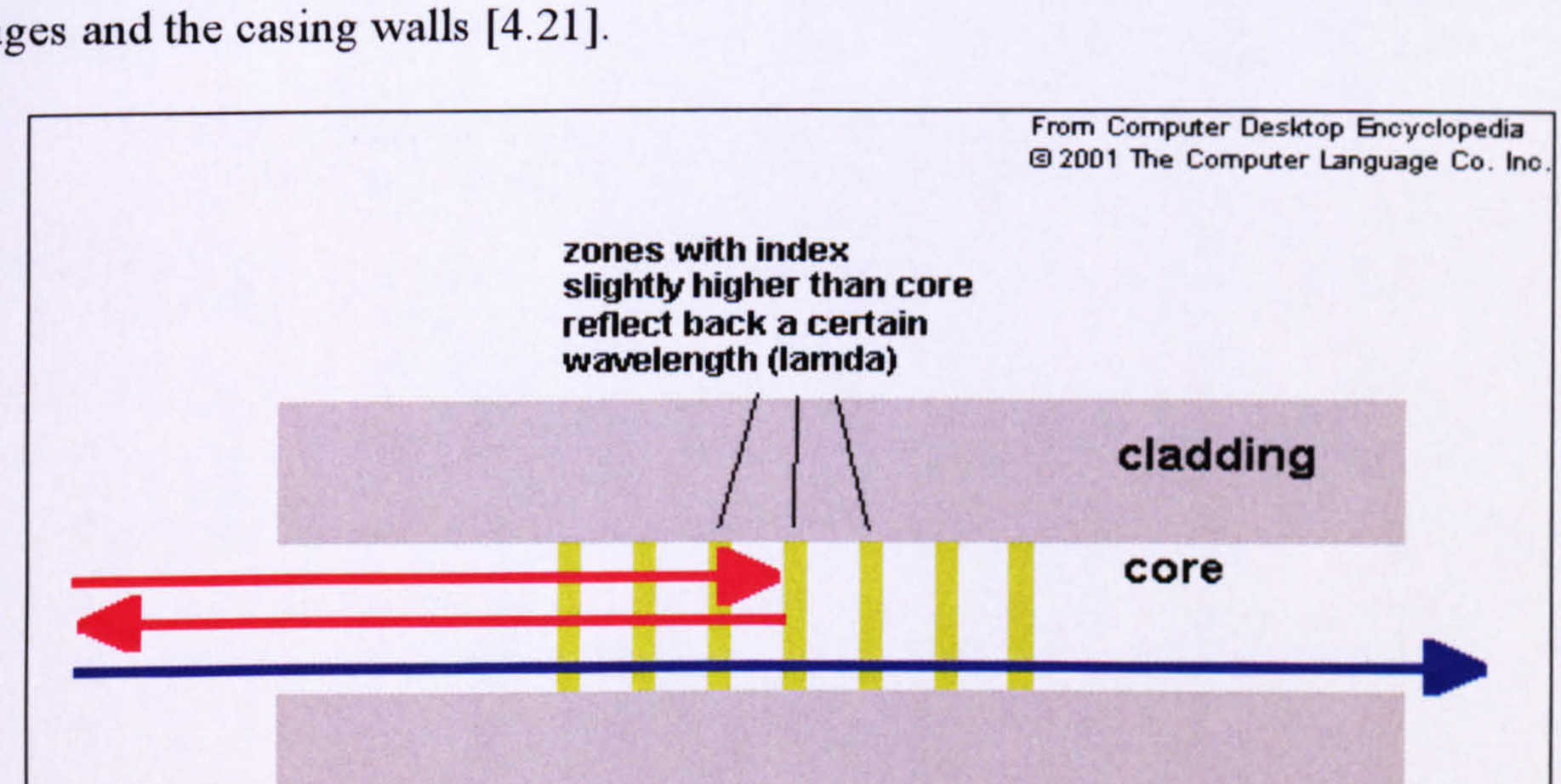

Figure 4-3. Fibre Bragg Grating Principle of operation

4.4 DTS Systems Installation Practices:

DTS optical fibre lines can be installed at different locations within the wellbore, depending on the type of completion and the required temperature measurements. For example, DTS measurements across the producing interval of a gravel packed well requires that the fibre optic is encapsulated in a control line that is placed outside both the production tubing and the sand-screen (Figure 4-4). Such wells can be found in the BP operated Azeri field development in Azerbaijan [4.4]. The flat packed, optic fibre lines are placed outside the production tubing with penetrations through the elastomer of the swell packers that will provide isolation between the four production zones. Such installation can be referred to as permanent installation.

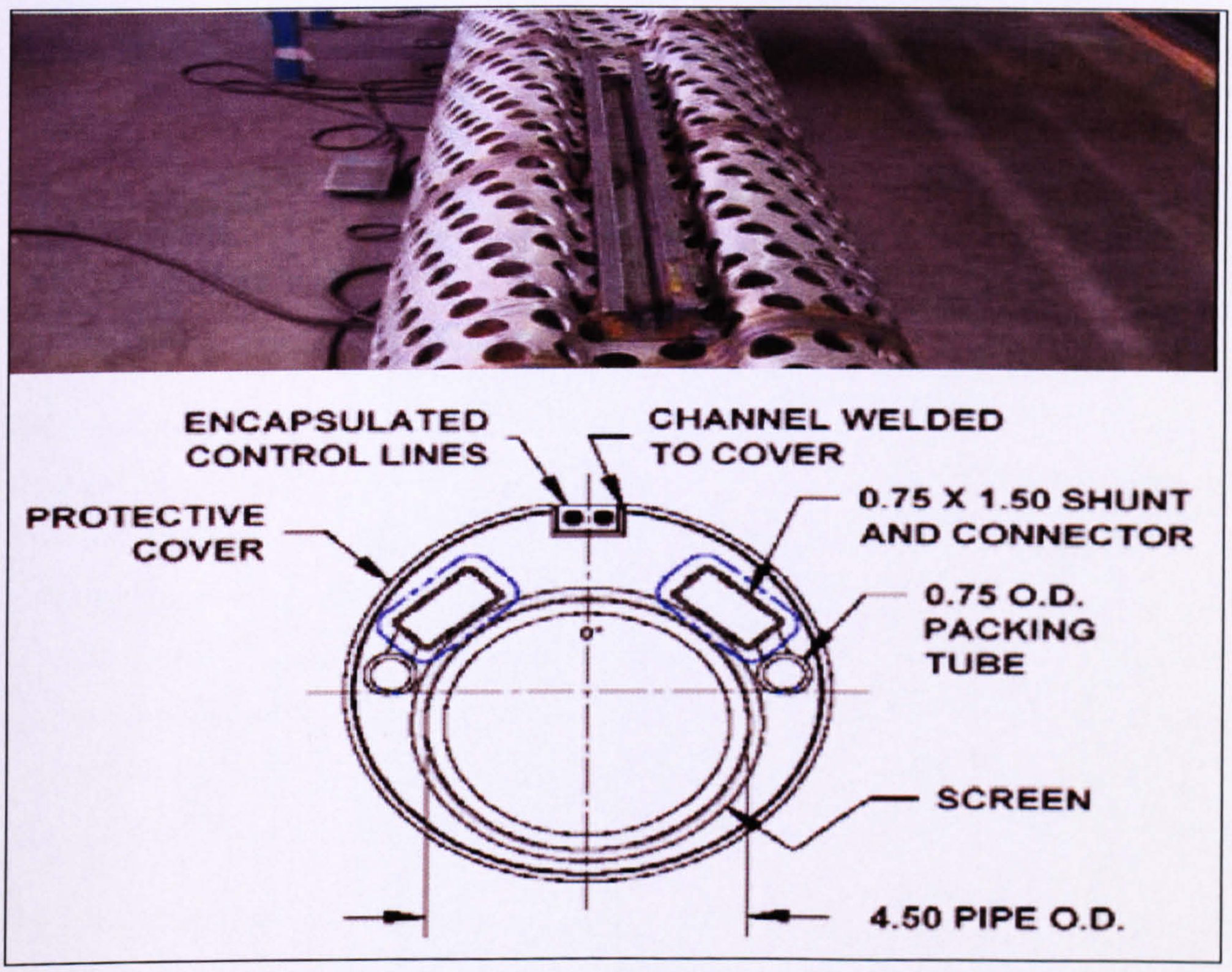

Figure 4-4. DTS in Sand-screen Completion in the BP Azeri Field Development [4.4]

Another type of installation is the semi-permanent installation, in which the fibre is "pumped-down" a capillary tube permanently attached to the tubing, the fibre can be retrieved when desired and if conditions allow such retrieval.

Installing an individual DTS cable for each well might prove uneconomical in fields that contain large number of production and injection wells which needs to be surveyed

for temperature data (e.g. monitoring steam flood operations). An alternative approach for DTS utilization employed in an Indonesia steam flood project [4.22] uses a pre-installed capillary tubing where a retrievable fibre is deployed through from the surface. The wellhead is modified to accommodate the capillary tubing and is equipped with a high-pressure relieve valve as a safety precaution in the event of steam breakthrough occurring through the capillary tubing. The fibre optic is inserted through the capillary tubing whenever a survey in a well is required and then retrieved and later deployed in another well. There are several advantages of this method in the steam-flood environment:

1. Increases the life of the fibre optic, as it minimizes the time the optic is exposed to high temperatures.
2. Reduction in the overall development CAPEX because of the reduced number of fibre cables deployed.
3. Requires less time and it is less affected by restrictions in the completion compared to the portable slick-line DTS units.

The Marco Polo field in the Gulf of Mexico is another multi-zone reservoir. The DTS system was coupled with a pressure/temperature fibre optic gauge system. Here, the DTS was run from above the production packer to the surface (i.e. DTS was not placed opposite the producing interval). An additional DTS fibre was also installed as a backup at a reported minimal, additional cost [4.5]. This case highlights the importance of defining the objective of the data gathering system. The main objective in the case of the Marco Polo field was flow assurance by monitoring the temperature profile along the tubing to avoid the formation of wax and hydrates; while gas lift surveillance was a secondary objective. By contrast, management of the Azeri field requires calculation of the flow contribution from each of the producing sand using the DTS temperature data.

One disadvantage when "pumping" the optical fibre into the well using fluid drag is that any hydraulic oil present will "wet" the optical fibres, causing it to stick to the wall of the control lines. The presence of hydraulic oil in the well can be due to several sources e.g. use of a coiled tubing to open the hydraulic isolation of an ICV [4.22]. This reference reports that complete removal of the hydraulic oil by detergent followed by flushing with water was not successful since the optical fibre was not deployed across all three zones. It is believed that the optical fibre lodged at the first ICV.

A portable (retrievable) fibre optic unit can be employed on a well-to-well basis if permanent installation of a DTS fibre optic can not be financially justified. It operates in

a similar manner to a slick-line unit. A 3/16th inch diameter tube with the optical fibre installed inside it is inserted into the well [4.13]. Temperature logs can be measured for the required period of time (e.g. to monitor any particular event or for a specific purpose such as evolution of the water injection profile over time, evaluation of the efficiency of a hydraulic fracture treatment, etc.) However, restrictions in the completion may prevent placing the optical line across the reservoir interval [4.13].

The key impediment for installation of fibre optic DTS in horizontal well is not the sensing technology but the deployment technology. Several strategies for optics deployment in horizontal wells have been developed e.g. deployment through extended tail pipe (i.e. a "stinger" completion) or through a groove in the sand-screen (N.B. the fibre cable has to be pre-attached to the completion). A clear disadvantage of the deployment of the fibre optic cable with the completion is that cable damage can only be repaired by recovering the whole completion to the surface, removing all clamps from the tubing in the process, etc. prior to replacing the cable.

4.5 Configurations of DTS systems:

DTS systems can be installed in different configurations using a range of techniques. Knowledge of the type of installation is vital for the correct interpretation of the data generated and hence to ensure accurate calculation of reservoir, tubing and/or annulus flow parameters. Two DTS wellbore configurations are available [4.15]:

4.5.1 Double Ended temperature measurement

This configuration is also called differential-light-loss-compensated temperature measurement. The optical fibre is pumped down in small-diameter tubing that was installed during the well completion process. The fibre returns to the surface via a "turn-around sub" installed at the bottom of the small diameter tubing. The measurement is made by alternately directing the laser signal into each of the two ends of the fibre optic at the surface. The Raman "Stokes" and "Anti-Stokes" spectrum is obtained for both sets of measurements. A software program geometrically averages both sets of measurements to produce a temperature trace that is automatically corrected for differential-light-losses [4.23]. These losses are attributed to manufacturing imperfections in the fibre itself or to the material used (Rayleigh or Mie scattering). The advantages of the double-ended system are mostly associated with a semi-permanent installations. It should be noted that in some instances the fibre cable does not fully return to the surface, in which case the system is called partially returned fibres.

4.5.2 Single Ended Temperature measurements:

The laser signal is now directed into the surface end of the fibre optic and the Raman "Stokes" and "Anti-Stokes" spectrum is measured for this single measurement. Any light loss due to manufacturing imperfections, etc. is now compensated for by using a differential light correction factor that assumes that the losses are constant along the fibre length.

The advantages of double ended measurement over single ended measurement are more prominent in pump-down installations and include [4.15]:

1. In the case of a semi-permanent system (pump-down), the absolute accuracy of the double-ended measurement can be determined. This is not the case for a single ended measurement due to uncertainties in knowledge of the light-loss correction factor.

2. Any such non-uniform light loss can result in apparent thermal anomalies when using single-ended measurement. These can be misinterpreted as flow or other well events.

3. Single-ended temperature measurements will apparently change over time as the loss characteristic of the fibre changes (due to new connections, reconnected fibres, different DTS measurement equipment, fibre deterioration with time, changes in the fibre environment, etc.).

4. In theory, the existing fibre can be recovered and replaced with a new, double-ended fibre; a challenge might arise if the installed fibre is stuck in the initial installation.

5. The system can be switched to act as two, independent, single-ended measurements in the case of damage or break to the double-ended DTS fibre i.e. the system integrity is maintained providing there is only one break in the fibre [4.23].

The disadvantages of a double-ended systems are [4.24]:

1. More costly (twice the length of a single-ended installation), although single ended system cost depends on the well and system configuration.

2. Cannot be used in wire-line deployments unlike the single ended system.

3. Cannot be linearly calibrated with a downhole temperature gauge.

On the other hand, the double-ended fibre configuration increases the complexity in the installation procedure; especially in highly deviated or horizontal wells. Hence it is more expensive and carries a greater installation risk. In addition, the resolution for the same acquisition time may be less than for a single end measurement due to the increased observed computational time required for the double end measurement.

The above highlights the importance of understanding the details of fibre optic technology to ensure an accurate interpretation of the measured data.

4.6 Thermal and Temporal Resolution:

Probably the most important factors concerning DTS measurements are the issues of resolution and accuracy, since temperature changes of only a few degrees centigrade can lead to radically different interpretations of the phenomenon being observed. Field experience has shown how both thermal and temporal resolution can be improved by normalizing the data at the fibre "turn-around" sub, particularly when this is placed below the reservoir [4.4, 4.25].

Application of box average statistical technique to the data can also be used to reduce the statistical noise characteristic of the measurement. A simple "box average" involves replacing each point with the average of several adjacent points. Thus, for a 5 point box average:

$$\overline{T}_{(x)} = \frac{T_{(X-2)} + T_{(X-1)} + T_{(X)} + T_{(X+1)} + T_{(X+2)}}{5} \qquad \text{Equation 4.3}$$

Bragg grating pressure and temperature sensors have an accuracy of ±2 psi and ±0.1 °C respectively with a resolution of 0.03 psi and 0.02 °C. For comparison, the DTS temperature resolution is up to 0.1 °C at a 1 meter measurement spacing [4.5]. It should be noted that conventional temperature logging instrument have a reduced absolute accuracy of ±2.5 °C, but do have an improved resolution, allowing observation of changes as small as 0.025 °C [4.1]. This is better than DTS, but slightly less accurate than that achieved by the Bragg grating temperature sensors.

The achieved temperature resolution is closely linked to the chosen measurement time, with shorter measurement times giving a reduced temperature resolution [4.15]. A sampling or measurement period of 1.5 hours has been reported as being suitable to achieve the temperature resolution discussed above [4.25]. This is a relatively long period compared to some events that occur within a well, hence short-term events (i.e.

temperature changes with a time scale shorter than the measurement period) will be missed. A long measurement time is thus typically used for flow profiling rather than for anomaly detection.

A horizontal well in a thin oil column (≈13 ft), completed with a multimode fibre-optic DTS reported temperature resolution of 0.50 °C and 0.22 °C for measurement times of 1 minute and 20 minutes, respectively [4.26]. This example highlights the impact of longer measurement acquisition time on the DTS resolution.

The depth of a particular measurement for the DTS system can be externally calibrated since it is possible to identify the exact location of the swell packers. A temperature decrease is noticed at the swell packer location due to the significantly lower thermal conductivity of the elastomer of the swell packer compared to its surrounding. The fibre measures the internal temperature of the packer rather than the flowing fluid temperature [4.4], thus providing an extra "depth calibration check" for the measured profile.

4.7 Production Management Applications:

In many wells the major objective for a DTS or a point measurement fibre optic system installation is to obtain data to be used for optimizing well production and reservoir management. Defining the planned application of the DTS fibre optic system is the first step in developing a "fit-for-purpose" system design. This includes specification of the deployment strategy. Some of the published applications of DTS systems are:

4.7.1 Cool Down Times:

DTS can provide accurate an estimation of the amount of time that a well or flowline can be left untreated during a shut-in period before hydrate or wax formation will start and flow assurance will impact future operations issues. This is particularly important for deepwater fields [4.5].

4.7.2 Diagnosis of Gas Lift Problems:

DTS data can be used to establish the required operating parameters for gas lift valves when replacing the dummy valves installed in a lower side pocket mandrel with live valves. In addition, DTS can identify the injection point of gas and whether the well has successfully unloaded to the planned injection valve. The injected gas will cool the produced fluids, a signal that can be clearly identified on DTS logs [4.5].

In addition to providing confirmation of proper valve operation, DTS can give an indication about the integrity of the gas lift completion system (e.g. a minor cooling effect above the operating injection valve location is indicative of a tubing leak [4.13]). Similarly, intermittent activity at one or more gas lift valves or continuous injection through two or more valves can be diagnosed.

4.7.3 Electric Submersible Pump (ESP) Monitoring:

Nowadays ESPs are often equipped with their own temperature gauge, the DTS can provide additional backup temperature measurement that is immune from the electrical interference of the ESP. DTS data can confirm the speed of well cleanup after the start of an ESP operation [4.27].

4.7.4 Reduce Wax or hydrate inhibitor Usage:

DTS continuously monitor temperature changes so that the exact time that inhibitor injection is needed can be identified. This is particularly important when volume of chemical usage is high or when the inhibitor has a high unit cost [4.5].

4.7.5 Water Breakthrough Detection:

Water breakthrough can be detected using temperature data since the presence of water will cause an increase in the temperature due to the Joule-Thompson effect (JTE). DTS was deployed in Douglas field [4.22] for water production management. Reservoir simulation had predicted that water cuts as high as 80% could be expected. Continuous monitoring of the temperature coupled with the ability of controlling the flow from each production zone lead to a greater oil recovery through efficient water management. It was claimed that conventional logging would not have provided such a complete picture of the well's water influx profile and would have reduced the well and field water management efficiency.

4.7.6 Gas Breakthrough Detection:

Gas influx can be efficiently detected using the principles of the Joule-Thompson coefficient, where gas is cooled upon expansion. Thus a horizontal oil production well showed a cooling of 0.75 °C at its heel because of the high GOR influx at this point due to the near wellbore pressure drop [4.25].

4.7.7 Back Flow Detection:

Low pressure zones can be detected by DTS based on back flow from surrounding high pressure zones when the well is shut-in (Figure 4-5) [4.27].

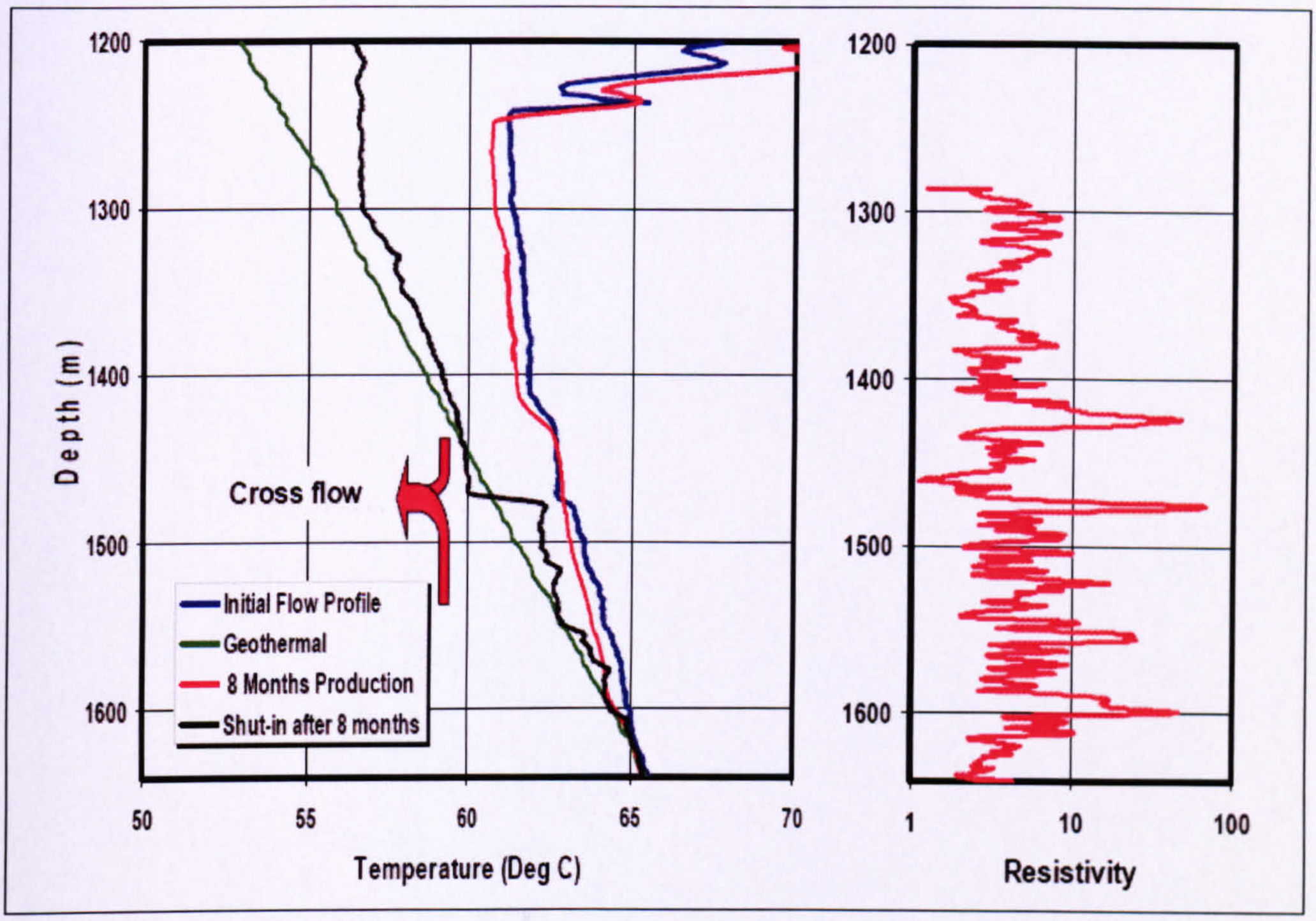

Figure 4-5. Temperature Profile Showing Back Flow on Shut-In [4.27]

4.7.8 Flow Profiling Interpretation:

DTS data can be interpreted to profile the flow from producing zones (e.g. by use of the THERMA™ software from Schlumberger or iFlow™ software from Halliburton). The concept behind the program is to compare the DTS log against the predicted temperature profile. A genetic algorithm is then used to adjust the prediction temperature profile to the DTS data by adjusting the individual layer permeability. The layer permeability values that give the best temperature comparison are thus identified and can then be used to calculate the layer flow rates [4.4].

This application of DTS data can be extended by using it to estimate the reservoir pressure at any time during the reservoir depletion process. The technique involves estimating the permeability profile during the initial stages of the well production using the techniques described above. It is then assumed that the permeability and near wellbore skin remain constant with time (i.e. they do not change due to sand failure, fines migration, scale build up, etc.). It is also assumed that all fluids properties and the

total flow rate are known from surface or other measurements. The reservoir pressure at any time can then be estimated by re-arranging the Darcy equation [4.27]:

$$P_r = P_w + \frac{Q.\left(s + \mu.\ln\left(r_e / r_w\right)\right)}{7.08(k.h)}$$ Equation 4.4

Where,

P_r = Reservoir Pressure, psi

P_w = Wellbore Pressure, psi

Q = Volumetric Flow Rate, STB/Day

S = Skin Factor, Dimensionless

μ = Viscosity, cp

r_e = Reservoir Radius, ft

r_w = Wellbore Radius, ft

k = Permeability, mD

h = reservoir thickness, ft

DTS data could then be used to determine the drawdown and skin combination that lead to the high GOR at the heel in a horizontal well [4.25]. This approach does not present a unique solution to the problem; but it does provide a good production analysis tool that can be used to manage developments within the well.

The iFlow^{TM} (by Halliburton) software is another DTS data analysis commercial package, it uses the same flow profiling procedure as the one used by THERMA (Schlumberger). Figure 4-6 shows a comparison between a constructed flow chart based on THERMA as described from published papers [4.4, 4.27] and the published flow chart for iFlow package flow profiling [4.28]. This figure show that the two packages use the same procedures for the flow profiling which is based on history matching the DTS data with the simulated/predicted temperature.

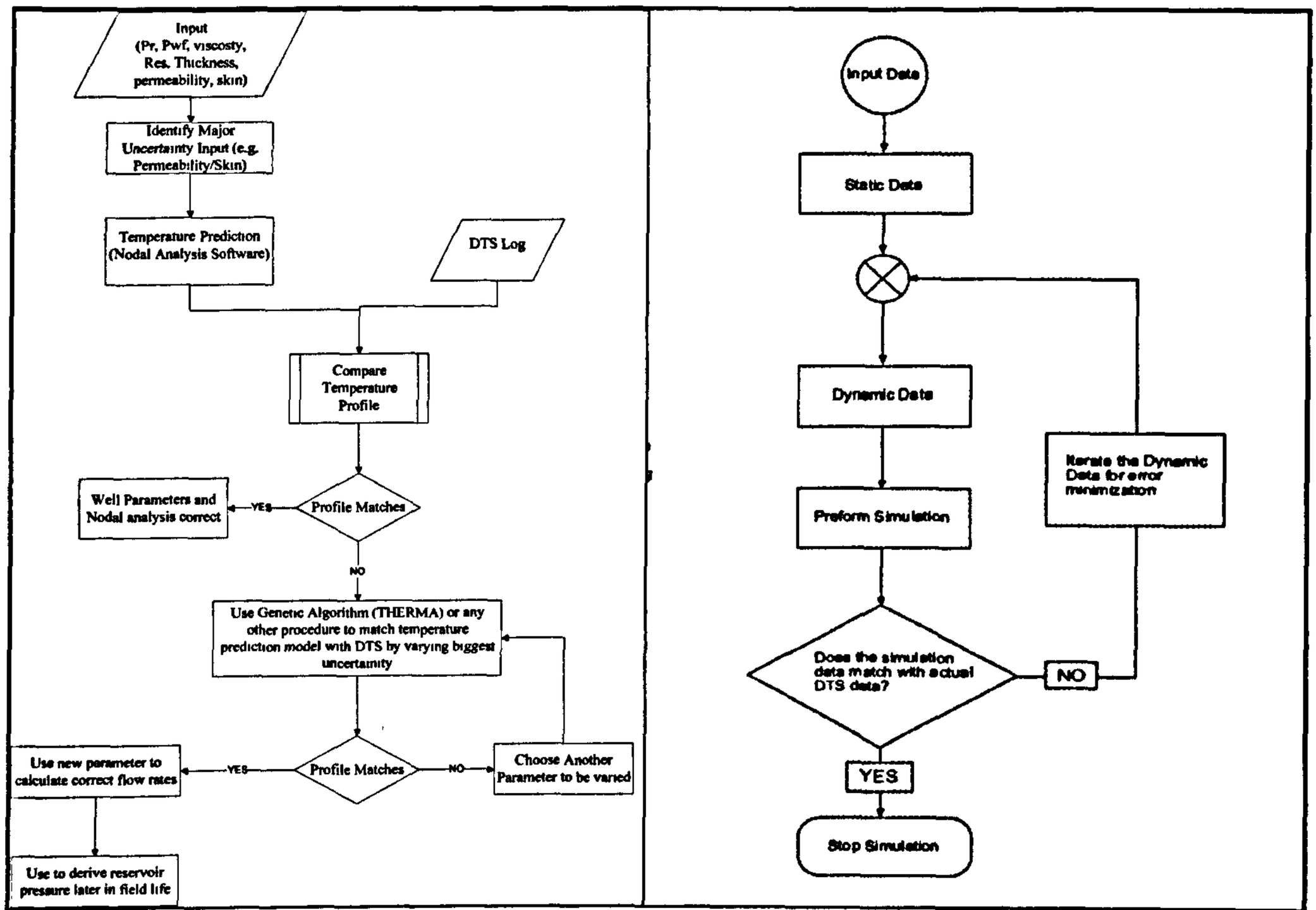

a) Temperature Profiling based on THERMA™ (inferred from 4.4 and 4.27)

b) Temperature Profiling Flowchart based on iFlow™ [4.28]

Figure 4-6. Flow Charts for a) THERMA & b) iFlow DTS Analysis and Flow Profiling Packages

The iFlow package uses the DTS data to confirm the geothermal gradient for the input into the temperature/pressure simulator. This method is based on determining the Geothermal Pivot Point (GPP). This is a depth at which the temperature of the flowing gas equals that of the geothermal gradient (i.e. the gas that cooled during flow through perforations, has gained enough temperature from the formation to be at thermal equilibrium with the formation). This idea originated from a paper by Kunz and Tixier [4.29] discussing analysis of temperature surveys in gas production wells. Identification of the GPP helps determine the thickness of the producing zones and estimate their respective contributions to the flow rate. The paper by Johnson et. al. [4.28], describing the iFlow package, only references their work in discussing the updating of the geothermal gradient by locating the GPPs. The contribution from each producing sands is said to be determined by iterating for the Joule-Thompson Coefficient and flow rate.

It is not possible to determine local oil and water flows from DTS data alone unless reservoir modelling is used to "history match" the data [4.3]. This conclusion was based on analysis of the results of simulation studies of well production and of the reservoir

performance of heterogeneous fields. Simulations of horizontal well performance indicate that DTS will not provide sufficient data for quantifying reservoir inflows.

Several studies have developed workflows for flow profiling using DTS data. Major challenges that remain still to be solved include the [4.2]:

1. Dependence of the interpretation on a number of parameters. Some of these parameters are difficult to determine with a high degree of certainty e.g. geothermal gradient, well deviation, fluid properties, wellbore completion (casing weight and size, cement, etc)

2. Correct identification of the complete oil, gas and water production zones from the temperature data; (correct rephrasing of this challenge is that the fluid entry point can be determined, but the exact length of the flow zone, especially if it is not at the heel of the horizontal well or at the top of the pay zone in a vertical or deviated well, can not be evaluated [4.30]).

3. Requirement for pressure drawdown information and well production history in addition to DTS data.

4. Difficulties in calculation of the energy balance with sufficient confidence if two-phase or multiphase flow exists, or if there is mass transfer between the phases during flow within the well.

4.7.9 Reservoir Characterization:

Reservoir layering can be inferred since the shape of the observed temperature profile will be dependent on the inflow rate and hence the reservoir characteristics.

4.7.10 Water Flooding Management:

Studies have shown that a thermal front moves from the injection well towards the producers with an average speed some 3-4 times slower than the speed at which saturation front moves through the reservoir [4.3]. This means that DTS can not, independently, be used as a monitoring tool for water flooding projects.

4.7.11 Water Injection Profiling:

DTS systems can provide useful data in injection wells. The water injection profile can be interpreted from DTS measurements by monitoring the warm-back temperature profile during a 24-hour shut-in period after water injection into the well at a variety of rates. A clear relationship between the injection rate and the injectivity profile can thus

be established. Such analyses might not work if the well was under injection for long periods due to the length of time required for the geothermal temperature front to re-establish at the wellbore. The changes in the DTS temperature profile during the shut-in period will be small in this case.

The same phenomenon will be observed if part of the completion zone has a lower permeability. The reduced injection rate into the lower permeability zone means that it will take a longer time for the temperature to change. An example of the data that can be derived from this technique is illustrated by the following field example (Figure 4-7). Temperature profiling showed that the lower perforated zone was taking the majority of the injected water [4.13] with the upper zone taking a negligible volume of the injected water at the initial well injection rate. Injection into the upper zone increased as the total well injection rate was increased. This was attributed to the elevated injection rates (and pressure) inducing a hydraulic fracture in the upper interval. The temperature warm back profile survey was then used to derive a more accurate permeability calculation using the injection conditions observed at the upper layer [4.13].

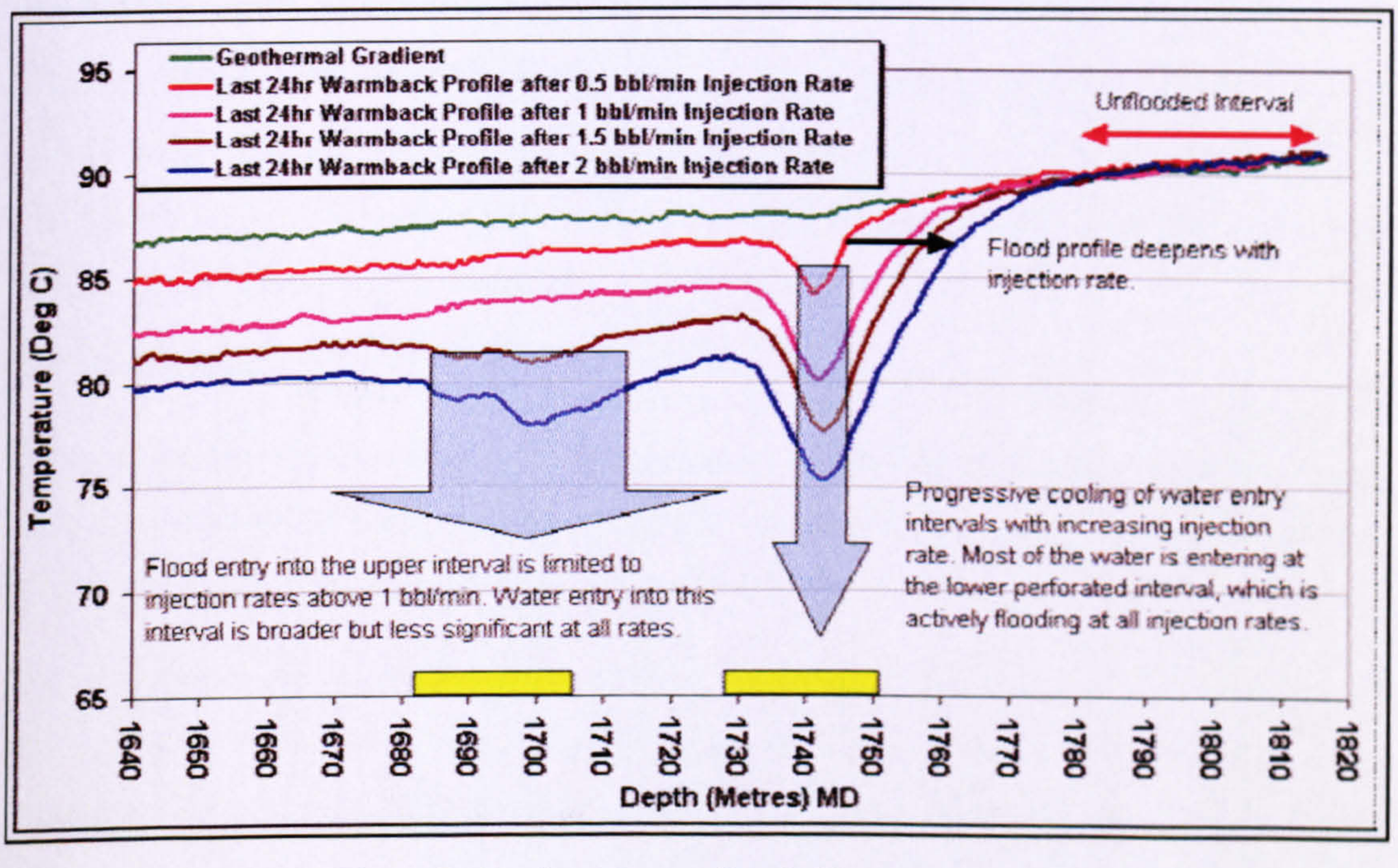

Figure 4-7. Water Injection Warm-Back Temperature Profile [4.13]

4.7.12 Steam Flood Management:

The first major application of DTS systems was in the area of steam flood monitoring. Here, temperature differences are high and are easily detected and interpreted with DTS. DTS installations in observation wells can be used to estimate formation heating rate,

steam-zone pressure, type of recovery mechanism, etc. information that will aid improved reservoir modelling of the steam flood and optimization of the oil recovery.
In addition, steam breakthrough in a producer can be determined by injecting relatively cooler water and monitoring the well during the subsequent shut-down. Also, DTS can aid in increasing the safety of steam flood operations by detecting potential shallow hazards, capable of becoming a ground eruption of steam. Another application of DTS in steam flood operation is the surveying of the injector wells to detect leaks that may lead to shallow, hot breakthroughs and the detection of cold production zones [4.31].

DTS systems have proved valuable in Steam Assisted Gravity Drained (SAGD) wells in the Joslyn field in Canada, where two horizontal wells are placed on top of each other in a 5 Darcy sand sands. Steam is injected at the upper horizontal to reduce the viscosity of Bitumen in the region between the injector and the production well [4.32]. DTS data was used to vary the injector-producer temperature to arrive at a match between the two sets of data to calculate the fluid viscosity in the region between the injector and producer. This later can be used to determine the flow distribution along the horizontal producer.

The installation of the DTS in the SAGD wells in the Joslyn field shed light on the huge temperature difference ($\approx 20\ ^{\circ}C$) that can be encountered across the wellbore of the producing wells. This was observed by accidental helical buckling of the capillary tube while reinstalling the DTS string after a workover [4.32].

4.8 Discussion

Fibre optic distributed temperature sensors offer a powerful downhole monitoring tool to the production engineer, allowing improved knowledge of the producing conditions and hence better optimisation of the well production.

The foundation for qualitative analysis of the temperature profiles was well established, during the development of the conventional production logging tool. The real-time and continuous nature of the DTS profiles gives the engineers the opportunity to infer more information about the well. The most important data required for production optimisation are the inflow rates and the detection of unwanted fluid entry. The only approach to quantify these parameters is to match the downhole temperature profile to a prediction model that resembles the well conditions as accurately as possible. One can construct reliable inflow profiles by evaluating the most likely values of the least known data; (the permeability, pressure and fluid cuts).

Therefore, it is essential to understand the temperature prediction models and the underlying heat transfer fundamentals that control the development of such models for a producing well environment.

The next chapter (Chapter 5) reviews the published steady-state temperature prediction models. It briefly reviews transient temperature prediction models and their application areas. It also discusses the Joule-Thompson effect, which has been used as the main indicator for changes in temperature profiles caused by phase changes.

4.9 References

4.1. Hill, A.D., *Production Logging - Theoretical and Interpretive Elements*: Published by Society of Petroleum Engineers in 1990.

4.2. Ouyang, L.-B. and D. Belanger. *Flow Profiling via Distributed Temperature Sensor (DTS) System - Expectation and Reality*. Paper SPE90541 presented at SPE Annual Technical Conference and Exhibition, Houston, Texas, U.S.A., 26-29 September 2004, Society of Petroleum Engineers.

4.3. Element, D.J., S.G. Goodyear, and A.J. Jayasekera. *The Use Of Distributed Well Temperature Measurements In Waterflood Management*. Paper presented at IEA Collaborative Project on Enhanced Oil Recovery 23rd International Workshop and Symposium, Caracas, Venezuela, September 2002,

4.4. Brown, G., et al. *Production Monitoring through Openhole Gravel-Pack Completions Using Permanently Installed Fibre-Optic Distributed Temperature Systems in the BP-Operated Azeri Field in Azerbaijan*. Paper SPE95419 presented at SPE Annual Technical Conference and Exhibition, Dallas, Texas, U.S.A., 9-12 October 2005, Society of Petroleum Engineers.

4.5. Weaver, M., et al. *Installation and Application of Permanent Downhole Optical Pressure/Temperature Gauges and Distributed Temperature Sensing in Production Deepwater Wells at Marco Polo*. Paper SPE95798 presented at SPE Annual Technical Conference and Exhibition, Dallas, Texas, U.S.A., 9-12 October 2005, Society of Petroleum Engineers.

4.6. Senior, J., *Optical Fibre Communications: Principles and Practice*. Prentice-Hall International series in optoelectronics: Published by Englewood Cliffs, NJ : Prentice-Hall International in 1985.

4.7. *Oxford Dictionary of Science*: Published by Oxford University Press in 2003.

4.8. Powers, J., *An Introduction to Fibre Optic Systems*. 2nd ed: Published by McGraw-Hill College in 1996.

4.9. Weatherford, *Optical Fibre Technology, An introduction to the fundamentals.*, in *Intelligent Wells*. 2002. p. 4-6.

4.10. Eriksson, K. *Fibre Optic Sensing - Case of "Solutions Looking for Problems"*. Paper SPE71829 presented at Offshore Europe Conference, Aberdeen, Scotland, 4-7 September 2001, Society of Petroleum Engineering.

4.11. Wright, P. *The Development and Application Of HT/HP Fibre-Optic Connectors For Use On Subsea Intelligent Wells*. Paper OTC15323 presented at 2003

Offshore Technology Conference, Houston, Texas, U.S.A., 5–8 May 2003, Society of Petroleum Engineers.

4.12. Sensornet *Multimode vs. Single mode Fibre for Distributed Sensing* http://www.sensornet.co.uk/index.cfm?page=99&zone=1&techtalk_id=10&tech_talk_action=view_techtalk Accessed On: 19 Feb 2007

4.13. Brown, G., et al. *Slickline With Fibre-Optic Distributed Temperature Monitoring for Water-Injection and Gas Lift Systems Optimization in Mexico.* Paper SPE94989 presented at SPE Latin American and Caribbean Petroleum Engineering Conference, Rio De Janiro, Brazil, 20-23 June 2005, Society of Petroleum Engineers.

4.14. Shahimin, M.M., *Investigation Of The Role Of Coherent Rayleigh Noise In The Accurate Determination Of The Backscattered Brillouin Signal*, in *School of Electronics and Computer Science*. 2004, Faculty of Engineering, Sciences and Mathematics, University of Southampton: Southampton, UK.

4.15. Schlumberger, *The Essential of Fibre-Optic Distributed Temperature Analysis*: Published by Schlumberger Educational Services in 2005.

4.16. Bass, M. and E.W.V. Stryland, eds. *Fibre Optics Handbook: Fibre, Devices, and Systems for Optical Communications*. McGraw-Hill Telecom Engineering. 2002, McGraw-Hill Professional. 416.

4.17. Sensornet *Measuring with light: distributed temperature AND strain sensing* http://www.sensornet.co.uk/index.cfm?page=99&zone=1&techtalk_id=6&tech_talk_action=view_techtalk Accessed On: 19 Feb 2007

4.18. Simonits, D. and A. Franzen. *Permanent Downhole Temperature Sensing - A Success Even for Low Cost Wells*. Paper presented at Intelligent Wells Asia 2006, Kuala Lumpur, Malaysia, 29-30 August 2006, IQPC.

4.19. Franzen, A. and H.d. Boer, *Low Cost Downhole Sensing: Basis for Design.* 2006, SHELL International E&P.

4.20. Kragas, T.K., et al., *Downhole Fibre-Optic Flowmeter: Design, Operating Principle, Testing, and Field Installations.* SPE Production & Facilities, 2003(November 2003): SPE87086 p. 257-268.

4.21. Kragas, T.K., et al. *Downhole Fibre-Optic Multiphase Flowmeter: Field Installation.* Paper SPE77654 presented at 2002 SPE Annual Technical Conference and Exhibition, San Antonio, Texas, U.S.A., 29 September–2 October 2002, Society of Petroleum Engineers.

4.22. Tolan, M., M. Boyle, and G. Williams. *The Use of Fibre-Optic Distributed Temperature Sensing and Remote Hydraulically Operated Interval Control Valves for The Management of Water Production in the Douglas Field.* Paper SPE71676 presented at SPE Annual Technical Conference and Exhibition, New Orleans, Louisiana, U.S.A., 30 September - 3 October 2001, Society of Petroleum Engineers.

4.23. SensaSolutions *What is Distributed Temperature Sensing?* http://www.sensa.org/userDocs/IS-TEC-Iss04-BASE.pdf Accessed On: 19 Feb 2007

4.24. Smolen, J.J. and A.v.d. Spek, *Distributed Temperature Sensing: A DTS Primer for Oil & Gas Production.* EP 2003-7100 ed: Published by Shell International Exploration and Production B.V in 2003.

4.25. Lanier, G.H. and G. Brown. *Brunei Field Trial of a Fibre Optic Distributed Temperature Sensor (DTS) System in a 1,000m Open Hole Horizontal Oil Producer.* Paper SPE84324 presented at SPE Annual Technical Conference and Exhibition, Denver, Colorado, U.S.A., 5-8 October 2003, Society of Petroleum Engineers.

4.26. Bryant, I.D., et al. *Real-Time Monitoring and Control of Water Influx to a Horizontal Well Using Advanced Completion Equipped with Permanent Sensors.* Paper SPE77522 presented at SPE Annual Technical Conference and Exhibition, San Antonio, Texas, U.S.A., 29 Sept. - 2 Oct. 2002, Society of Petroleum Engineers.

4.27. Fryer, V. *Monitoring of Real-Time Temperature Profiles Across Multizone Reservoirs During Production and Shut-In Periods Using Permanent Fibre-Optic Distributed Temperature Systems.* Paper SPE92962 presented at SPE Asian Pacific Oil & Gas Conference, Jakarta, Indonesia, 5-7 April 2005, Society of Petroleum Engineers.

4.28. Johnson, D., et al. *Successful Flow Profiling of Gas Wells Using Distributed Temperature Sensing Data.* Paper SPE103097 presented at 2006 SPE Annual Technical Conference and Exhibition, San Antonio, Texas, U.S.A., 24-27 September 2006, Society of Petroleum Engineers.

4.29. Kunz, K.S. and M.P. Tixier. *Temperature Surveys in Gas Production Wells.* Paper SPE472-G presented at AIME Annual Meeting, Chicago, Illinois, U.S.A., 13-17 February 1955, Society of Petroleum Engineering.

4.30. Yoshioka, K., et al. *Interpretation of Temperature and Pressure Profiles Measured in Multilateral Wells Equipped with Intelligent Completions*. Paper SPE94097 presented at SPE Europec/EAGE Annual Conference, Madrid, Spain, 13-16 June 2005, Society of Petroleum Engineers.

4.31. Nath, D.K., R. Sugianto, and D. Finley. *Fibre-Optic Distributed-Temperature-Sensing Technology Used for Reservoir Monitoring in an Indonesian Steamflood*. Paper SPE97912 presented at 2005 SPE International Thermal Operations and Heavy Oil Symposium, Calgary, Alberta, Canada, 1-3 November 2005, Society of Petroleum Engineers.

4.32. Krawchuck, P., et al. *Predicting the Flow Distribution on Total E&P Canada's Joslyn Project Horizontal SAGD Producing Wells Using Permanently Installed Fibre-Optic Monitoring*. Paper SPE102159 presented at 2006 SPE Annual Technical Conference and Exhibition, San Antonio, Texas, U.S.A., 24-27 September 2006, Society of Petroleum Engineers.

Chapter 5 Wellbore Temperature Modelling Review

5.1 Introduction:

The idea of value creation is the foundation of intelligent well systems application through measurement of fluid flow rates and subsequent flow control. The increasing use of the DTS systems contributes to the measurement aspect of this process. DTS make a huge amount of data available for engineers to use in several different ways (see Chapter 2). The potentially most significant application of those described in chapter 2 is the ability to infer an inflow profile so as to be able to optimise and manage production or injection in the well. The main driver of fluid flow from the reservoir to the wellbore and then to the surface is the reservoir pressure. Monitoring this by use of the temperature requires understanding the subtle heat transfer effects that occur both inside the wellbore and between the fluid and its surroundings. The "real-time" and continuous nature of the temperature log produced by the DTS system allows it to be compared with the temperature predictions derived from a nodal analysis flow processes that occur within the well. The DTS log accurately reflects the "real" temperature profile. Hence it may be used to modify the "uncertain" parameters in the well model (such as permeability, skin, pay zone thickness, etc) by improving the program's

prediction until it matches the DTS log. This calibration process (See Figure 4-6 in Chapter 4) will have increased the accuracy of the nodal analysis flow model calculations of the well production rate as well as the inflow profile under a range of well operating conditions.

Wellbore temperature modelling dates back to the early years of well logging. It was pioneered in the field by Schlumberger et. al in 1937 [5.1]. Ramey's work [5.2] on heat transport in a wellbore in 1963 was the first paper that discussed the steady state modelling of a flowing fluid within the wellbore. It spawned great interest in the study of the wellbore temperature behaviour due to its ability to shed light on field observations during drilling and production operations. Temperature data derived from production logging has traditionally been sparse since well interventions are normally infrequent; operational and economic constraints restricting the frequency of production logging. The growing deployment of downhole fibre optic temperature sensors, sometimes coupled with downhole flow control, has resulted in a step charge in the availability of temperature data and renewed interest in temperature data interpretation. Hence, attention paid to the modelling of the temperature behaviour and the in-depth study of heat transfer phenomenon inside the wellbore has increased. This chapter will review the fundamental thermodynamic and heat transfer processes related to flow in oil and gas wells. It will focus on wellbore temperature modelling, the models available in the literature and related issues.

5.2 Applications of Temperature Predictions in Production Engineering:

An accurate temperature prediction can have an important role in well design. In the 1970's arctic operations lead to the development of several wellbore thermal simulators as prediction of the flowing wellhead temperature, the extent of permafrost thaw and the subsequent freeze-back were needed for operational design [5.3]. It proved possible to replace over-conservative well designs with "Fit-for-Purpose" alternatives once confidence was achieved that these models were producing accurate predictions for temperature and pressure [5.3].

Temperature prediction models for transient conditions in multiphase pipelines have been developed to improve the pressure drop modelling and, most importantly, to minimize the risk of hydrate and wax formation [5.4]. In addition, surface temperature prediction of HPHT (High Pressure – High Temperature) condensate production is important for maximum wellhead temperature control due to Christmas tree design limitations.

Temperature prediction can also aid in drilling operations. Estimates of the circulating and the shut-in temperatures are needed for designing the thickening time and the wait-on-cement time during and after casing cementation operation. Mud viscosity, and hence friction losses and equivalent circulating densities, are a strong function of temperature; particularly in oil based systems [5.3]. Estimation of the static reservoir temperature is a necessary step for exploration wells.

Estimation of the magnitude of temperature and pressure changes are critical to tubing and casing design in terms of buckling forces. Other applications include estimation of wellhead temperature due to heat losses from the produced fluid and of downhole injection temperature since small changes in the value can affect the enhanced oil recovery. Important Hydraulic Fracture treatment parameters, such as proppant carrying capacity, leak-off, and fracture clean up are all highly dependant on the temperature.

It should be noted that many of these application involve highly transient behaviour of the temperature. A 50 °C Temperature change during drilling, cementing, fracturing and well production start-up that occurs over a time period of a few minutes are not unusual [5.4].

5.3 Wellbore Fluid Temperature Modelling Literature Review:

5.3.1 Steady State Temperature Modelling:

Temperature modelling started with Ramey's 1963 paper on "Wellbore heat transmission" [5.2]. He discussed a steady state, analytical solution to the energy balance problem for the prediction of the temperature during injection. The assumptions that Ramey used in his model are that the:

1. Physical and thermal properties of the earth and wellbore fluids do not vary with temperature.
2. Heat will transfer radially from the well in the earth
3. Heat transmission in the wellbore is rapid compared to heat flow in the formation
4. The well is vertical

The equations for the flowing fluid temperature prediction that Ramey derived from his enthalpy-energy balance are:

For Liquid:

$$T_t(z,t) = g_G Z + T_{sG} - g_G A + (T_0 + g_G A - T_{sG})e^{-z/A} \qquad \text{Equation 5.1}$$

For Gas:

$$T_t(z,t) = g_G Z + T_{sG} - A\left(g_G + \frac{1}{JC_p}\right) + \left[T_0 - T_{sG} + A\left(g_G + \frac{1}{JC_p}\right)\right]e^{-Z/A} \qquad \text{Equation 5.2}$$

Where,

A= Relaxation Distance defined by Equation 5.3, ft

$$A = \frac{wC_p[k + r_{ti}Uf(t)]}{2\pi r_{ti}Uk} \qquad \text{Equation 5.3}$$

f(t) = time function defined by

$$f(t) = -\ln\left(\frac{r_{co}}{2\sqrt{\alpha t}}\right) - 0.290 + O\left(r_{co}/4\alpha t\right) \qquad \text{Equation 5.4}$$

g_G = geothermal gradient, °F/ft

T_{sG} = Surface geothermal temperature, °F

C_p = specific heat at constant pressure of fluid, Btu/lb.°F

T_o = Surface temperature of injected fluid, °F

Z = measured well depth from surface, ft

w = fluid injection mass rate, lb/day

r_{ti} = inside radius of tubing, ft

r_{co} = outside radius of casing, ft

t = time from the start of injection/production, days

α = Thermal diffusivity of Earth, ft^2/day

O = "on the order of"

U = Overall Heat Transfer Coefficient between inside of the tubing and outside of casing based on r_{ti}, Btu/day.ft^2.°F

k = thermal conductivity of earth, Btu/day.ft^2.°F

J = Mechanical Equivalent of heat, 778 ft.lb/Btu

Ramey highlighted the significance of the overall heat transfer coefficient (U) and the time function f(t). The overall heat transfer coefficient considers the net resistance to heat flow offered by fluid inside the tubing, the tubing wall, fluids or solids in the annulus, and of the casing wall. The resistance to heat flow caused by scale or wax on the tubing or casing may also be included in addition to the effect of radiant heat transfer from the tubing wall to the casing (This subject will be explored in detail later on). In his paper Ramey's highlighted several physical phenomena that were not included E.g. expansion of gas (the Joule-Thompson Effect), heat generated by friction and heat effects linked to phase changes [5.2]. Ramey's model is still considered to be very reliable, especially for long times when the transient period has finished. Many of the later models build on Ramey's work as a foundation.

Jacques Hagoort [5.5] analyzed Ramey's work and concluded that Ramey's solution to the wellbore heat transmission problem is an excellent approximation apart from during the early transient period where the modelled temperatures are overestimated. Hagoort arrived at this conclusion after rigorously solving the tubing heat balance equation and the associated Fourier equation by using Laplace's transformation.

The heat balance equation in dimensionless form used is:

$$\frac{\partial T_{tD}}{\partial t_D} + \frac{\partial T_{tD}}{\partial x_D} = -N_{RA} \int_0^{t_D} \frac{\partial T_{tD}(\tau)}{\partial \tau} q_{uD}\left[N_{Gz}(t_D - \tau); U_D\right] d\tau \qquad \text{Equation 5.5}$$

Where,

N_{RA} = Dimensionless Ramey's Number

N_{GZ} = Dimensionless Graetz Number

T_D = Dimensionless Temperature in the Tubing $T_D = \dfrac{T - T_{top}}{T_{bot} - T_{top}}$

t_D = Dimensionless Time for convention $t_D = \dfrac{u}{L} t$

x_D = dimensionless distance from bottom of the tubing

q_u = unit heat-loss function

subscript D designates dimensionless numbers

The associated initial and boundary condition are, respectively:

$$t_D = 0: \quad T_D = 1 - x_D, \qquad \text{and}$$

$$t_D > 0,\ x_D = 0:\ T_D = 1$$

The dimensionless form of the Fourier heat conduction equation is:

$$\frac{1}{r_D}\frac{\partial}{\partial r_D}\left(r_D \frac{\partial T_{fD}}{\partial r_D}\right) = \frac{\partial T_{fD}}{\partial t_{DFo}} \qquad \text{Equation 5.6}$$

Where the initial condition is:

$$t_{DFo} = 0, r_D \geq 1 \ ; T_{fD} = 0$$

At the inner and outer boundary we have, respectively:

$$t_{DFo} > 0,\ r_D = 1: -\frac{\partial T_{fD}}{\partial r_D} = U_D(1 - T_{fD}) \qquad \text{and}$$

$$t_{DFo} > 0,\ r_D = \infty: T_{fD} = 0$$

Hagoort's inspection analysis of Ramey's wellbore heat transmission equations showed that three dimensionless numbers govern the temperature distribution in a wellbore:

The Graetz number:

$$N_{Gz} = \frac{t_{DF}}{t_D} = \frac{L\alpha}{vr_{wb}^2} \qquad \text{Equation 5.7}$$

Where,

L = Tubing Length, ft

α = Heat Diffusivity of the formation, ft^2/s

v = fluid velocity inside the tubing, ft/s

r_{wb} = wellbore radius, ft

The Ramey number:

$$N_{RA} = \frac{2kL}{\rho C_p v r_n^2} = \frac{2\pi kL}{C_p w} \qquad \text{Equation 5.8}$$

The Thermal skin factor: is the reciprocal of the dimensionless over-all heat transfer coefficient U_D and defined as:

$$U_D = \frac{Ur_{wb}}{k}$$ Equation 5.9

In addition, he confirmed that Ramey's method for estimating the overall heat transfer coefficient is good only for large values of the Fourier time.

Kabir & Hasan [5.1, 5.6, 5.7] made a significant contribution to the area of temperature modelling in wellbores. They provided a range of equations for different fluid flow situations in the wellbore (Figure 5-1). including [5.1]:

$$\frac{dT_f}{dz} = \pm\frac{1}{A}(T_f - T_{ei}) + \frac{g\sin\theta}{C_p J g_c} - \phi$$ Equation 5.10

Where,

$$\phi = \frac{v}{C_p J g_c}\frac{dv}{dZ} - \mu_{JT}\frac{dp}{dz}$$ Equation 5.11

T_{ei} = formation temperature at initial condition, °F

g = acceleration due to gravity, 32.17 ft/s^2

θ = Wellbore inclination from the horizontal, degrees

μ_{JT} = Joule-Thompson Coefficient, °F/psi

g_c = Conversion factor, 32.17 (lbm.ft)/(lbf.s^2)

p = pressure, psi

Note that the relaxation length parameter (A) parameter is the same as the one defined by Ramey in Equation 5.3. Table 5-1 lists the different assumptions used by Hasan and Kabir while developing these wellbore fluid temperature expressions.

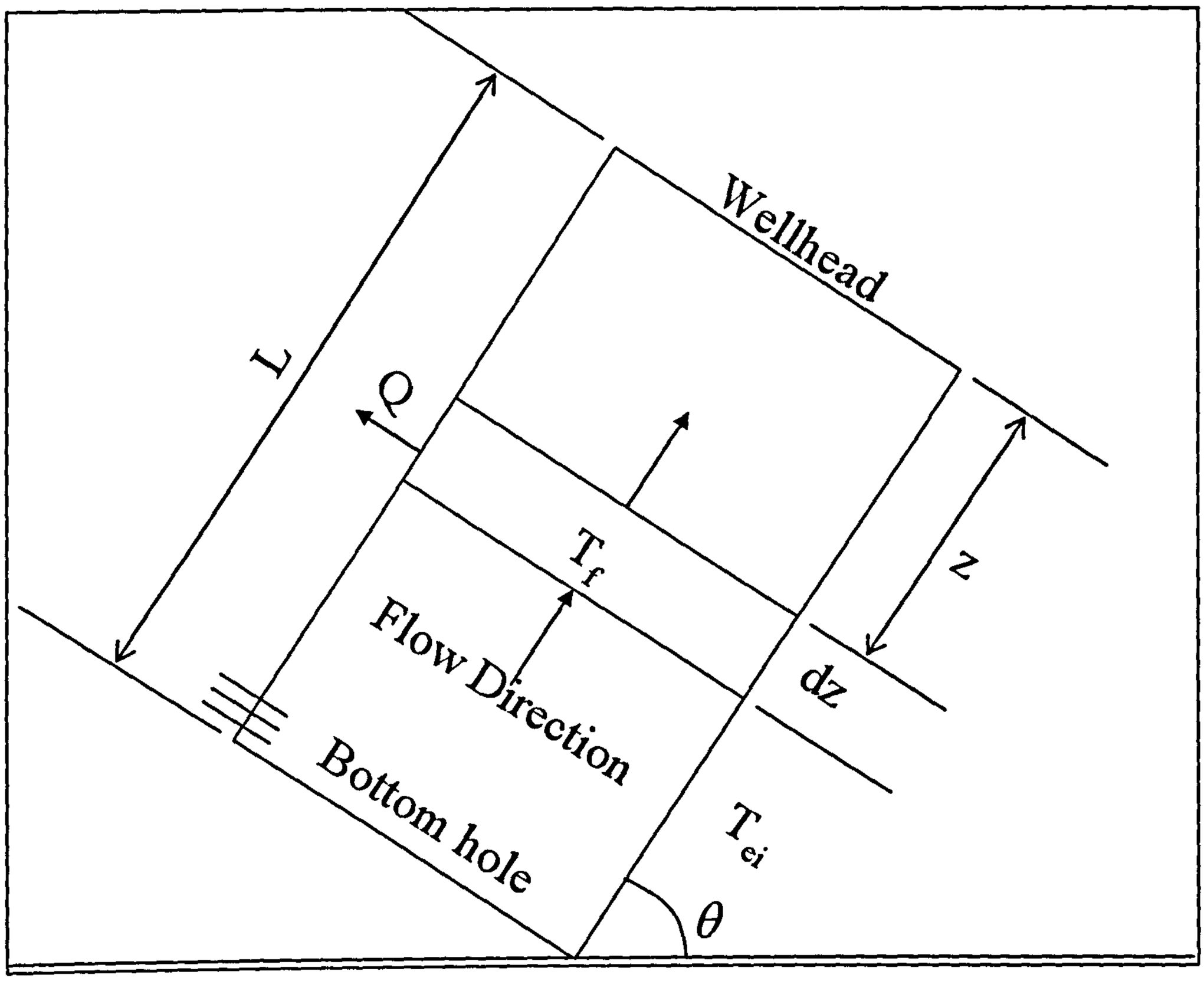

Figure 5-1. Energy Balance for Wellbore Fluid [5.1]

Table 5-1. Hasan and Kabir Wellbore Fluid Temperature Models

Case	Assumptions	Expression
Single Phase Liquid	1. Negligible fluid velocity change with depth (dv/dz) 2. Liquid density variation with pressure is usually very small➔ $\mu_J = \frac{1}{\rho c_p}$ 3. The static head loss is approximately equal the total pressure gradient ➔ dp/dz ~ ρ(g/gc)sinα 4. Relaxation Length (A) does not change with depth	$T_f = T_{eibh} - g_G \sin\theta\left[(L-Z) - A\left(1-e^{(Z-L)/A}\right)\right]$ For deep wells: $T_f = T_{ei} + g_G A \sin\theta$
Single Phase Gas	1. For gases at low pressure the term ϕ is usually small and may be neglected 2. Gas density at high pressure becomes comparable to that of liquids; use the equation for liquid temperature in deep wells	$T_f = T_{ei} + A\left(1-e^{(z-L)/A}\right)\left[g_G \sin\theta - \frac{g\sin\theta}{C_p J g_c}\right]$
Gas/Liquid Flow	1. Equation 5.10 must be solved in its entirety 2. ϕ and A are independent of well depth 3. ϕ can be determined using an empirical correlation developed by Sager et.al. [5.8]	$T_f = T_{ei} + A\left(1-e^{(z-L)/A}\right)\left[g_G \sin\theta + \phi - \frac{g\sin\theta}{C_p J g_c}\right]$

Many other models that are comparable to Ramey's solution are available in the literature. E.g. Alves et. al [5.9], proposed a general model for predicting flowing temperature distribution by applying the conservation laws of mass, momentum and energy balance to a differential control volume (dz). The differential equation for their model, without any simplifications or assumptions, is:

$$\frac{dT_f}{dz}+\frac{1}{A}T_f=\frac{1}{A}T_{ei}+\frac{1}{\rho C_p}\frac{dp}{dz}\Phi \qquad \text{Equation 5.12}$$

Where,

$$\Phi=\left(\rho\mu_{JT}C_p\frac{dp}{dz}-\rho g\sin\theta-\rho v\frac{dv}{dz}\right)\Big/\frac{dp}{dz}$$

T_{ei} = Undisturbed formation temperature, °F

Various assumptions are necessary to solve this equation analytically and arrive at an explicit expression of the flowing fluid temperature in the wellbore. The first stage of simplifying Equation 5.12 is to assume the geothermal gradient is linear:

$$T_{ei}=T_{eibh}-g_G z\sin\theta \qquad \text{Equation 5.13}$$

Where,

T_{eibh} = Static formation temperature at the bottom hole, °F

Equation 5.12 then becomes:

$$\frac{dT_f}{dz}+\frac{1}{A}T_f=\frac{1}{A}T_{eibh}-\frac{1}{A}g_G z\sin\theta+\frac{1}{\rho C_p}\frac{dp}{dz}\Phi \qquad \text{Equation 5.14}$$

The general explicit equation for temperature (Equation 5.15) can be derived by assuming that, for a certain differential segment (dz), U, c_p, μ_{JT}, g_G, θ, vdv/dZ, and dp/dz are approximately constant.:

$$T_t=(T_{eibh}-g_G z\sin\theta)+(T_i-T_{eibh})e^{-(L-z)/A}+g_G A\sin\theta[1-e^{-(L-z)/A}]+\frac{1}{\rho C_p}\frac{dp}{dZ}\Phi\Big/A[1-e^{-(L-z)/A}] \qquad \text{Equation 5.15}$$

Where,

T_i = Temperature at pipe intake, °F

L = Total Measured Depth of the Well, ft

The above assumptions imply that significant simplifications have been made. E.g. the Joule-Thompson effect (JTE) is assumed to be constant. This is not correct since the JTE can change significantly over a very small differential element for a gas system in cases where the pressure drop changes rapidly because of changes in the flow path diameter or because of the introduction of second fluid such as water. The differential element has thus to be very small to account for changes in the flow conditions from a one solution segment to the next one in order to satisfy the above assumption.

The advantage of Equation 5.15 is that, once appropriate assumptions are applied, it becomes equivalent to either the Coulter and Bardon [5.10] pipeline temperature prediction equation or to the Ramey equation [5.2]. Table 5-2 summarize the different assumptions and models derived by Alves [5.9].

Equation 5.15 is Ramey's solution for single phase liquid modified by a correction term which is a function of both the total pressure gradient (dp/dz) and of the dimensionless term Φ. The frictional pressure gradient is normally only a small fraction of the total pressure gradient in a vertical or slightly deviated well. The Φ term is small for single-phase liquid flow in vertical pipes at low flow rates and hence Ramey's solution will provide *good* results for this particular case [5.9]. Cases where Ramey's solution is less accurate are when the dimensionless term Φ is important e.g. flow conditions with a large free gas fraction, highly inclined pipes and horizontal wells where gravitational pressure drop (hydrostatic head) is reduced and large flow rates where the frictional pressure drop is no longer a small fraction of the total pressure drop.

Table 5-2. Alves et. al General Unified Model Assumptions and Explicit Temperature Expression

Case	Assumptions	Temperature Expression
Horizontal Pipe (θ=0)	- The potential and acceleration energy term can be neglected - Term $\Phi = \rho \mu_{JT} C_p$	$T_t = T_{eibh} + (T_i - T_{eibh}) e^{-(L-Z)/A} + \mu_{JT} \frac{dp}{dZ} A\left[1 - e^{-(L-Z)/A}\right]$ • Equivalent to Coulter and Bardon Equation [5.10]
Ideal Gas Flow	- Neglect acceleration term	$T_t = (T_{eibh} - g_G (L-Z)\sin\theta) + (T_i - T_{eibh}) e^{-(L-Z)/A} + g_G A \sin\theta [1 - e^{-(L-Z)/A}] + [-(1/C_p) g \sin\theta] A [1 - e^{-(L-Z)/A}]$ • Equivalent to Ramey's equation for ideal gas [5.2]
Incompressible liquid	- JTE for liquid = $\mu_{JT_L} = -1/C_{pL}\rho_L$ - Neglect friction - $\Phi = 0$	$T_t = (T_{eibh} - g_G (L-Z)\sin\theta) + (T_i - T_{eibh}) e^{-(L-Z)/A} + g_G A \sin\theta [1 - e^{-(L-Z)/A}]$ • Equivalent to Ramey's equation for incompressible liquid flow [5.2]

Sagar et. al's. [5.8] model incorporates a correlation developed with measured temperature data from 392 wells. This model was intended to simplify the complex equations usually resulting from the complex total energy balance equations previously used. The model derived using a total energy balance equation is similar to that of Ramey [5.2] and of Hasan and Kabir [5.6]:

$$\frac{dT_f}{dz} = -\frac{1}{A}\left[\left(T_f - T_{ei}\right) + A\frac{g}{g_c}\frac{\sin\theta}{JC_p} - \mu_{JT}A\frac{dp}{dz} + A\frac{vdv}{g_cJC_p}\right] \qquad \text{Equation 5.16}$$

Sagar simplified his model by assuming that the Joule-Thompson effect and the kinetic energy terms are smaller than the other terms in the equation. He combined those two terms into a single function (F_c); reducing Equation 5.16 to:

$$\frac{dT_f}{dz} = -\frac{1}{A}\left[\left(T_f - T_{ei}\right) + A\frac{g}{g_c}\frac{\sin\theta}{JC_p} - AF_c\right] \qquad \text{Equation 5.17}$$

Equation 5.17 can be integrated to provide an explicit expression for the flowing fluid temperature by assuming that the parameter F_c, the relaxation distance (A), the geothermal gradient, the specific heat C_{pm} and the inclination angle θ are all constants:

$$T_f = T_{ei} - A\frac{g}{g_c}\frac{\sin\theta}{JC_p} + AF_C + g_GA\sin\theta + e^{-(L-z)/A}\left(T_{fin} - T_{ein} + A\frac{g}{g_c}\frac{\sin\theta}{JC_p} - AF_c - g_GA\sin\theta\right) \qquad \text{Equation 5.18}$$

The development of the correlation used for calculating the F_c value in Equation 5.17 and Equation 5.18 involves the back calculation of the F_c value from Equation 5.18 to calculate an average value of F_c for each well. These were then correlated for all the wells as a function of known physical properties [5.8]. This correlation can only be used for wells with conditions falling within the range of values for oil, gas and water flow rates, gas and oil gravities, geothermal gradients, bottom-hole temperature, Gas-Oil Ratios (GORs), depths and total mass flow rate that were used in the correlation's development.

There is a further error in the F_c correlation in that the values used to derive it came from temperature logs and data from different wells. In addition to the assumption that all the wells are vertical, the assumptions made while integrating Equation 5.17 might not be applicable to the conditions within all the wells used in the correlation

development. A more accurate approach would be to use a numerical methods to solve Equation 5.17.

5.4 Horizontal & Multilateral Wells Temperature Modelling:

Horizontal wells present a unique challenge for temperature modelling and temperature data interpretation. Here the vertical depth of the well and the (geothermal) temperature of the well completion only change by a small amount along its length. Therefore temperature analysis can not use changes in the geothermal temperature as a significant variable; as is the practice in vertical wells where the geothermal temperature acts as a reference when analyzing the temperature profile. The horizontal well flow characteristics will greatly influence the temperature response in the well, so that the two main tools to analyze the temperature profile are:

1. The temperature prediction model and
2. Its relationship with time

A more rigorous temperature prediction model is required for horizontal well than that for a vertical well. It should take into account all the flow characteristics and heat transfer phenomenon that occur in the wellbore, in addition to the changes of the fluid properties along the wellbore. An example of such a model is that of Yoshika et. al. [5.11]. This is a horizontal well temperature model that couples the temperature in the reservoir with the temperature in the wellbore. In all previous temperature models only the flow in the wellbore was analyzed. Yoshika's coupled model consists of a reservoir flow model, where conservation of mass and energy is solved along with Darcy's Law, and a wellbore model that solves the conservation equations in a similar manner to the temperature models discussed previously. Yoshika's model assumed:

1. Steady-State flow
2. **Isolated reservoir segments:** each segment is completely isolated from the other segments.
3. **Single phase reservoir flow:** Multiphase flow only occurs in the wellbore as a result of the combination of single phase flows of different phases from the reservoir segments

The equation for temperature in the wellbore is:

$$\frac{dT_t}{dx} = \frac{2U_I}{r_{ti}(\rho v C_p)_T}(T_{ei} - T_t) + \frac{(\rho v C_p \mu_{JT})_T}{(\rho v C_p)_T}\frac{dp}{dx} + \frac{(\rho v)_T}{(\rho v C_p)_T} g \sin\theta \qquad \text{Equation 5.19}$$

Where,

x = Measured distance of the horizontal length, ft

$$(\rho v)_T = \sum_i \rho_i v_i y_i \qquad \text{Equation 5.20}$$

$$(\rho v C_p)_T = \sum_i \rho_i v_i y_i C_{pi} \qquad \text{Equation 5.21}$$

$$(\rho v C_p \mu_{JT})_T = \sum_i \rho_i v_i y_i C_{pi} \mu_{JT,i} \qquad \text{Equation 5.22}$$

U_I is the combined convection and conduction overall inflow heat transfer coefficient. It is defined as:

$$U_I = \gamma(\rho v C_p)_{T,I} + (1-\gamma)U \qquad \text{Equation 5.23}$$

Where:

γ = average open pipe ratio over a finite length

For reservoir temperature behaviour the model gives:

$$\rho C_p \mathrm{u}.\nabla T - \beta T \mathrm{u}.\nabla p - \nabla(K_T.\nabla T) + \mathrm{u}.\nabla p = 0 \qquad \text{Equation 5.24}$$

Where:

u = Darcy velocity vector,

β = Thermal expansion Coefficient

K_T = Thermal Conductivity

The first term in Equation 5.24 represents the thermal energy transported by convection in the reservoir, the second term refers to the thermal energy change caused by fluid expansion, the third term represents the thermal energy transported by heat conduction while the last term is the viscous dissipative heating. Equation 5.24 can be analytically solved to provide the temperature for linear and radial flow.

For linear flow:

$$T_{res} = L_1 e^{m_+ y} + L_2 e^{m_- y} + \frac{1}{\beta}$$ Equation 5.25

And for radial flow:

$$T_{res} = R_1 r^{n_+} + R_2 r^{n_-} + \frac{1}{\beta}$$ Equation 5.26

Where y is the linear coordinate and r is the radial coordinate. Details of the derivation and the parameters in Equation 5.25 and Equation 5.26 can be found in [5.11].

The coupling of the temperature in the wellbore and in the reservoir is necessary to provide a sufficiently complete representation of the effect of different phases flowing in the wellbore since the geothermal temperature gradient is no longer available as a reference. The DTS data measured in the wellbore is compared to the different temperatures predicted for different inflow scenarios. It is thus possible to determine the source of a temperature anomaly observed in the DTS data by simulating different phase flow rates within the well, different inclinations from the horizontal and different points of gas or water breakthrough. Matching the modelled results with the actual DTS temperature profile allows the modeller to gain insight into the performance of the well.

Romero et. al. [5.12] presented a model to predict the temperature in a multilateral well. Their model was based on the Ramey's model with the addition of calculation of a mixing temperature at the multilateral well junction. The algorithm employed was based on the mixing method used in conventional well logging in which the temperature at the junction is derived from an enthalpy balance at that point:

$$T_m = \frac{w_1 C_{p1} T_1 + w_2 C_{p2} T_2}{w_1 C_{p1} + w_2 C_{p2}}$$ Equation 5.27

The mixed stream mass flow rate is:

$$w_m = w_1 + w_2$$ Equation 5.28

If it is assumed the branches are producing the same fluids with the same heat capacities then:

$$\frac{w_1}{w_m} = \frac{T_m - T_2}{T_1 - T_2}$$ Equation 5.29

Equation 5.29 allows estimation of the fraction of the total flow from each lateral (N.B. this approach is also used in the Schlumberger "quick look" interpretation method for multilayer reservoirs [5.13]). The application of the mixing method described in Equation 5.29 requires that the inflow from the laterals are not at the same depth, otherwise streams would have similar temperatures, as dictated by the local geothermal temperature. A minimum difference of 0.1 °C is required to ensure detection with current sensing technology [5.13, 5.14, 5.15]. The production rate from each lateral will influence the mixing temperature; different flow rates from the two laterals will have a significantly different temperature at the junction compared to when the laterals produce similar flow rates. This is due to the effect of increased convective heat transfer at the higher flow rates. This applies to both liquid and gas wells [5.12]. The fluid composition can also affect the mixing temperature as heat conductivity is dependent on the fluid composition and the thermal diffusivity (α). This term is "the ratio of the heat conducted through the material to the heat stored per unit volume" [5.16].

$$\alpha = \frac{\text{Heat Conducted}}{\text{Heat Stored}} = \frac{k}{\rho C_p} \qquad \text{Equation 5.30}$$

N.B. Liquid water conducts heat 10 times more rapidly than oil [5.16].

Yoshika et. al. [5.17] tested the temperature prediction model for the horizontal well (Equation 5.19) with different production and completion scenarios such as open holes, cased & perforated, discontinuous perforation interval, gas and water entry and the effect of elevation. To summarize their findings:

1. The heat transfer is higher in open-hole wellbores than for perforated/slotted liner wells because the increased fluid temperature compared to the geothermal surrounding caused by large friction due to the increased wall roughness.

2. For oil wells, the temperature profile shows a greater sensitivity to the location of production zones than does the pressure profile. It is thus a useful tool for identifying the location and the length of the intervals contributing to the production.

3. The temperature profile contains more information about the water entry interval (e.g. its length) when the breakthrough occurs closer to the heel as the deviation from the single phase temperature profile will occur close to the bottom of the well.

5.5 Transient Temperature Modelling:

The models in the previous section assumed a steady-state fluid flow accompanied by unsteady-state, heat flow. However, transient temperature modelling is required for accurate predictions in many situations e.g. well start-up and shutdown. Erickson [5.4] developed a transient multiphase temperature prediction program for monitoring temperature behaviour in buried pipelines. The thermal model uses a two dimensional version of the Fourier heat conduction equations to determine how much energy is transferred to or from the soil surrounding the pipeline:

$$\rho c_p \frac{\partial T}{\partial t} = \frac{\partial}{\partial x}\left(k\frac{\partial T}{\partial x}\right) + \frac{\partial}{\partial y}\left(k\frac{\partial T}{\partial y}\right) \qquad \text{Equation 5.31}$$

The development of deep water, subsea, satellite wells has become a major application of this model. It is used to predict the time required for the pipeline to warm-up and cool down to avoid hydrate and/or wax formation.

Wellbore and formation temperature behaviour during fluid circulation in the well is also a transient phenomenon e.g. for designing cement slurries. Inaccurate wellbore temperature estimation can lead to problems such as excessive waiting-on-cement time and the drilling-out of cement-filled casing. Zhongming et. al. [5.18] presented a finite difference model that solves the governing energy conservation equations for the transient temperature profile inside the drill-pipe, the annulus, the formation and at the interface between the annulus and formation. It uses a finite difference technique and assumes that the heat transfer between the tubing and annulus is a steady-state heat flow while the heat transfer between the annulus and formation is an unsteady state process. Results from testing the model on two onshore and two offshore wells show a good agreement between the measured and the predicted temperatures. Fluid properties such as viscosity, heat conductivity and heat capacity have the greatest impact on the Bottom Hole Circulating Temperature (BHCT). The study also highlighted that the temperature predicted from a finite difference model represents the instantaneous or real-time temperature. The importance of understanding the measurement technology employed was illustrated by the need to modify the values recorded by conventional temperature gauges to allow for their thermal response time of 2 minutes or more. The measured temperature also need to be adjusted thus allowing for the intrinsic sensitivity of the gauge.

5.6 Joule-Thompson Effect:

One of the main causes of temperature change in oil and gas wells, for both production and injection wells, is the Joule-Thompson effect (JTE). This is defined as "the change in temperature of a fluid upon expansion (i.e. pressure decrease) in a steady flow process involving no heat transfer or work (i.e. at constant enthalpy)" [5.19]. Examples of such a "throttling" process are flow through a porous media, a capillary tube or a valve. The Joule-Thompson coefficient, μ_{JT}, quantifies this effect:

$$\mu_{JT} = \left(\frac{\partial T}{\partial p}\right)_H = -\frac{1}{C_p}\left[v - T\left(\frac{\partial v}{\partial T}\right)_p\right] \qquad \text{Equation 5.32}$$

Joule-Thompson coefficient is a measure of the change in temperature with pressure during a constant-enthalpy process [5.16]. Figure 5-2 illustrate when the cooling and heating occurs in a throttling process.

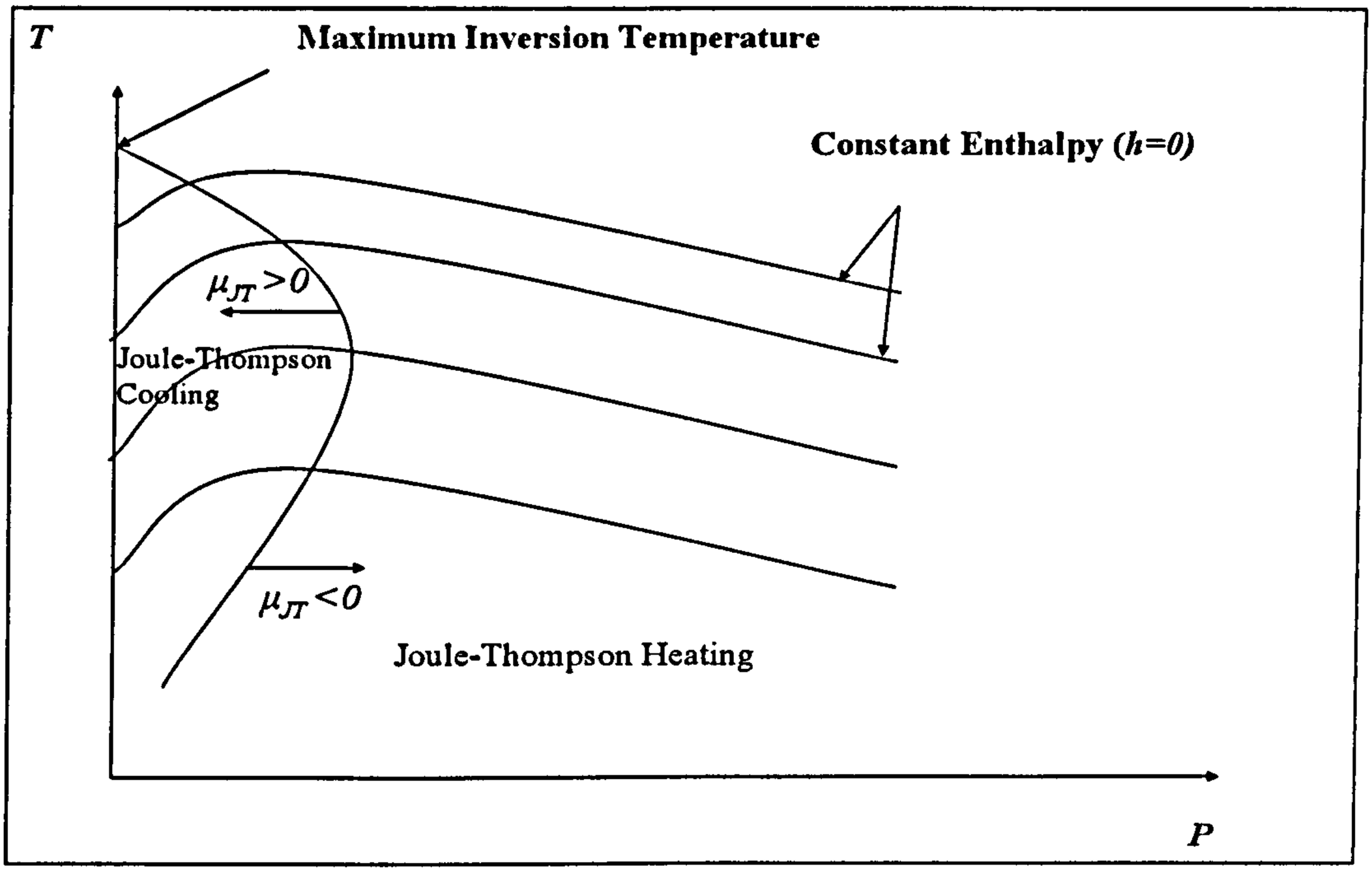

Figure 5-2. Constant Enthalpy Curves for a substance on a T-P diagram

Joule-Thompson heating is sometimes referred to as frictional heating as it is caused by the viscous dissipation of pressure during flow [5.19], e.g. water injection wells usually experience Joule-Thompson heating since a column of water increases the hydrostatic head, causing a pressure increase.

Field observations showed that Joule-Thompson cooling exists in many gas wells. This cooling effect may extend up to 50 meters into the formation after long production periods. A considerable shut-in time will be required before the original geothermal temperature is re-established [5.20].

Alves et. al. [5.9], proposed a method to approximate Joule-Thompson coefficient for black-oil systems where detailed enthalpy tables are not available. They assumed that the total enthalpy of a mixture is the sum of the enthalpies of individual phases (neglecting effects such as mass transfer, non-ideal mixing, etc.). The average Joule-Thompson coefficient is then given by:

$$\overline{\mu_{JT}} = -\frac{1}{\overline{C_p}\rho_n}\left\{y_g\left[-\frac{T}{z}\left(\frac{\partial z}{\partial T}\right)_p\right]+y_L\right\} \qquad \text{Equation 5.33}$$

Where,

Z = Gas compressibility factor

γ_g = Gas volume fraction

γ_L = Liquid volume fraction

$\overline{C}_p$ = Average heat capacity for the two-phase mixture, defined as:

$$\overline{C_p} = \left(w_g C_{pg} + w_L C_{pL}\right)/w \qquad \text{Equation 5.34}$$

Application of the average Joule-Thompson coefficient by Alves el.al [5.9] showed excellent agreement when compared to the temperatures predicted using values obtained from enthalpy tables.

5.6.1 JTE for Water Flow:

Water flow is considered to be an incompressible flow. The liquid volume fraction (γ_L) will have a value of unity when the gas volume fraction (γ_g) is equal to zero. Equation 5.33 can then be reduced to:

$$\mu_{JT} = -\frac{1}{c_{pw}\rho_w} \qquad \text{Equation 5.35}$$

For field units:

$$\mu_{JTw} = -\frac{144}{JC_{pw}\rho_w}$$ Equation 5.36

The Joule-Thompson coefficient will be ≈ -3.3 °F/1000psi, assuming the water has a density of 62.38 lbm/ft^3 and a specific heat value of 0.9 Btu/(lbm.°F). This implies that the temperature of the water will increase by almost 3 °F for a pressure drop of 1000 psia. Such pressures drops and the consequent temperature change, are rarely encountered in production wells.

5.6.2 JTE for Oil Flow:

The density of the oil at reservoir conditions is a function of the temperature and pressure [5.21]. Therefore, the Joule-Thompson coefficient will vary with different temperatures:

$$\mu_{JTo} = -\frac{144}{JC_{po}(T)\rho_o(T)}$$ Equation 5.37

The heat capacity for crude oil can be estimated from the correlation developed by Gambil [5.22]:

$$C_{po} = \frac{(0.388 + 0.00045T)}{\sqrt{\gamma_o}}$$ Equation 5.38

Where,

γ_o= Specific Gravity of Oil

Figure 5-3 was constructed by using the values of the oil density and the heat capacity as a function of temperature in Equation 5.36.

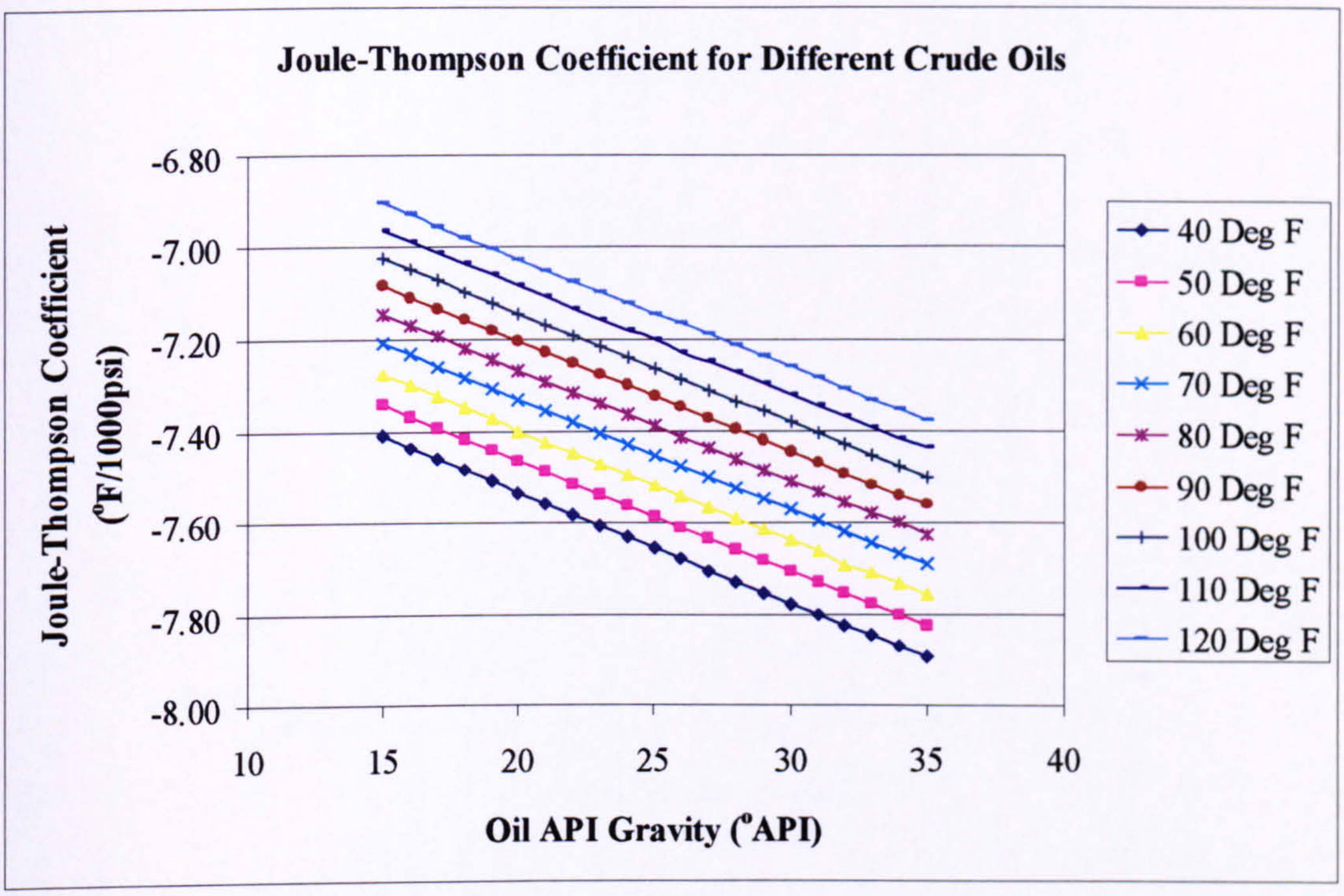

Figure 5-3. Joule-Thompson Coefficient for Different Oil Densities (Densities vs. Temp. from [5.23])

For a constant value of oil gravity the temperature rise caused by the Joule-Thompson effect will increase with increasing temperature and at constant temperature the temperature rise will be greater for the less dense oil (higher API oil gravity).

5.6.3 JTE for Hydrocarbon Mixtures

Equation 5.33 requires that the z-factor at both the producing temperature and pressure have to be calculated in addition to the rate of change of the gas compressibility with the temperature (dz/dT). To examine the effect of the introduction of gas, a sensitivity on the effect on the Joule-Thompson coefficient of increasing the gas volume faction (γ_g) for a constant pressure and temperature of 2000 psia and 150 °F, respectively was studied (Figure 5-4). This figure shows that at low gas volume fraction the fluid will experience heating rather than cooling when it is expanded. Cooling is observed once the gas volume fraction becomes higher than 25%. This is a crucial observation for the application of DTS to detect gas production in oil producing wells.

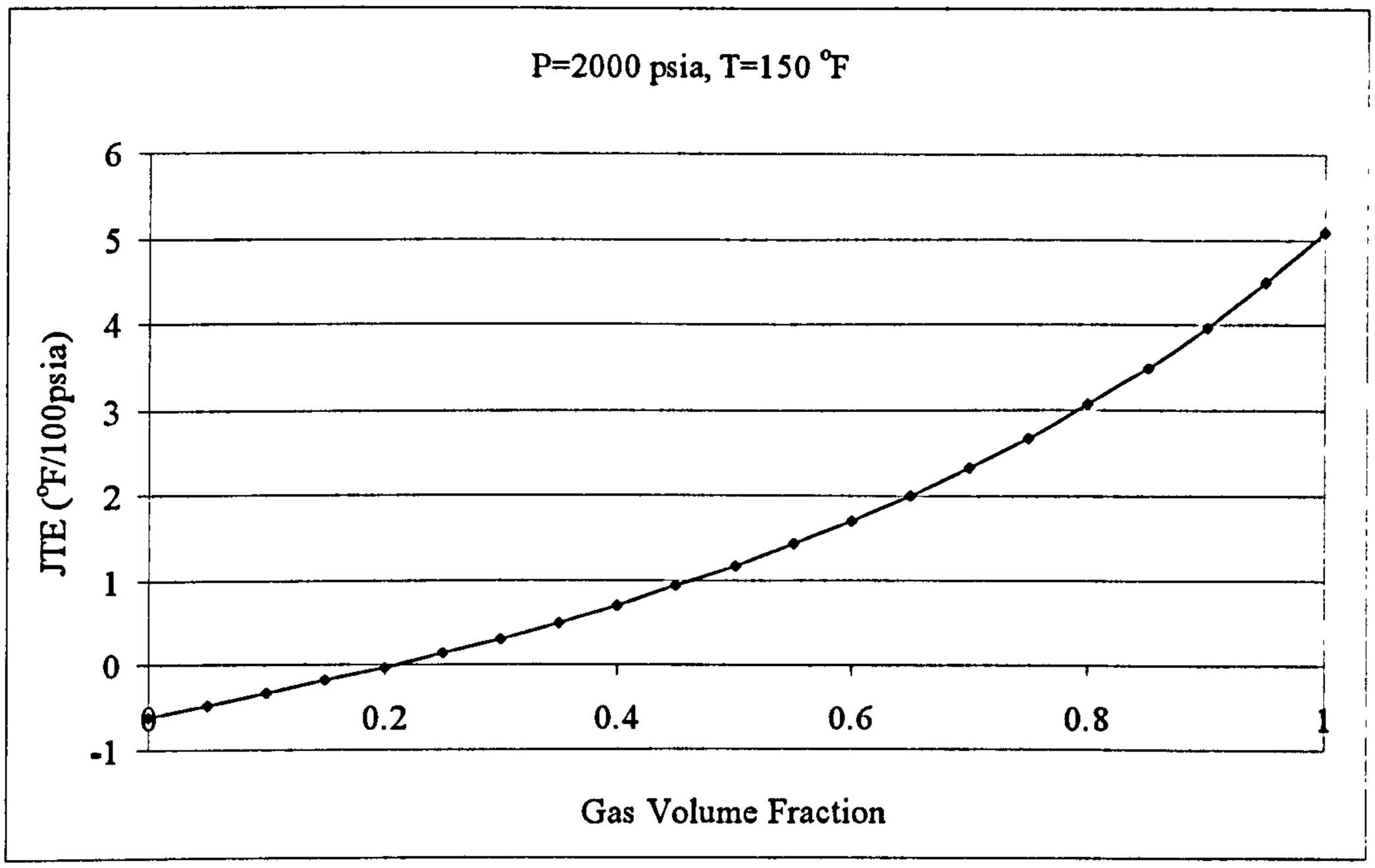

Figure 5-4. Effect of Increasing Gas Production on a Hydrocarbon Mixture

5.7 Temperature Modelling Issues in Intelligent Wells

5.7.1 Convection Phenomenon in Wellbore:

Intelligent well completions allow simultaneous flow in the annulus and in the tubing. Heat transfer caused by convection between the two flow streams is a very important issue. Heat transfer occurs in three forms:

1. *Conduction:* the mechanism of heat transfer through a solid or a quiescent fluid.
2. *Convection:* the mechanism of heat transfer through a fluid in the presence of bulk fluid motion.
3. *Radiation:* is the energy emitted by matter in the form of electromagnetic waves (or photons) as a result of the changes in the electronic configurations of the atoms or molecules.

Conductive heat transfer between the tubing and annulus occurs when the well is produced through the tubing and while the annulus is filled with a static fluid. The type of fluids and their thermal conductivity will dictate the rate of heat transfer between the annulus and the tubing. Also, conductive heat transfer is very important when studying temperature behaviour in buried pipelines [5.4]. Fourier's first law of conduction

governs the relationship between the rate of heat transfer by conduction, the thermal conductivity and the temperature difference:

$$\dot{Q}_{cond} = -kA_s \frac{dT}{dx} \qquad \text{Equation 5.39}$$

Where,

A_s = Surface Area, ft^2

x = distance

Convection involves the combined effect of conduction and fluid motion and can be classified as natural (free) convection or forced convection. Forced Convection occurs when the fluid is forced to flow across a surface by an external means, such as a fan, a pump or the wind. Natural (free) convection occurs if the fluid motion is only caused by buoyancy forces induced by density differences due to the variation in the temperature of the fluid. Convective heat transfer is a more complex process than the conduction, due to the parameters involved. The rate of convection heat transfer ($\dot{Q}_{conv}$) is expressed by Newton's law of cooling:

$$\dot{Q}_{conv} = hA_s(T_s - T_\infty) \qquad \text{Equation 5.40}$$

Where,

h = Convection heat transfer coefficient, $Btu/(hr.ft^2.{}^\circ F)$

T_s = Tubing Surface Temperature, °F

T_∞ = Temperature of the fluid sufficiently far from the surface of the tubing (e.g. T_{ci}), °F

The convection heat transfer coefficient (h) is not just a fluid property but depend on variables such as the surface geometry, the nature of the fluid motion, the fluid velocity as well as the properties of the fluid. Convection greatly influences heat transfer within the wellbores, especially when flow is simultaneously occurring in the annulus and in the tubing (e.g. gas lift operations, annulus/tubing production).

Forced convection is also classified into two categories, depending on the type of boundary layers that exists in the system. External forced convection is characterized by the freely growing boundary layers surrounded by a free flow region that involves no

velocity and temperature gradient. A typical example of external forced convection is flow over flat plates and flow across cylinders and spheres. For internal forced convection, the fluid is confined by the inner surfaces of the tube and there is a limit on the extent of the boundary layer (Figure 5-6). The boundary can not grow indefinitely, unlike external forced convection (Figure 5-5). Examples of internal flow that causes internal forced convection are flow in pipes and heat exchangers.

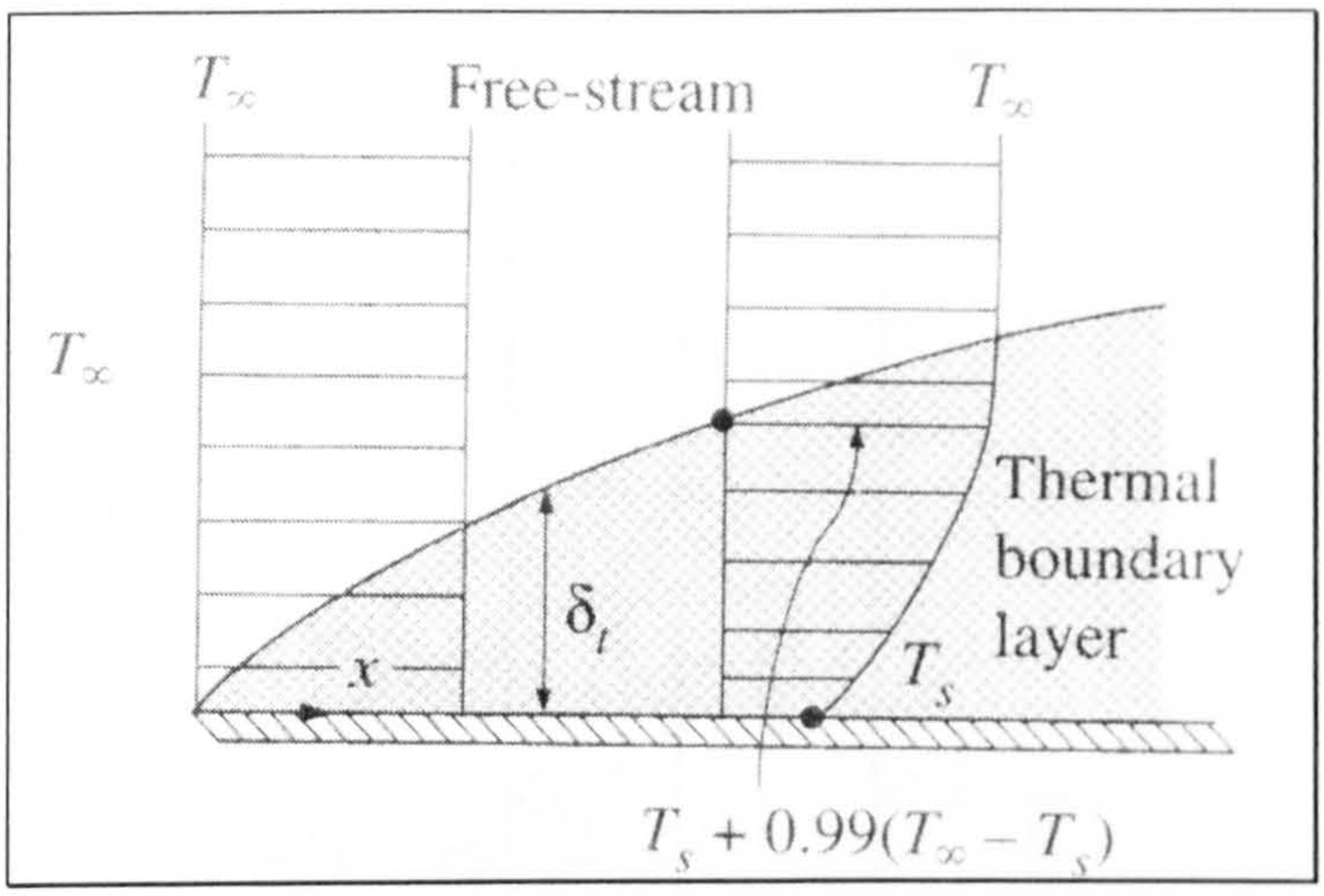

Figure 5-5. Thermal Boundary Development in External Forced Convection [5.16]

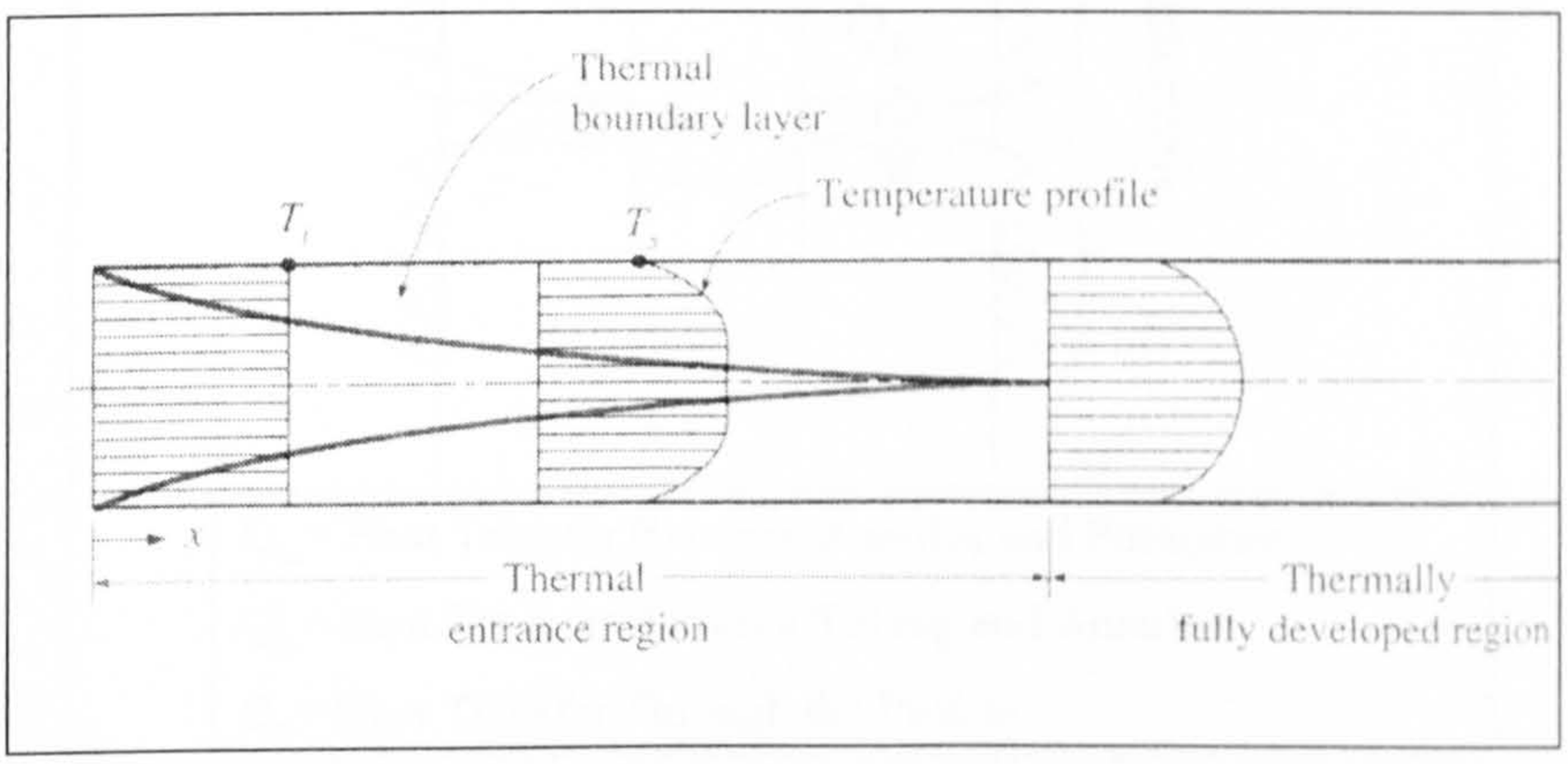

Figure 5-6. Thermal Boundary Development in Internal Forced Convection [5.16]

5.7.2 Temperature Modelling Issues in Intelligent Wells:

Intelligent completions involve complex wellbores geometries, increasing the number of parameters that affect the heat transfer in the well. For example, in the case of a multilayered reservoir, fluids can have different physical and thermal properties. There will be multiple inflows into the wellbore, with different flow rates and characteristics depending on the number of zones controlled by the intelligent completion. Also, the completion equipment, such as ICVs and packers, will complicate the calculation of the

overall-heat transfer coefficient. The simultaneous flow in the annulus and in the tubing is the greatest complication that the intelligent completion adds to the temperature prediction in the well. Heat transfer will occur between the formation and the annulus and between the annulus and the tubing. In addition, heat transfer can occur between the fluids in the annulus and through the packers in the time period before the fluids flows into the tubing (Figure 5-7).

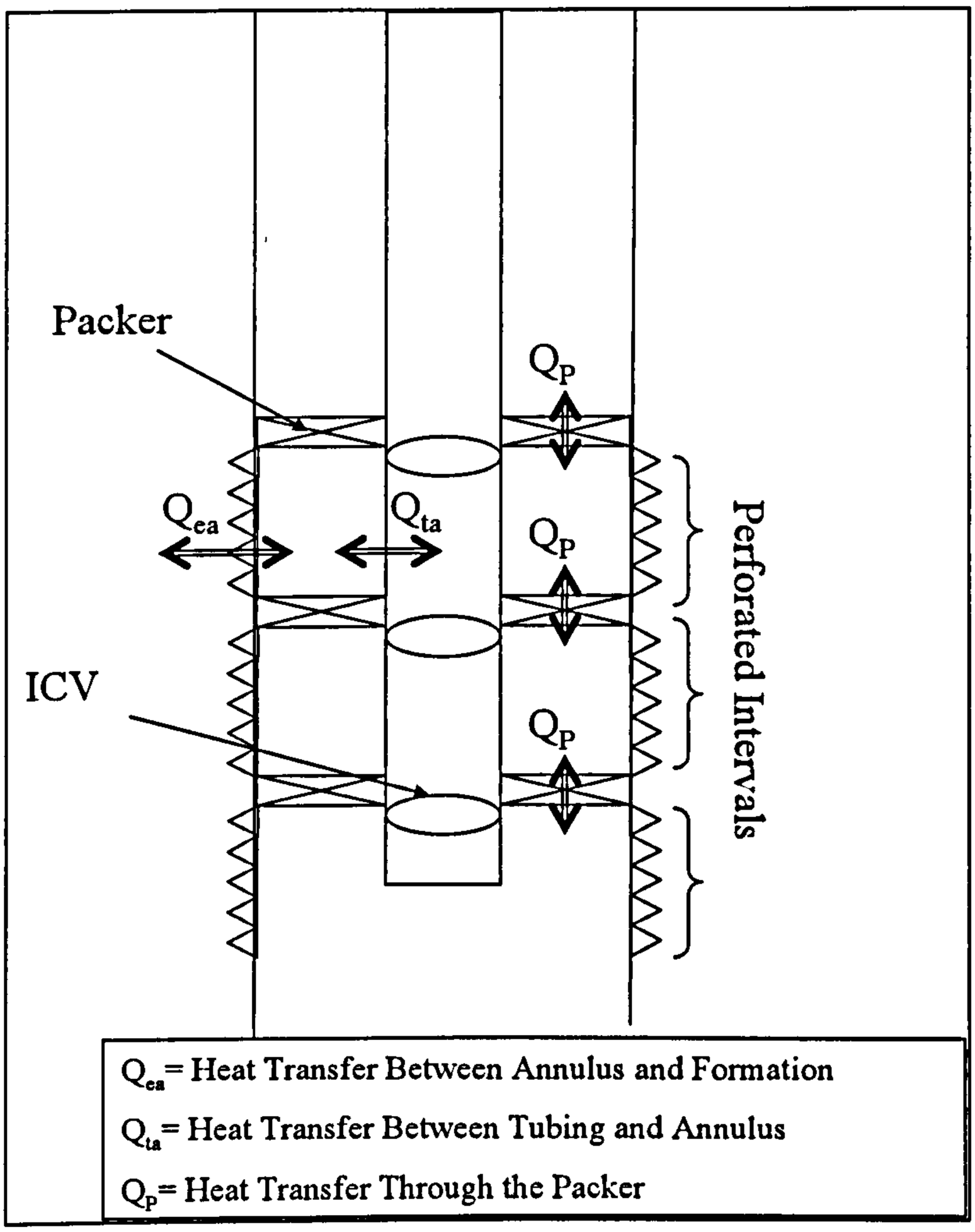

Figure 5-7. Heat Transfer in an Intelligent Completion

The majority of temperature prediction models calculate the flowing temperature in the tubing. Predicting the temperature in the tubing has wide application especially in the area of flow assurance (e.g. hydrate and wax management), but may not be sufficient for inflow profile analysis based on DTS temperature data. The DTS fibre optic is usually installed outside the tubing or in the grove on the outside of the sandscreen. The temperature profile in the annulus will thus need to be calculated. Hasan and Kabir [5.1, 5.24] developed a model that will predict the temperature profile for simultaneous flow

in the annulus and tubing. It takes into consideration the formation-annulus and annulus-tubing heat transfer. The differential equations for the tubing temperature (T_t) equivalent to (T_f) are:

$$-AB'\frac{d^2T_t}{dz^2}+B''\frac{dT_t}{dZ}-T_t+T_{es}+g_G Z\sin\theta+D'=0 \qquad \text{Equation 5.41}$$

Where,

T_{es}= the geothermal temperature at the surface, °F

For the temperature in the annulus T_a:

$$\frac{dT_a}{dz}=-\left(\frac{1}{A}\right)(T_{ei}-T_a)+\frac{1}{B_a}(T_a-T_t)-\frac{D_a}{C_{pa}} \qquad \text{Equation 5.42}$$

The analytical solution to the above differential equations results in very complicated equations that involve many of parameters that are required to account for the heat transfer between the annulus and the tubing. Nevertheless, it is expected to play an important role in the analysis of DTS data from intelligent wells since flow in the annulus will cause a lower temperature in the tubing due to accelerated heat transfer caused by forced convection.

5.8 Conclusion and Discussion:

This chapter show that temperature modelling for the flowing wellbore fluid uses the same principles of energy, mass and momentum balance for vertical and horizontal wells. Most steady-state temperature prediction models uses Ramey's approach to heat transmission in wellbore, thus the relaxation parameter *(A)* appears in almost all the subsequent models; though these models differ in some of the assumption used.

The Joule-Thompson effect range of values under various production conditions have been examined. Presence of gas can cool the temperature of the produced fluid; but this requires a certain percentage of gas to be flowing with the liquid. Large pressure drop is required before significant Joule-Thompson heating can occur in two-phase oil and water wells.

Understanding the heat transfer phenomena and the available models is important to accurately model and capture the temperature profile in intelligent wells. Only Hasan and Kabir tackled the modelling of the temperature in a well with annulus and tubing

production. This model forms the basis of a detailed study of the complexity heat transfer and flow behaviour in intelligent completions and the resultant temperature prediction profiles.

The next two chapters (6 & 7) will use Hasan & Kabir (H&K) models to investigate the possibility of detecting scale in a conventional well using DTS (Chapter 6). In Chapter 7 modifications will be proposed to the solution for H&K model for temperature prediction in annular and tubular flow to accommodate the complexities of an intelligent completion well. This chapter will also investigate the detection of water cut in multizone intelligent wells.

5.9 References

5.1. Hasan, A.R. and C.S. Kabir, *Fluid Flow and Heat Transfer in Wellbores*: Published by Society of Petroleum Engineering in 2002.

5.2. H.J. Ramey, J., *Wellbore Heat Transmission.* Journal of Petroleum Technology, 1962(April 1962): SPE96 p. 427-435.

5.3. Mitchell, R.F. and I. H. F. Wedelich. *Prediction of Downhole Temperatures Can Be Key for Optimal Wellbore Design.* Paper SPE18900 presented at SPE Production Operations Symposium, Oklahoma City, Oklahoma, U.S.A., 13-14 March 1989, Society of Petroleum Engineers.

5.4. Erickson, D.D. and M.C. Mai. *A Transient Multiphase Temperature Prediction Program.* Paper SPE24790 presented at SPE 67th Annual Technical Conference and Exhibition, Washington, DC, U.S.A, 4-7 October 1992, Society of Petroleum Engineers.

5.5. Hagoort, J., *Ramey's Wellbore Heat Transmission Revisited.* SPE Journal, 2004(December 2004): SPE87305 p. 465-474.

5.6. Hasan, A.R. and C.S. Kabir, *Aspects of Wellbore Heat Transfer During Two-Phase Flow.* SPE Production & Facilities, 1994: SPE22948 p. 221-216.

5.7. Hasan, A.R. and C.S. Kabir. *Heat Transfer During Two-Phase Flow in Wellbores: Part I - Formation Temperature.* Paper SPE22866 presented at 66th Annual Technical Conference and Exhibition of the Society of Petroleum Engineers, Dallas, Texas, U.S.A., 6-9 October 1991, Society of Petroleum Engineers.

5.8. Sagar, R. and Z. Schmidt, *Predicting Temperature Profiles in a Flowing Well.* SPE Production Engineering, 1991: SPE19702 p. 441-448.

5.9. Alves, I.N., F.J.S. Alhanatl, and O. Shoham, *A Unified Model for Predicting Flowing Temperature Distribution in Wellbores and Pipelines.* SPE Production Engineering, 1992(November 1992): SPE20632 p. 363-367.

5.10. Coulter, D.M. and M.F. Bordon, *Revised Equation Improves Flowing Gas Temperature Prediction.* Oil & Gas Journal, 1979(February 26, 1979): p. 107-108.

5.11. Yoshioka, K., et al. *A Comprehensive Model for Temperature Behaviour in a Horizontal Well.* Paper SPE95656 presented at SPE Annual Technical

Conference and Exhibition, Dallas, Texas, U.S.A., 9-12 October 2005, Society of Petroleum Engineers.

5.12. Romero, A., D. Zhu, and A.D. Hill. *Temperature Behaviour in Multilateral Wells: Application to Intelligent Wells*. Paper SPE94982 presented at SPE Latin American and Caribbean Petroleum Engineering Conference, Rio De Janiro, Brazil, 20-23 June 2005, Society of Petroleum Engineers.

5.13. Schlumberger, *The Essential of Fibre-Optic Distributed Temperature Analysis*: Published by Schlumberger Educational Services in 2005.

5.14. SensaSolutions *What is Distributed Temperature Sensing?* http://www.sensa.org/userDocs/IS-TEC-Iss04-BASE.pdf, accessed: 23-May-2007

5.15. Sensornet *Sentinel DTS Product Range* http://www.sensornet.co.uk/download.cfm?type=document&document=112, accessed: 23-May-2007

5.16. Cengel, Y.A., *Heat Transfer - A Practical Approach.* Second ed: Published by McGraw-Hill Higher Education in 2003.

5.17. Yoshioka, K., et al. *Interpretation of Temperature and Pressure Profiles Measured in Multilateral Wells Equipped with Intelligent Completions*. Paper SPE94097 presented at SPE Europec/EAGE Annual Conference, Madrid, Spain, 13-16 June 2005, Society of Petroleum Engineers.

5.18. Chen, Z. *Accurate Prediction Wellbore Transient Temperature Profile Under Multiple Temperature Gradients: Finite Difference Approach and Case History.* Paper SPE84583 presented at SPE Annual Technical Conference and Exhibition, Denver, Colorado, U.S.A., 5-8 October 2003, Society of Petroleum Engineers.

5.19. Steffensen, R.J. and R.C. Smith. *The Importance of Joule-Thompson Heating (or Cooling) in Temperature Log Interpretation.* Paper SPE4636 presented at 48th Annual Fall Meeting of the Society of Petroleum Engineers of AIME, Las Vegas, Nevada, U.S.A., Sept. 30 - Oct. 3 1973, American Institute of Mining, Metallurgical and Petroleum Engineers, Inc.

5.20. Hawkes, R.V., Z. Su, and D. Leech, *Field Data Demonstrate Thermal Effects Important in Gas Well Pressure Buildup Tests.* Journal of Canadian Petroleum Technology, 2001. **40**(11): p. 56-60.

5.21. McCain, W.D., *The Properties of Petroleum Fluids*: Published by PennWell Books in 1990.

5.22. Gambill, W.R., *You Can Predict Heat Capacities.* Chemical Engineering, 1957: p. p. 42-46.

5.23. RefiningDept, *Design and Operation of Oil-Water Separators*. Monographs on Refinery Environmental Control - Management of Water Discharges: Published by American Petroleum Institute in 1990.

5.24. Hasan, A.R. and C.S. Kabir, *A Mechanistic Model for Computing Fluid Temperature Profiles in Gas-Lift Wells.* SPE Production & Facilities, 1996: SPE26098 p. 179-185.

Chapter 6 Detection of Scale using Fibre Optic Distributed Temperature Sensors

6.1 Introduction

Solid deposition in the production tubing presents a big challenge for the production engineer; solids deposition can reduce well production, increase project operating costs due to the scale dissolver treatment requirements, and in certain situations, create health and safety issues. Examples of production solid deposition problems are:

1. *Organic Deposits*
    a. Wax Deposition
    b. Hydrate Formation
2. *Inorganic Scale Deposits*
    a. Carbonate Scales (e.g. Calcium Carbonate $CaCO_3$): precipitated by decreasing pressure (e.g. Venturi flow meters) and increasing temperature (ESPs)

b. Sulphate Scales (e.g. Barium Sulphate $BaSO_4$) forms when two different brine streams mixes.

Deposition of scale in the tubing can severely affect the well productivity and causes a decline in the production rate. Inorganic scale deposition is one of the most frequently encountered production problems and forms the focus of this study. Scale deposition renders valves inoperable; while precipitation on electric submersible pumps (ESPs) can lead to over-heating and pump motor failure. Project economics will be affected by scale formation due to increased project operating expenditure (OPEX) to mitigate the scale deposition problem.

The detection of scale is conventionally detected at the surface by reduction in the production flow rate or by wireline intervention using a calliper log. Alternatively, the Attenuated Total Reflectance (ATR) probe, a direct measurement surface analysis technique utilizing an energy loss mechanism, has been used for real-time and in-situ detection of Calcium Carbonate scale. Its main function is to test the water composition for the tendency to scale and the severity of the $CaCO_3$ scaling [6.1]. Other methods to monitor scale deposition include [6.2]:

1. Soluble scaling ion concentration analysis of brine
2. Inspection of visual signs of scaling (increase in pressure, equipments failure)

Using downhole monitoring for scale deposition would provide a great tool for the engineers overseeing wells in environments where logging is not practical such as subsea developments. In North Sea Visund field [6.3], which is a subsea development, the impracticality of calliper logging did not allow the correct determination of the depth where CaCO3 scaling deposition started. Scale deposition can extend to long distances in the tubing as shown in the case of Brage field in the North Sea, where $CaCO_3$ scaling extended for 400m (≈1300 ft) [6.3]. The Miller field in the North Sea is a represent the most severe case of scaling where scale treatment is carried out on weekly basis to avoid complete loss of the well [6.4].

6.2 Objective and Motivation:

The objective of this chapter is to investigate the temperature behaviour in wells where scale deposition is occurring and to quantify the temperature changes that occur within the scaled region. Understanding this behaviour can aid in determining the possibility of

detecting scale deposits in the production tubing using Distributed Temperature Sensor (DTS) downhole temperature data.

Understanding the temperature behaviour and the factors affecting it will provide engineers with guidelines to examine the prospect of scale detection using fibre optic DTS before installation. Although, scale detection is never, and never will be a major application of DTS, such a secondary application can form an extra incentive to justify installation of a DTS system.

The main driver for this study is the low conductivity of the scale deposits. Calcium carbonate ($CaCO_3$) scale has a thermal conductivity that ranges between 2.1 Btu/(hr.ft.°F) to 3.2 Btu/(hr.ft.°F); while the Barium Sulphate scales have an even lower thermal conductivity around 1.4 Btu/(hr.ft.°F). Typical thermal conductivity of the production tubing usually ranges between 26 Btu/(hr.ft.°F) for mild steel to 14 Btu/(hr.ft.°F) for stainless steel.

6.3 Model Description:

The flowing tubing temperature prediction model developed by Hasan and Kabir [6.5, 6.6], was used to determine if the scale presence will cause any significant change in the temperature profile. (N.B. The equation are updated from the references using an errata sent by the author of the book)

$$\frac{dT_f}{dz} = \frac{1}{A}\left(T_f - T_{ei}\right) + \frac{g\sin\theta}{C_p} - \phi \qquad \text{Equation 6.1}$$

Where,

$$A = \frac{C_p w}{2\pi}\left[\frac{k_e + \left(r_{to}U_{to}T_D\right)}{r_{to}U_{to}k_e}\right] \qquad \text{Equation 6.2}$$

$$\phi = \frac{v}{C_p J g_c}\frac{dv}{dz} - \mu_{JT}\frac{dp}{dz} \qquad \text{Equation 6.3}$$

T_f = Flowing Fluid Temperature in the tubing, °F

z = Measured Depth, ft

T_{ei} = Earth initial (geothermal) temperature, °F

g = Gravitational Acceleration Constant = 32.17 ft/s^2

C_p = Fluid Heat Capacity, Btu/(lbm.°F)

w = mass flow rate, lbm/hr

k_e = Formation Thermal Conductivity, Btu/(hr.ft.°F)

r_{to} = Tubing outside diameter, ft

U_{to} = Overall Heat Transfer Coefficient, Btu/(hr.ft^2.°F)

v = velocity, ft/s

μ_{JT} = Joule-Thompson Coefficient, °F/psi

6.3.1 Overall Heat Transfer Coefficient (U_{to}):

The overall heat transfer coefficient (U_{to}) can be defined as the sum of the individual resistances to heat flow from the flowing fluid in the tubing to the formation. A typical definition of the overall heat transfer coefficient for a conventional well with stationary fluid or gas in the annulus and insulation around the tubing (Figure 6-1) is [6.6]:

$$U_{to}=\left[\frac{r_{to}}{r_{ti}h_t}+\frac{r_{to}\ln\left(r_{to}/r_{ti}\right)}{k_t}+\frac{r_{to}\ln\left(r_{ins}/r_{to}\right)}{k_{ins}}+\frac{r_{to}}{r_{ins}(h_{nc}+h_r)}+\frac{r_{to}\ln\left(r_{co}/r_{ci}\right)}{k_{cas}}+\frac{r_{to}\ln\left(r_{wb}/r_{co}\right)}{k_{cem}}\right]^{-1} \quad \text{Equation 6.4}$$

Where,

r_{to} = Outside Tubing Radius, ft

r_{ti} = Inside Tubing Radius, ft

r_{ins} = Insulation Radius, ft

r_{ci} = Casing Inside Radius, ft

r_{co} = Casing outside radius, ft

r_{wb} = Wellbore Radius, ft

h_t = Tubing Convection Heat Transfer Coefficient, Btu/(hr.ft^2.°F)

h_r = Radiation Heat Transfer Coefficient, Btu/(hr.ft^2.°F)

h_{nc} = Natural Convection Heat Transfer Coefficient in Casing Annulus, Btu/(hr.ft^2.°F)

k_t = Tubing Thermal Conductivity, Btu/(hr.ft.°F)

k_{cas} = Casing Thermal Conductivity, Btu/(hr.ft.°F)

k_{ins} = Insulation Thermal Conductivity, Btu/(hr.ft.°F)

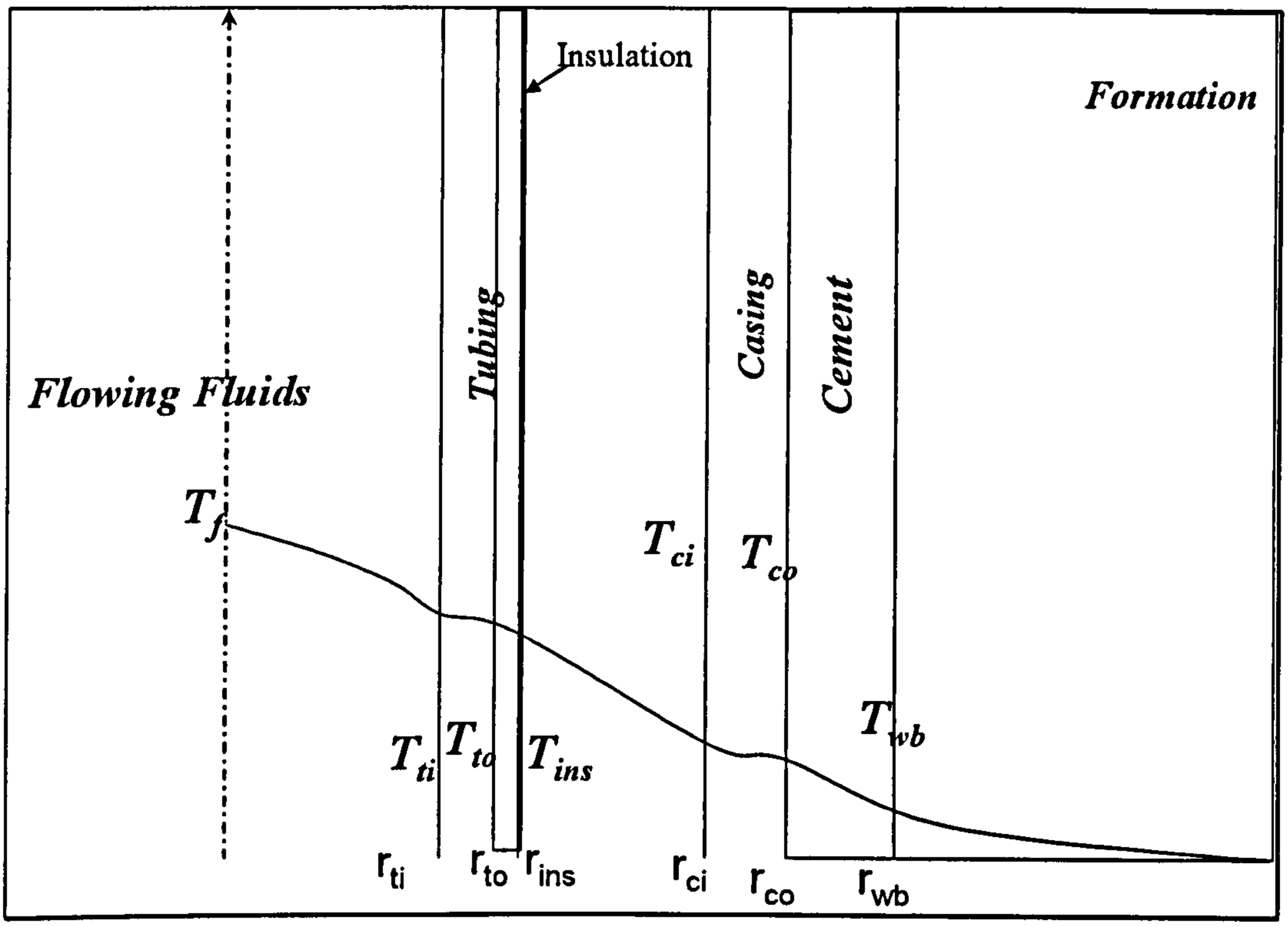

Figure 6-1. Heat Resistance in a Conventional Well

When the tubing insulation is absent, the term containing the thermal conductivity of the insulation (k_{ins}) is omitted and Equation 6.4 reduces to:

$$U_{to} = \left[\frac{r_{to}}{r_{ti} h_t} + \frac{r_{to} \ln\left(r_{to}/r_{ti}\right)}{k_t} + \frac{1}{(h_{nc} + h_r)} + \frac{r_{to} \ln\left(r_{co}/r_{ci}\right)}{k_{cas}} + \frac{r_{to} \ln\left(r_{wb}/r_{co}\right)}{k_{cem}} \right]^{-1} \qquad \text{Equation 6.5}$$

Most tubings and casings are made of steel which is highly conductive and the ratio between the inside and outside radii of the tubing and casing is small. The temperature on the outside and inside of the tubing and casing are thus almost identical allowing the terms containing k_t and k_{cas} also to be omitted. Further, the convective heat flow in the production tubing can be assumed to be large so that the temperature for the fluid flow (T_f) will be equal to the temperature at the inside radius of the tubing (T_{ti}). I.E. there is negligible resistance to heat flow between the centre of the tubing and the tubing wall. This allows the term containing h_t also to be omitted [6.6], reducing Equation 6.5 to:

$$U_{to} = \left[\frac{1}{(h_{nc} + h_r)} + \frac{r_{to} \ln\left(r_{wb}/r_{co}\right)}{k_{cem}} \right]^{-1} \qquad \text{Equation 6.6}$$

The above definition of the overall heat transfer coefficient is based on the assumption of steady state heat transfer that is independent of time. The overall heat transfer coefficient value will be depend on time for the unsteady-state or transient case. An example of an unsteady state condition would be the heat transfer coefficient from the reservoir to adjacent strata. Zolutokhin [6.7] proposed an analytical definition of the overall heat transfer coefficient for heat transfer in the reservoir. The assumption of constant U value was questioned by some experimental results that showed the value of U decreases with time [6.7]. The treatment of heat flow in the reservoir as an unsteady-state process was analysed in the Ramey's paper on wellbore heat transmission [6.8]. Transient conditions certainly occur during well start-up and during drilling operations [6.9]. The dependency of the overall heat transfer coefficient on time will result in the Newton Law of cooling being written in the following differential format:

$$dQ = U(t)A.(T_{res} - T_l).dt \qquad \text{Equation 6.7}$$

Where,

T_{res} = Temperature of the reservoir, °F.

T_l = Temperature of the adjacent strata, °F.

The overall heat transfer coefficient allows of simplification for complex heat loss calculations (e.g. during thermal steam injection) where one has to solve a two dimensional (2D) (for 1D flow geometry) or 3D (for 2D flow geometry) energy Equation [6.7].

6.3.2 Kinetic Term and Pressure Drop

The term ϕ in Equation 6.1, which is defined in Equation 6.3, consists of the kinetic energy term, Joule-Thompson coefficient and the pressure drop. For incompressible liquid flow, the velocity change with depth is negligible and liquid density variation with pressure is usually very small. Using these assumptions, the enthalpy for liquids can be written as:

$$dH = C_p dT + \left[v - T\left(\frac{dv}{dT}\right)_P \right] dp \qquad \text{Equation 6.8}$$

Where,

H = Fluid Enthalpy, Btu

v = specific volume (1/density), ft^3/lbm

And

$$\mu_{JT} \equiv \frac{1}{C_p}\left[\frac{\partial H}{\partial p}\right]_T = \frac{v}{C_p} = \frac{1}{\rho C_p} \qquad \text{Equation 6.9}$$

Therefore for liquids:

$$\phi \equiv \frac{v}{C_p J g_c}\frac{dv}{dz} - \mu_{JT}\frac{dp}{dz} = -\frac{1}{C_p \rho}\frac{dp}{dz} \qquad \text{Equation 6.10}$$

Then Equation 6.10 will become:

$$\frac{dT_f}{dz} = \frac{1}{A}\left(T_f - T_{ei}\right) + \frac{g\sin\theta}{C_p J g_c} + \frac{1}{C_p \rho}\frac{dp}{dz} \qquad \text{Equation 6.11}$$

Equation 6.11 forms the basis of the computer coding developed to simulate the impact of the presence of scale on the flowing fluid temperature.

Chapter 3 discussed how Joule-Thompson heating during incompressible flow requires large pressure drop (typically a 1000 psi pressure drop is required to raise the temperature of flowing water by 3 °F and 8 °F for oil flow). Therefore, unless the flow is large and there is significant deposition of the scale in the tubing to create large pressure drop, the effect of Joule-Thompson heating will be small.

Since we are interested in the early detection of scales, the increase in pressure drop and the resulted heating from the increase in velocity due to smaller flow diameter and t Joule-Thompson Effect in the scale deposited region will be neglected. This investigation will focus on the insulation effect provided by the scale layer on the temperature profile. The model divides the tubing into 10 ft segments; the initial condition for the temperature in each segment is the temperature of the previous segment. The temperature change over each segment is calculated by solving Equation 6.11 using a differential equation solver provided by MATLAB™ [6.10].

6.4 Incorporation of Deposited Scale in Temperature Prediction Model:

The deposited scale layer alters the well configuration by reducing the tubing flow diameter (Figure 6-2). The scale impact on heat transfer within the wellbore is captured in the overall heat transfer coefficient (U_{to}). Heat transfer through the scale layer in the tubing is by conduction. The overall heat transfer coefficient **(Equation 6.6)** was modified to add a term incorporating the effect of the scale conductivity.

$$U_{to} = \left[\frac{r_{to} \ln\left(r_{ti}/r_{si}\right)}{k_{scale}} + \frac{1}{(h_{nc} + h_r)} + \frac{r_{to} \ln\left(r_{wb}/r_{co}\right)}{k_{cem}} \right]^{-1} \qquad \text{Equation 6.12}$$

Where,

r_{si} = Scale Layer inside Radius, ft

k_{scale} = Scale Layer Thermal Conductivity, Btu/(hr.ft.°F)

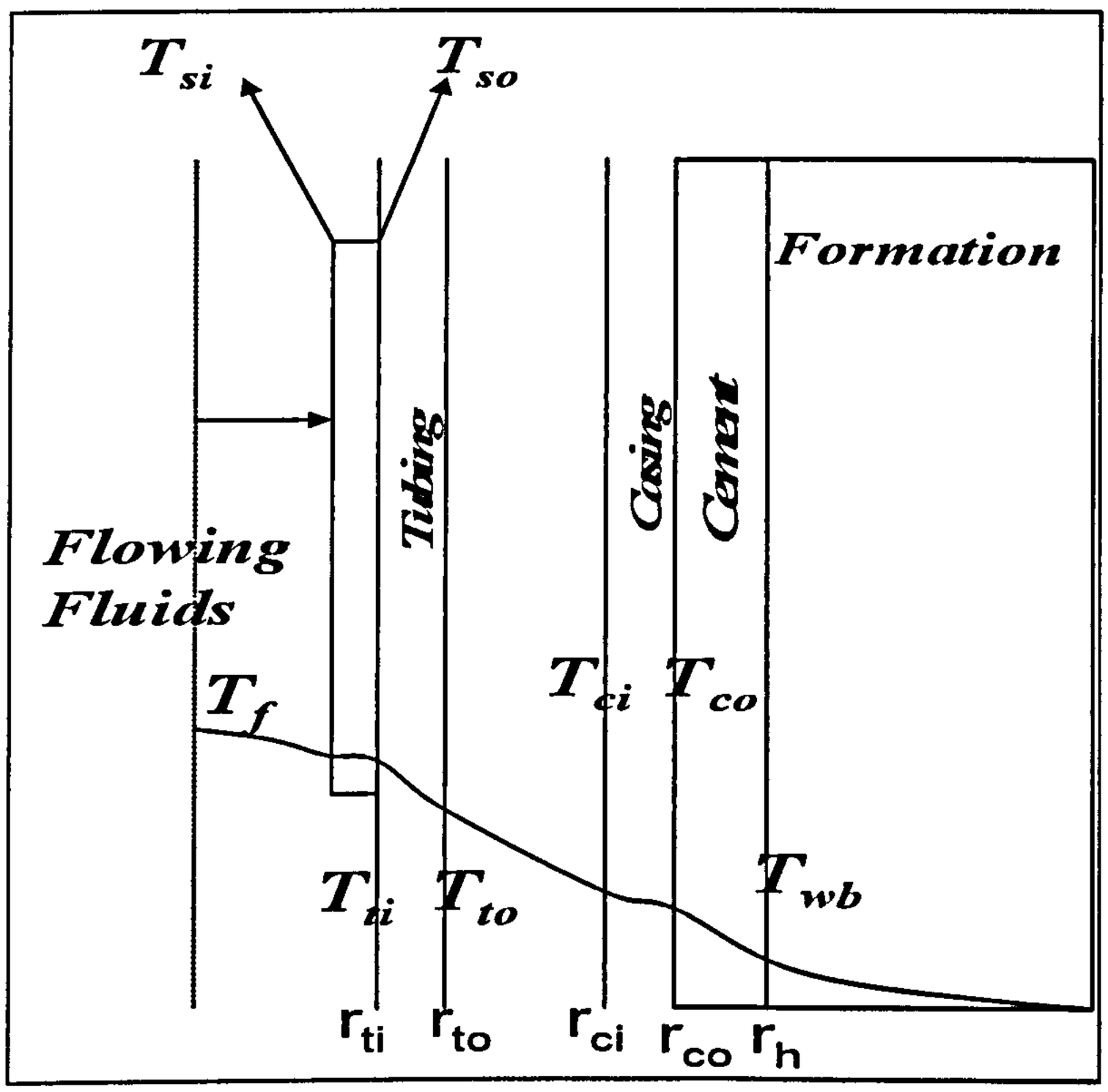

Figure 6-2. Scale Deposited Layer Effect the Well Configuration

6.5 Assumptions:

This work assumes:

1. A Vertical Well

2. Ideal case of uniform scale deposition in the tubing (constant thickness)
3. Steady-State flow in the tubing (Equation 6.11)
4. The thermal properties of the fluid remain unchanged within the scale deposition region.
5. The mass flow rate of the flowing fluid does not change as the scale deposition increases in thickness.
6. The minimum resolution of the DTS measurement is of 0.18 °F. All DTS manufacturers have claimed this value. Some manufacturers also report a resolution of 0.018 °F [6.11].

Table 6-1. Base Case Simulation Data

Well Configuration & Properties

Tubing Outside Diameter	4.5	in
Tubing Inside Diameter	4	in
Wellbore Radius	9	in
Casing Inside Diameter	6.46	in
Casing Outside Diameter	7	in
Well Length	6000	ft
Emmisivity	0.9	dimensionless
Roughness	0.0015	ft

Fluid Properties

Liquid Production Rate	1,250	bbl/day
Water Cut	20%	
Oil Gravity	34.4	°API
Water Gravity	1.01	-
Oil Viscosity	4	cp
Water Viscosity	1	cp

Tubing Fluid Thermal Properties

Oil Thermal Conductivity	0.081	Btu/(hr.ft.°F)
Water Thermal Conductivity	0.383	Btu/(hr.ft.°F)
Oil Heat Capacity	0.507	Btu/(lbm.°F)
Water Heat Capacity	0.947	Btu/(lbm.°F)

Annulus Fluid Thermal Properties (Seawater + KCl) [6.12]

Heat Capacity	0.949	Btu/(lbm.°F)
Thermal Conductivity	0.37	Btu/(hr.ft.F)
Viscosity	0. 52	cp
Density	65.83	lbm/ft^3
Thermal Expansion	0.00027	$°F^{-1}$

Formation and Production Properties

Thermal Conductivity	3.33	Btu/(hr.ft.°F)	Sandstone
Formation Heat Capacity	0.625	Btu/(lbm.°F)	Sandstone
Formation Density	135	lbm/ft^3	
Bottom Hole Static Temperature	150	°F	
Well Head Temperature	76	°F	
Time since production started	158	Hours	
Cement Thermal Conductivity	4.02	Btu/(hr.ft.°F)	

Scale Properties

$CaCO_3$ Scale Thermal Conductivity	2.08	Btu/(hr.ft.°F)
Scale Roughness	0.003	ft
Scale Top Depth	4,000	ft
Scale Bottom Depth	5,000	ft

6.6 Impact of Scale on Temperature Profiles in Conventional Wells:

Tubing scale deposition mainly occurs in oil wells that produce some water. The effect of scale deposition on the flowing temperature profile of an oil well with the base case parameters listed in Table 6-1 has been evaluated for various scale layer thicknesses (SLT). The results using the computer code to solve Equation 6.11 are illustrated in Figure 6-3. The presence of the scale layer increases the temperature of the flowing tubing fluid. This temperature increase becomes greater as the thickness of the deposited scale layer increases, as expected from the increased insulation provided by the scale.

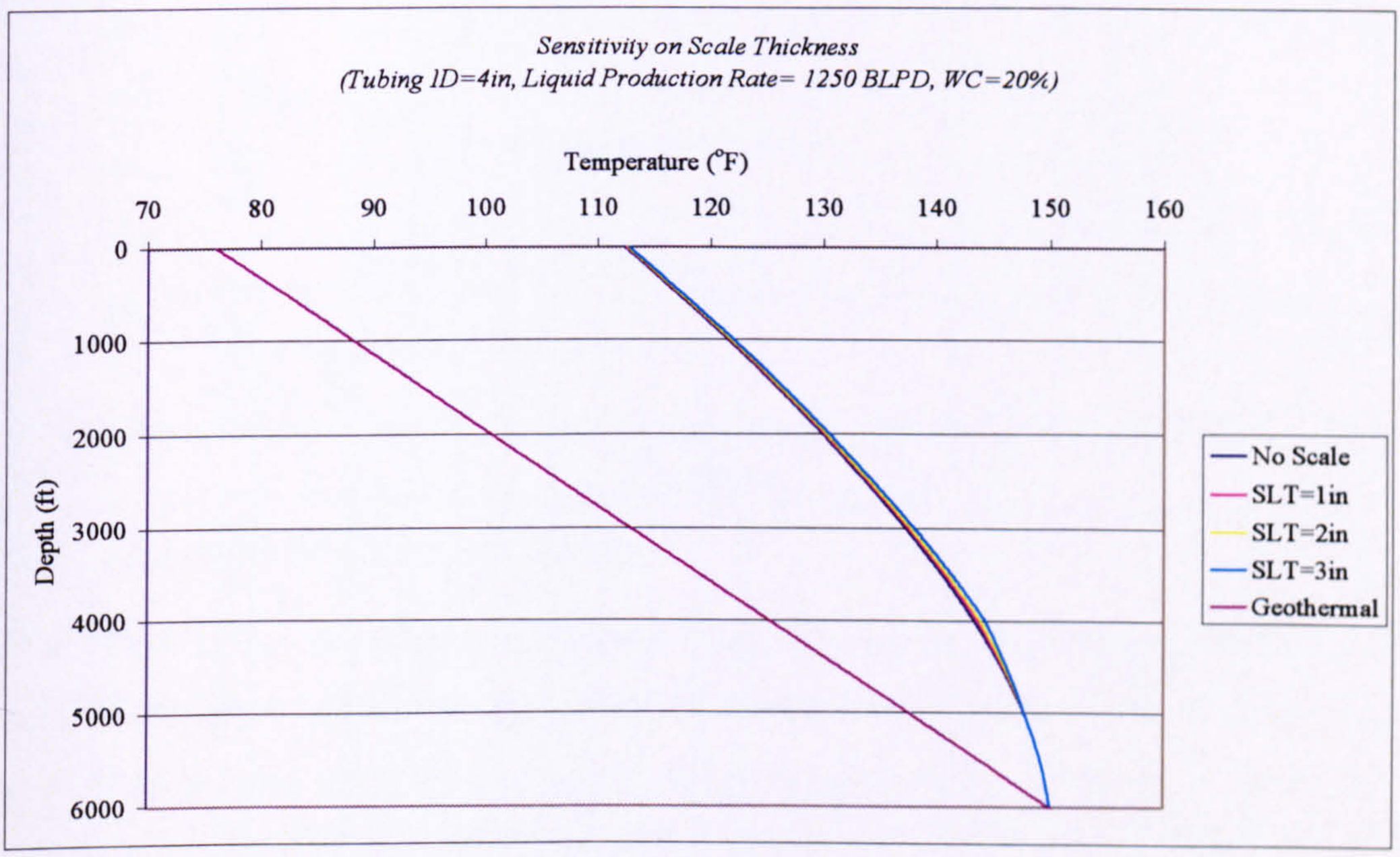

Figure 6-3. Temperature of Tubing Fluid Increases as Scale Layer Thickness Increases

Figure 6-4 indicates that the fluid will exit the scaled region with a higher temperature than the normal flowing temperature (≈0.2 °F higher in case of scale thickness of 1 in) when no scale deposited in the tubing. The increase in temperature can be recognized using fibre optic DTS technology, though this temperature change will occur inside the tubing.

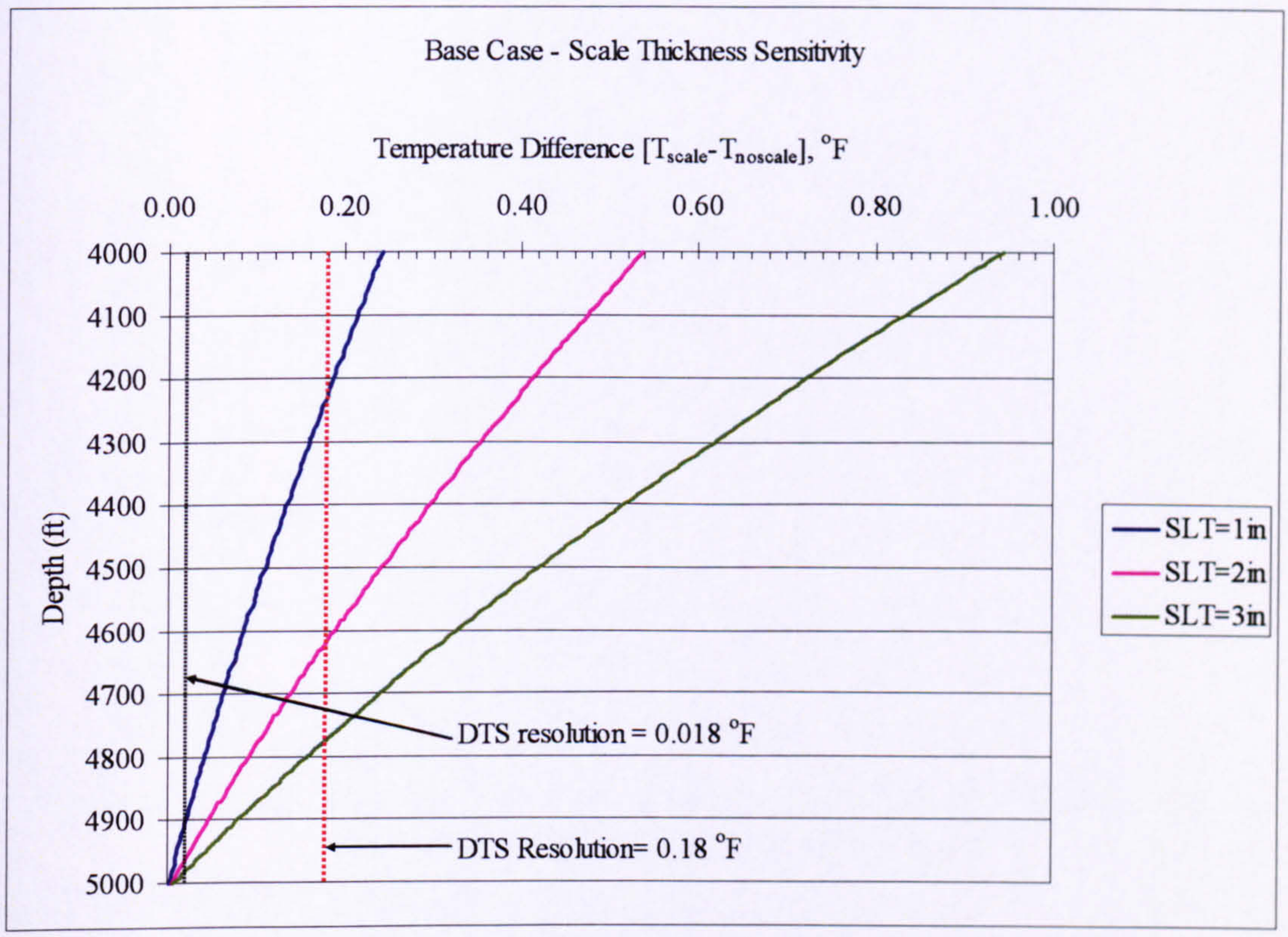

Figure 6-4. Magnitude of Temperature Increase due to Scale Deposition for the Base Case

6.6.1 Time since production Sensitivity:

The time elapsed since the start of production influences the dimensionless formation temperature. This formation temperature is an important parameter when calculating the relaxation distance *(A)* which can be viewed as the total overall heat transfer coefficient that includes the heat transfer effects of the wellbore and the formation. The relaxation parameter function may then be used then to calculate the temperature in the tubing.

Figure 6-5 shows that the temperature difference caused by the presence of the scale layer decreases as the production time increases. This is due to, heat losses to the surrounding formation decreasing for longer production time [6.13].

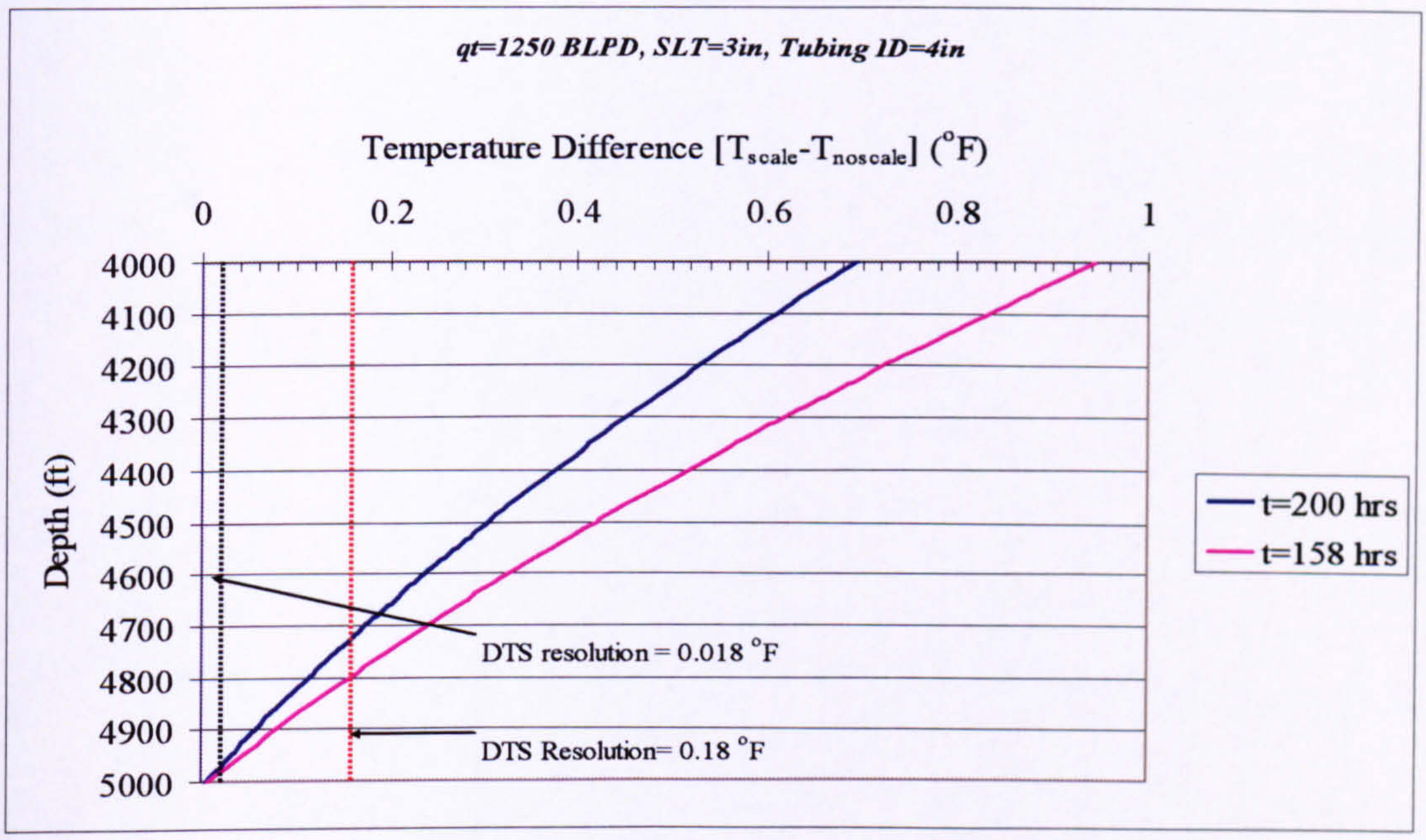

Figure 6-5. Effect of Elapsed Time since Production Started on the Temperature Difference Caused by the Presence of Scale

6.6.2 Well Production Rate Sensitivity:

The production rate is the main parameter that affects the temperature profile in the well. Higher flow rate decreases the residence time of the fluid in the tubing, resulting in a smaller heat loss from the flowing fluid in the tubing to the formation. Figure 6-6 shows the effect of increasing production flow rate on the temperature profile and on the increase in temperature caused by the presence of scale deposits in the tubing.

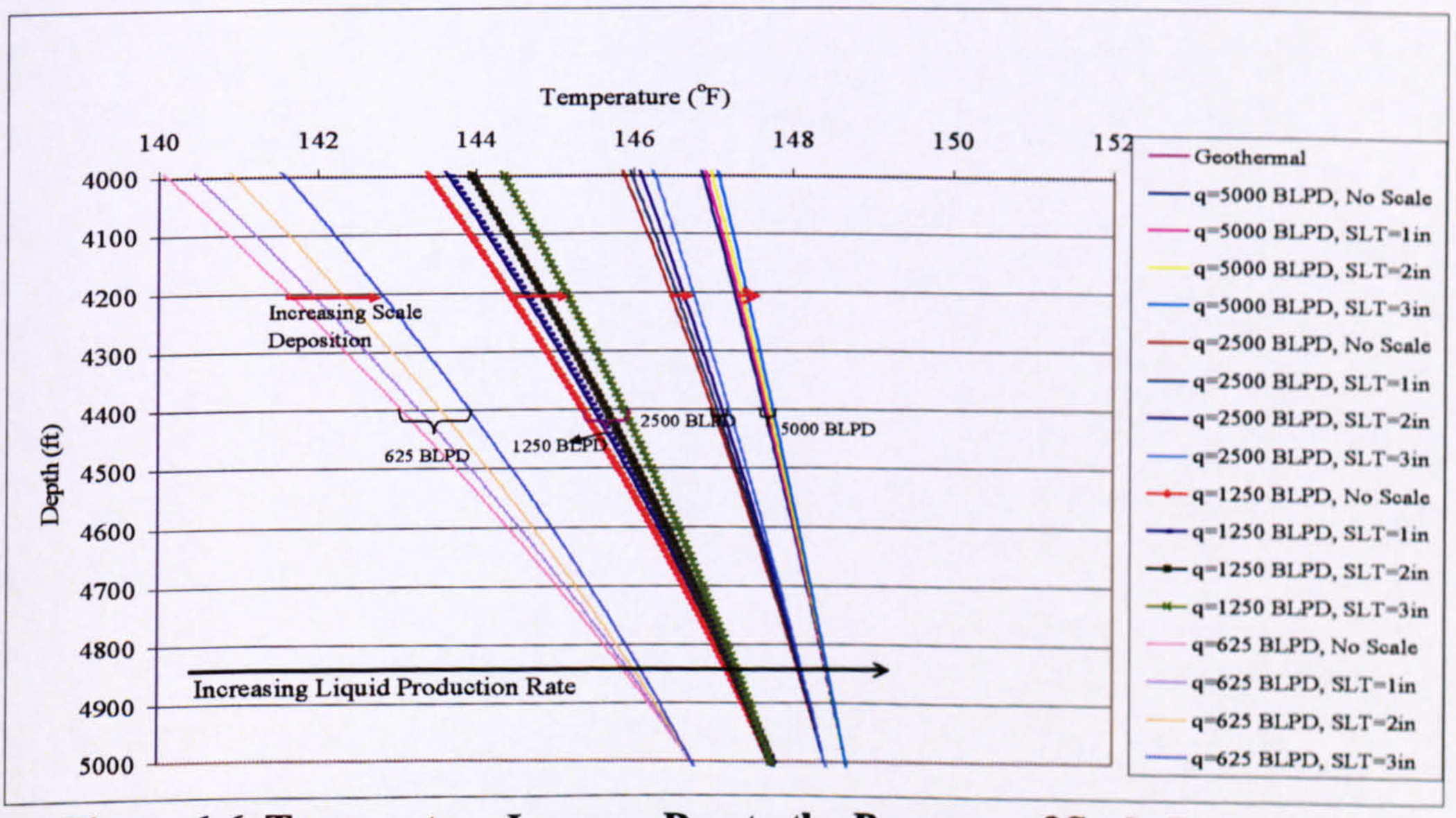

Figure 6-6. Temperature Increase Due to the Presence of Scale Decreases as Production Rate Increases

Figure 6-6 shows that, as the liquid production rate increases, the difference in temperature profiles caused by the presence of the scale layer becomes smaller; reducing the possibility of detection by DTS. Figure 6-7 presents the temperature difference between the temperature profiles for the no scale and the 1 in scale layer cases.

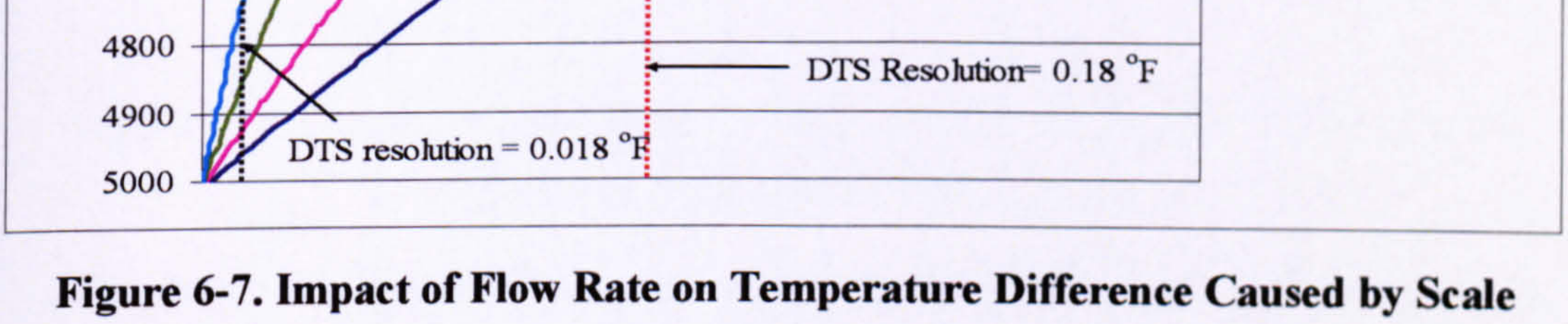

Figure 6-7. Impact of Flow Rate on Temperature Difference Caused by Scale

The temperature difference becomes smaller than the reported accuracy of the DTS systems of ±0.18 °F for the higher flow rates of 2,500 and 5,000 BLPD. Availability of equipment with an improved resolution would radically alter this conclusion.

Figure 6-8 illustrates the length of the scaled region that is required to register a temperature increase higher than DTS resolution of 0.18 °F as a function of the liquid production rate and the scale layer thickness. The figure shows that, for the high production rates, an increased length of scaled tubing is required to register specific increase in the temperature. Lower production rates make it easier to detect the presence of scaled deposits.

Another observation is that, even at the low rate (625 BLPD) with the largest scale layer thickness of 3in, a minimum length of 130 ft of scaled tubing was required. This is due to the masking effect by the fluid entering from a non-scaled region at the bottom of the

scale region. The fluid temperature requires a sufficient residence time to show the effect of the insulation provided by the scale region.

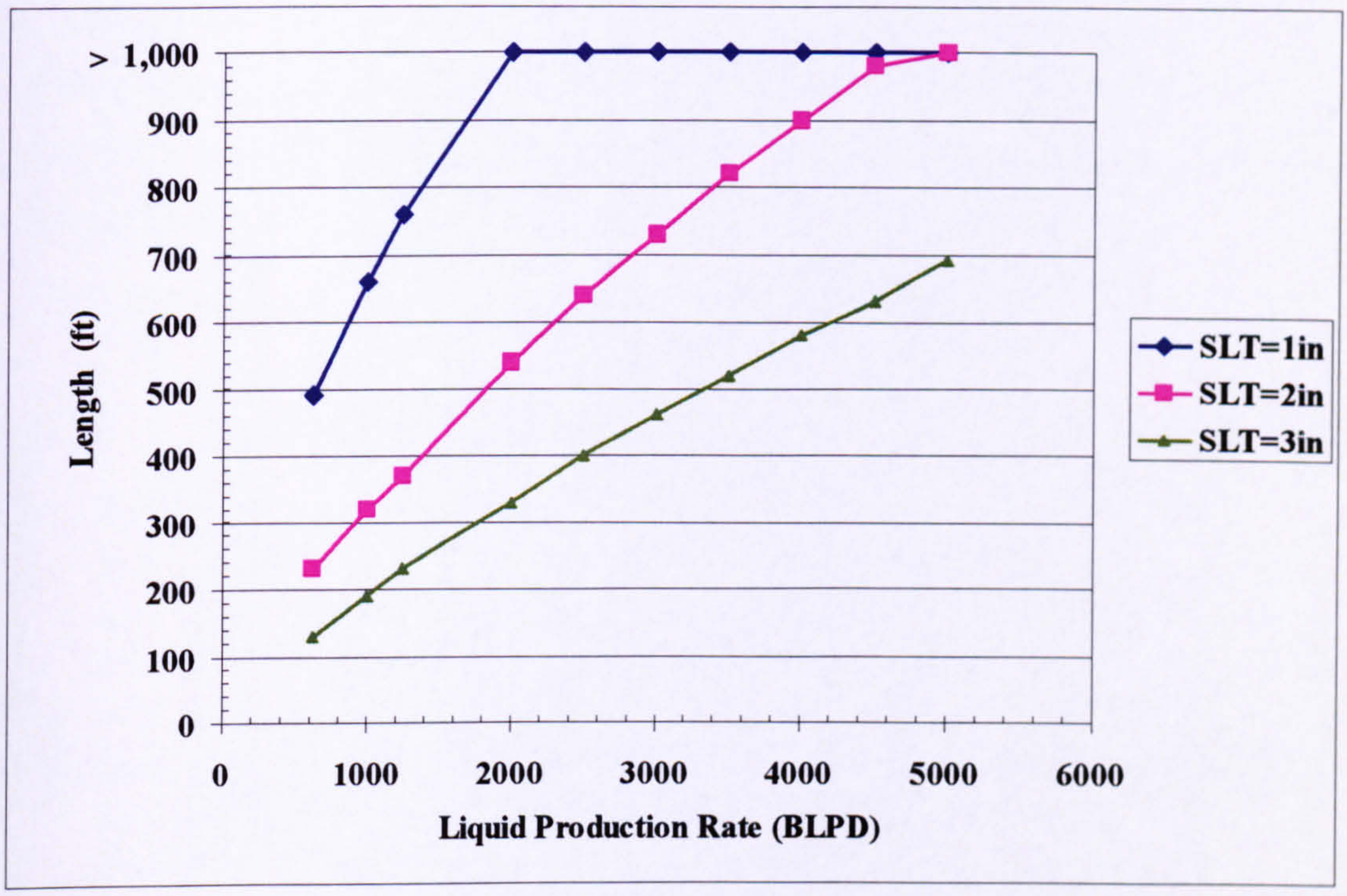

Figure 6-8. Length of Scaled Tubing Required for Measurable Temperature Increase by DTS (0.18 °F Resolution)

The above figure shows that the scale deposits can cause a temperature difference that can be registered using DTS. Ease of detection increases with increasing scale layer thickness and with decreasing production flow rate. Other factors, such as the water cut and well design related issues, need to be also investigated if a complete view of this application area is to be developed.

6.6.3 Impact of Increased Pressure Drop in Scaled Region:

The effect of an increased pressure drop due to the reduced internal diameter of the tubing was omitted in the previous section. The validity of ignoring this pressure drop have been investigated for a case when the scale roughness was assumed to be twice that of the roughness of the tubing.

Figure 6-9 shows that, for a small scale layer thickness of 1in, the effect of the increase pressure drop is small for the base case production rate of 1250 BLPD. The temperature increase attributed to the increased pressure drop in the tubing will increase as the scale layer thickness increases. This is illustrated in Figure 6-10 for a scale layer thickness of

3in. Inclusion of the pressure drop in the temperature calculations is essential for thicker scale layers.

A complete analysis requires that this thermal model should be coupled to an inflow/outflow model for the well to allow determination of the exact flow conditions; particularly whether the well can sustain the required production rate when a large scale deposited thickness has been deposited on the tubing.

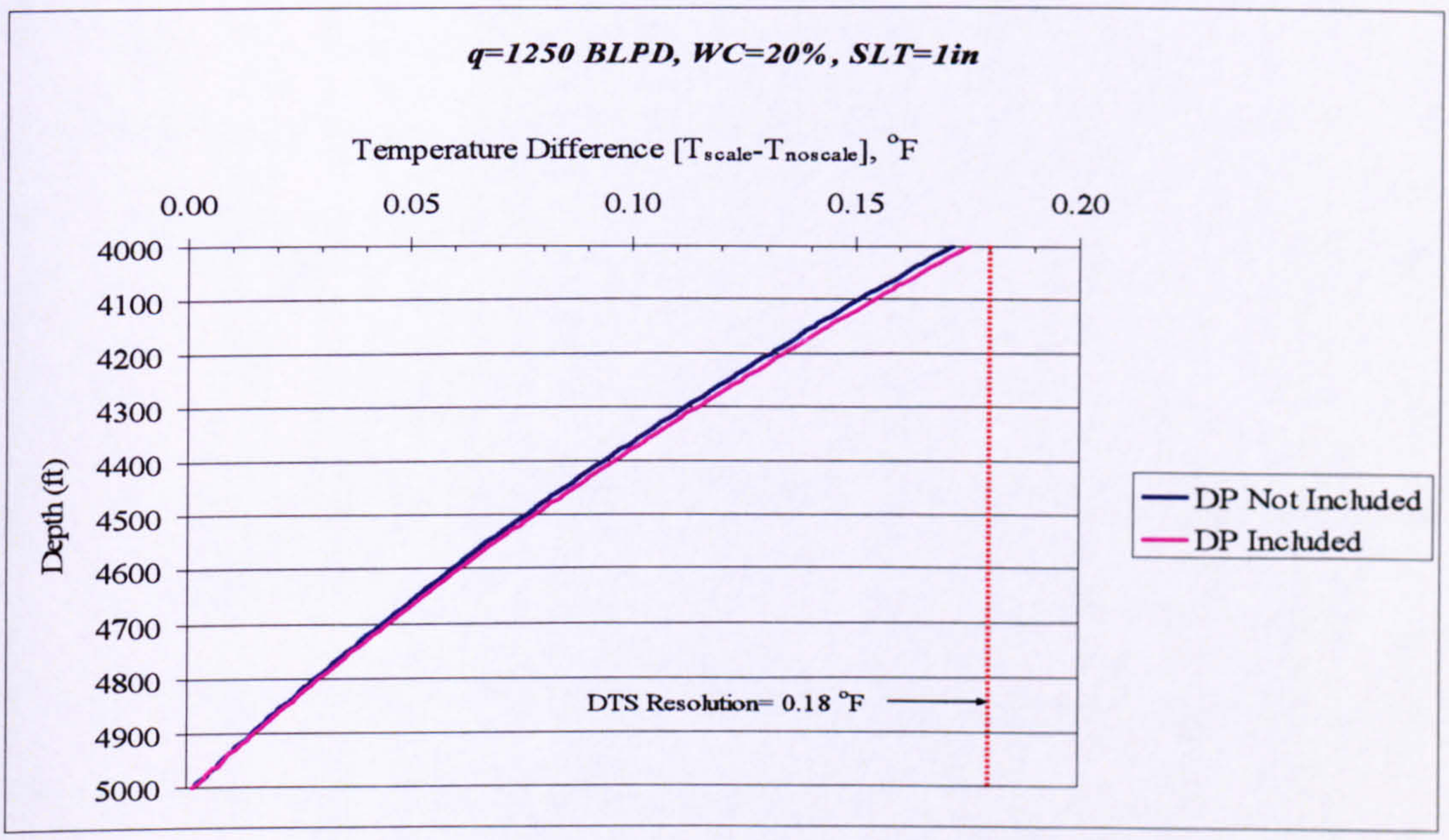

Figure 6-9. Scale Region Pressure Drop Effect on Temperature Difference (Small Scale Layer Thickness=1in)

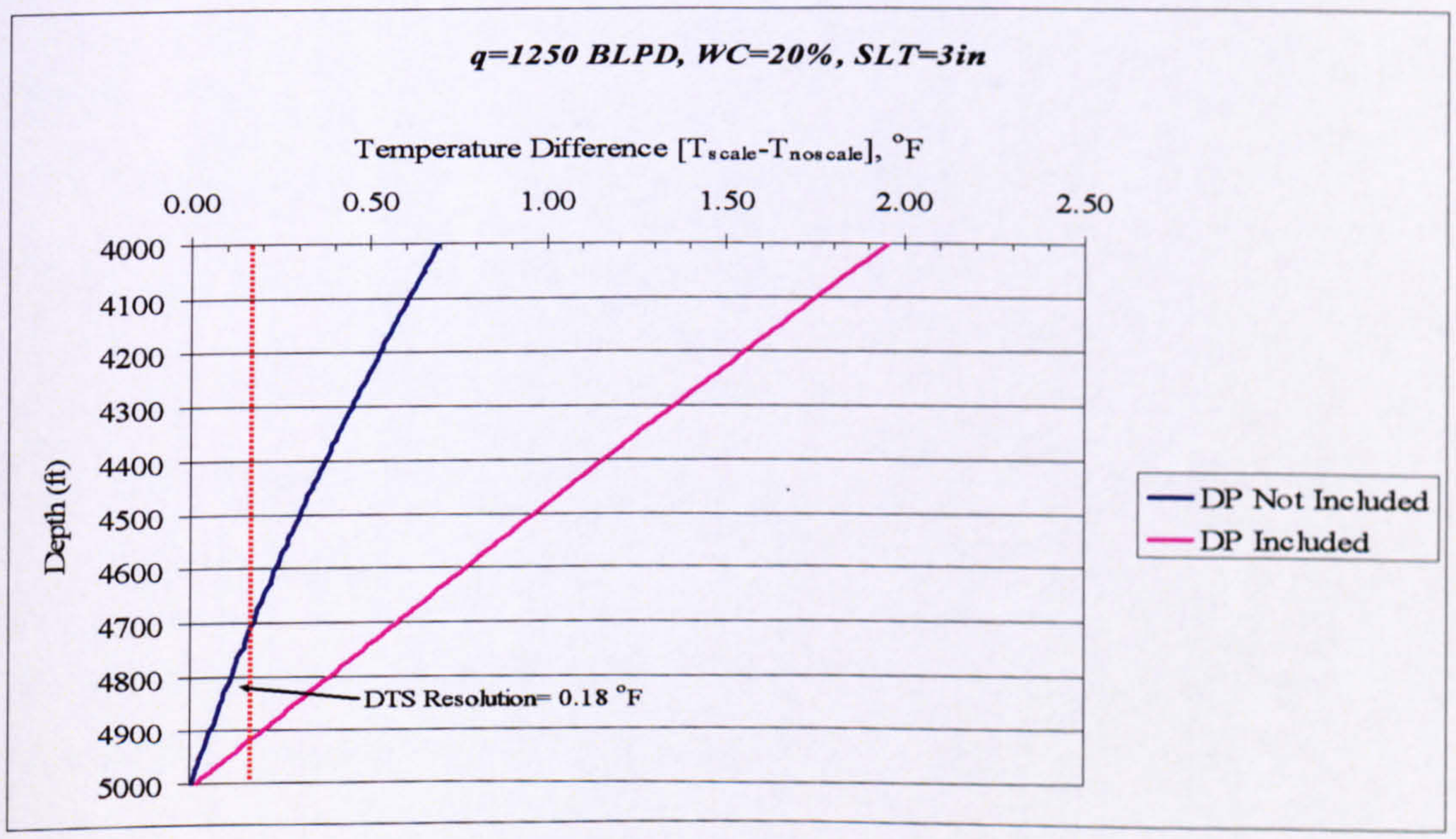

Figure 6-10. Scale Region Pressure Drop Effect on Temperature Difference (Large Scale Layer Thickness=3in)

6.6.4 Increasing Water Cut Impact on Scale Region Temperature Profile:

Influx of water in the wellbore can greatly affect the heat transfer phenomenon within the wellbore. Water has a higher heat capacity than the oil; typical heat capacity value for water ranges between 0.94 – 1.12 Btu/(lbm.°F) for the temperature range 32 to 450 °F. Typical values for heat capacity for crude oil are only 50% of that for water (Table 6-1).

The Heat capacity for crude can be estimated by the following correlation [6.14]:

$$C_{po} = \frac{(0.388 + 0.00045 * T)}{\sqrt{\gamma_o}} \qquad \text{Equation 6.13}$$

Where,

C_{po} = Crude oil heat capacity, Btu/(lbm.°F)

T =Reservoir Temperature, °F

γ_o = Oil specific gravity, dimensionless (ρ_o/ρ_w)

The liquid mixture heat capacity is calculated as:

$$C_{pL} = \frac{q_o}{q_t} C_{po} + \left(1 - \frac{q_o}{q_t}\right) C_{pw} \qquad \text{Equation 6.14}$$

Where,

C_{pL} = Liquid Mixture Heat Capacity, Btu/(lbm.°F)

C_{pw} = Water Heat Capacity, Btu/(lbm.°F)

q_o = Oil Flow Rate, STB/D

q_w = Water Flow Rate, STB/D

q_t = Total Flow Rate, STB/D

The heat capacity is a measure of how much energy a material stores per unit volume. An increased heat capacity will decrease the thermal diffusivity (α) where [6.15]:

$$\alpha = \frac{k}{\rho C_p} \qquad \text{Equation 6.15}$$

A decrease in the value of the thermal diffusivity of the liquid implies that the rate of heat loss to the formation and the surroundings will be reduced. The effect of an increasing water cut on the temperature difference between the scale and the no-scale case for a 1 inch scale layer deposited in the tubing is plotted in Figure 6-11.

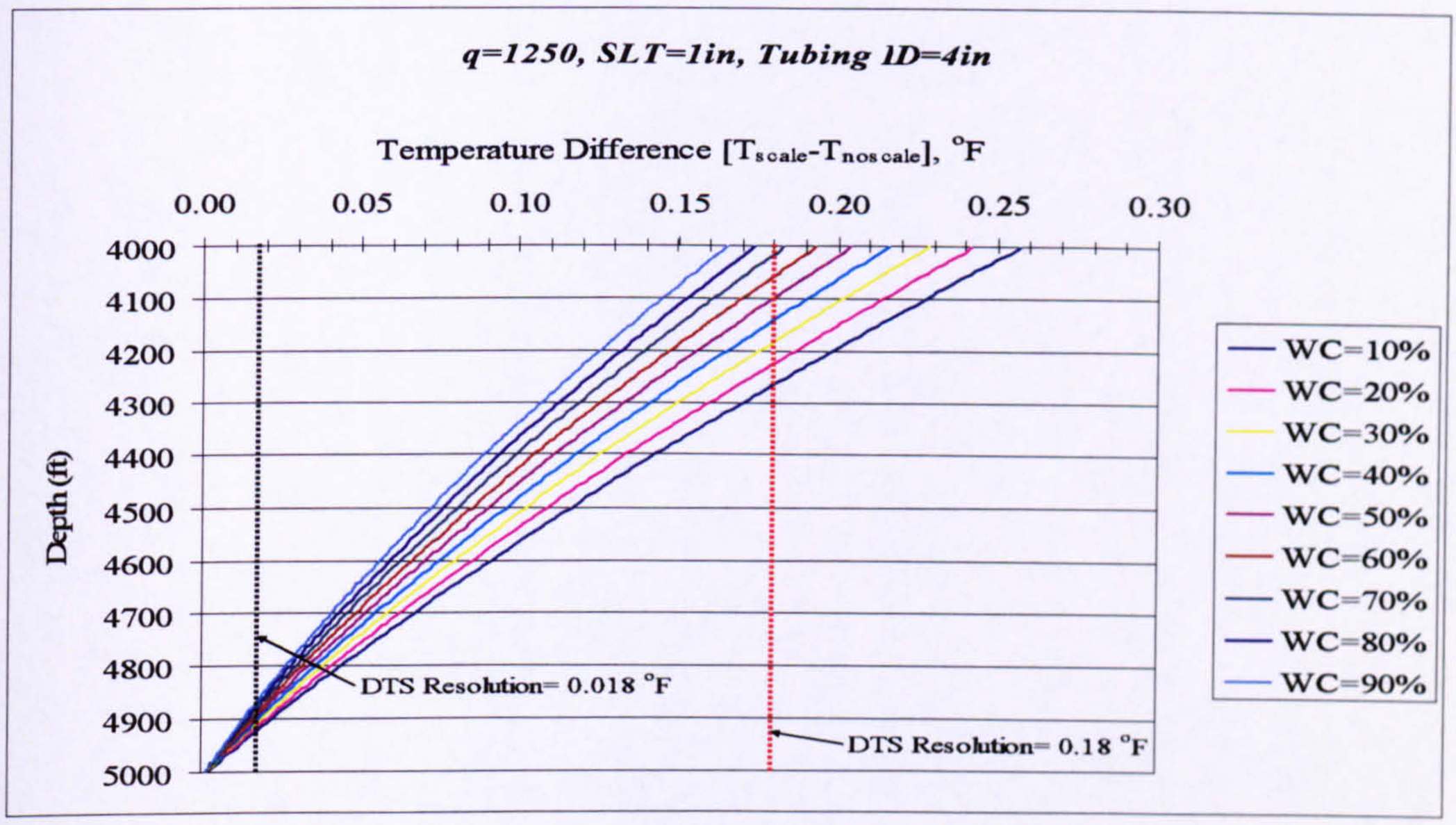

Figure 6-11. Impact of Increased Water Cut on the Temperature Increase Caused by Scale Deposits in the tubing

The increase in water cut decreases the temperature difference between the scale and the no scale temperature profiles. The reason behind the small difference is that the temperature of the fluid as it enters the scale region (i.e. at 5,000 ft depth) increases as the water cut increases. This increase in the fluid temperature due to the presence of water is itself also due to the increased mixture heat capacity.

Figure 6-11 showed that detection of a thin (1in) scale deposit is difficult. Increasing the scale layer thickness to 3 inches creates a very clear temperature difference (Figure 6-12); allowing detection over quite a short length of scaled tubing. As discussed earlier the pressure drop will increase for the tubing with the thick scale layer. This can cause Joule-Thompson heating if the reservoir is able to sustain the tubing flow rate. This heating will also increase with the presence of water under the appropriate conditions.

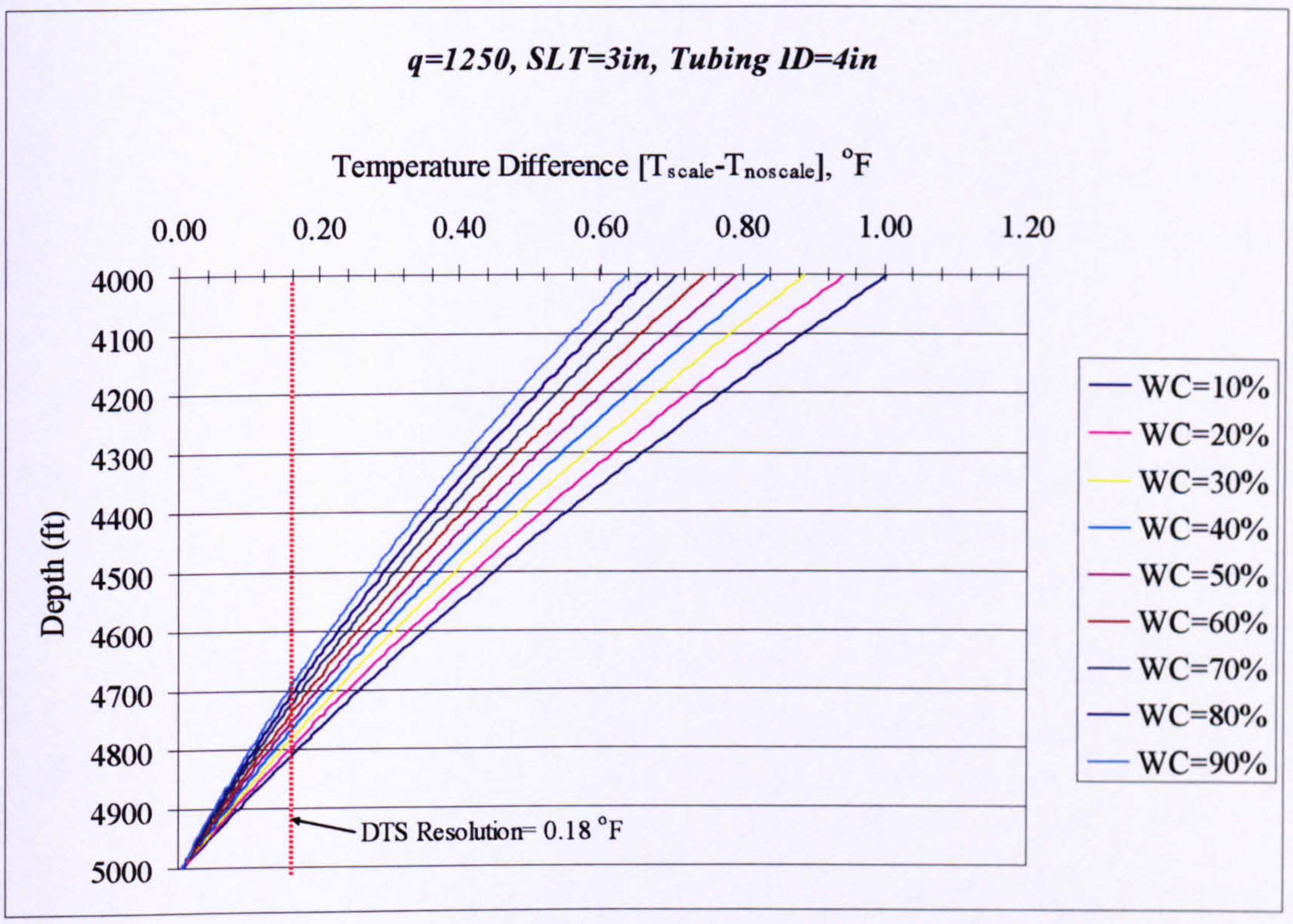

Figure 6-12. Temperature Difference in Scale Zone with SLT=3in (Water Cut Sensitivty)

6.6.5 Discussion on Impact of Production Conditions:

The discussion in the previous sections showed how the temperature difference that indicates of the presence of scale deposits in the tubing will be affected by the production conditions of the well. The average temperature difference caused by the presence of the scale is inversely proportional to the water cut and the total production rate values, and can be expressed as (α denotes inverse proportionality relationship):

$$\Delta T_{avg} \alpha \frac{1}{W.C.}$$

And

$$\Delta T_{avg} \alpha \frac{1}{q_{TL}}$$

Where,

q_{TL} = total liquid production rate

6.7 Completion Design Effect:

Natural convection heat transfer [6.15] due to static packer fluids is an important contributor to the overall heat transfer coefficient for the annulus (Equation 6.12). The tubing external diameter and the casing internal diameter determine the dimensions of the annulus.

6.7.1 Changing Annulus Area Effect on Overall Heat Transfer Coefficient (U_{to}):

Analysis of the effect of tubing and casing sizes employs the dimensionless completion area (D_{ca}), the ratio between the annulus area and the tubing area.

$$D_{ca} = \frac{A_{an}}{A_t} = \frac{d_{ci}^2 - d_{to}^2}{d_{ti}^2} \qquad \text{Equation 6.16}$$

Where,

A_{an} = Area of the annulus, ft^2

A_t = Area of the tubing, ft^2

For a 7-inch casing, with 6.094-in inside diameter, the D_{ca} value ranges from 0.9 for a 4.5-in tubing to 10 for a 2-in tubing. D_{ca} has a smaller range if the value of the tubing size is fixed and the casing size is varied.

D_{ca} is the ratio between the annulus area available for natural convection heat transfer and the tubing area. Larger values of D_{ca}, imply a larger annulus volume and hence a larger volume of packer fluids available for natural heat convection. Examining the sensitivity if the heat transfer to the D_{ca} highlights the importance of the annulus area occupied by the packer fluid, rather than the tubing or casing size.

It was decided to investigate the effect of the annulus area is by fixing the tubing size and increasing the casing size. Although this does not simulate how actual completions are designed, it focuses the investigation on the annulus area at a constant tubing size. The alternative, varying the tubing size, would have introduced an additional parameter such as an increased pressure drop, caused by increased fluid velocity; which will cause a change in the temperature profile not related to the size of the annulus.

Figure 6-13 shows that the overall heat transfer coefficient increases with an increasing value of D_{ca}. Larger heat losses from the producing fluid to the surrounding formation

result in a cooler fluid temperature profile compared to the case when the annulus area available for natural convection is smaller (Figure 6-14).

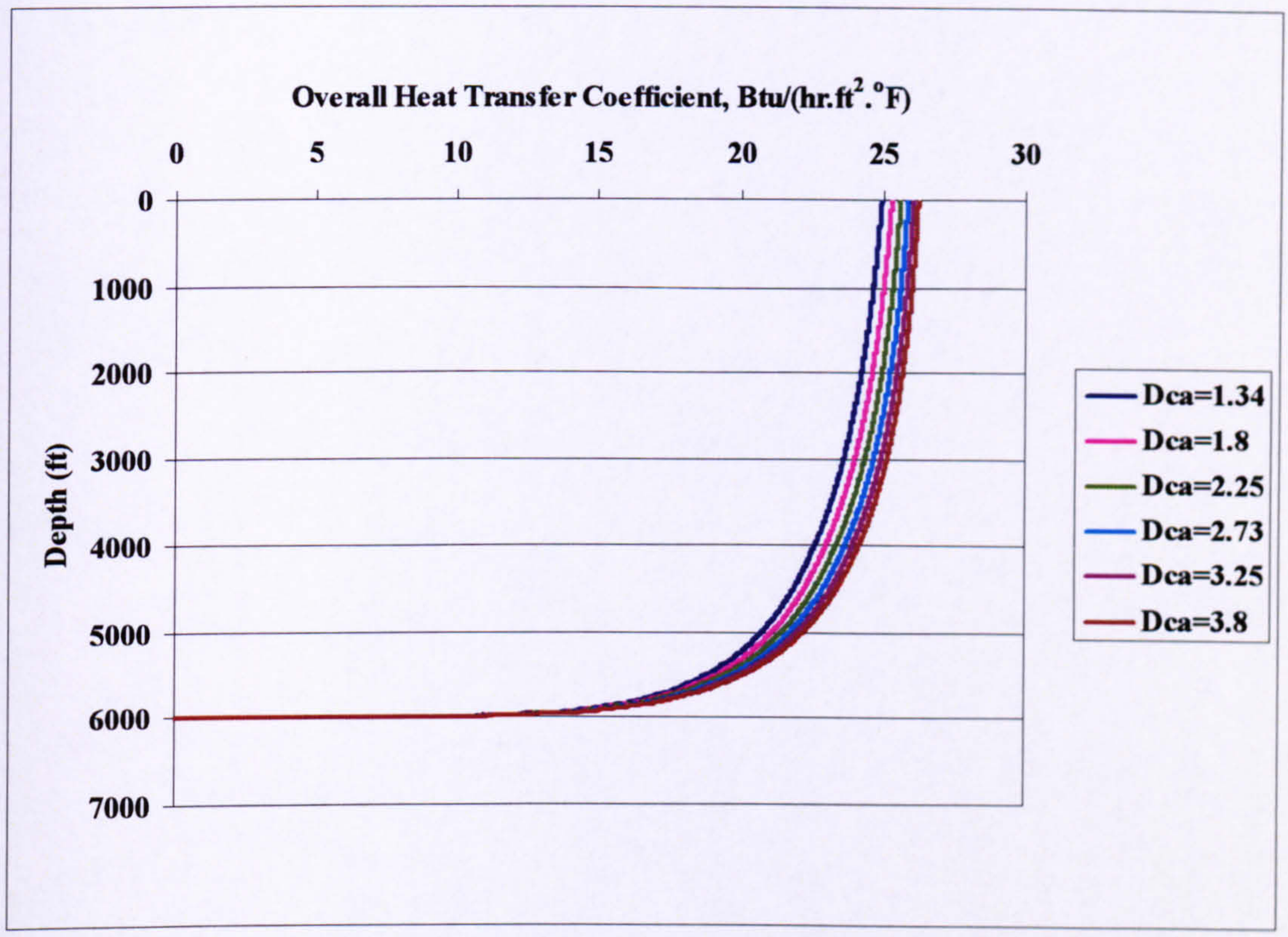

Figure 6-13. Effect of increasing annulus area on the overall heat transfer coefficient in the annulus (No Scale Deposition Case)

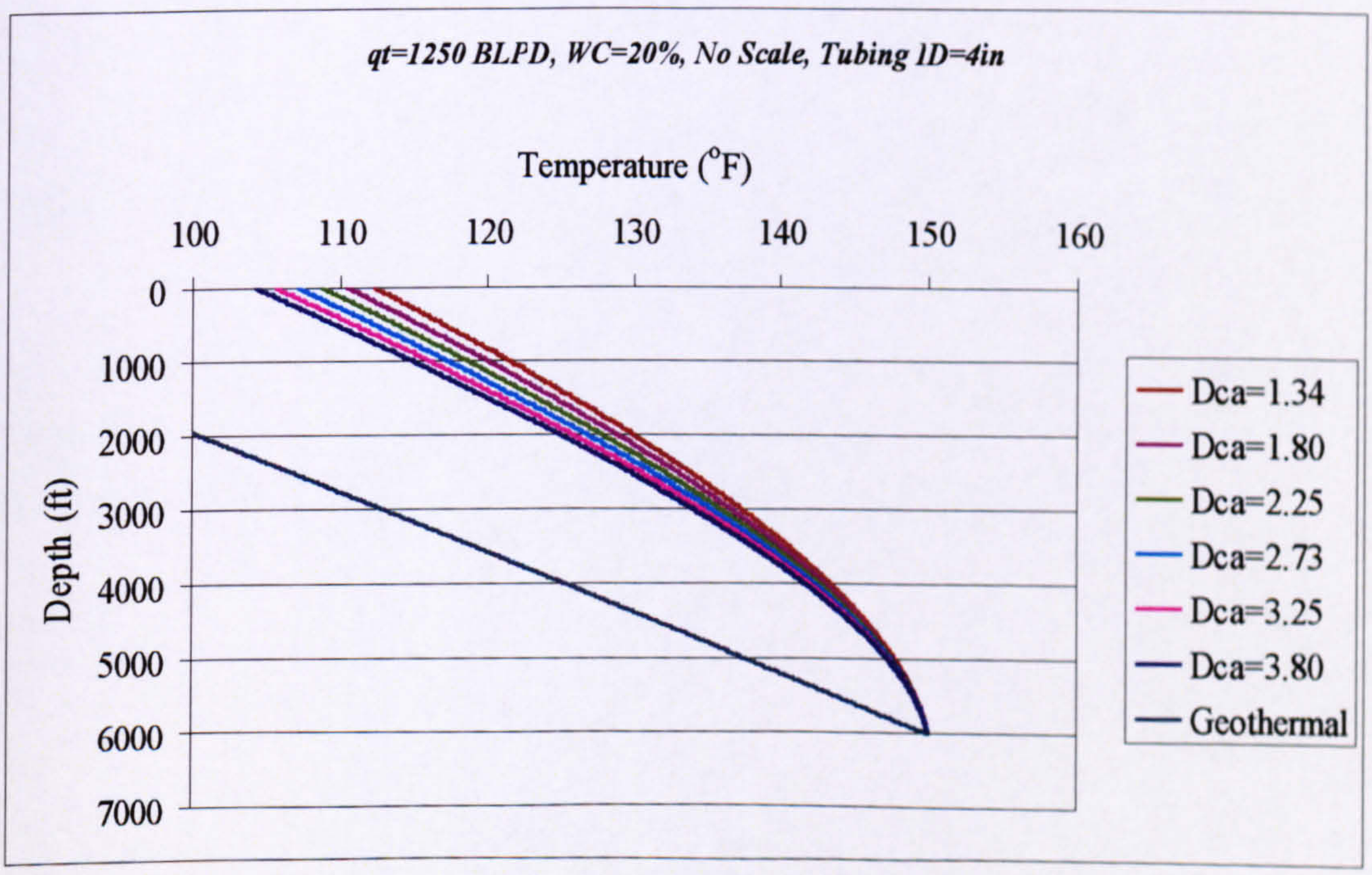

Figure 6-14. Temperature Profiles for Increasing Annulus Area

6.7.2 Impact of Annulus Area Size on Detection of Scale:

The insulation effect, due to the low thermal conductivity of any scale deposits on the inside of the tubing will reduce the overall heat transfer coefficient in the scaled-up region. This reduction will cause an increase in the temperature difference between the fluid in the tubing and in the annulus, reducing heat losses from the tubing to the formation. Figure 6-15 shows that, as the ratio of the annulus area to the tubing area increases, the temperature difference caused by the presence of scale deposits inside the tubing increases.

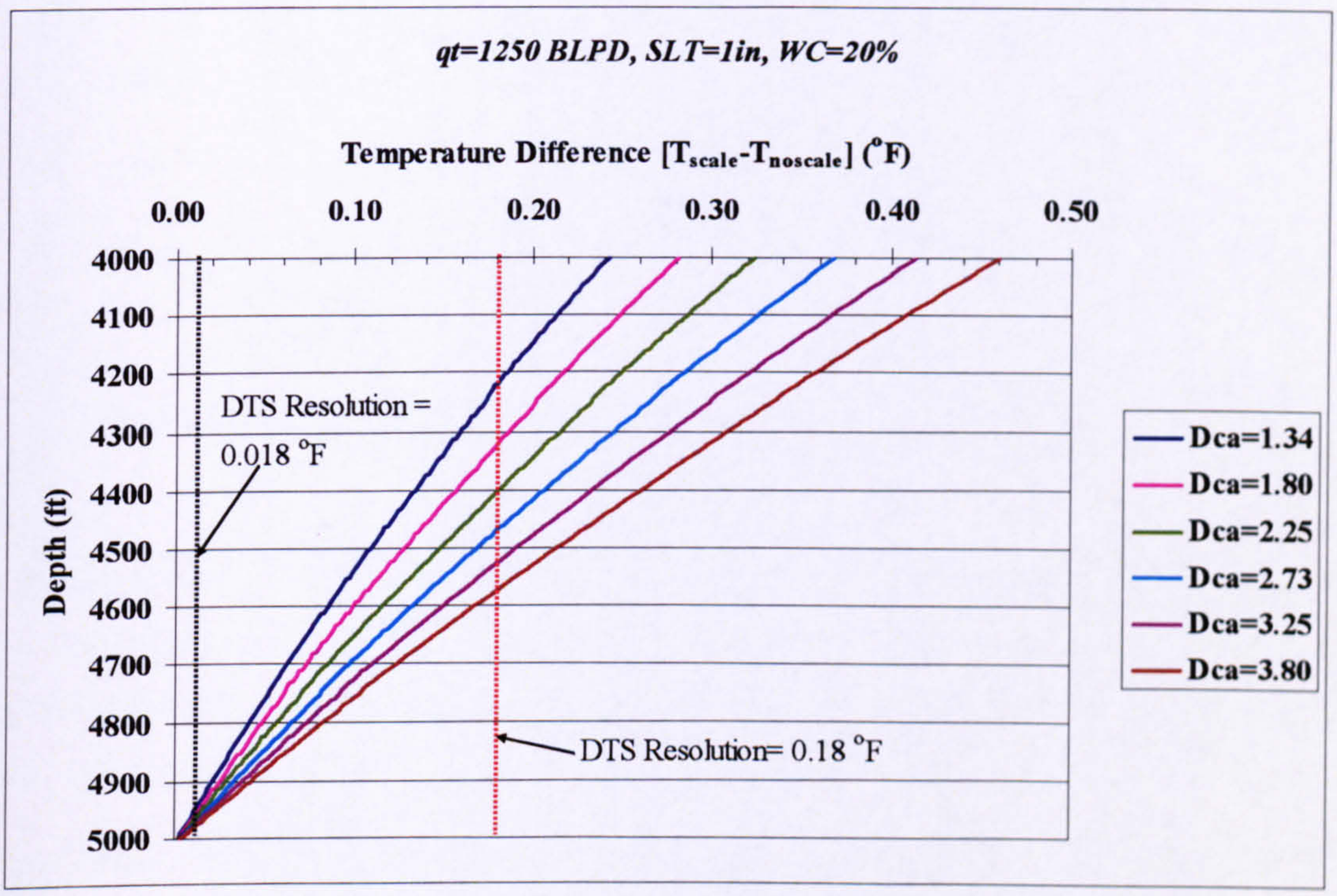

Figure 6-15. Effect of Increasing the Annulus Area on the Temperature Difference Caused by Scale Deposition in the Tubing

The low conductivity of the scale layer will dominate the overall heat transfer coefficient (U_{to}) in Equation 6.12 for the scaled length of the tubing. Figure 6-16 shows the impact of the scaled-up zone on overall heat transfer coefficient values.

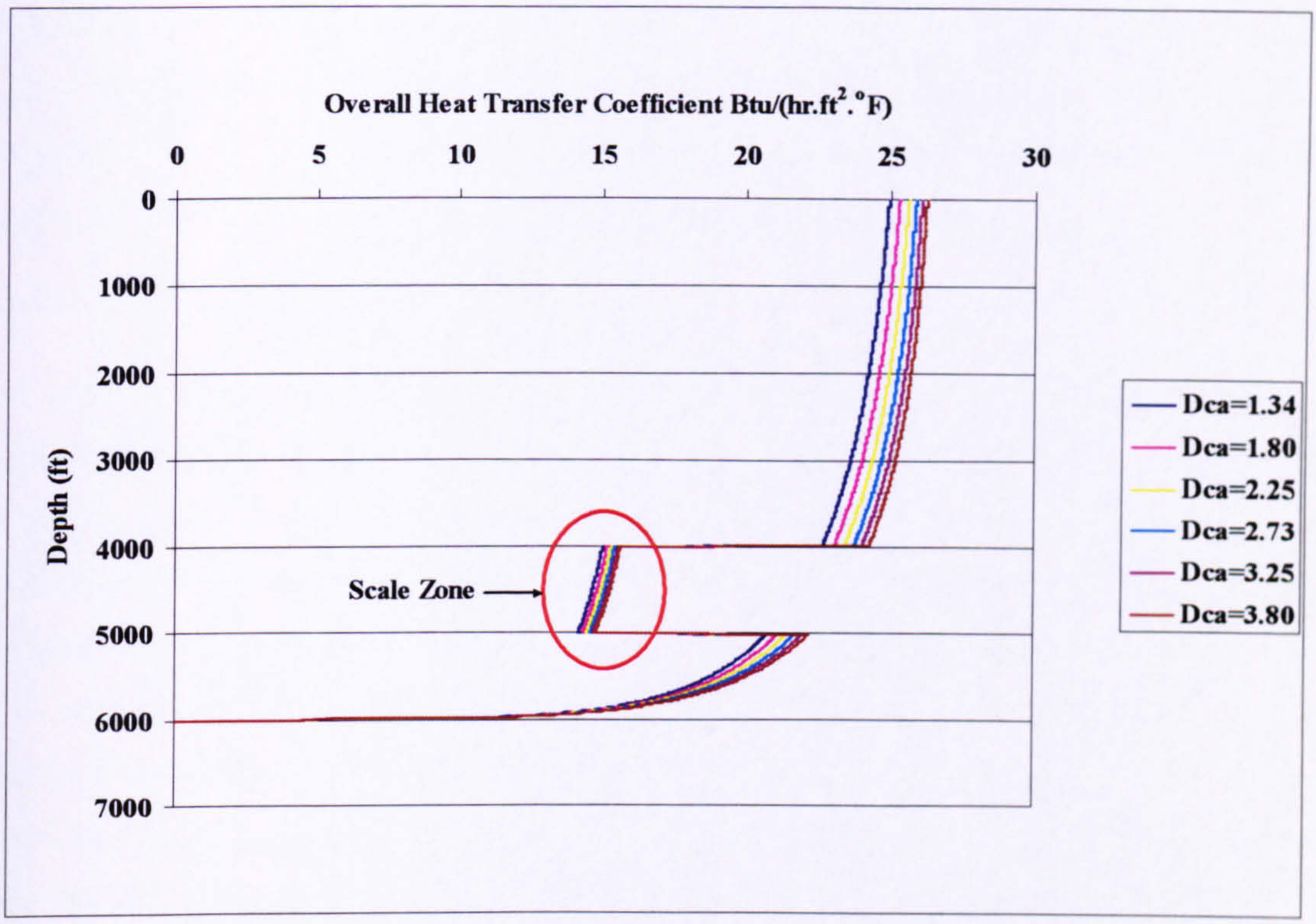

Figure 6-16. Overall Heat Transfer Coefficient in Scaled-Up zones (Completion Sizes Sensitivity)

A more noticeable increase in the temperature of the fluid in the tubing will be observed as the difference in the U_{to} value between the tubing with scale deposits, and the non-scaled tubing increases. A greater temperature difference over time is created because of the scale insulation.

Therefore, the average temperature difference caused by the presence of scale layer will increase as the ratio of the annulus area to the tubing area increases.

6.8 Impact of Packer Fluids on Temperature Increase Caused by Scale Deposition:

The importance of the natural convection heat transfer occurring in the annulus was highlighted by the previous section examining the effect of changing the completion design and, hence, the annulus area.

The medium in which this natural convection occurs is the packer fluid. Operator's move to develop deep water field has focused the industry attention on the impact of the packer's fluid on the heat loss from the tubing to the surrounding formation. Heat loss in a deep water environment can lead to many problems such as wax and hydrate formation, which ultimately affect the well productivity. In addition, steam injection operations require good insulation to prevent reduction of steam temperature which

might affect the effectiveness of the operations. This lead the industry to move from gas-filled annuli to annuli filled with specially designed thermal insulated packer fluids [6.16]. Other factors that influence the selection of the packer fluids are, bottom-hole pressure, corrosion, carbon dioxide content in flowing fluid [6.17].

6.8.1 Types of Packer's Fluid:

A wide range of packer fluids are available; gas is the least desirable packer fluid when heat-loss to the formation is of high concern as it causes wellbore refluxing (condensation of gas and the convection current creation caused by change in the annulus fluid properties) that can cause the heat losses to be some three to six times higher than for insulated tubing. Oil emerged as a suitable material for reduced heat loss because of its low conductivity, but this low conductivity was counter-acted by the natural convection. Gelled oil has been considered as a replacement for oil, but environmental considerations rendered this to be undesirable [6.16]. Aqueous based packer fluids recently emerged as the favourite among production engineers for their good insulation and favourable environmental properties [6.16, 6.18].

6.8.2 Packer's Fluid Properties and Convection in the Annulus:

Natural convection occurs in the annulus due to fluid motion caused by differences in density within the fluid column. Hence, density and viscosity emerge as the main properties that affect the natural convection heat transfer. The natural convection heat transfer coefficient (h_{nc}) is a function of the Grashof number (Gr). The Grashof number represents "the ratio of the buoyancy force to the viscous force acting on the fluid" in the annulus [6.15]. It is defined as:

$$Gr = \frac{(r_{ci} - r_{to})^3 g \rho_a^2 \beta (T_f - T_{ci})}{\mu_a^2} \qquad \text{Equation 6.17}$$

Where,

β = Volume Expansion Coefficient of the fluid in the annulus, 1/°F

μ_a = Dynamic viscosity of annulus fluid, cp

ρ_a = Density of annulus fluid, lbm/ft^3

Equation 6.17 shows that increasing the fluid viscosity will decrease the natural convection in the annulus while increasing the density will increase the natural

convection. These properties have been investigated in order to complete the investigation for the application guidelines for detection of scale using DTS temperature data.

6.8.3 Impact of Varying Packer's Fluid Properties:

The packer's fluid properties used in the base case (Table 6-1) were taken from Vollmer et. al. [6.12]. Packer fluids with viscosities between 0.52 cp to 4300 cp and densities between 64 lbm/ft^3 for KCl solution to 157 lbm/ft^3 for $ZnBr_2$ are available [6.17]. Figure 6-17 shows that, as expected, an increased packer fluid viscosity decreases the average temperature difference caused by scale deposition.

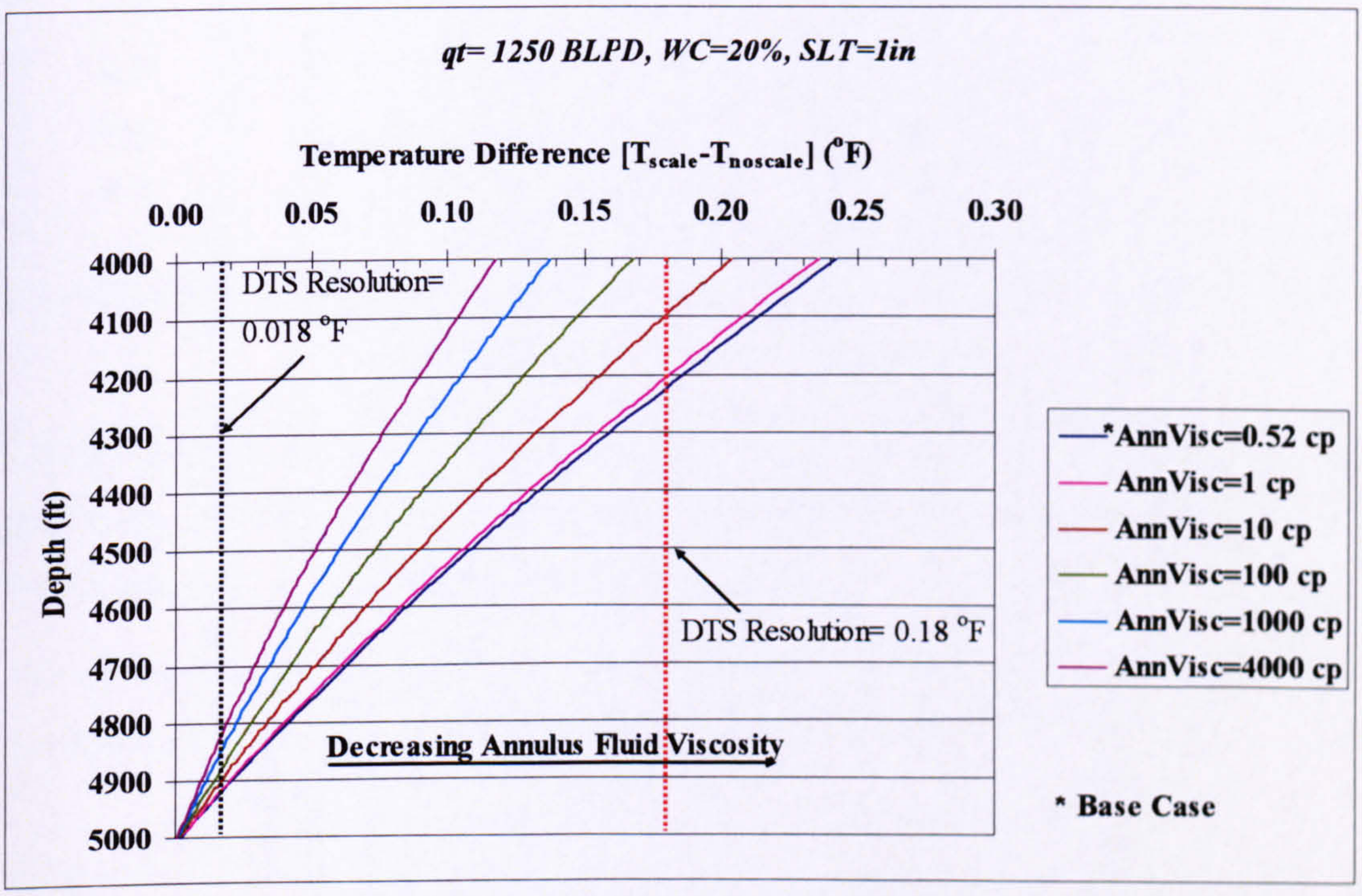

Figure 6-17. Effect Of Annulus Fluid Viscosity On The Temperature Increase Caused By The Scale Deposits In The Tubing

An increased fluid density has the opposite effect to that of an increased viscosity. An increased density causes higher heat losses from the produced fluid to the formation prior to the region where the scale is deposited in the tubing due to increased natural convection. The low thermal conductivity of the scale thus causes an increase in the temperature difference between the scale/no-scale cases. However, this is a minor effect and the temperature differences due scale deposition are not significant due to the narrow range of packer fluid densities (Figure 6-18).

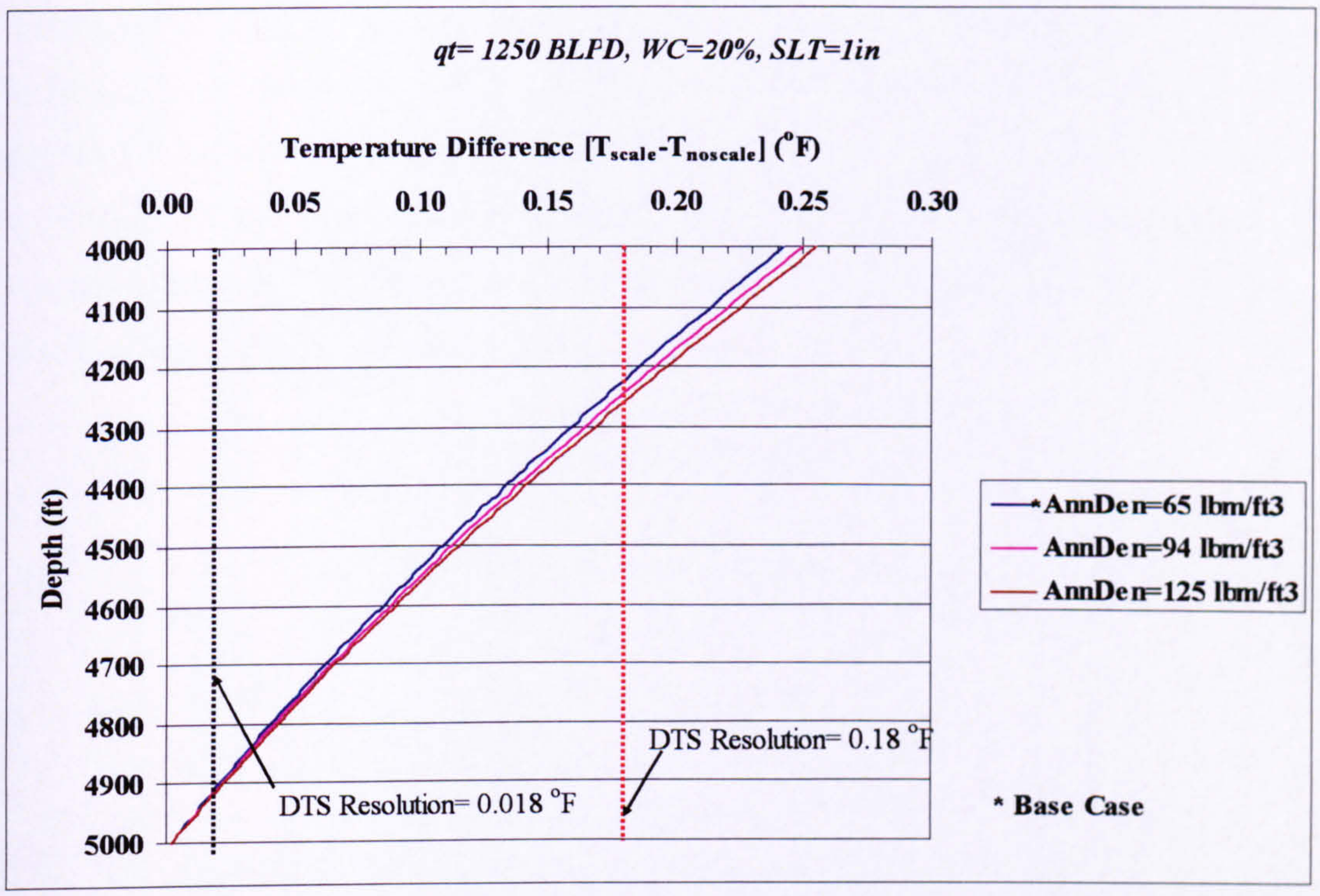

Figure 6-18. Small Impact on Temperature Difference Caused by Presence of Scale with Changing Packer Fluid Density

This leads to the conclusion that the properties of the packer fluid play an important role, particularly the viscosity, in determining if there is a potential in using the DTS temperature data to detect scale deposits in the tubing.

The relationship between the properties and the average temperature difference can be summarized as:

$$\Delta T_{avg,scale} \alpha \frac{1}{\mu_a}$$

$$\Delta T_{avg,scale} \alpha \rho_a$$

6.9 Impact of Scale Deposits Location and Length:

The depth in the well where the scale is deposited is as important as the previously discussed parameters. The fluid flowing up the tubing continuously losses heat to the formation. This heat loss is higher toward the top of the well since the difference between the formation temperature and that of the produced fluid is larger, causing greater natural convection in the annulus. The presence of scale will reduce the heat loss from the tubing because of the dominance of the low scale conductivity on the overall heat transfer coefficient.

A sensitivity analysis was carried out from the base case by moving the 1,000ft long scale zone up the well. The average temperature difference caused by the scale deposition increases at shallower depths (Figure 6-19). It is thus easier to detect the scale using DTS if scaling occurs towards the top of the well. This occurs because the average temperature difference between the fluid in the tubing and the surrounding is greater at the shallower depths.

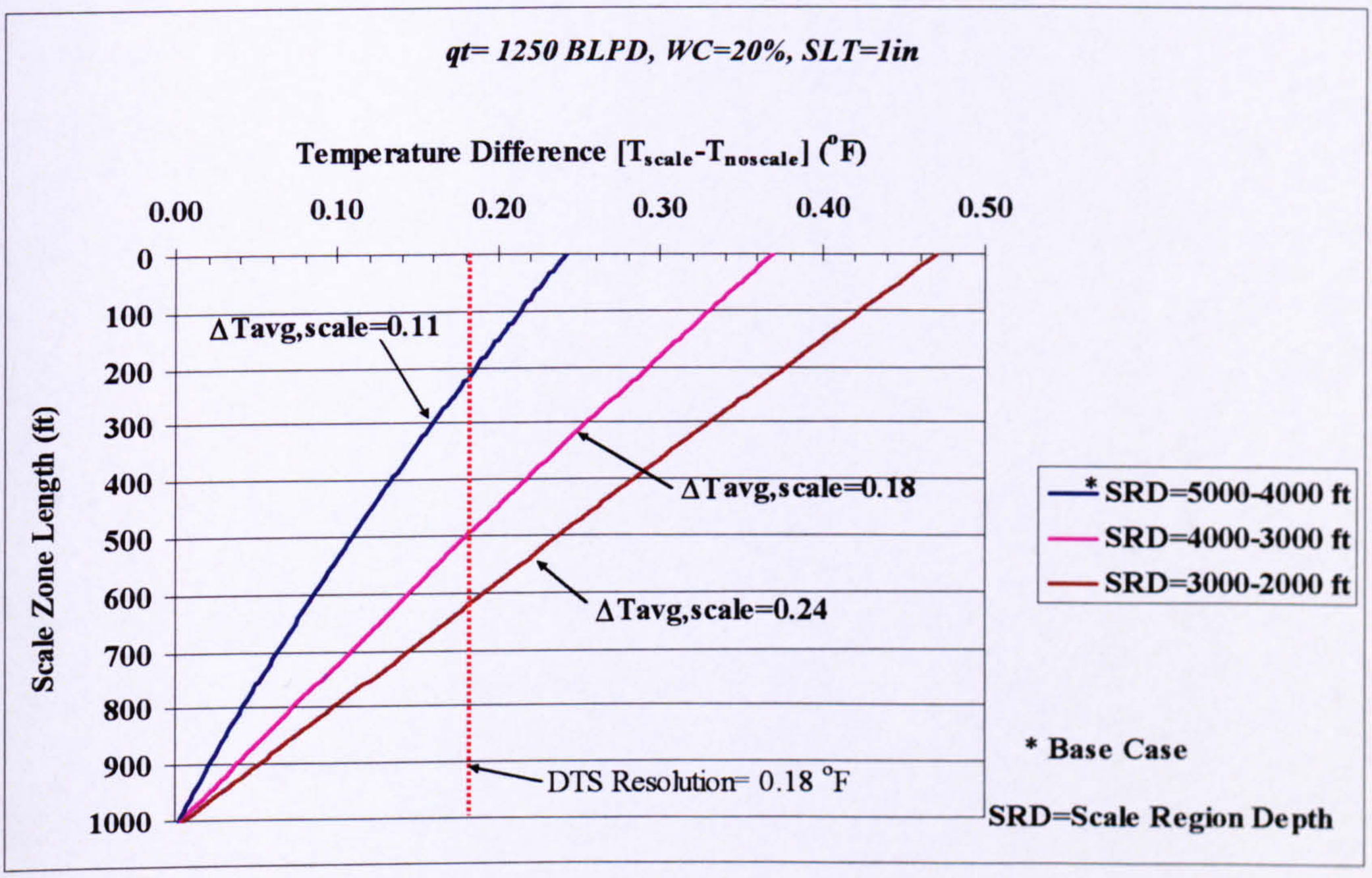

Figure 6-19. Influence of the Scale Region Location on the Tubing Temperature Difference Caused by the Presence of Scale

Figure 6-20 shows that, as the scaled-up region length increases, the average temperature difference caused by scale increases for the base case, while decreasing the length lead to the temperature difference to fall below the 0.18 °F threshold for DTS resolution.

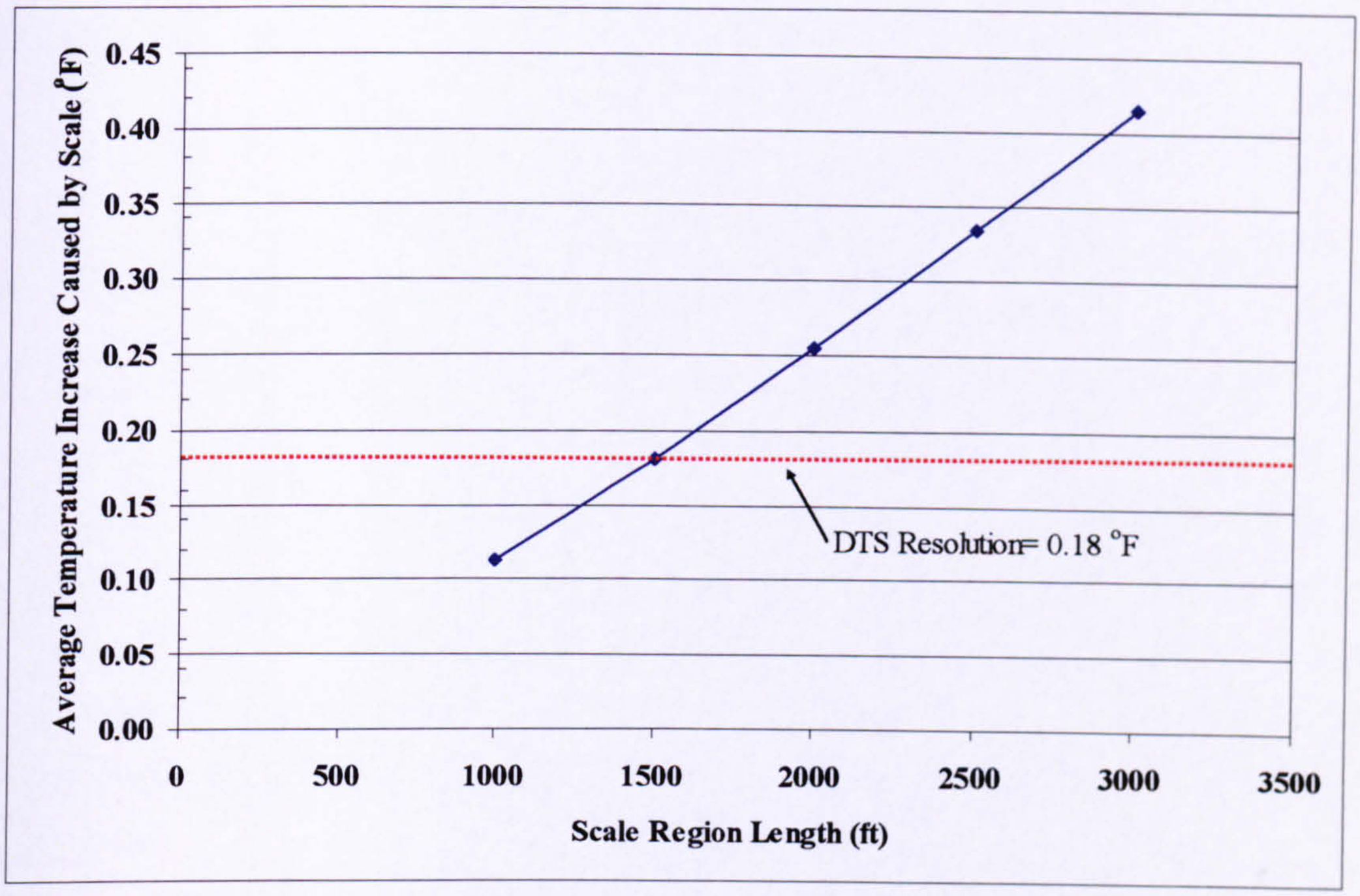

Figure 6-20. Scale Region Length Sensitivity

The length of the scale region influences the residence time during that the fluid experiences reduced heat losses due to the insulation effect caused by the presence of scale in the tubing. If the scale region length is small, the residence time across the scale insulated region is short, and there is only a small difference in temperature between the scale and the no scale cases.

6.10 General Observations on Temperature Behaviour in Scaled Regions:

Temperature deviations caused by scale deposition in production tubular are most visible under the following conditions and the assumptions listed in section 6.5 :

1. Production Parameters:
    a. Low-to-moderate liquid production rate
    b. Low water cut
2. Completion Design:
    a. Large annulus area
    b. Low viscosity packer fluids
    c. No thermal insulation

3. Scale Location and Length:

    a. Long scale zone

    b. Scale Region Located Toward the top of the well.

6.11 Application of DTS in Detecting Scale Deposition:

It has been shown that the temperature of the fluid will increase in the scaled region compared to the case when there is no scale. This increase will depend on various production and well design related conditions. Standard DTS installation practices attach the fibre optic cable to the outside wall of the tubing. The DTS will thus register a decrease in the temperature-depth profile when a low conductivity scale layer is deposited inside the tubing. In addition, the DTS will register a higher-than-usual temperature after the scale region. This is a second indication that scale has been deposited.

Figure 6-21 illustrate a constructed temperature profile from the results of the simulation of what the DTS profile would look like in the case of scale deposition. The scale region temperature was replaced with the temperature of the casing, which has been assumed to be the annulus temperature. The casing temperature is calculated using:

$$T_{co} = T_{wb} + \frac{\log\left(r_{wb}/r_{co}\right)}{k_{cem}} U_{to}\left(T_f - T_{wb}\right) \qquad \text{Equation 6.18}$$

Where,

T_{co}= Casing Temperature, °F

T_{wb}= Wellbore Temperature, °F

Figure 6-22 is an enlargement of the temperature profile in the scaled zone. It shows the temperature increase in the DTS profile after the scale region compared to the case where there is no scale deposited in the tubing. Temperature decrease in a flowing production well is usually associated with gas expansion (Joule-Thompson cooling). It is not followed by a temperature increase or (heating). Therefore, the effect of scale in the DTS depth-temperature profile (decrease followed by an increase) is unique in a conventional production well, this shows the potential of DTS to be used as a complimentary tool for scale detection and monitoring.

Another indication of the scale deposition from the DTS profile can be notice by the large increase in temperature after the scale region due to the insulation provided by the low thermal conductivity of the scale (e.g. for a scale layer thickness of 1 in. the increase after the cooling caused by the insulation is 3.5 °F). The temperature increase is expected to be higher if the pressure drop and the temperature increase due to the increase velocity was included.

The final temperature of the flowing fluid at the surface will show no differences for any scale layer thickness when compared to the no scale case. The surface temperature can not be used as an indicator of scale deposition. This highlights the importance of the continuous downhole monitoring provided by the DTS.

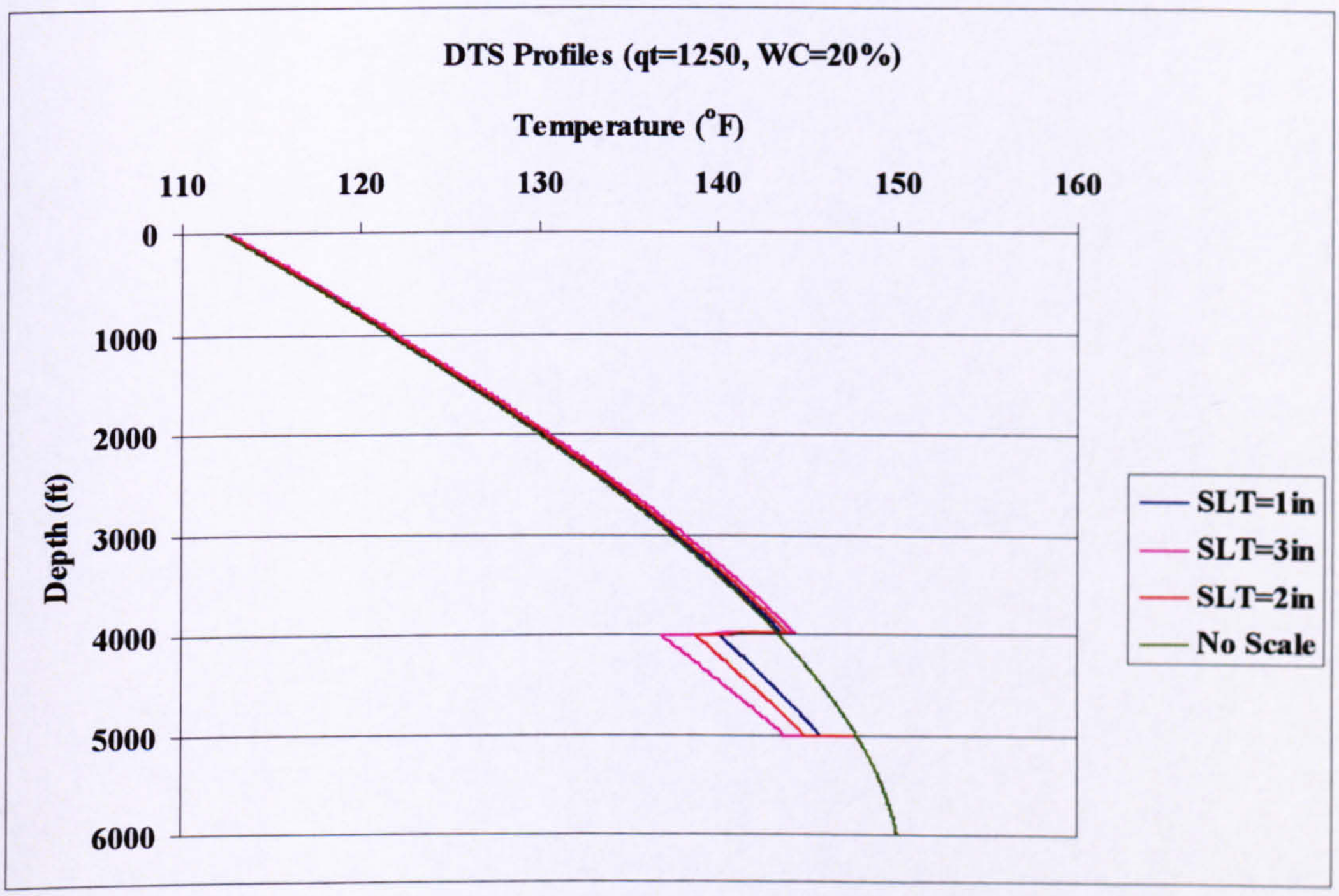

Figure 6-21. Calculated DTS Profile for Scale Detection of Base Case

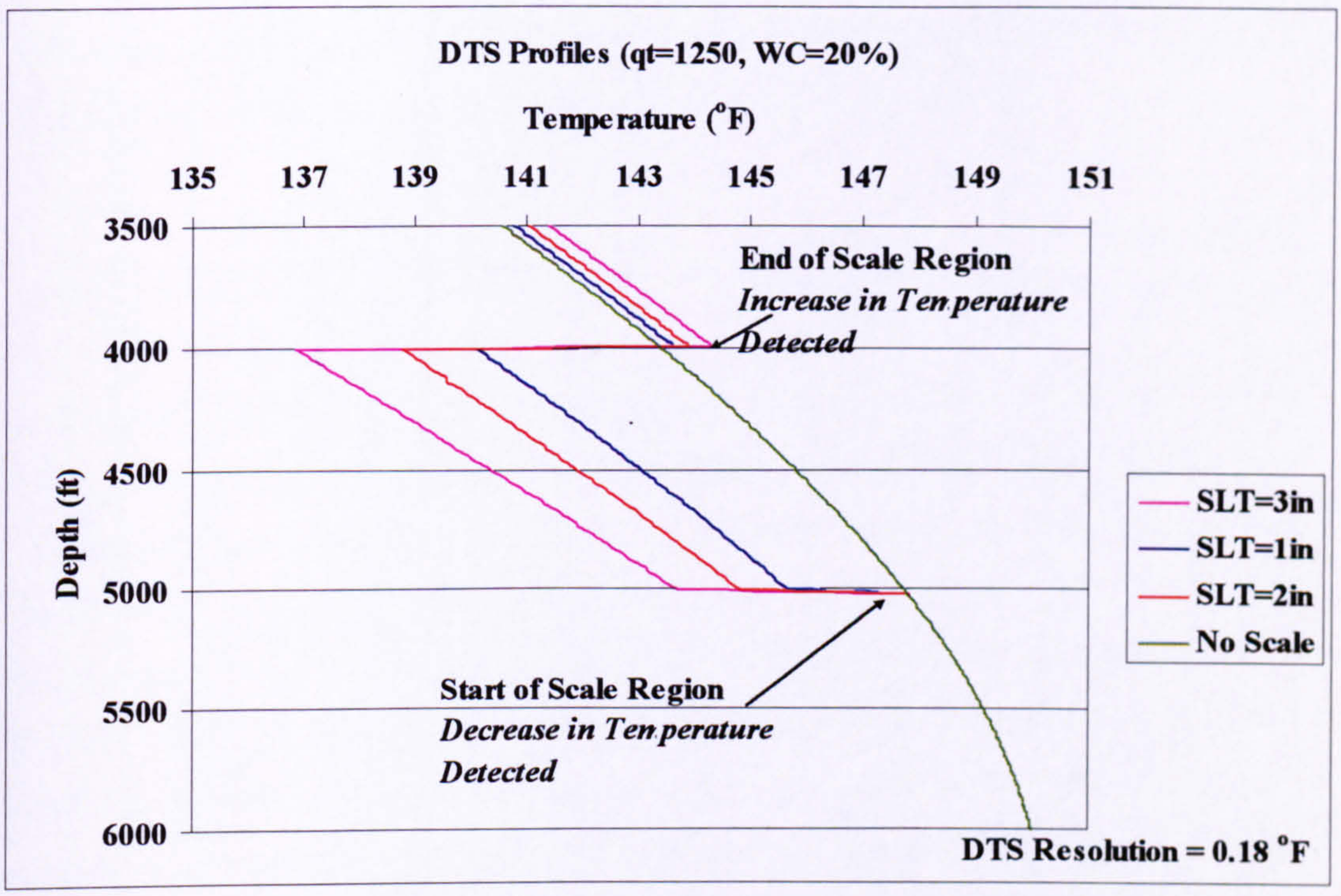

Figure 6-22. Calculated DTS Profile Focusing on the Scale Region

6.12 Calculation of scale inside radius (r_{si}) from Temperature Profiles:

The real-time and continuous nature of the DTS data allows the monitoring of the conditions downhole and, in the case of scale deposition, can provide a good tool to estimate the thickness of the deposited scale layer within the tubing. This piece of information is very important for the production engineer as it can aid in:

1. The indication of the severity of the scaling problem in the well
2. Planning for the proper treatment operation
3. Future simulation of scale deposition in the wellbore

The presence of scale can be detected, by using the DTS or by observing a reduced production rate at the surface or through other detection method such as calliper logging. The DTS temperature profile data from before and after scale deposition can be used to estimate the thickness of the scale layer. The assumption of sustained well deliverability to maintain the production flow rate is fundamental in this study due to the wide range of parameters that can affect the temperature profile in the wellbore; such as a fluctuating flow rate and a changing production fluid cut (WC, GOR).

The inside radius of scaled-up region of the tubing (r_{si}) expression is derived from the overall heat transfer coefficient for the scaled up region (Equation 6.12). The derivation

for the radius of the scaled region is illustrated in Appendix 1. The inside radius of scaled up tubing (r_{si}) can be calculated using the following expression:

$$r_{si} = \frac{r_{ti}}{\exp\left(\frac{k_{scale}}{r_{to}}\left[U_{scale}^{-1} - U_{noscale}^{-1}\right]\right)} \qquad \text{Equation 6.19}$$

The main unknowns in Equation 6.19 are the overall heat transfer coefficients for the well (U_{scale} and $U_{noscale}$) when there is no scale deposited and when the scale is deposited at a particular time. Determination of these unknowns is the main advantage of the downhole DTS temperature data. Historically, for conventional well temperature prediction, the overall heat transfer coefficient is determined by an iterative procedure [6.6, 19]. Figure 6-23 illustrates this procedure. An iterative solution is required for the overall heat transfer coefficient in the conventional wells due to the need to determine the natural convection heat transfer coefficient (h_{nc}) for the static fluid in the annulus (packer fluid, air, gas). Calculation of the natural convection heat transfer coefficient requires the determination of the Grashof number (Equation 6.17). The Grashof number is a function of the temperature drop across the annulus. This, in turn, requires knowledge of the temperature of the fluid in the tubing which is the parameter required to be predicted. Therefore an iterative determination of the U coefficient is required to predict the temperature.

The availability of DTS data eliminates the need for such an iterative procedure. Knowledge of the flowing fluid temperature in the tubing allows direct estimation of the overall heat transfer coefficient (U_{to}) factor by back-calculating it from the temperature prediction model (i.e. Figure 6-11)

The inside radius of the scaled-up region can be determined and thickness of the scale layer can be estimated from the determination of the U factors in Equation 6.19. The algorithm in Figure 6-24 illustrates the method to calculate the layer thickness of the deposited scale by estimating the inside radius of the scaled up region.

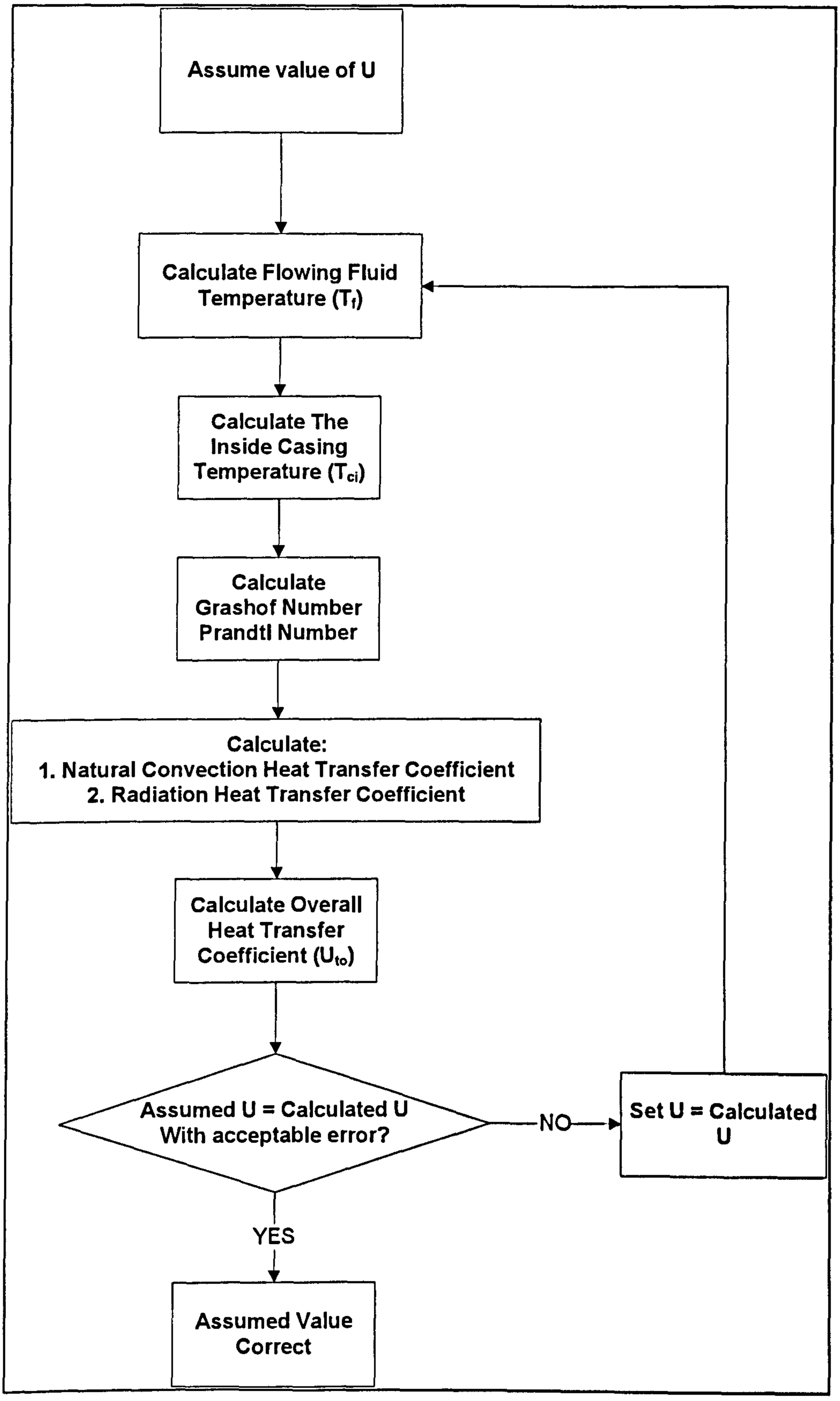

Figure 6-23. Overall Heat Transfer Coefficient with Natural Convection

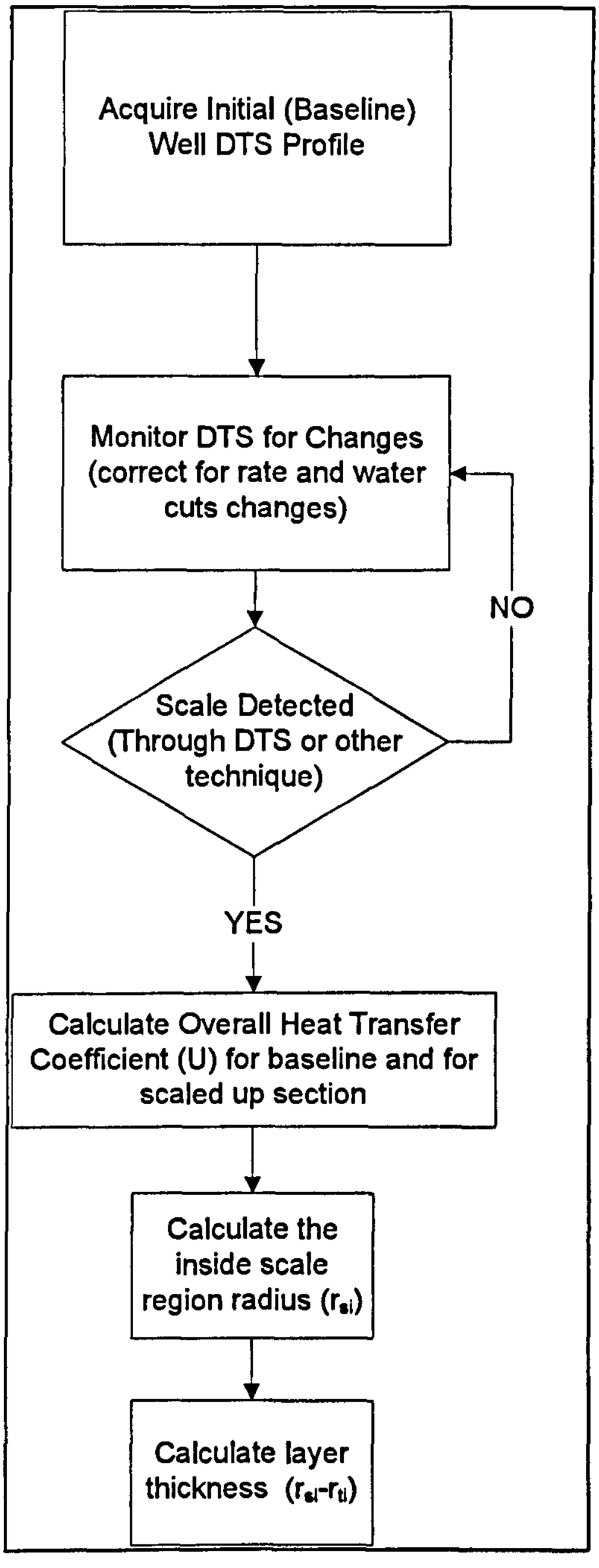

Figure 6-24. Scale Layer Thickness Determination Algorithm

6.13 Discussion and Conclusions:

1. DTS is being employed as a remote sensing tool as part of the I-field concept. This chapter has examined if, and under what conditions, DTS can be used to detect scale deposition in the tubing.

2. In general, scale detection using DTS temperature data can be best achieved when the well is experiencing large heat losses to the formation. The scale layer can acts as an insulator and an increased temperature-depth profile can be observed compared to the base line (initial well temperature profile).

3. Similar to all other DTS applications, DTS is not an independent tool for scale detection. However, it can serve as a complimentary tool to the engineer, which in favourable circumstances, can be used to determine if the scale is present as well as the thickness of the deposited scale. This tool is thus useful for treatment and intervention planning.

4. The DTS resolution determines the sensitivity with which scale deposition can be detected. A higher resolution will detect smaller changes in the wellbore (a smaller scale layer thickness). The DTS resolution is closely linked to the measurement time. A longer measurement time will provide a better resolution. Therefore, it is important to establish an adequate measurement time to achieve the resolution needed for the desired application.

5. The concepts discussed here can also be applied to an open-hole horizontal well by first modelling the temperature in the horizontal section to determine the temperature at the heel of the horizontal section. The same procedure discussed in this chapter can then be applied.

Temperature behaviour and modelling in intelligent completion vertical wells will be discussed in the next chapter.

6.14 References

6.1. Smith, J.K., et al., *Real-Time and In-Situ Detection of Calcium Carbonate Scale in a West Texas Oil Field.* SPE Production & Facilities, 2004: SPE87376 p. 94-99.

6.2. Emmons, D.H., et al. *On-Site, Near-Real-Time Monitoring of Scale Deposition.* Paper SPE56776 presented at 1999 SPE Annual Technical Conference and Exhibition, Houston, Texas, U.S.A., 3–6 October 1999, Society of Petroleum Engineers.

6.3. Ramstad, K., et al., *Predicting Carbonate Scale in Oil Producers From High-Temperature Reservoirs.* SPE Journal, 2005(December 2005): SPE87430 p. 363-373.

6.4. Bourne, H.M., G. Williams, and C.T. Hughes. *Increasing Squeeze Life on Miller with New Inhibitor Chemistry.* Paper SPE60198 presented at SPE 2nd International Symposium on Oilfield Scale, Aberdeen, Scotland, 26-27 January 2000, Society of Petroleum Engineers.

6.5. Hasan, A.R. and C.S. Kabir, *Aspects of Wellbore Heat Transfer During Two-Phase Flow.* SPE Production & Facilities, 1994: SPE22948 p. 221-216.

6.6. Hasan, A.R. and C.S. Kabir, *Fluid Flow and Heat Transfer in Wellbores*: Published by Society of Petroleum Engineering in 2002.

6.7. Zolotukhin, A.B. *Analytical Definition of The Overall Heat Transfer Coefficient.* Paper SPE7964 presented at California Regional Meeting of the Society of Petroleum Engineers of AIME, Ventura, California, U.S.A., 18-20 April 1979, American Institute of Mining, Metallurgical and Petroleum Engineers, Inc.

6.8. H.J. Ramey, J., *Wellbore Heat Transmission.* Journal of Petroleum Technology, 1962(April 1962): SPE96 p. 427-435.

6.9. Erickson, D.D. and M.C. Mai. *A Transient Multiphase Temperature Prediction Program.* Paper SPE24790 presented at SPE 67th Annual Technical Conference and Exhibition, Washington, DC, U.S.A, 4-7 October 1992, Society of Petroleum Engineers.

6.10. The MathWorks, I., *MATLAB*. 1994-2006, The MathWorks, Inc.

6.11. Sensornet, *Sentinel DTS Product Range* http://www.sensornet.co.uk/download.cfm?type=document&document=112 Accessed On:19 Feb 2007

6.12. Vollmer, D.P., et al. *Convective Heat Transfer in Turbulent Flow: Effect of Packer Fluids on Predicting Flowing Well Surface Temperatures.* Paper SPE86546 presented at SPE International Symposium and Exhibition on Formation Damage Control, Lafayette, Louisiana, U.S.A, 18-20 February 2004, Society of Petroleum Engineers.

6.13. Hasan, A.R. and C.S. Kabir. *Heat Transfer During Two-Phase Flow in Wellbores: Part I - Formation Temperature.* Paper SPE22866 presented at 66th Annual Technical Conference and Exhibition of the Society of Petroleum Engineers, Dallas, Texas, U.S.A., 6-9 October 1991, Society of Petroleum Engineers.

6.14. Gambill, W.R., *You Can Predict Heat Capacities.* Chemical Engineering, 1957: p. p. 42-46.

6.15. Cengel, Y.A., *Heat Transfer - A Practical Approach.* Second ed: Published by McGraw-Hill Higher Education in 2003.

6.16. Wang, X., et al. *A New Thermal Insulating Fluid and Its Application in Deepwater Riser Insulation in the Gulf of Mexico.* Paper SPE84422 presented at SPE Annual Technical Conference and Exhibition, Denver, Colorado, U.S.A., 5-8 October 2003, Society of Petroleum Engineers.

6.17. Fang, C.S. and D. Vollmer, *Method obtains alkali formate packer fluid thermal conductivity.* Oil & Gas Journal, 2002. **100**(52): p. 49-53.

6.18. Wang, X., et al. *Factors Controlling the Proper Design of Effective Insulation Fluids for Oilfields*. Paper SPE103132 presented at 2006 SPE Annual Technical Conference and Exhibition, San Antonio, Texas, U.S.A., 24-27 November 2006, Society of Petroleum Engineers.

6.19. Willhite, G.P. *Over-all Heat Transfer Coefficients in Steam and Hot Water Injection Wells*. Paper SPE1449 presented at SPE Rocky Mountain Regional Meeting, Denver, Colorado, May 24-24 1966, SPE.

Chapter 7 Temperature Modelling and Behaviour in Intelligent Wells

7.1 Introduction:

The complexities of an intelligent completion complicate the analysis of the temperature profile behaviour across the completion interval. This chapter investigates the impact that the different flow paths, fluid properties and the added equipments have on the temperature profile in the wellbore and how their effects should be modelled.

This chapter extends the enthalpy/energy balance temperature prediction model developed by Hasan & Kabir [7.1] for a conventional well so that it can be applied to an intelligent completion. This new solution can be used for steady-state modelling of the temperature profile in the intelligent completion. The extension is based on altering their initial and boundary conditions to represent the intelligent well's completions.

The annulus, and its static fluid, plays an important role in the heat transfer from the tubing to the surrounding formation in conventional wells, was discussed in Chapter 6. It is even more important when annular flow occurs, as is the case for an intelligent

well, since natural, convection heat transfer process (caused by density variations) changes to forced convection due to fluid flow. Forced convection may increase or decrease the heat transfer rate from the tubing to the formation depending on the type of flow (turbulent or laminar) and the thermo-physical properties of the produced fluids.

Understanding the added complexities of the intelligent wells have implications when DTS or any other temperature sensor data is being interpreted for the detection of fluid/flow anomalies or when the DTS data is being is matched with the modelled wellbore temperature for zonal flow allocation. Accounting for the various production scenarios encountered in intelligent completions can help the engineer avoid misinterpretation of the available data. The cooler annulus fluid can also directly influence the temperature profile by mixing with the warmer produced tubing fluid.

The effect of the annulus has been studied before from the point of view of conventional wells. However, an intelligent completion offers a different scenario due to the varying inflow profile. Conventional well temperature modelling, assumes that the inflow enters the well at a single point at the bottom of the completion. This is different for the intelligent completion where the perforated interval or open-hole, inflow zone may have a length of many hundreds of or even thousands feet. The effect of this extended annulus inflow profile will also be studied in this chapter.

The main objective of this chapter is to provide the basis of a temperature data analysis methodology for the different production environments encountered in intelligent completions. This will aid in accurate matching to DTS data and hence provide a better interpretation, enhancing the decision making to better optimize the well's production strategy.

7.2 Application of H&K model in Intelligent Completion Environments:

Identifying the effect of the intelligent completion equipment (annular flow, zonal isolation through packers, mixing of temperature at the valves) and their effect on the temperature profile in the I-Well are the main focus of this study. This section examines the extension required to the H&K temperature behaviour model [7.1, 7.2] to model I-Well production environments.

A complex well completion modifies the initial and the boundary conditions imposed on the solution of the energy balance equation for any well segments that describe the completion opposite the producing zones where the intelligent completion is installed.

The main equations developed by Hasan and Kabir [7.1, 7.2] that will be used in this work are:

For tubing flow temperature (describing the heat transfer from the tubing to the annulus):

$$\frac{dT_t}{dz} = \frac{1}{B'}(T_t - T_a) - \frac{D_t}{C_{pt}} \qquad \text{Equation 7.1}$$

For the annulus flow temperature:

$$\frac{dT_a}{dz} = -\left(\frac{1}{A}\right)(T_{ei} - T_a) + \frac{1}{B_a}(T_a - T_t) - \frac{D_a}{C_{pa}} \qquad \text{Equation 7.2}$$

By substituting Equation 7.1 into Equation 7.2 then the tubing temperature profile can be expressed in the following second order differential equation:

$$-AB' \frac{d^2T_t}{dz^2} + B'' \frac{dT_t}{dz} - T_t + T_{ei} + D' = 0 \qquad \text{Equation 7.3}$$

Where,

T_t = Temperature of the tubing, °F

T_a = Temperature of the annulus, °F

T_{ei} = Geothermal Temperature, °F

And

$$B' = \frac{w_t C_{pt}}{2\pi r_{to} U_{ta}} \qquad \text{Equation 7.4}$$

$$B_a = \frac{w_a C_{pa}}{2\pi r_{to} U_{ta}} \qquad \text{Equation 7.5}$$

$$A = \frac{w_a C_{pa}}{2\pi}\left[\frac{k_e + r_{co} U_{fa} T_D}{r_{co} U_{fa} T_D}\right] \qquad \text{Equation 7.6}$$

$$B'' = B' + \frac{AB'}{B_a} + A \qquad \text{Equation 7.7}$$

$$D_a = -\frac{\mu_{JT} C_{pa}}{J}\frac{dp_a}{dz} + \frac{g\sin\alpha}{g_c J} + \frac{v_a}{g_c J}\frac{dv_a}{dz}$$ Equation 7.8

$$D' = B'\frac{D_t}{C_{pt}} + \frac{AB'}{B_a}\frac{D_t}{C_{pt}} - A\frac{D_t}{C_{pa}}$$ Equation 7.9

Equation 7.2 describes the energy balance for the temperature in the annulus. The term B_a (Equation 7.5) describes the heat transfer from the annulus to the tubing, while A, the relaxation parameter (Equation 7.6) describes the heat loss from the annulus to the formation. The D_a term (Equation 7.8) combines the effect of the pressure drop, the Joule-Thompson effect, the elevation and kinetic energy terms. This latter is usually very small for incompressible fluid flow in vertical wells. The term D' in Equation 7.3 combines the D_a and D_t terms. D_t is analogous to the D_a, but represents the tubing plus all the associated heat transfer mechanisms described in Equation 7.4, Equation 7.5 and Equation 7.6. This term is also negligible for incompressible fluid flow. The B' term represents the heat transfer from the tubing fluid flow to the annulus.

The above equations were coded in MATLAB and the algorithm illustrated in Figure 7-1 applied to model the I-Well temperature using the assumptions and modifications described in the following sections.

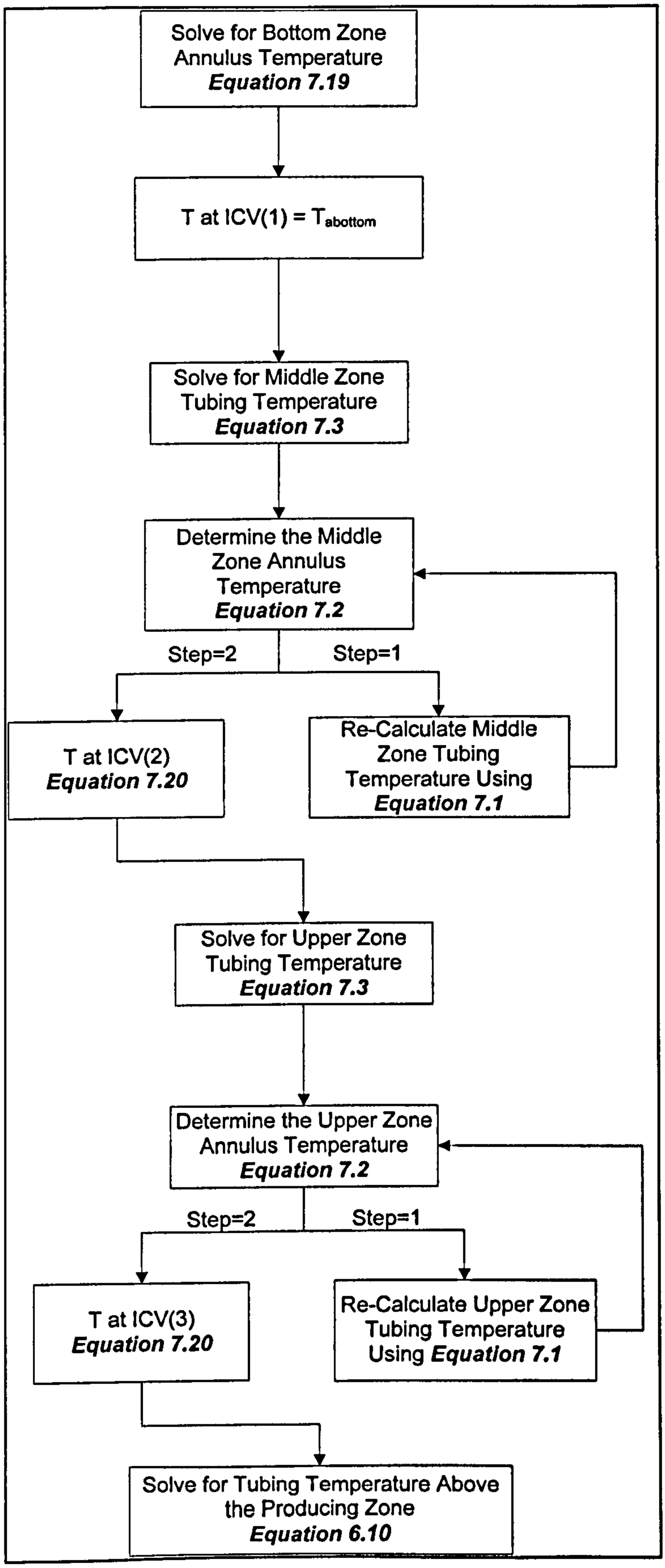

Figure 7-1. Model Solution Algorithm

7.2.1 Bottom Zone Treatment:

The tubing does not usually extend to the bottom of the well in intelligent completions. It usually ends a few feet below the bottom packer and the ICV. Thus, temperature modelling in the majority of the bottom zone resembles that for an open-hole or perforated casing production. However, in this work we will simulate the case when the tubing is fully extended to the bottom of the well. This will simplify the modelling and will focus our efforts on the effect of the completion, the aim of this work. The temperature in the tubing in the bottom zone can be derived using a heat transfer balance between the annulus and the tubing (Figure 7-2).

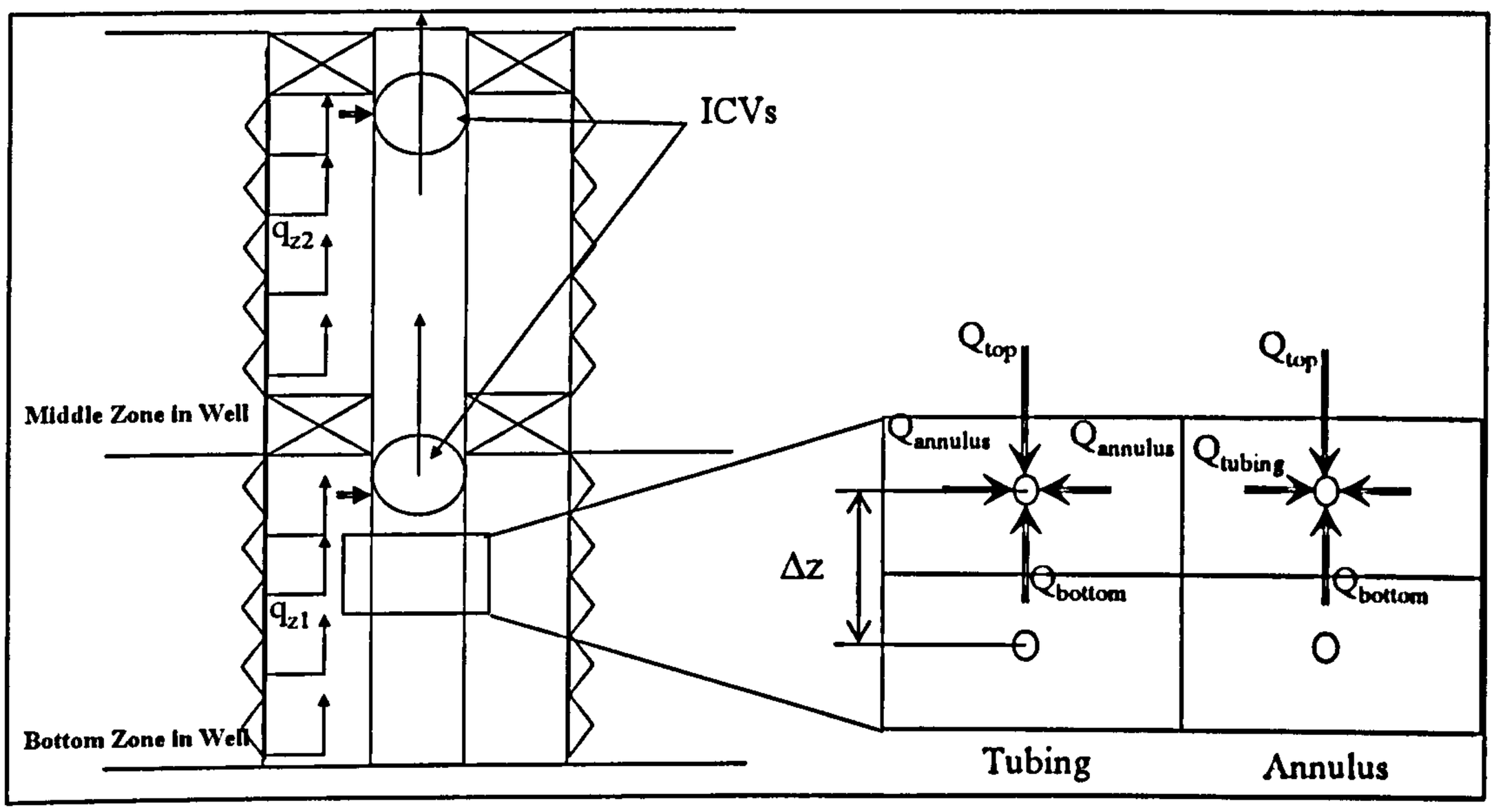

Figure 7-2 Heat Transfer Balance on Tubing Section for Bottom Zone where No Flow Occurs

Assuming steady state conditions, the heat transfer balance for a tubing node where the flow only occurs in the annulus is:

$$Q_{t,top} + Q_{t,bottom} + 2Q_{annulus} = 0 \qquad \text{Equation 7.10}$$

Where,

$Q_{t,top}$ = Heat transfer in the tubing from subsequent segment

$Q_{t,bottom}$ = Heat transfer in the tubing from the previous segment

$Q_{annulus}$ = Heat Transfer from the annulus (left and right)

Convective heat transfer occurs in the tubing once the well is flowing. This is expressed as:

$$Q_{t,top} = h_{tubing} A(T_t(Z + \Delta Z) - T(Z))$$ Equation 7.11

$$Q_{t,bottom} = h_{tubing} A(T_t(Z - \Delta Z) - T(Z))$$ Equation 7.12

Heat transfer from the annulus to the tubing is via heat conduction through the tubing:

$$Q_{annulus} = \frac{2\pi \Delta Z k_t}{\ln\left(r_{ci}/r_{to}\right)}\left(T_a(z) - T_t(z)\right)$$ Equation 7.13

The heat transfer balance becomes on substituting Equation 7.11, Equation 7.12 and Equation 7.13 into Equation 7.10:

$$h_{tubing} A(T_t(Z+\Delta Z) - T(Z)) + h_{tubing} A(T_t(Z-\Delta Z) - T(Z)) + \frac{4\pi \Delta Z k_t}{\ln\left(r_{ci}/r_{to}\right)}\left(T_a(z) - T_t(z)\right) = 0$$ Equation 7.14

There is no flow in the tubing. The forced convection heat transfer coefficient can thus be assumed to be zero, cancelling the first two terms of Equation 7.14. This reduces the heat transfer mechanisms to only the conductive heat transfer i.e. the temperature in the tubing will be equivalent to the temperature in the annulus when there is no flow in the tubing.

$$T_a(z) = T_t(z)$$ Equation 7.15

The other heat transfer mechanism that can occur is the natural convection heat transfer. Its coefficient (h_{nc}) is governed by the Rayleigh Number which is itself a function of the Grashoff number (Gr) (see chapter 6), and the Prandtl number (Pr), which describes the relative thickness of the velocity and thermal boundary layers (Equation 7.18):

$$h_{nc} = \frac{Nu.k}{d_{ti}} = CRa_L^n$$ Equation 7.16

Where C and n are constants depending on the geometry and the flow regime. The Rayleigh number is expressed in field units as:

$$Ra_L = Gr\,\mathrm{Pr} = \left(2.22E6\frac{r_{ti}^3 g\beta\rho^2\Delta T}{\mu^2}\right)\left(2.4191\frac{\mu C_p}{k}\right)$$ Equation 7.17

Where,

$$\Pr = \frac{\mu C_p}{k}$$ Equation 7.18

r_{ti} = Tubing inside radius, ft

g = Gravity Acceleration constant, ft/s^2

ρ = Tubing fluid density, lbm/ft^3

β = Volume expansion Coefficient, 1/°F

μ = Tubing fluid viscosity, cp

C_p = Specific Heat Capacity of the liquid, Btu/(lbm.°F)

k = Thermal Conductivity of the fluid, Btu/(hr.ft.°F)

ΔT = Temperature difference across the two surfaces, °F

We may assume that the natural convection heat transfer coefficient is zero i.e. we assume there are no temperature variations across this (imaginary) tubing wall, (Figure 7-3).

This assumption will simplify the solution for the energy balance for the annulus at the bottom of the well, since the annulus energy balance, when there is flow in both the tubing and the annulus, is also a function of the tubing temperature (Equation 7.19) [7.1].

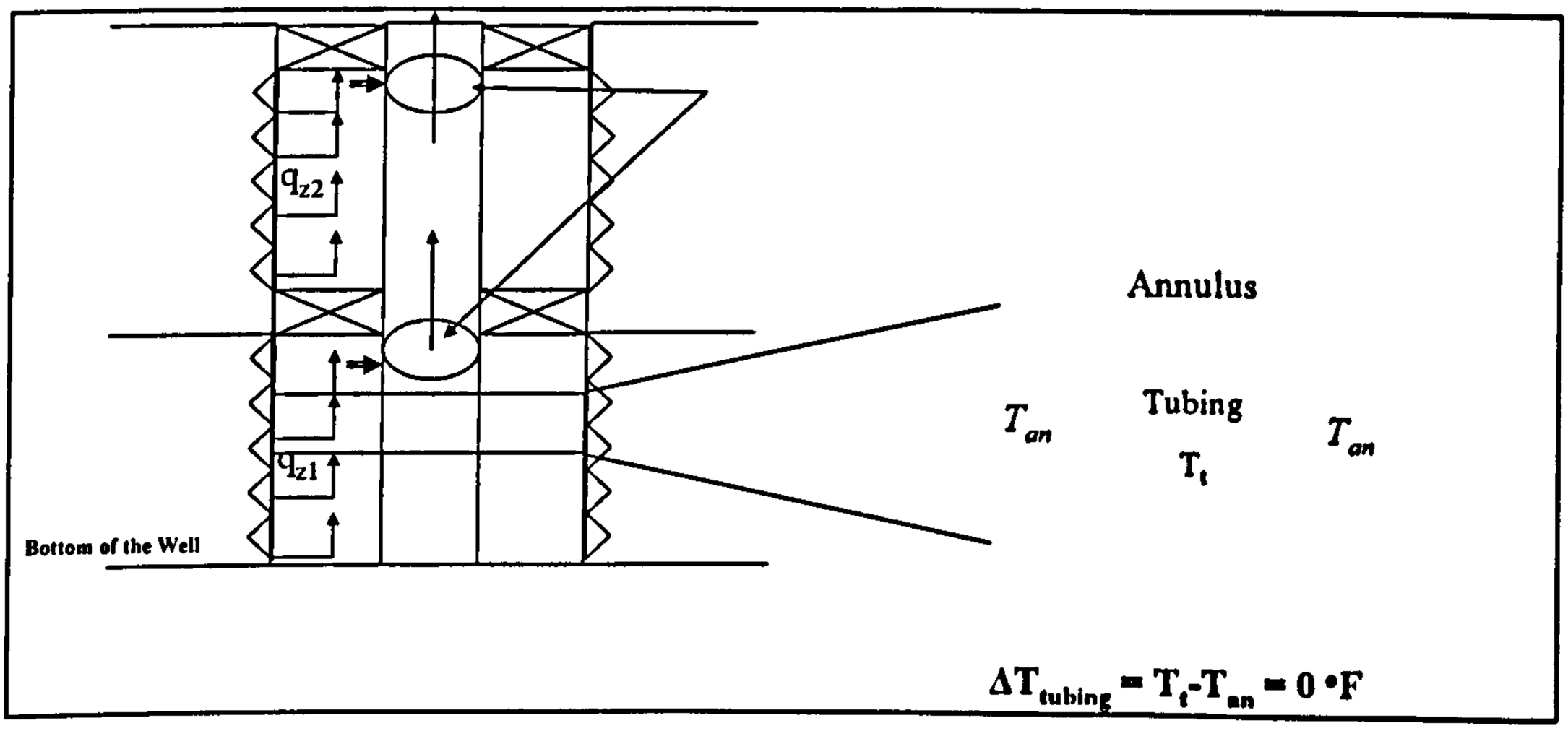

Figure 7-3 Temperature Difference Across the Bottom Zone Tubing = °F

Table 7-1. Annulus Energy Balance

Annulus Energy Balance	$\frac{dT_a}{dz} = -\left(\frac{1}{A}\right)(T_{ei} - T_a) + \frac{1}{B_a}(T_t - T_a) - \frac{D_a}{C_{pa}}$	Equation 7.19
Modified Annulus Energy Balance for the bottom zone segments	$\frac{dT_a}{dz} = -\left(\frac{1}{A}\right)(T_{ei} - T_a) - \frac{D_a}{C_{pa}}$	Equation 7.20

The first term in Equation 7.19 represents the heat transfer from the annulus to the formation while the second term represents the heat transfer from the tubing to the annulus or vice versa.

7.2.2 Importance of Mixing Temperature:

The annular flow joins the tubular flow at the top of each zone. Cooler fluid from the upper zones will mix with the warmer fluids from the bottom of the well, decreasing the temperature of the fluid in the tubing. The resulting cooler temperature will be the initial condition for calculating the temperature profile for the tubing segment of the following zone (e.g. the middle zone in Figure 7-3). (N.B. the temperature at the valve controlling the bottom zone will be the temperature of the fluid flowing from that zone).

Ideal mixing of the two streams is described by [7.3, 7.4]:

$$T_m = \frac{w_1 C_{p1} T_1 + w_2 C_{p2} T_2}{w_1 C_{p1} + w_2 C_{p2}} \qquad \text{Equation 7.21}$$

Where,

w = Mass flow rate, lbm/hr

T_m = Mixture temperature, °F

7.2.3 Annular Flow and Zonal Isolation through Packers:

One of the most important functions of an intelligent completion is the ability to divide the producing zones into isolated intervals so as to be able to control the production from each zone. The division of the producing zone into a number of intervals can be viewed as creating multiple wells within each (real) well.

Each isolated interval can be viewed as double pipe (co-current) heat exchanger from a heat transfer point of view. The inflow of the cooler formation fluid in the annulus will cool the warmer fluid in the tubing; providing there is sufficient heat transfer exist between the annulus and the tubing. The annulus temperature can be modelled using Equation 7.19. The initial formation temperature at the bottom of the targeted zone is used as the initial condition for this equation. The forced convection heat transfer is a function of the fluid properties and the flow regime (turbulent or laminar). Table 7-2 shows the forced convection heat transfer correlations used in the determinations of the convective heat transfer coefficients for the annulus and the tubing [7.5, 7.6]:

Table 7-2. Nusselt Number Correlations for Annulus and Tubing Heat Transfer Coefficient Calculations

Flow Regime	Correlation
Turbulent $3x10^3<Re<5x10^6$ $0.5 \leq Pr \leq 2000$	$Nu_t = \frac{(f/8)(Re-1000)Pr}{1+12.7(f/8)^{0.5}\left(Pr^{2/3}-1\right)}$ (Gnielinski Correlation, 1976)
Laminar $Re<3000$	$Nu_t = 4.364 + \frac{0.086\left(RePr\frac{D}{L}\right)^{1.33}}{1+0.1Pr\left(Re\frac{D}{L}\right)^{0.83}}$ (Setphan K. Correlation, 1962)

The forced convection heat transfer coefficient (h_{fc}) is calculated then from:

$$h_{fc} = \frac{Nu.k_{fl}}{D} \qquad \text{Equation 7.22}$$

Where,

k_{fl} = is the fluid thermal conductivity, Btu/hr.ft.°F

D = diameter, ft

Re=Reynolds Number

The diameter used for the annulus Nusselt number calculations is the hydraulic diameter of the annulus:

$$D_h = D_{ci} - D_{to}$$ Equation 7.23

The Prandtl Number (Pr) in field units is defined as:

$$\mathrm{Pr} = 2.4191\frac{\mu C_p}{k_{fl}}$$ Equation 7.24

The correlations presented in Table 7-2 were mainly orientated towards the chemical processing industry, these correlations were mostly developed in laboratory experiments. It has been assumed that they are representative of downhole conditions, but almost no work has been done on examining the applicability of these correlations in oil and gas wells environments. The development of new correlations based on the extensive data being collected from downhole using DTS could form an area of future research.

7.2.4 Inflow distribution Effect:

The inflow in the annulus can influence many parameters when modelling the temperature in both the annulus and the tubing. The annulus-formation overall heat transfer coefficient is expressed as:

$$U_{fa} = \left[\frac{r_{wb}\ln\left(r_{co}/r_{ci}\right)}{k_{\text{casing}}} + \frac{r_{wb}\ln\left(r_{wb}/r_{co}\right)}{k_{\text{cement}}}\right]^{-1}$$ Equation 7.25

The above equation assumes that the heat will be only be transferred from the annulus to the formation through conduction via the casing walls and the cement sheath. It will have a constant value as long as the casing/liner dimensions and properties do not change and the drilled hole has a constant diameter. Heat loss in the formation is modelled using transient heat diffusion. It is incorporated into the relaxation length parameter *(A)* (equation 7.2), using the dimensionless formation temperature (T_D), (defined by Equation 7.26 as [7.1, 7.7]):

$$T_D = \ln\left[e^{-0.2t_D} + \left(1.5 - 0.3719e^{-t_D}\right)\sqrt{t_D}\right]$$ Equation 7.26

t_D is the dimensionless time. It is defined as:

$$t_D = \frac{k_e t}{\rho_e C_{pe} r_{wb}^2}$$ Equation 7.27

Where,

k_e = formation conductivity, Btu/(hr.ft.°F)

ρ_e = formation density, lbm/ft^3

C_{pe} = formation heat capacity, Btu/(lbm.°F)

t = production/injection time, hr

Let us assume at this stage that it is fully perforated (Figure 7-4). The flowing fluid enters the annulus at the geothermal temperature of the formation via the perforations at that particular depth (Figure 7-5).

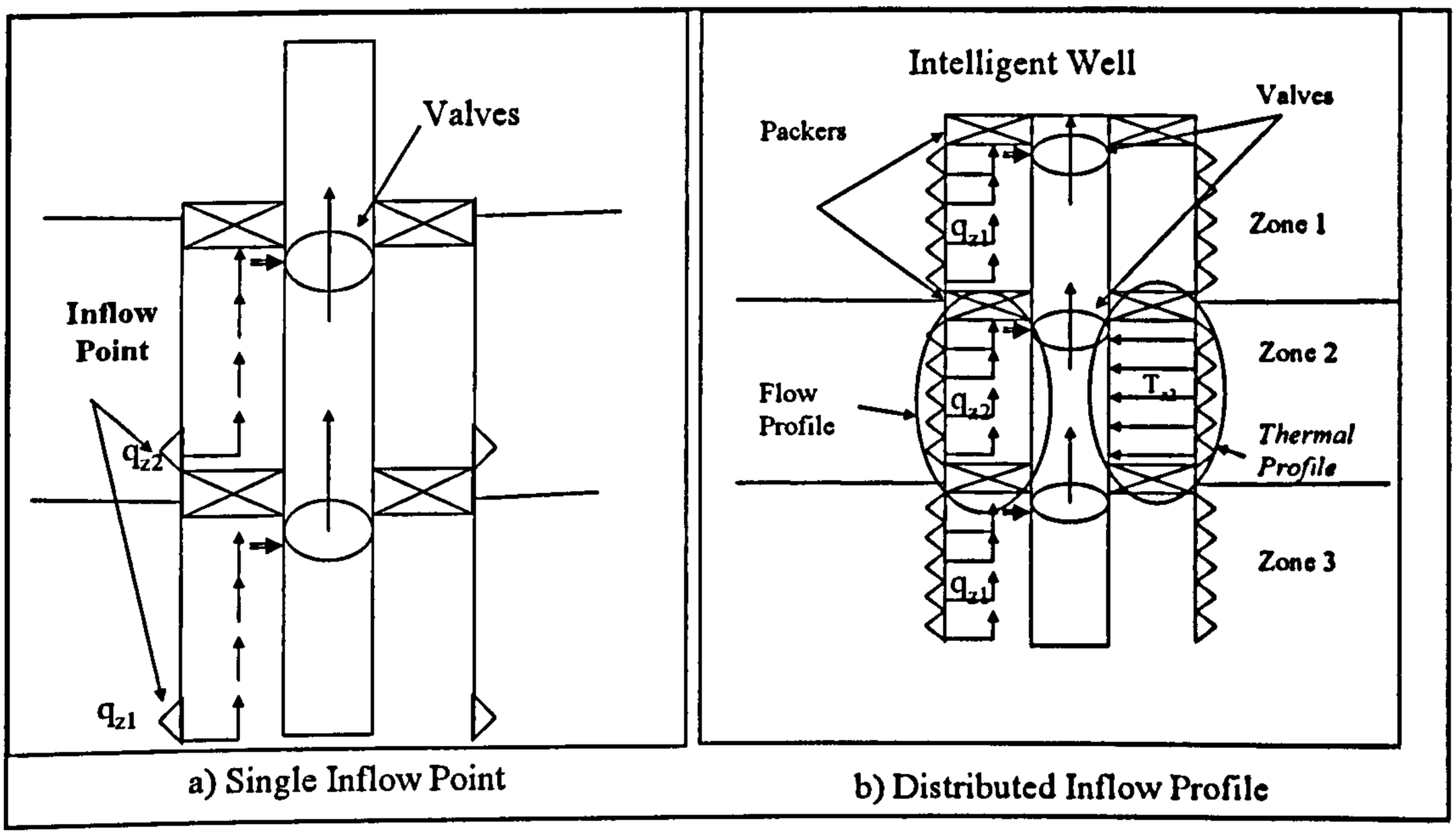

Figure 7-4. I-Well vs. Conventional Wells Inflow Profile

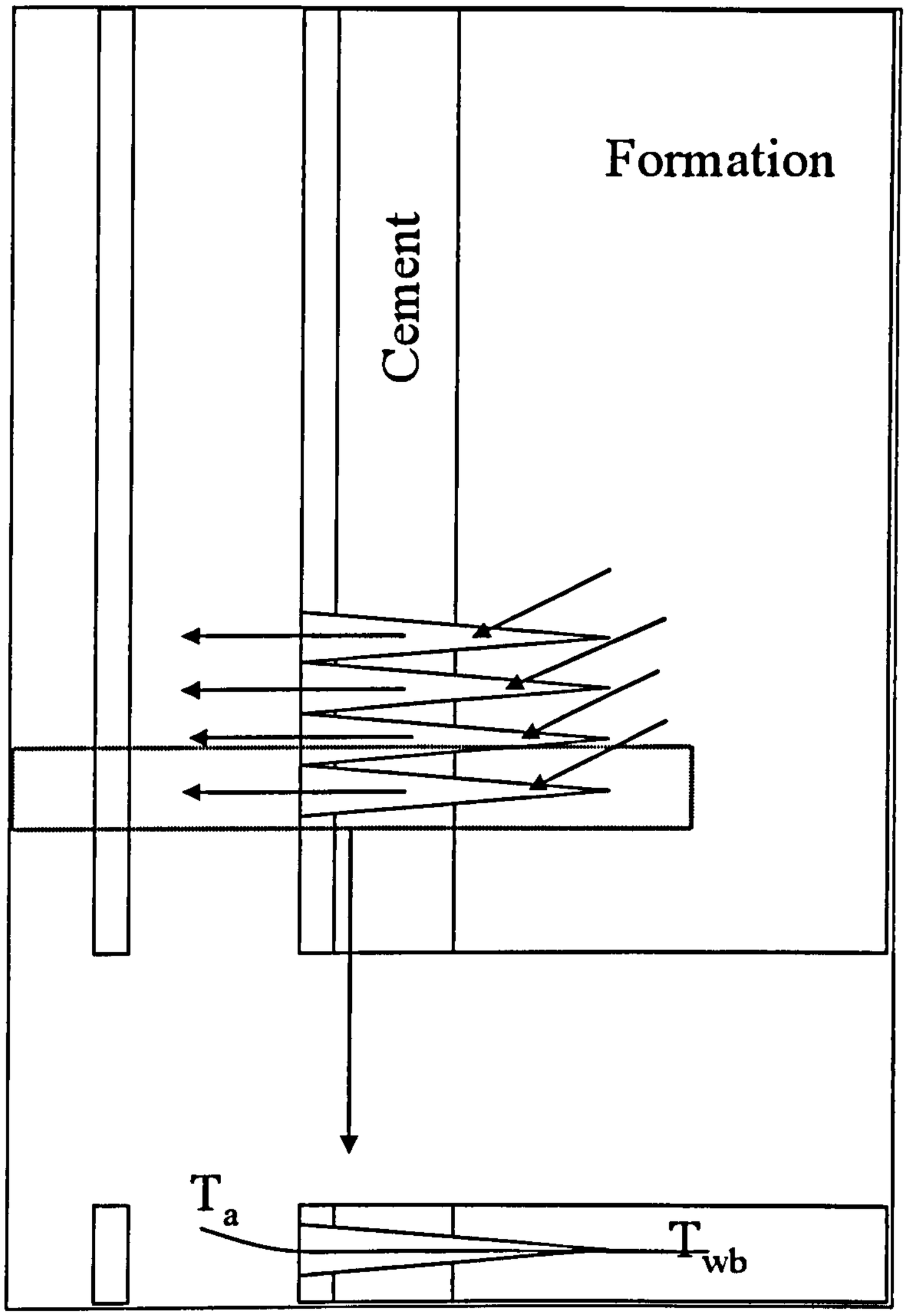

Figure 7-5. Perforation Treatment in I-Well Temperature Modelling

The influx of fluid at the geothermal temperature will cause cooling of the warmer fluid flowing from the bottom of the zone. This cooling effect will decrease as the fluid flows up the annulus because of the ever increasing upwards, mass flow rate of the warmer fluid. This is a reasonable assumption for incompressible fluid (oil/water) production. This type of fluid has a small negative Joule-Thompson coefficient. Hence, significant Joule-Thompson heating will require a substantial pressure drop across the sandface. Highly uneven, inflow profiles due to heterogeneous geology or layer reservoir pressure may affect this simple conclusion. In addition, this is not the case for gas due to its much larger, positive Joule-Thompson coefficient. Gas wells show Joule-Thompson cooling due to expansion at the perforations causes the flowing fluid to be cooler than the geothermal temperature.

The initial condition for each annulus segment is:

$$InitT(N) = \frac{w_f(N-1)T_a(N-1)C_p + w_i(N)T_{ei}(N)C_p}{w_f(N-1)C_p + w_i(N)C_p} \qquad \text{Equation 7.28}$$

Where,

N= segment number

w_i = influx mass flow rate from the segment, lbm/hr

w_f= cumulative mass flow rate from the previous segment, lbm/hr, where:

$$w_f(N) = w_f(N-1) + w_i(N) \qquad \text{Equation 7.29}$$

The initial condition of the first segment will be the geothermal temperature of that segment (Figure 7-6) since we will assume gas is not present. The initial conditions will be applied to Equation 7.2 to solve for the annulus temperature. This has to be done after the solution of Equation 7.3 to determine the tubing temperature since Equation 7.2 is also a function of the tubing temperature.

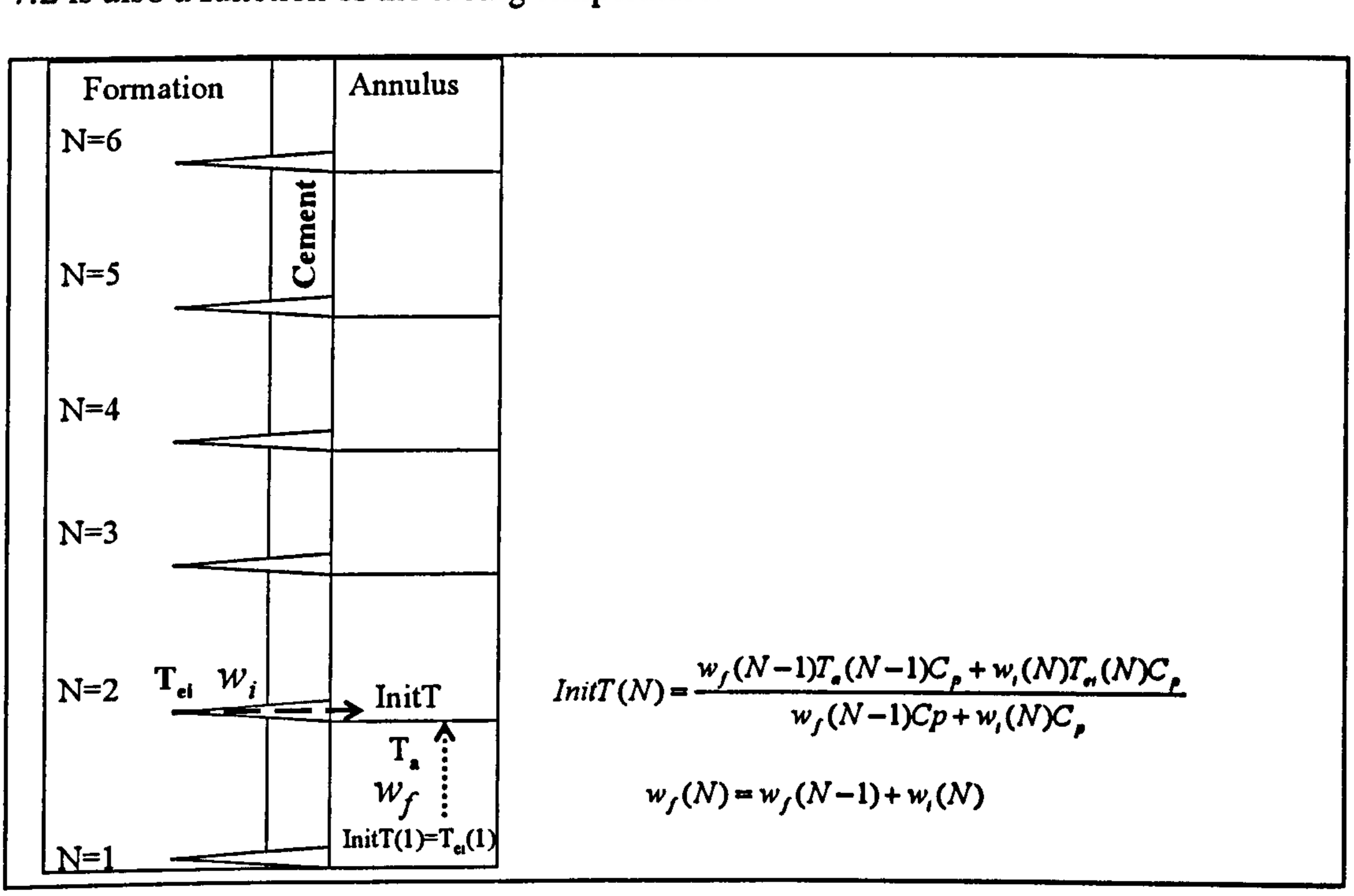

Figure 7-6. Annulus Segments Initial Conditions

The annulus-formation overall heat transfer coefficient need not be taken into account as there is no casing and cement sheath conductivity that will cause a temperature drop in open hole completions. Open-hole completions in horizontal wells require rigorous accounting of the flow effect and pressure drop at the sand face and of any thermal

property changes since all fluids enter at the same geothermal temperature. Dawkrajai's thesis [7.8] presented a temperature prediction model for producing horizontal wells. He discussed and modelled most aspects of horizontal well production which were then coupled to a wellbore flow simulator. However, his work did not include the effect of completions, an area he recommended as future research.

7.3 Assumptions Employed in This Study:

The assumptions underlying this work are:

1. The Well is Vertical.
2. Steady state heat transfer occurs in the wellbore.
3. Incompressible fluids are flowing in the tubing and annulus (oil and/or water with no gas)
4. The production rate is uniformly distributed along the completion zone with an inflow point situated at every 5ft along the whole perforated interval.
5. Ideal mixing of the two streams occurs at the ICV.

7.4 Base Case Selection:

A vertical, intelligent well with three isolated zones will be used to demonstrate the effect of the I-completion's added complexities on the temperature profile. The three zones well will provide an opportunity to:

1. Apply the tubing bottom zone model described in section 7.2.1.
2. Study the impact of mixing temperature on the two zones above the bottom zone, particularly its impact on the flowing fluid temperature along the tubing above the producing zones.
3. The vertical nature of the well will avoid well deviation effects on the geothermal temperature profile. Such effects can be accounted for by an extension of the model.

The base case assumes a production rate of 500 BOPD (no gas) from each of the three, fully perforated zones of equal length (300 ft). The fluid data and the well configuration used for the base case are the same as that used in the scale detection study in Chapter 6 (See Table 6-1).

7.5 Base Case Performance Analysis:

Figure 7-7 shows the production fluid temperature profile for the I-completion used in the base case well. The "Stair Steps" in the lower part of the figure are the temperature profile for the producing zones (the bottom 900 ft of the well). This is shown in greater detail in Figure 7-8. A small increase in the annulus temperature for the bottom inflow point of each zone is observed. This is due to heat transfer from the tubing.

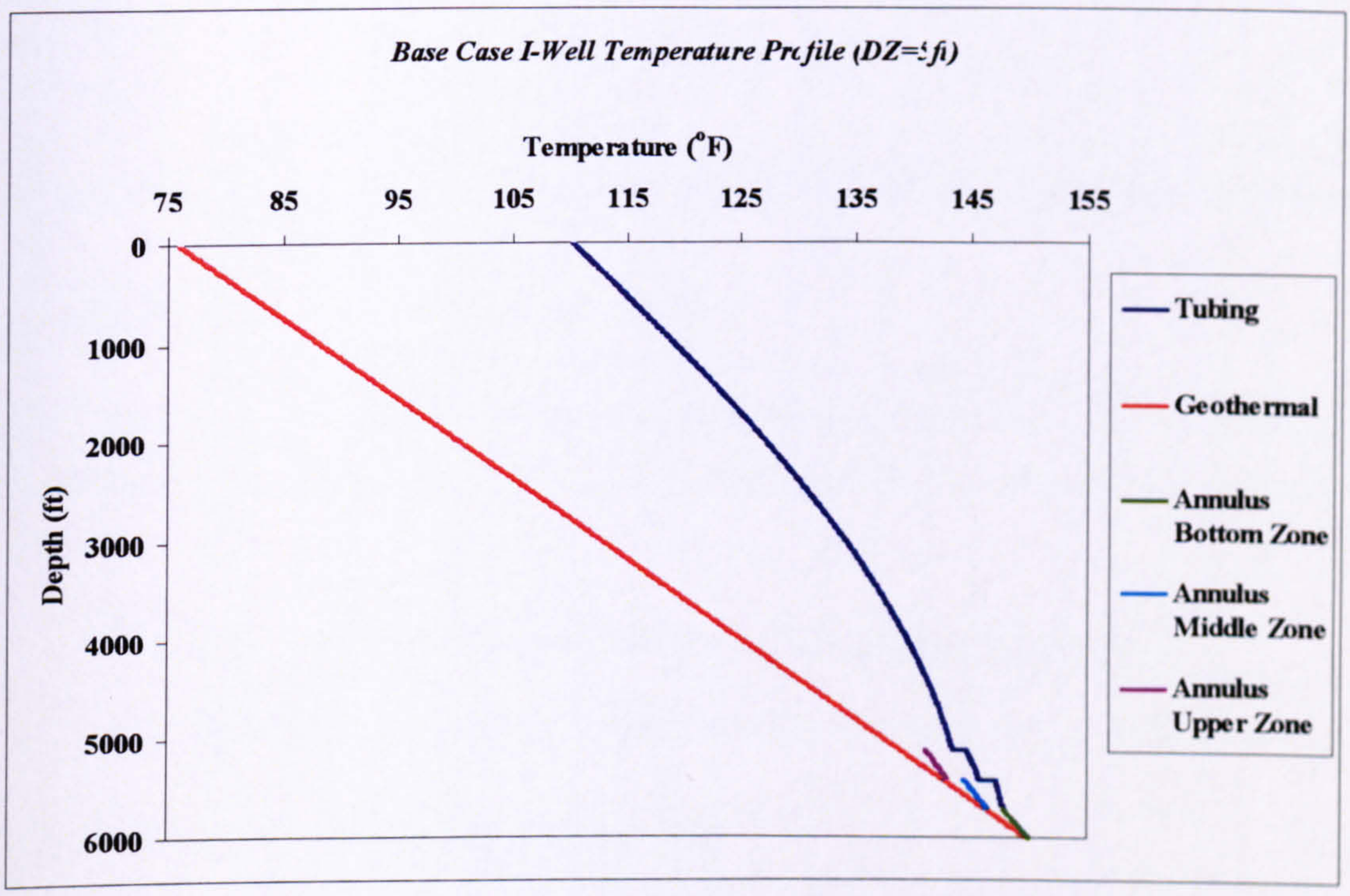

Figure 7-7. Complete Temperature Profile for the I-Well Base Case

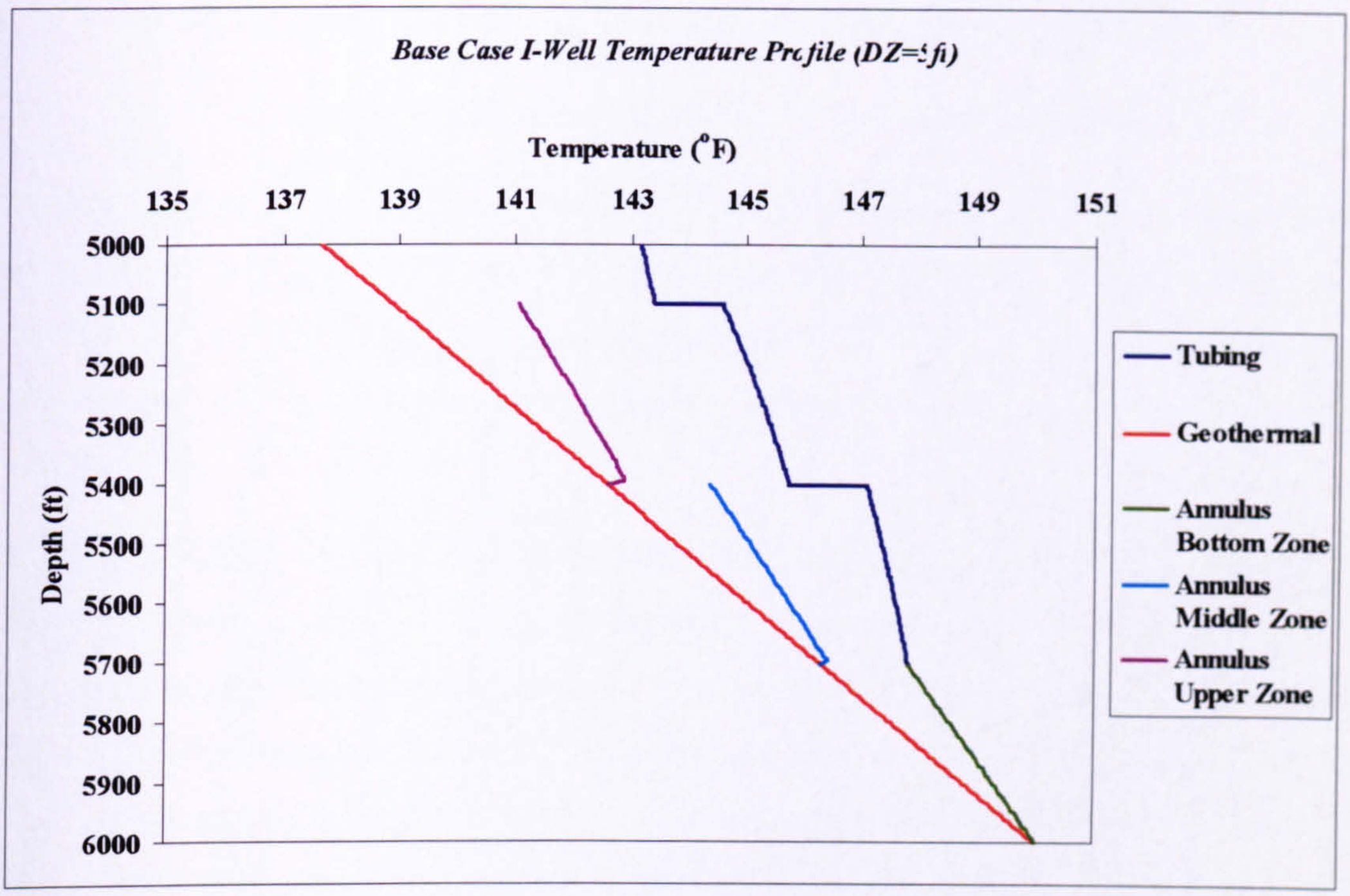

Figure 7-8. Base Case Zone Temperature Profile for the I-Well Completion Zone

7.5.1 Base Case Tubing Temperature Analysis:

The indication of the "Stair-Step" tubing profile indicates heat loss from the tubing to the annulus. The heat loss from the tubing is governed by two main factors (Equation 7.1):

1. The overall heat transfer coefficient between the tubing and annulus
2. The temperature difference between the fluids in the tubing and annulus

Overall Heat Transfer Coefficients Analysis:

The tubing-annulus overall heat transfer coefficient (U_{ta}) has a low value because of the low thermal conductivity (0.081 Btu/(ft.hr.°F)) of the produced oil flowing in the annulus. This low thermal conductivity reduces the value of the forced convection heat transfer coefficient both in the annulus and in the tubing.

The tubing-annulus overall heat transfer coefficient U_{ta} is defined as:

$$U_{ta} = \left(\frac{1}{h_a} + \frac{1}{h_t} \right)^{-1}$$ Equation 7.30

Where,

h_a = Convection Heat Transfer Coefficient in the Annulus, Btu/(hr.ft^2.°F)

h_t = Convection Heat Transfer Coefficient in the Tubing, Btu/(hr.ft^2.°F)

The tubing-annulus overall heat transfer coefficient is analogous to that for a double-pipe (co-current) heat exchanger. The overall heat transfer coefficient will be dominated by the lower convective heat transfer coefficient [7.5] for cases where there is a significant difference between the tubing and annulus convection heat transfer coefficients.

Figure 7-9 shows the large contrast between the convective heat transfer coefficient for both the producing zones and above the top production packer. Natural convection is the dominant heat transfer mechanism in the water filled annulus above the top packer. A lower rate of heat transfer will occur if the annulus was filled with drilling mud which had gelled on aging. Figure 7-10 shows the heat transfer coefficient profiles for the I-Well base case across the producing zones. The tubing overall heat transfer coefficient for the bottom zone's (imaginary) tubing section is assumed to be zero since there is no flow here (see section 7.2.1). Figure 7-10 also shows the convection heat transfer coefficient increases across each producing zones as the fluid flow rate up the annulus increases. This increasing flow rate is due to the constant fluid influx rate per unit completion length and resulting distributed inflow in the annulus.

The tubing convection heat transfer coefficient is constant for each zone since the tubing flow rate does not change within the zone. It increases as the flow rate increases after inflow from each ICV. This increases the forced convection heat transfer in the tubing; resulting in a small increase in the tubing-annulus overall heat transfer coefficient. N.B. The tubing-annulus overall heat transfer is smaller than either the convective heat transfer for the tubing or that for the annulus because, as expressed by Equation 7.30, these resistances to heat transfer are placed in series with each other.

The annulus contains a water based packer fluid (3% KCl brine) above the producing zone. The higher thermal conductivity of water compared to oil increases the convection heat transfer coefficient and the overall heat transfer coefficient for the annulus. It also includes the effect of radiation within the static annulus (Equation 7.31). Chapter 6 provided a description of the model for the temperature in conventional wells, which appropriate above the producing zones. The temperature of the tubing is modelled using the Equation 6.1 and the overall heat transfer coefficient for the tubing (U_{to}) is given by:

$$U_{to} = \left[\frac{1}{(h_{nc} + h_r)} + \frac{r_{to} \ln\left(r_{wb} / r_{co}\right)}{k_{cem}} \right]^{-1}$$ Equation 7.31

Where,

r_{to} = Outside Tubing Radius, ft
r_{co} = Casing outside radius, ft
r_{wb} = Wellbore Radius, ft
h_r = Radiation Heat Transfer Coefficient, Btu/(hr.ft^2.°F)
h_{nc} = Natural Convection Heat Transfer Coefficient in Casing Annulus, Btu/(hr.ft^2.°F)
k_{ins} = Insulation Thermal Conductivity, Btu/(hr.ft.°F)

Understanding the behaviour of the heat transfer coefficient is essential for the understanding of the developing temperature profile in the intelligent well.

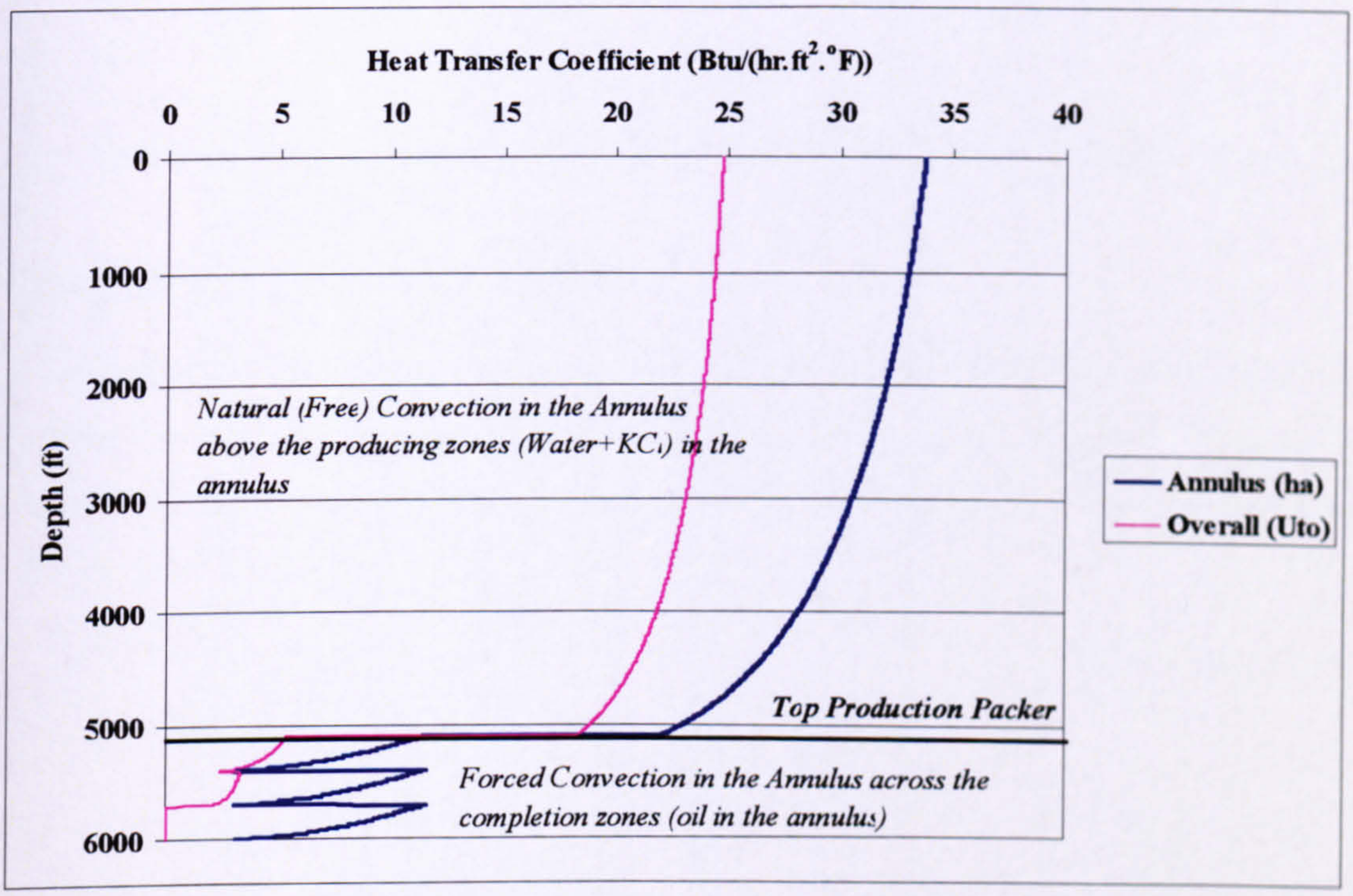

Figure 7-9. Comparison between the Annular Convective Heat Transfer Values in the I-Well Completion Zones and Above the Top Production Packer

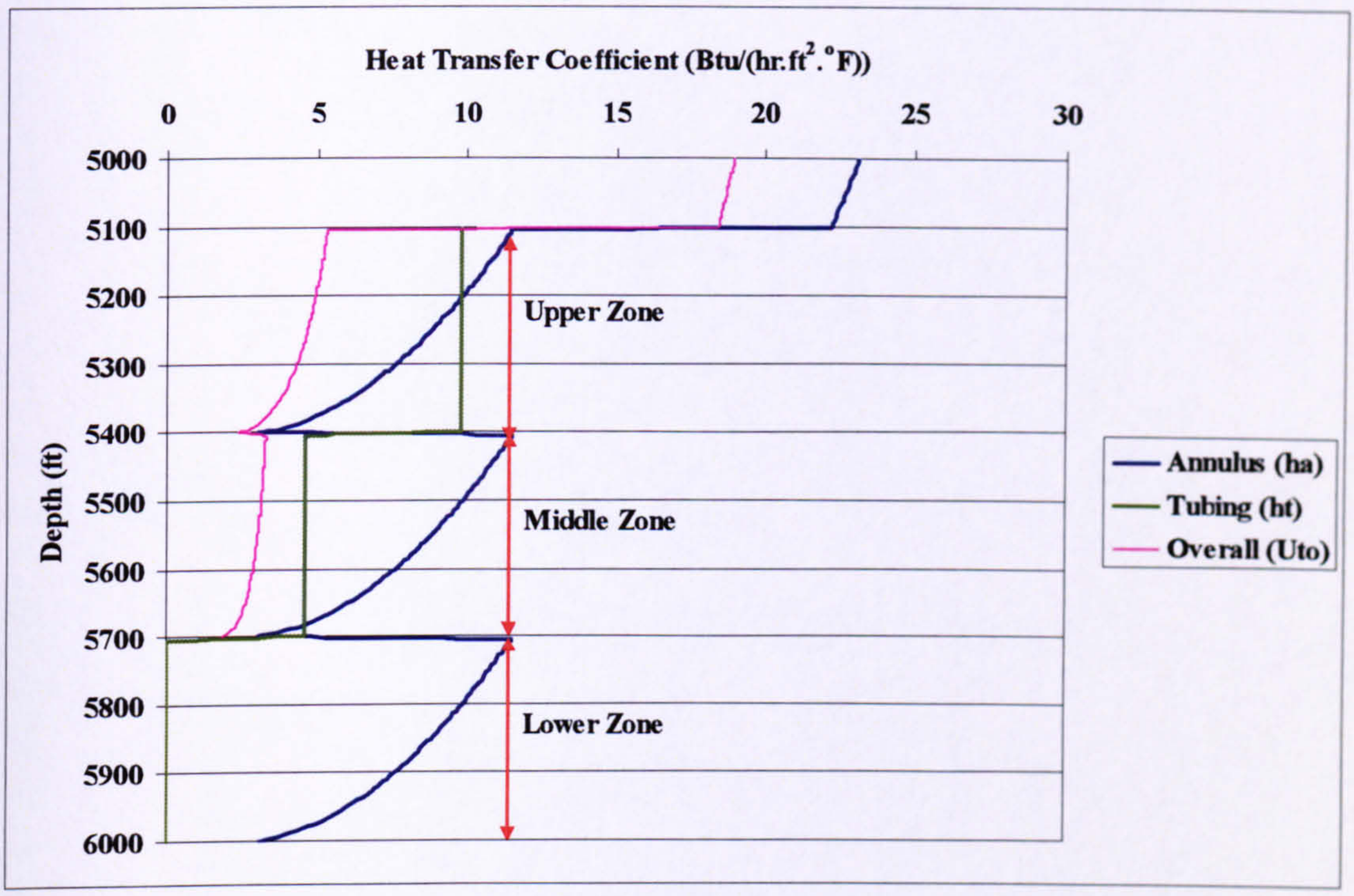

Figure 7-10. Base Case Heat Transfer Coefficient across Producing Zones

Tubing-Annulus Temperature Drop:

Fluid inflow into the tubing begins at the first ICV. The difference between the tubing and the annulus inlet temperature for the middle zone is 1.5 °F rising to 3.1 °F for the flow in the upper zone (Table 7-3). The locations of the inlet temperatures analyzed are illustrated in Figure 7-11.

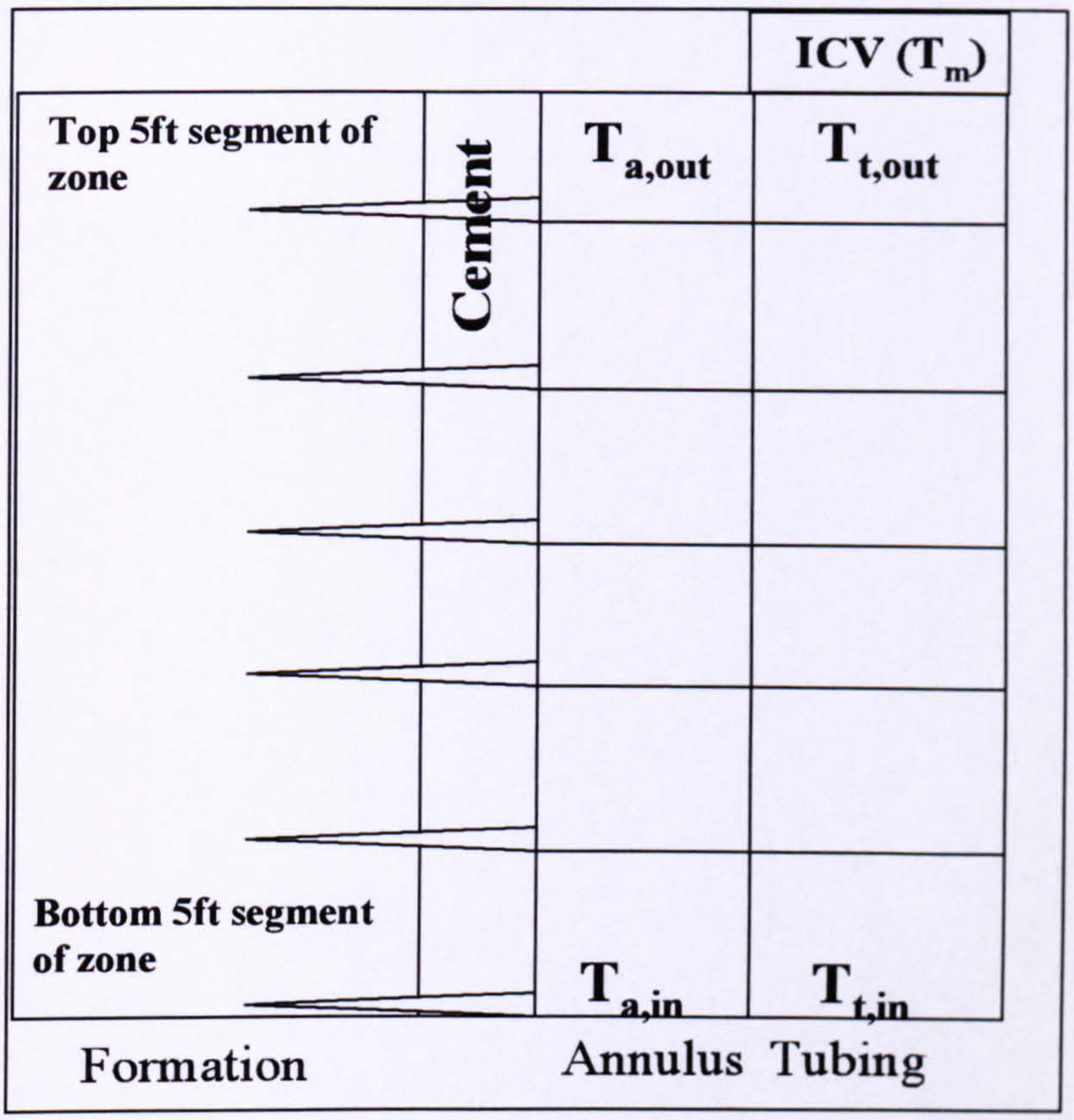

Figure 7-11. Location of Tubing and Annulus Inlet and Outlet Temperatures

Table 7-3. Temperature Difference between Annulus and Tubing Effect on Heat Loss in the Tubing

	Inlet Temperature Difference between Tubing and Annulus ($T_{t,in}$-$T_{a,in}$), °F	Tubing-Annulus Overall Heat Transfer Coefficient (U_{ta}), Btu/(hr.ft^2.°F)	Fluid Temperature Loss in the Tubing ($T_{t,in}$-$T_{t,out}$) (°F)
Middle Zone	1.5	2.9	0.7
Upper Zone	3.1	4.4	1.2

This table show that not only does the temperature difference between the annulus and the tubing increase for the upper zone, but the overall heat transfer coefficient is increasing due to the increase in the tubing flow rate. A high tubing-annulus overall heat transfer coefficient would allow the annulus and tubing temperature to reach an equilibrium. This is exemplified in Figure 7-12 by changing the thermal conductivity of oil from a typical value of 0.081 to a non-realistic value of 30 Btu/(hr.ft.°F). The tubing-annulus overall heat transfer coefficient values for the middle and upper zones now increase to 32 and 58 Btu/(hr.ft.°F), respectively and the tubing and annular temperature profiles become into equilibrium with each other.

Installation of an insulated tubing would have the reverse effect resulting in small increase in the temperature difference compared to the values in Table 7-3, the effect of

this small increase will be minimized by a further reduction in the overall heat transfer coefficient.

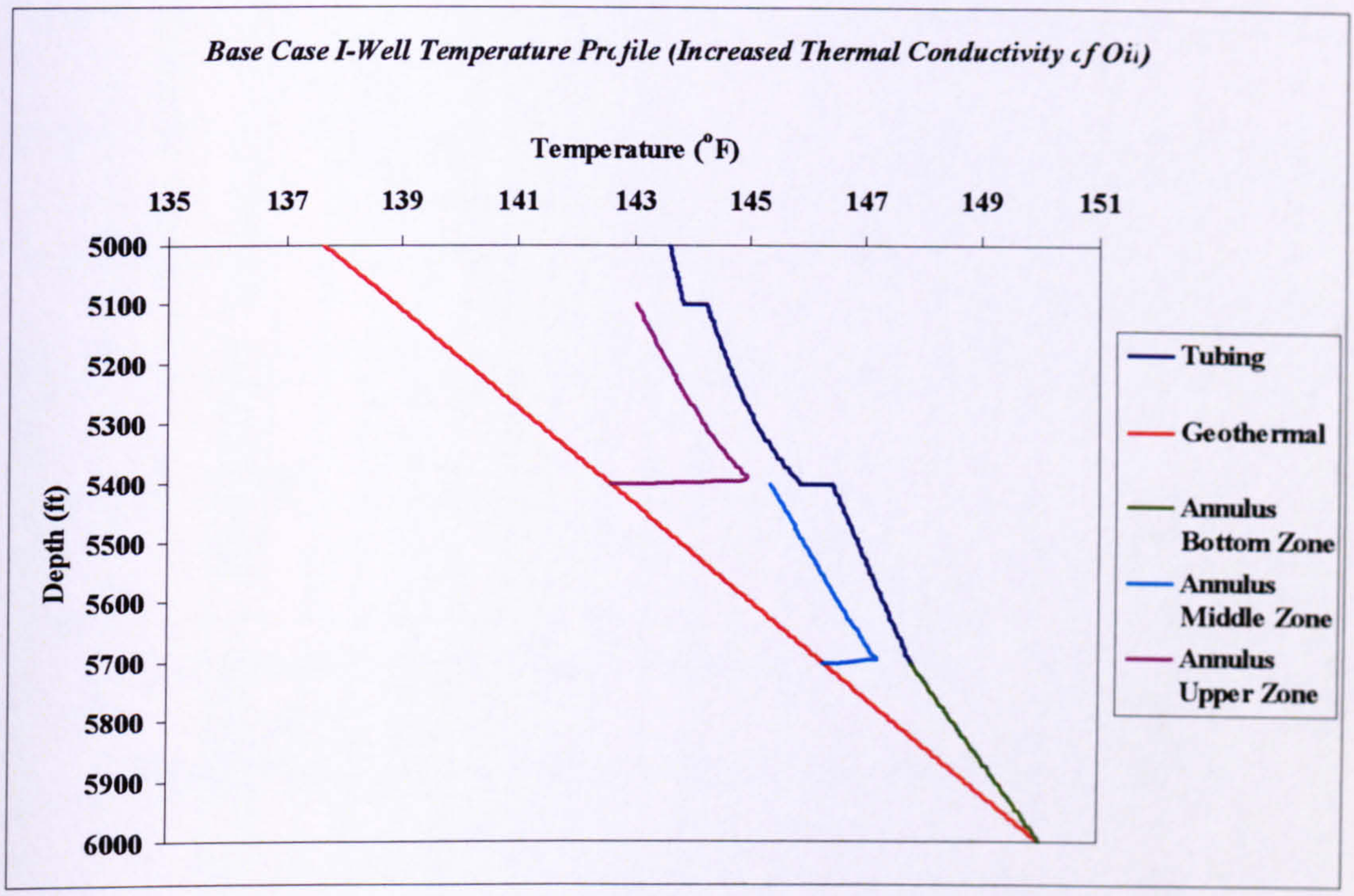

Figure 7-12. A Fluid with a Very High Thermal Conductivity Causes the Annular and Tubing Temperature Profiles to be in Equilibrium

7.5.2 Single Inflow Point Flow Rate Sensitivity Impact

Conventional thermal models employ a single inflow point placed at the bottom of the zone where the inflowing fluid will have the highest temperature. Figure 7-13 shows that using a single inflow point to model the temperature in an I-Well will over-estimate the temperature at the ICVs.

The main reason is the absence of cooling the fluid in the annulus experience from continuous influx of cooler fluid from the upper segments in the annulus. In addition, the small increase noticed at the bottom of the zone has been replaced by a much larger temperature increase (Figure 7-14) caused by large difference in the mass flow rate of fluid entering the annulus. The mass flow rate is 106 lbm/hr for distributed inflow (with 5ft segment), while it is 6352 lbm/hr in the single inflow case.

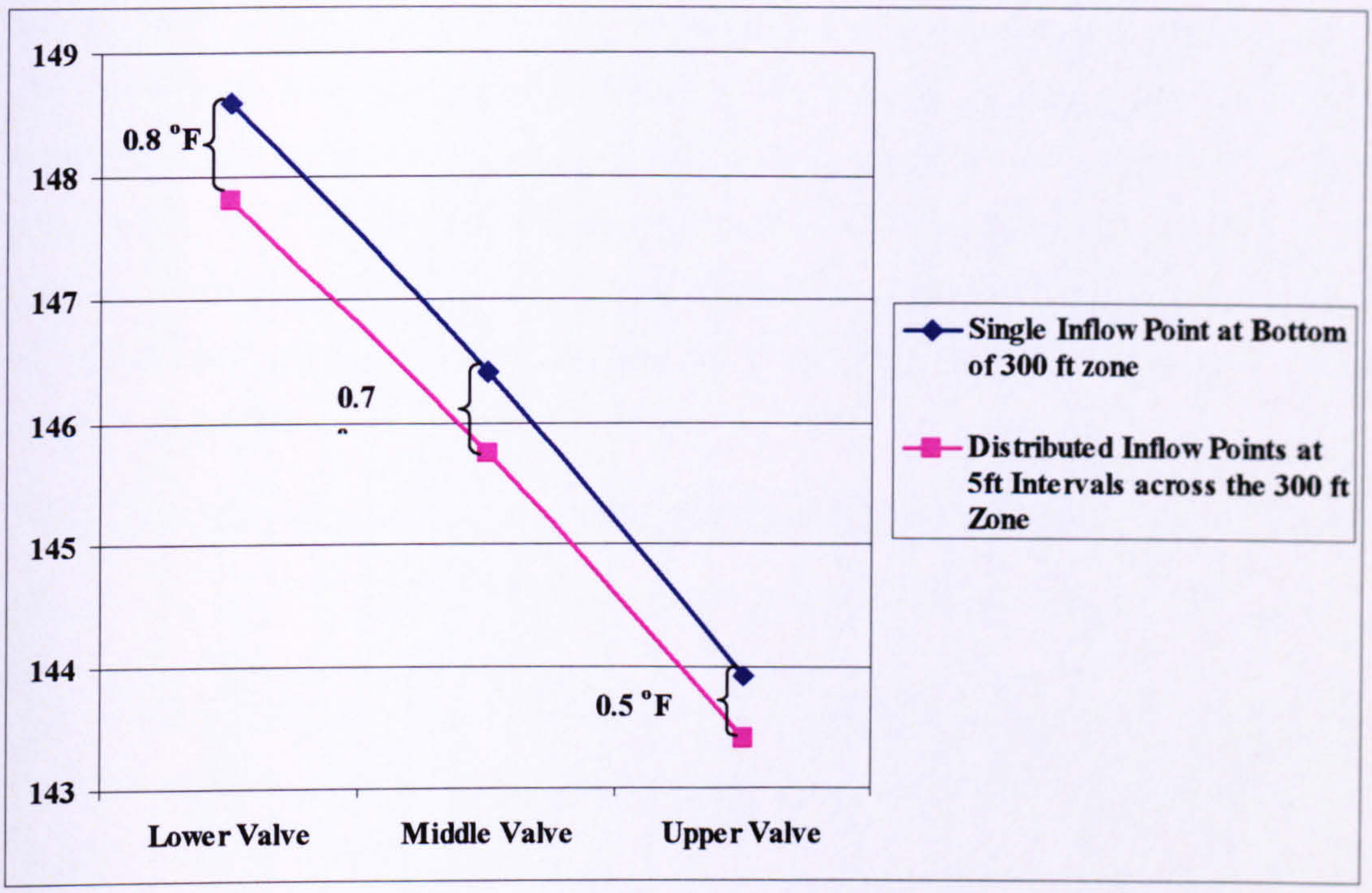

Figure 7-13. Impact of Inflow Points on Mixing Valve Temperature

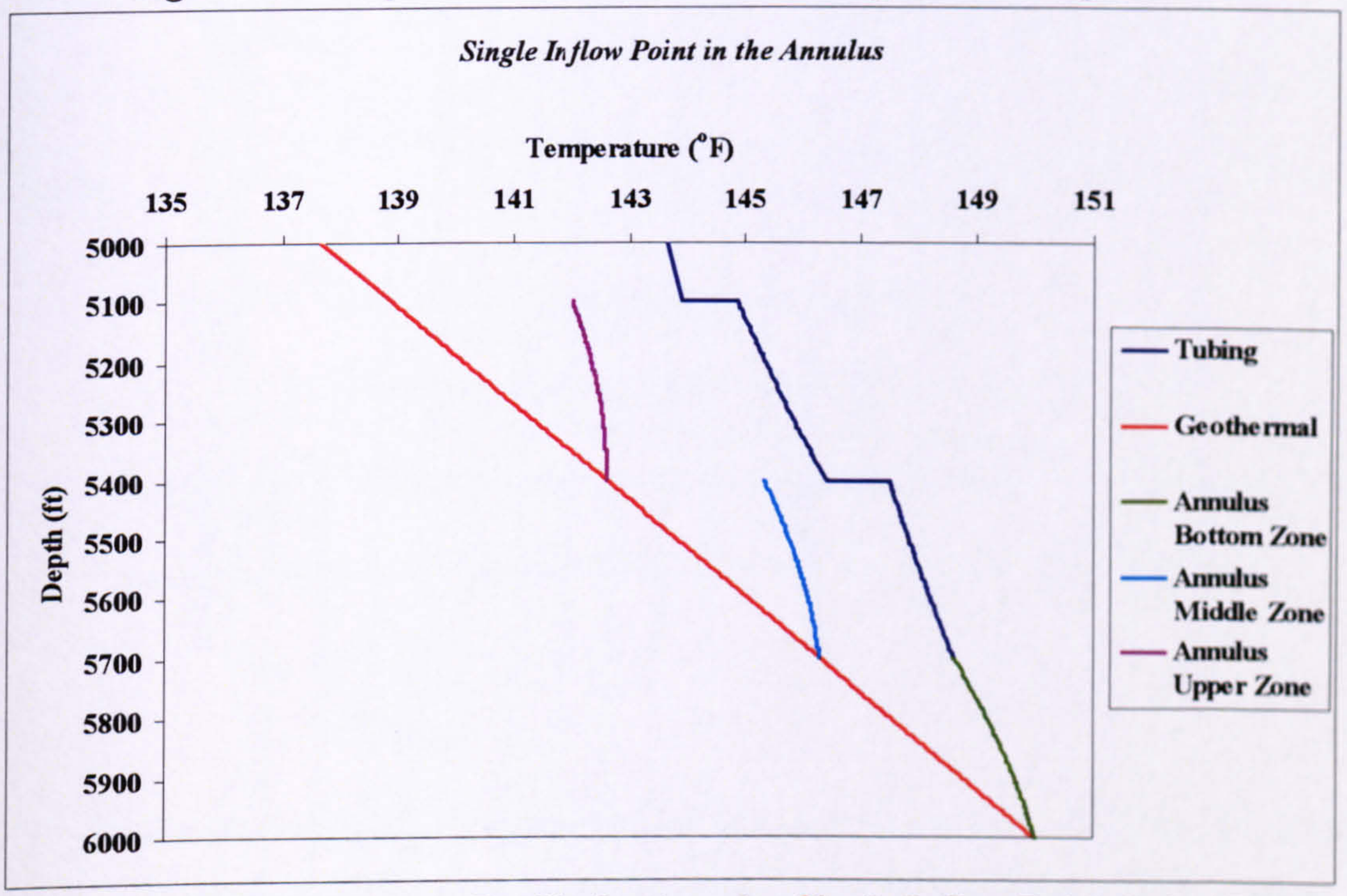

Figure 7-14. Temperature Profile for Annulus Single Inflow Point (using Base Case Rate =500 BLPD/zone)

This observation might be useful when interpreting temperature data from a multi-zone completion (e.g. triple zone selective completion with SSD, triple zone I-Well) producing at a constant total production rate.

The ICV mixing temperature will tend to be higher if the top section of the pay zone is not producing and the production is coming mainly from the warmer, bottom part of the zone (for a constant flow rate and phase cuts at the surface). On the other hand, a lower temperature indicates that the majority of the flow is coming from the top of the formation where the fluid is cooler. Localised scale formation, sand compaction or formation damage can lead to reduced or zero production from that part of the completion interval.

7.5.3 Estimating the Maximum Possible Heat Transfer for Tubing across Producing Zone:

The resemblance of the flow in the tubing and annulus in an I-Well to a double-pipe heat exchanger can also be used to explain why there is small heat transferred between the annulus and the tubing.

The maximum possible heat transfer rate in heat exchanger [7.5] is:

$$\dot{Q}_{\max} = C_{\min}(T_{tub,in} - T_{ann,in}) \qquad \text{Equation 7.32}$$

Where,

$\dot{Q}_{max}$ = The maximum possible heat transfer rate, Btu/hr

$T_{tub,in}$ = Tubing inlet temperature (initial temperature of the tubing), °F

$T_{ann,in}$ = Annulus inlet temperature (temperature at the bottom of the annulus), °F

C_{min} = Smallest Heat Capacity Rate of the two streams, Btu/(hr.°F), where:

$$C_{tub} = w_t C_{pt}$$
$$C_{ann} = w_{ann} C_{pa}$$

The initial mass flow rate for the annulus and the mass flow rate for the tubing flow can be used to determining the maximum heat transfer rate for the tubing segment for the middle and upper zones (Table 7-4). The maximum heat transfer rate (Q_{max}) for the middle and upper zone is low at 80.7 Btu/hr and 168 Btu/hr, respectively.

Table 7-4. Maximum Heat Transfer Rate for Upper and Middle Zones

		C_{ann} (C_{min}) Btu/(hr.°F)	C_{tub} Btu/(hr.°F)	$T_{a,in}$ (°F)	$T_{t,in}$ (°F)	Q_{max} (Btu/hr)
Distributed Inflow (Base Case)	Middle Zone	54	3,220	146.3	147.8	80.7
	Upper Zone	54	6,441	142.6	145.7	168.4
Single Point Inflow	Middle Zone	3,220	3,220	146.3	148.6	7,409
	Upper Zone	3,220	6,441	142.6	146.4	12,278

The assumption that the flow in the annulus and the tubing is analogous to a double-pipe (co-current) heat exchanger is correct if the annulus has a single point of inflow at the bottom of the annulus (Figure 7-4a). This analogue is not valid if the annulus inflow profile is distributed since the mass flow rate in the annulus continuously changes with depth (Figure 7-15). This increasing flow rate with varying temperature along the tubing is a marked difference from the heat exchanger concept where each stream is assumed to have the same mass flow rate at all position in the two streams and the inlet (or outlet) temperatures are both constant.

The same analysis show higher maximum heat transfer rate values when the flow is coming from a single point at the bottom of the zone, with 7,409 Btu/hr and 12,278 Btu/hr, for the middle and upper zones, respectively. The large inflow at the bottom of the annulus will also increase the tubing-annulus heat transfer coefficient.

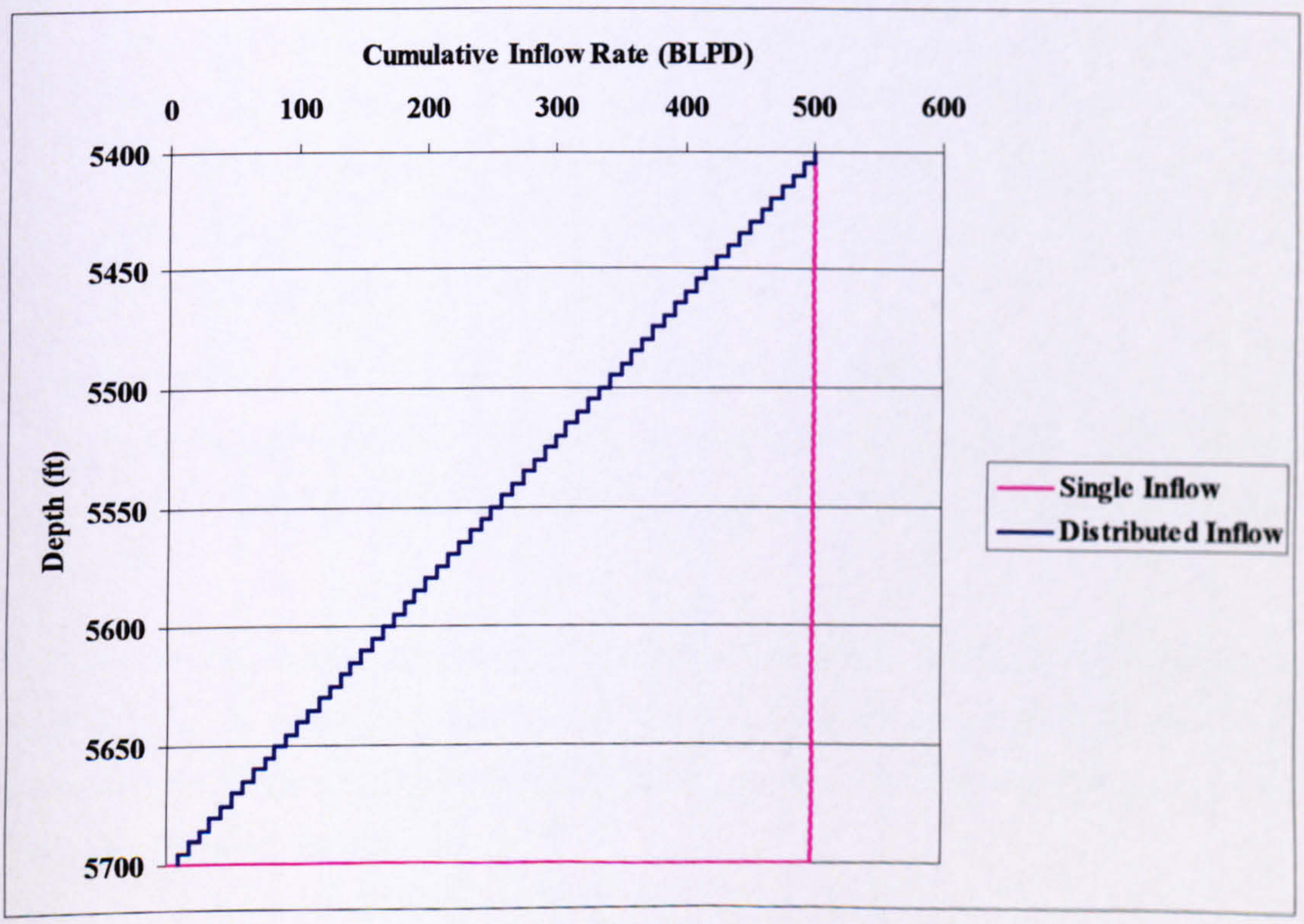

Figure 7-15. Middle Zone Flow Profile inside the Annulus

7.5.4 Producing Zones Annulus Temperature Analysis:

The tubing and annulus segment length selected for the base case calculations is 5 ft. Each segment has an inflow rate of 8.3 BOPD. The profile in Figure 7-8 shows that the modelled annulus flow temperature in the producing zones experience a small increase in the temperature immediately on entering the annulus due to the heat transferred from the warmer fluid in the tubing (in reality this would occur gradually over the complete length of the segment). The annulus temperature profile is closer to the geothermal gradient compared to the case where there is a single inflow point at the bottom of the annulus. The constant fluid inflow into the annulus from the perforations cools the warmer fluid flowing from the bottom of the zone. The difference between the geothermal temperature and the annulus temperature profile increases for the upper zones.

The heat transfer mechanisms that occur in the annulus for the three zones are:

1. *Bottom Zone:* There is no flow in the tubing, so there is NO heat transfer between the tubing and the annulus, and heat transfer is only to the formation.

2. *Middle Zone:* There is flow in the tubing and two heat transfer mechanisms are at work; to the formation and between the annulus and the tubing. In addition to the overall heat transfer coefficient, the temperature prediction formula for the annulus (Equation 7.2) is a function of the temperature difference between the annulus and the tubing (T_a-T_t). The temperature difference between the tubing and annulus inlet temperature in the middle zone (at 1.5 °F) is relatively small compared to that for the upper zone.

3. *Upper zone:* There is now more fluid flowing in the tubing so the overall heat transfer coefficient for the tubing-annulus is increased compared to the middle zone. Also the temperature difference between the two streams increases to 3 °F.

Figure 7-16 show a magnification of the annulus and tubing temperature profile for the middle zone. A segment size of 50 ft was used for these calculations. The figure illustrates the initial conditions for the annulus and the relatively small temperature loss from the tubing to the annulus.

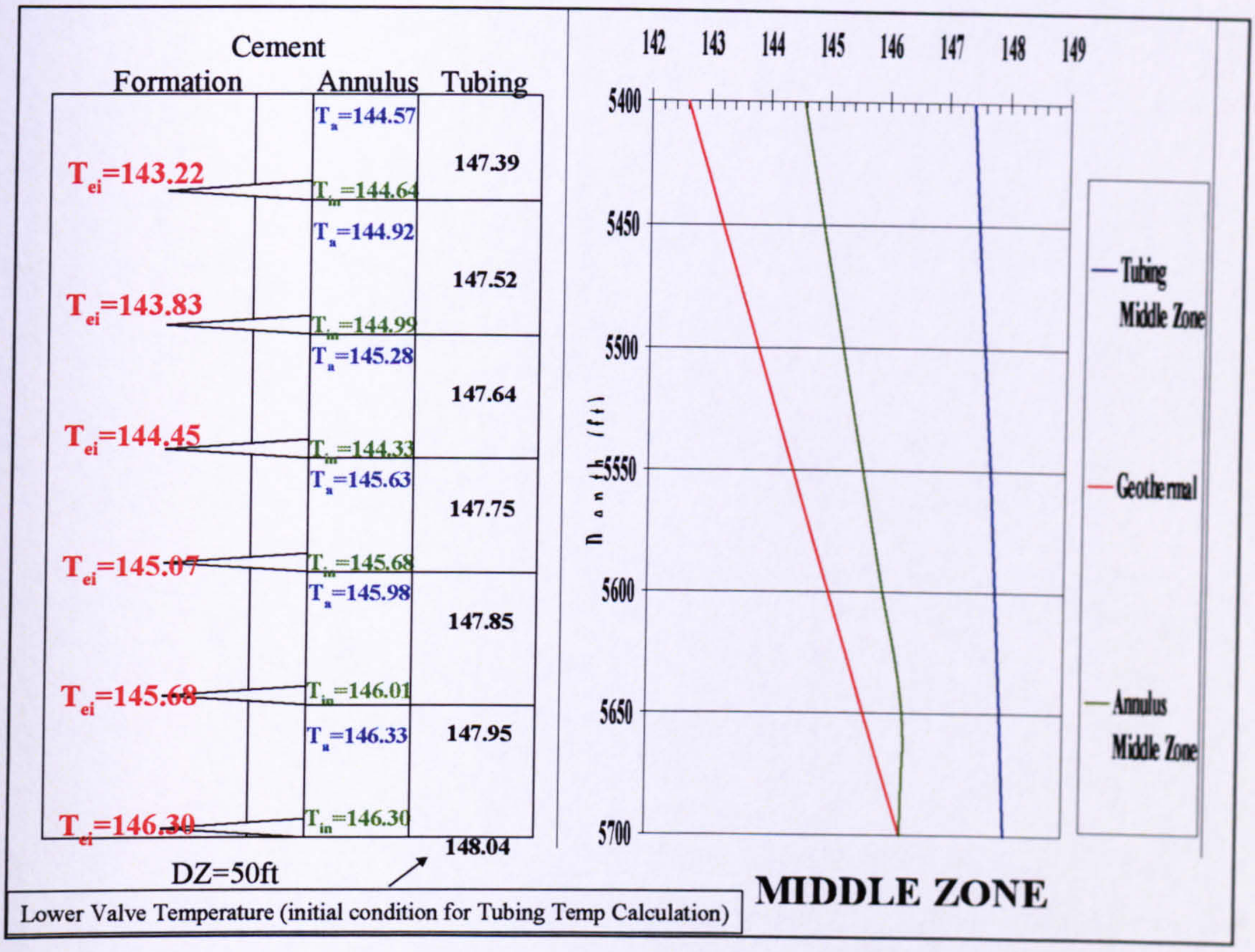

Figure 7-16. Magnified Temperature Profile for the Middle Zone Modelled with a Segment Length of 50ft

7.5.5 Inflow Points Separation Effect (Segment Size Effect):

The segment size of the model (or how many inflow points are included across the total zone length) plays an important role in the shape and value for the modelled temperature of both the annulus and the tubing temperatures. Figure 7-17 shows that, as the segment size increases, the modelled annulus temperature deviates further from the geothermal profile and the temperature in both the annulus and the tubing increases. The increase in the tubing temperature is due to the increase of the mixing point temperature.

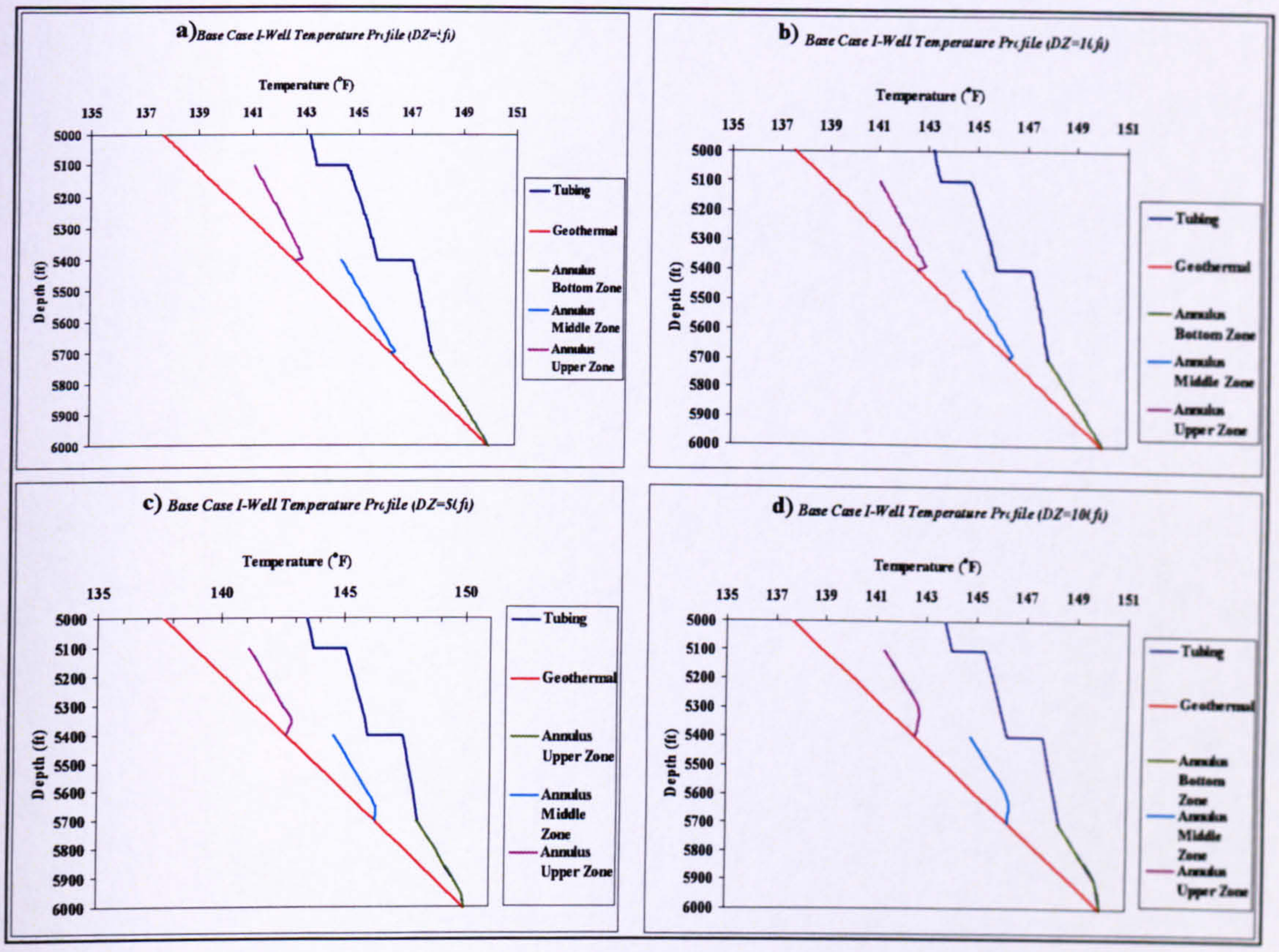

Figure 7-17. Effect of Segment Size (or Number of Inflow Points in the Zone) on Modelled Annulus and Tubing Temperature

Table 7-5 quantifies the effect of the segment size on the ICV mixing temperature that was illustrated in Figure 7-17. The calculated valve mixing temperature increases with increased segment length (due to the increasing distance between the inflow points). It is recommended that the segment length is selected based on the perforation data for the well when modelling the distributed flow in the annulus. It is recommended that the modeller uses either 5 or 10ft segments in any initial studies since only small differences were observed when using a 5ft or 10ft segment length. Smaller segment sizes may increase the running time of complex models (e.g. incorporation of rigorous pressure drop calculations for multiphase flow and thermal properties modelling).

Another feature of increasing the segment size is the increase in temperature for the first segment of the annulus caused by the heat transferred from the tubing. The increase in the segment size will delay the effect of cooling caused by the influx of cooler fluid from the upper segment.

Table 7-5. Effect of Model Segment Size on the ICV Mixing Temperature

Segment Size (ft)	5	10	50	100
Number of Inflow Points	60	30	6	3
Inflow Rate/Segment (BLPD)	8.3	16.7	83.3	166.7
	Mixing Temperature (°F)			
Upper Valve	143.4	143.5	143.7	144.0
Middle Valve	145.7	145.8	146.0	146.2
Lower Valve	147.8	147.8	148.0	148.3

7.5.6 Zonal Production Rate Effect on Mixing Temperature at the ICV:

An increase in the zonal production rate for all the zones (producing equally) in a single-phase I-Well leads to a minor increase in the mixing temperature (Table 7-6) since the increasing flow rate reduces the residence time in the tubing during which the fluid can lose heat to the annulus. The increase in temperature is small for uniformly distributed zonal inflow due to the cooling that the warmer fluid experience in the annulus as it flows up the annulus.

Table 7-6. Impact of Increase in Zonal Production Rate on the ICV Mixing Temperature for the I-Well Base Case

Zonal Rate	Lower Zone (°F)	Middle Zone (°F)	Upper Zone (°F)
500	147.8	145.7	143.4
1000	147.9	145.8	143.6
2000	147.9	145.9	143.6
3000	147.9	145.9	143.6

Increasing Zonal Production Rate from Lower Zone To the Upper Zone:

It has previously been assumed that the production rate of the three zones are the same. Table 7-7 examines the effect of the upper zones producing at a higher production rate than the lower zones. A higher mass flow rate from the cooler upper zones will increase the cool down of the warmer fluid in the tubing that was produced from the lower zones.

Table 7-7. Effect of a 2:1 Ratio Production Rate Increase on ICV mixing Temperature

	Lower Zone	Middle Zone	Upper Zone
Zonal Production Rate (BLPD)	1000	2000	4000
ICV Mixing Temperature (°F)	147.9	145.3	142.1
Zonal Production Rate (BLPD)	2000	4000	8000
ICV Mixing Temperature (°F)	147.9	145.3	142.1

Table 7-7 show that increasing all zonal flow rates in a ratio of 2:1 does not affect the temperature. Significant temperature differences are calculated for higher zonal inflow rates (Table 7-8). The decrease in temperature is only noticeable at the upper zone valve due to the increase in the (cooler) mass flow rate flowing from the upper zone (more than twice flow rate in the tubing from the middle and lower zones).

Table 7-8. Effect of a 3:1 Ratio Production Rate Increase on ICV mixing Temperature

	Lower Zone	Middle Zone	Upper Zone
Zonal Production Rate (BLPD)	500	1500	4500
Temperature (°F)	147.8	145.0	141.5
Zonal Production Rate (BLPD)	1500	4500	13500
Temperature (°F)	147.9	145.0	141.2

Decreasing Zonal Production Rate from Lower Zone To the Upper Zone:

When the bottom zone produces at higher production (mass flow) rate the fluid will be warmer as it will undergo relatively less cooling due to mixing with the fluid from the upper zones (Table 7-9). The temperature will decrease at the ICVs with increasing flow rate from the bottom zone. This is caused by the increasing in the tubing-annulus overall heat transfer coefficient as the increase in the flow rate in the tubing leads to increased convection.

Table 7-9. Effect of a 2:1 Ratio Production Rate Decrease on ICV mixing Temperature

	Lower Zone	Middle Zone	Upper Zone
Zonal Production Rate (BLPD)	4000	2000	1000
Temperature (°F)	147.9	146.4	145.0
Zonal Production Rate (BLPD)	8000	4000	2000
Temperature (°F)	147.8	146.2	144.6

Table 7-10. Effect of a 3:1 Ratio Production Rate Decrease on ICV mixing Temperature

	Lower Zone	Middle Zone	Upper Zone
Zonal Production Rate (BLPD)	4500	1500	500
Temperature (°F)	147.9	146.6	145.6
Zonal Production Rate (BLPD)	13500	4500	1500
Temperature (°F)	147.5	145.9	144.1

7.5.7 Effect of Increase Zone Length:

The geothermal gradient was altered so temperatures at the top and bottom of zones are the same and one then only focus on the effect of the change in zonal length. The ICV mixing temperature reduces as the zone length increases (Table 7-11) because the increase length will allow more heat transfer between the annulus and the tubing therefore causing more heat loss from the tubing compared to the shorter zone length. Figure 7-18 clearly shows that the tubing and annulus temperature profile are closer than the base case. A reduction in the zone length (with a constant zonal inflow temperatures) lead to the reverse effect (Table 7-11).

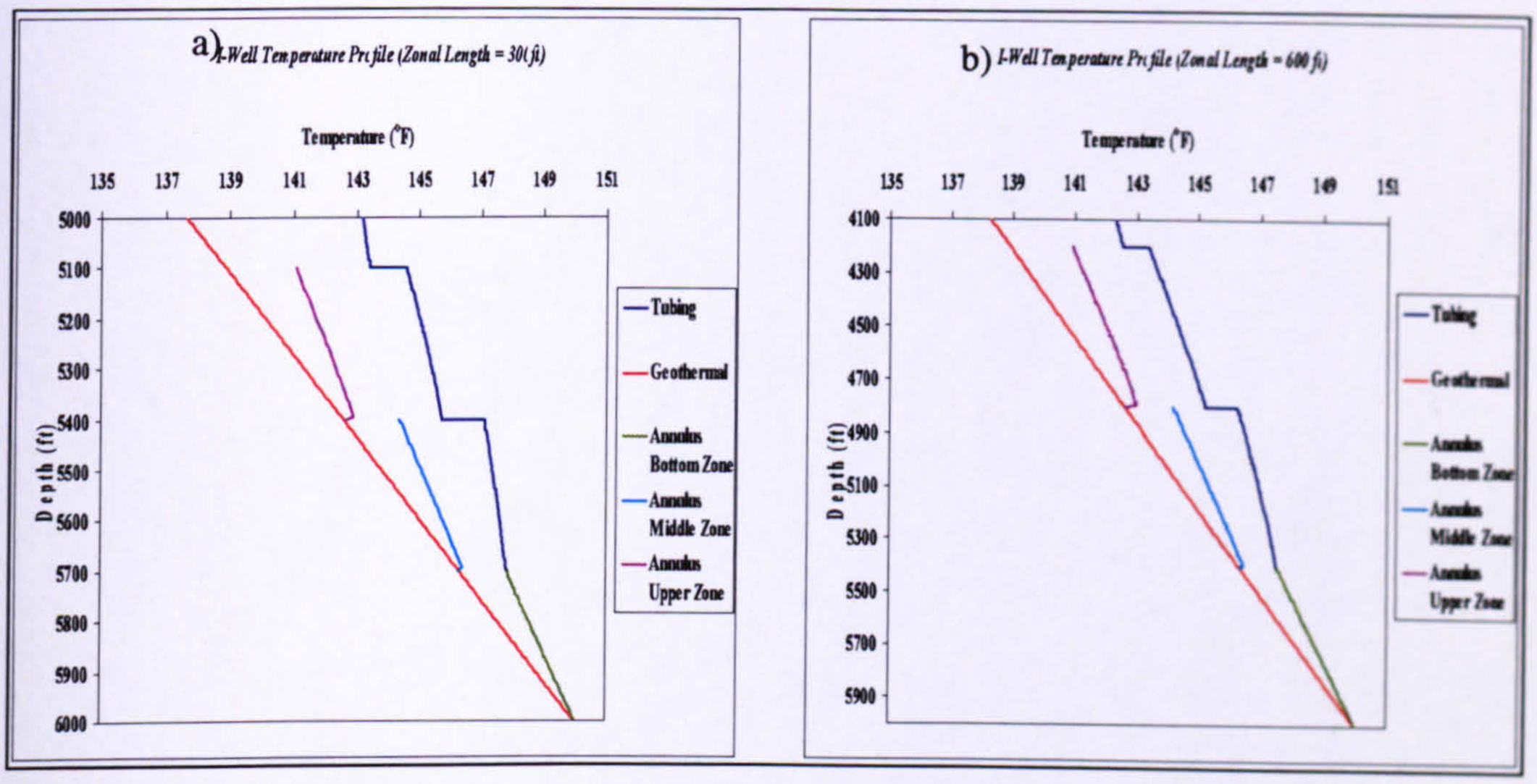

Figure 7-18. Effect of Increasing the Zonal Length on the Base Case Temperature Profile

Table 7-11. Effect of Altering the Zonal Length with Constant Zone Rate and Geothermal Temperature Profile

	ICV Mixing Temperature (°F)		
Zone Length (ft)	Lower Zone	Middle Zone	Upper Zone
600	147.5	145.2	142.5
300	147.8	145.7	143.4
150	148.0	146.1	143.9

7.6 Water Cut Effect on I-Well Temperature Profile:

Water inflow can alter the thermo physical properties of the produced fluid and the temperature profile of a producing well. This section will investigate the impact of water production on the temperature behaviour of an intelligent well with the aim of understanding when water detection using temperature data might be possible. The properties of the oil and water mixture will be calculated using the volume fraction of each phase:

For mixture heat capacity:

$$C_{pm} = \gamma_o C_{po} + \gamma_w C_{pw} \qquad \text{Equation 7.33}$$

Where,

γ_o= oil volume fraction

γ_w= water volume fraction

Similarly for mixture thermal conductivity:

$$k_m = \gamma_o k_o + \gamma_w k_w \qquad \text{Equation 7.34}$$

7.6.1 Equal Zonal Production Rate & Equal Zonal Water Cut:

The annulus temperature profile will increase with increasing water production because of the increase heat capacity of the mixture. Figure 7-19 shows the effect of increasing water cut on the upper zone annulus temperature profile. The increase in temperature is more apparent in the annulus temperature profile than at the ICV mixing temperature (Figure 7-20). The reason behind the lack of sensitivity of the ICV mixing temperature to an increase in the water cut is that all streams will have the same heat capacity. This results in Equation 7.21 becoming only a function of the mass flow rate and the temperature:

$$T_m = \frac{w_1 T_1 + w_2 T_2}{w_1 + w_2} \qquad \text{Equation 7.35}$$

An increase in the heat transfer coefficient will occur, since the increasing water fraction will increase the fluid thermal conductivity, causing a higher rate of heat transfer with the tubing. This is the main cause of the increase in temperature at the bottom of the annulus.

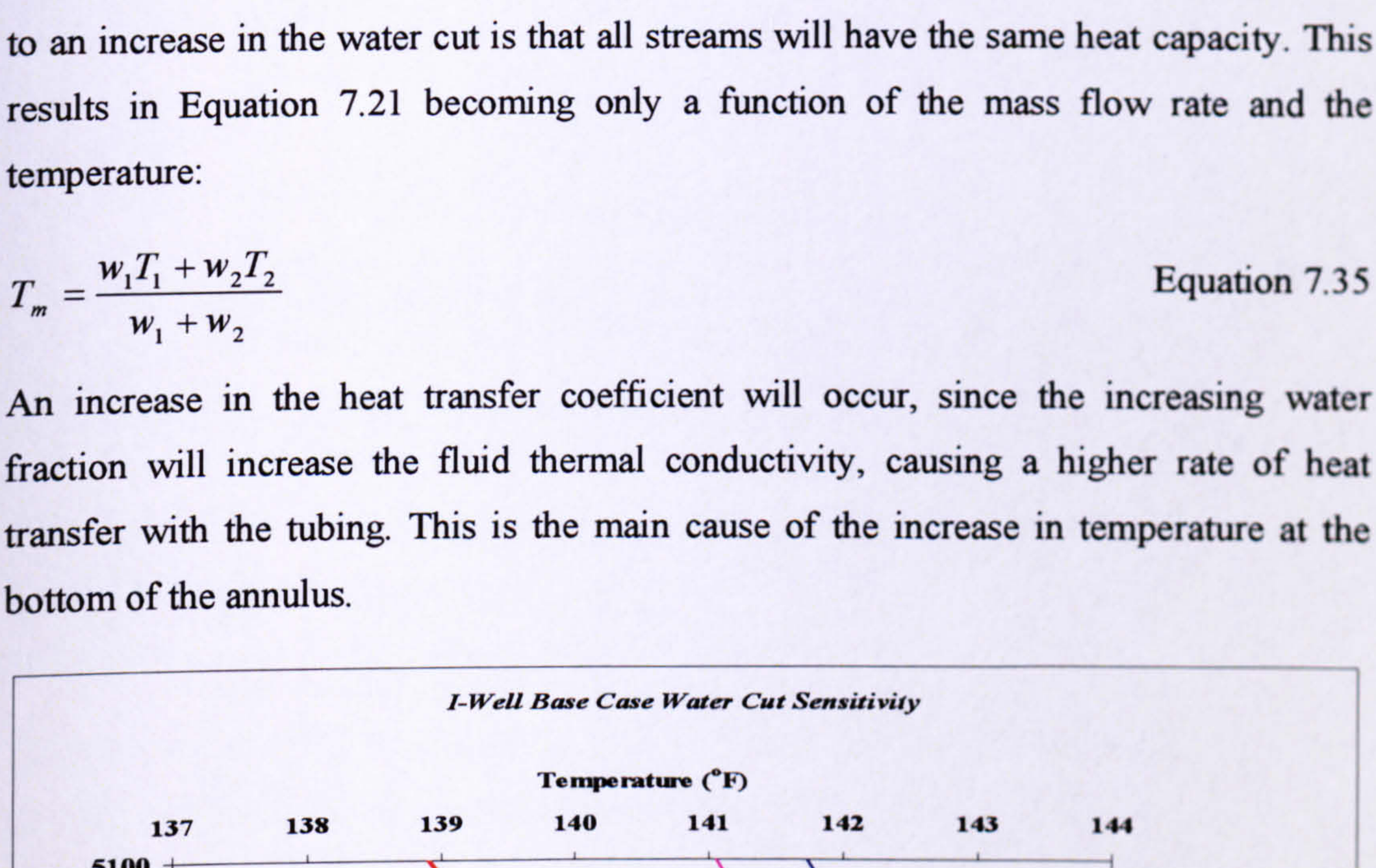

Figure 7-19. Upper Zone Annulus Temperature Profile for I-Well with Continuous influx in the Annulus

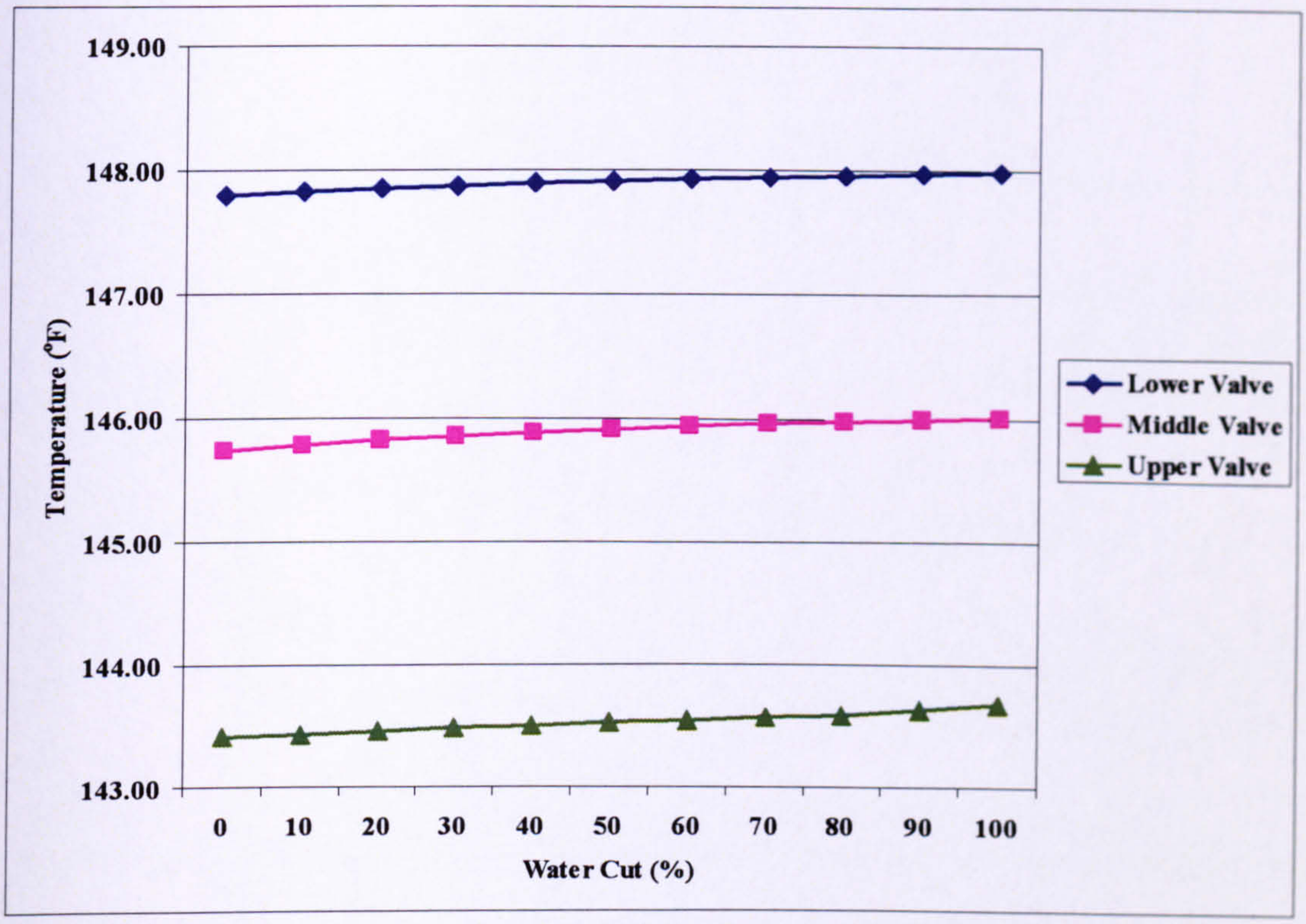

Figure 7-20. I-Well Base Case ICV Mixing Temperature for Equal Zonal Production Rate (500 BLPD) and Equal Zonal Water Cut

7.6.2 Equal Zonal Production Rate & Variable Zonal Water Cut:

The effect of water on the ICV mixing temperature is more visible when the water is being produced from a single zone. Figure 7-21 shows the valve mixing temperature when the water is produced from different zones.

High water cut (90%) production (Figure 7-21) from the lower zone results in a significant and measurable temperature increase for all ICV mixing temperatures with the strongest signal being observed at the top ICV. Water production from the middle zone causes a much smaller temperature decrease at the middle valve. The change in temperature is only twice the gauge resolution here, but it is even smaller at the other valves. A larger temperature change at this upper zone ICV is observed when it produces at 90% water cut.

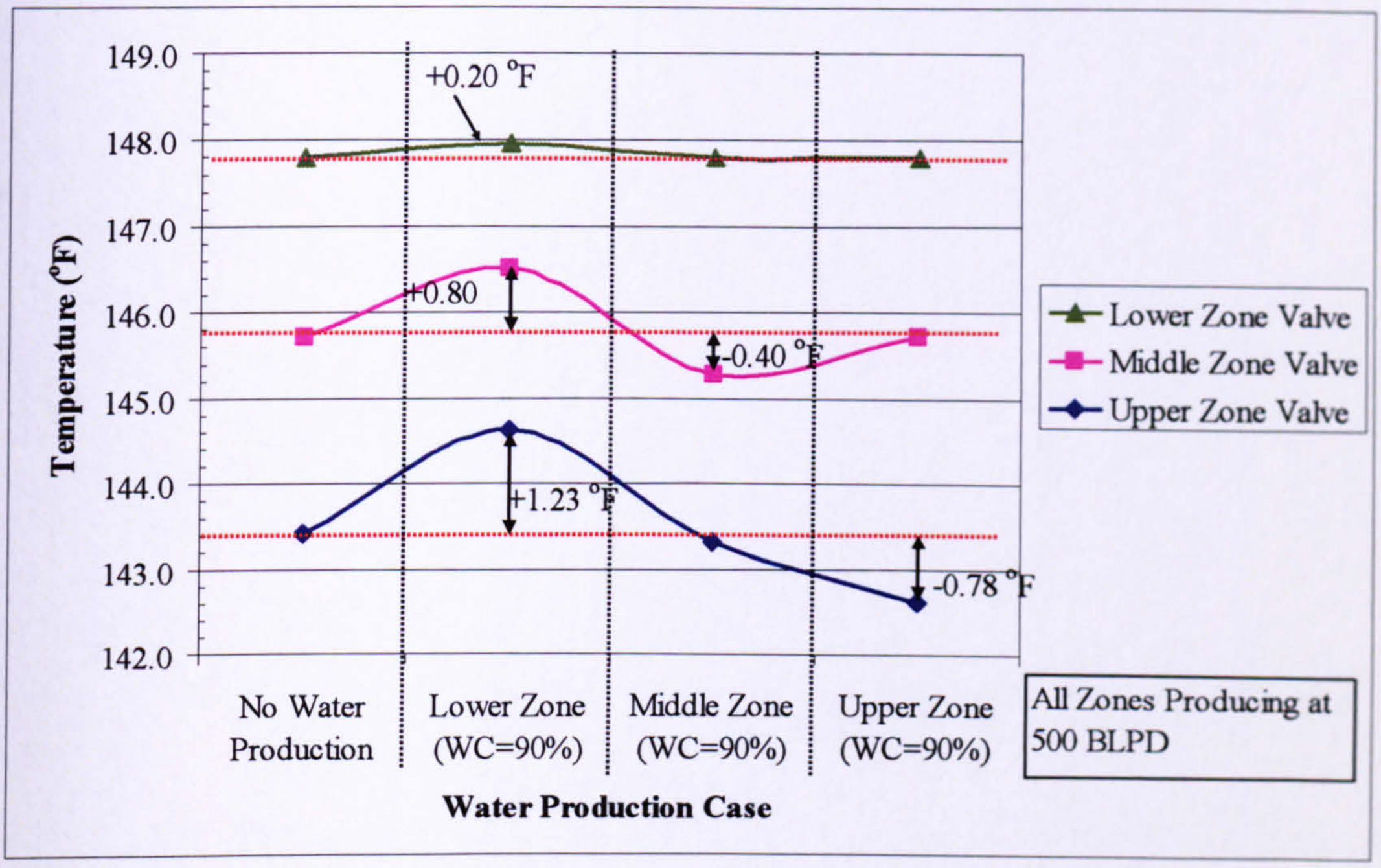

Figure 7-21. ICV Mixing Temperature when Different Zones Produce with a High Water Cut (90%)

Water Detectability with Lower WC:

The same behaviour pattern is observed with a lower water cut of 10% (Figure 7-22). However, the observed temperature differences compared to no water production are lower than the 0.18 °F resolution of the DTS [7.9], being +0.16 °F and -0.12 °F, respectively for the upper ICV when the lower and upper zones produce 10% water. Such a temperature difference is detectable based on the resolution of a fibre-optic pressure/temperature (P/T) sensor of 0.036 °F [7.10]. The detectability of the temperature change will diminish even further as the water cut decreases. For example, a water cut of 1% produced from the lower zone will increase the temperature at the upper valve by only 0.02 °F.

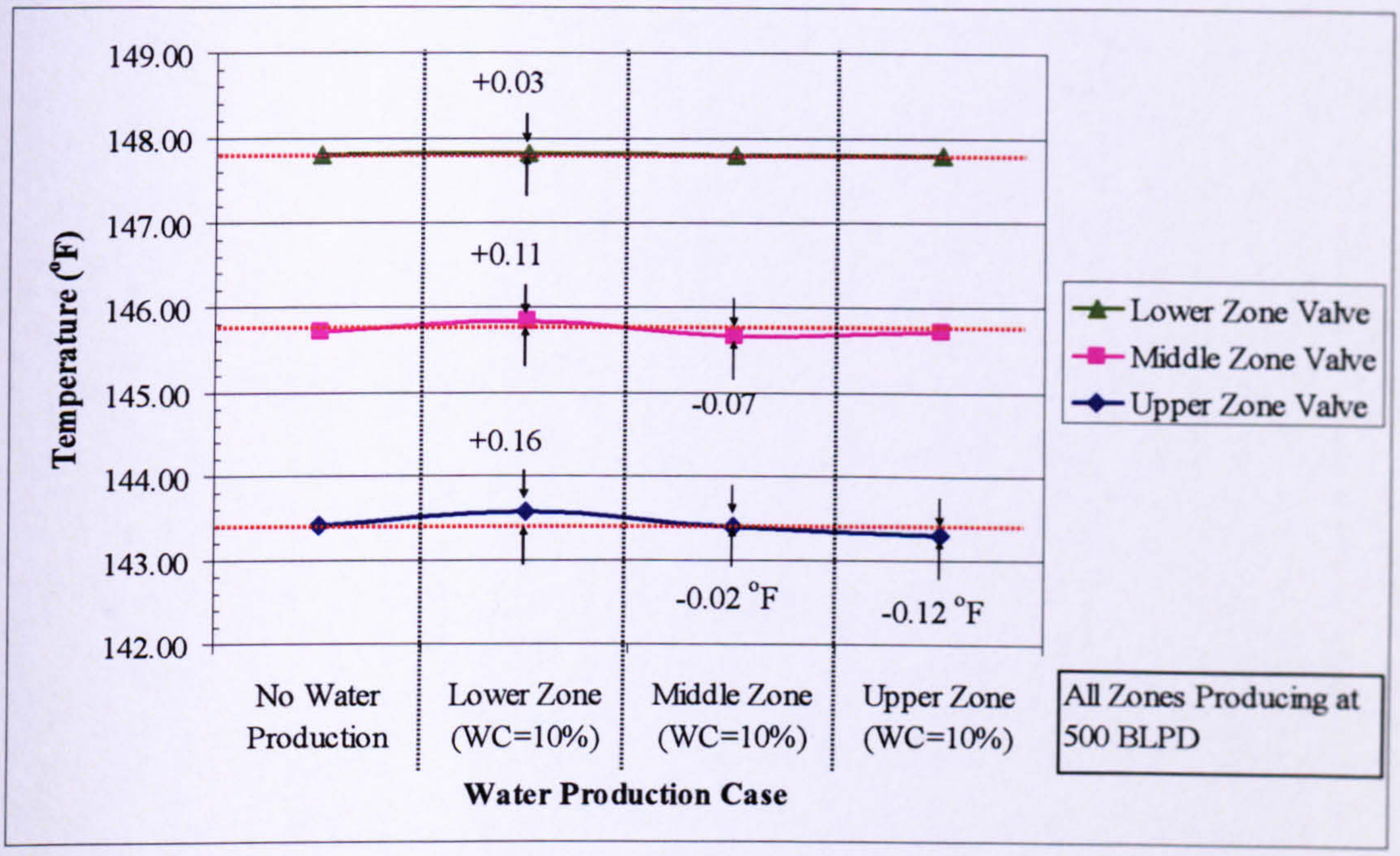

Figure 7-22. ICV Mixing Temperatures when Different Zones Produce with a Low Water Cut (10%)

7.6.3 Variable Zonal Production Rate & Variable Water Cuts:

The production flow rate is an important parameter when examining the effect of water production on the mixing temperature at the ICV since the mixing temperature is also a function of the mass flow rate. Figure 7-23 and Figure 7-24 show the effect of increasing liquid production rate on the valve mixing temperatures.

The water cut effect on the ICV mixing temperature is unchanged when there is an increasing production rate from the lower zone upward compared to the base case production rate of 500 BLPD (Figure 7-23).

The temperature differences to be detected decreases when the middle and upper zone produce at higher rates (Figure 7-24). However, most of the mixing temperature differences at the ICVs are greater than the detection limit for all cases.

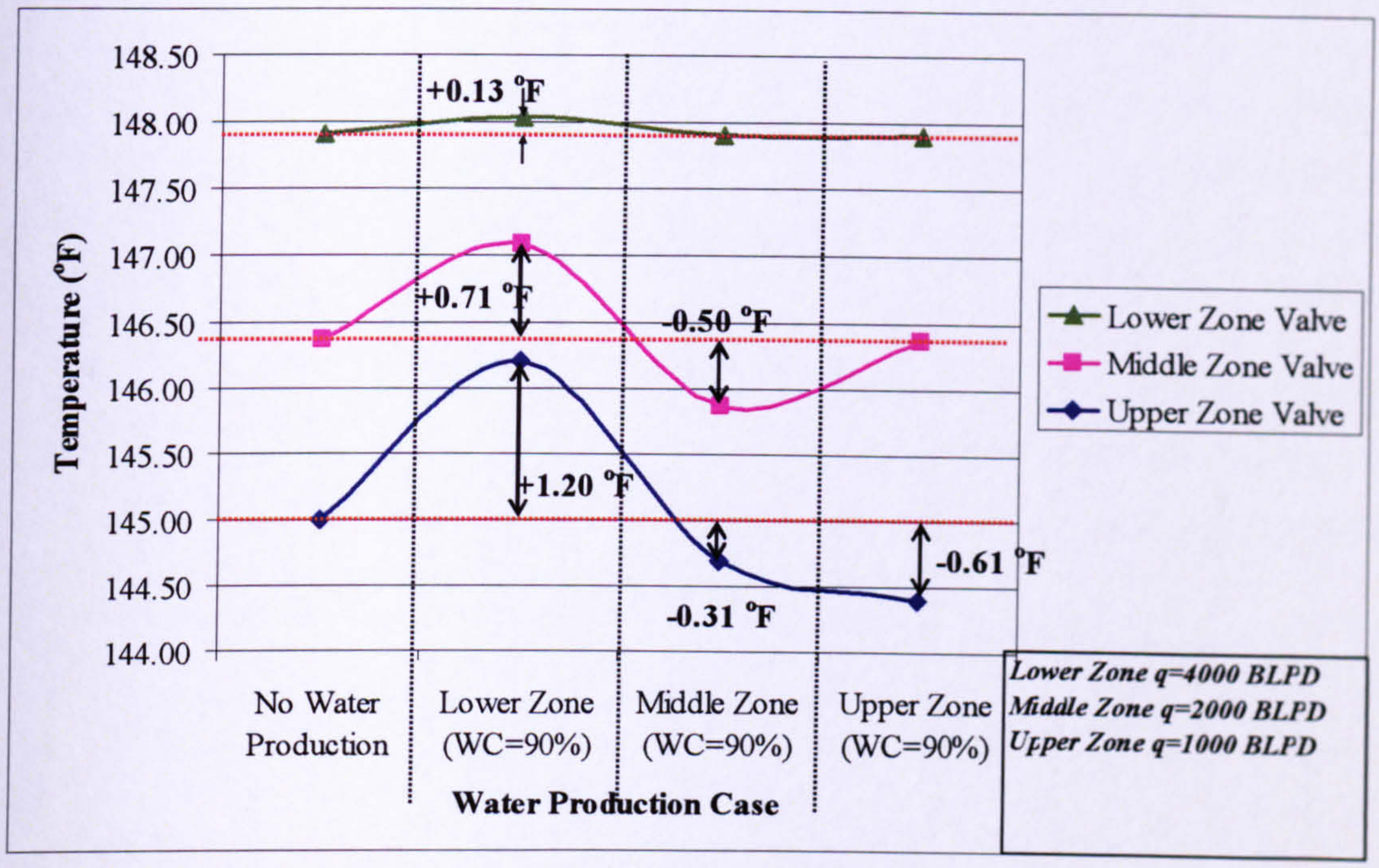

Figure 7-23. Increasing Production Rate Effect on the ICV Mixture Temperature with Water Production (Rate decreases from Bottom to Top zone)

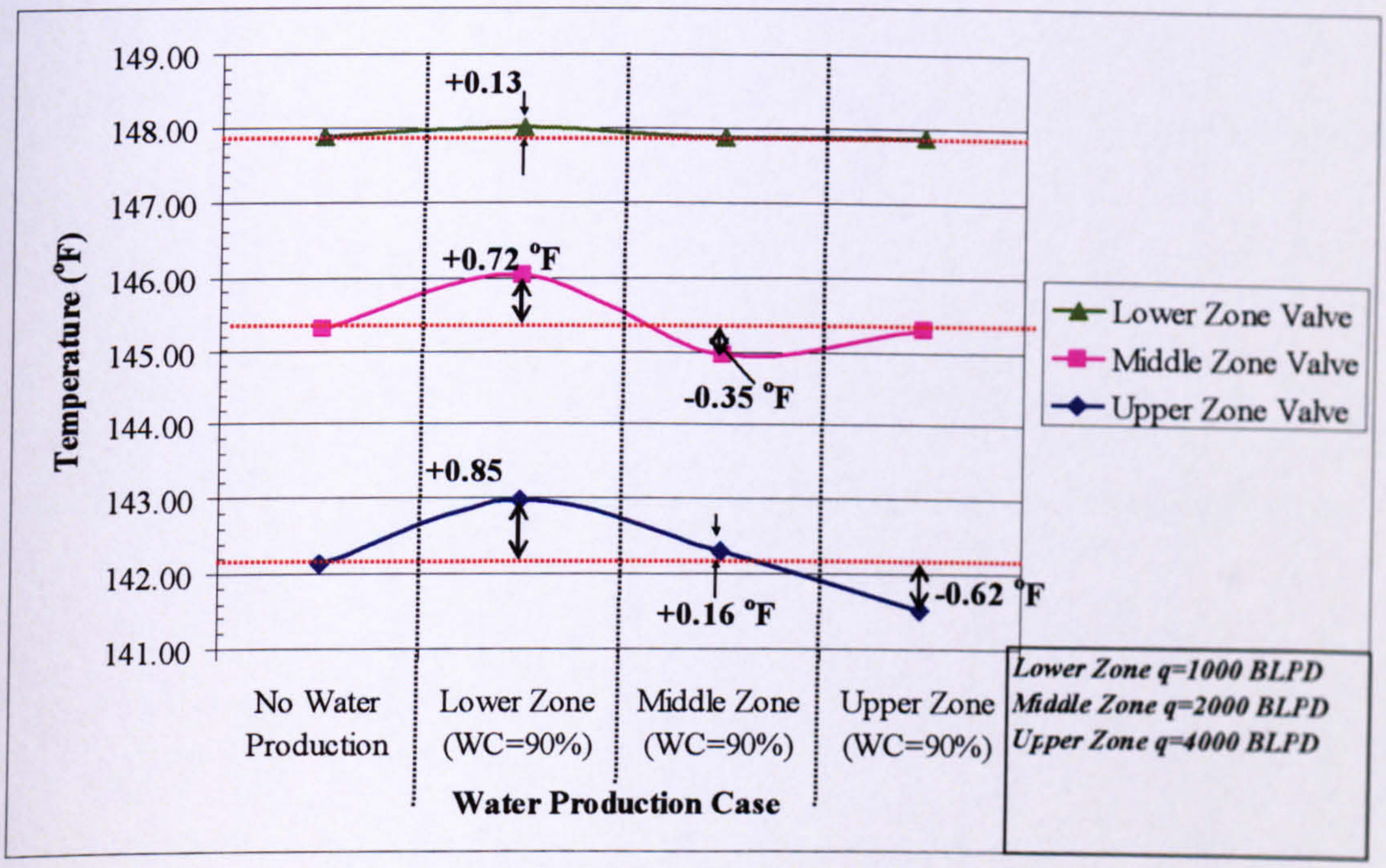

Figure 7-24. Increasing Production Rate Effect on the ICV Mixture Temperature with Water Production (Rate increases from Bottom to Top zone)

7.6.4 Effect of Water Production from all Producing Zones:

So far all the cases studied assumes that the water cut is breaking through in just one zone. Water is produced from all the producing zones in many production scenarios, as

occurred in the Chapter 2 field case study. Figure 7-25 and Figure 7-26 shows that the same principles discussed in sections 7.6.2 and 7.6.3 still applies even if the water is produced from all the zones at different rates; though the modelled temperature changes differ. N.B. The lower zone tubing temperature is assumed equal to the annulus temperature (see section 7.2.1).

Figure 7-25 illustrates that there is a decrease in the temperature of the tubing across the upper zone because the middle zone is producing with a 50% water cut. By contrast Figure 7-26, shows that the tubing temperature profile for all the other zones will be higher if the bottom zone produces with a high water cut.

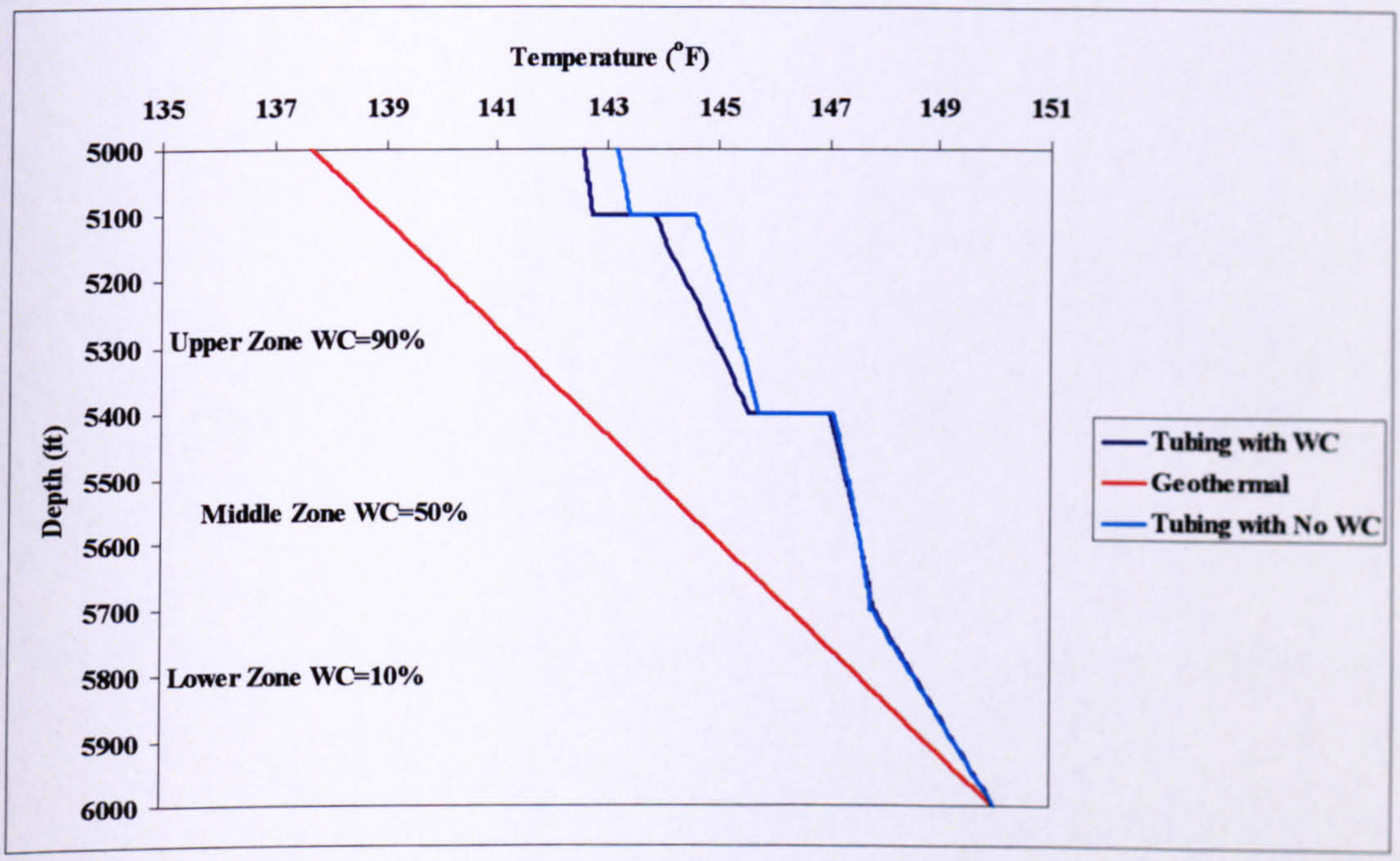

Figure 7-25. Effect of Variable Water Production from all Producing Zones (Water Cut Increases from Bottom to Top Zone)

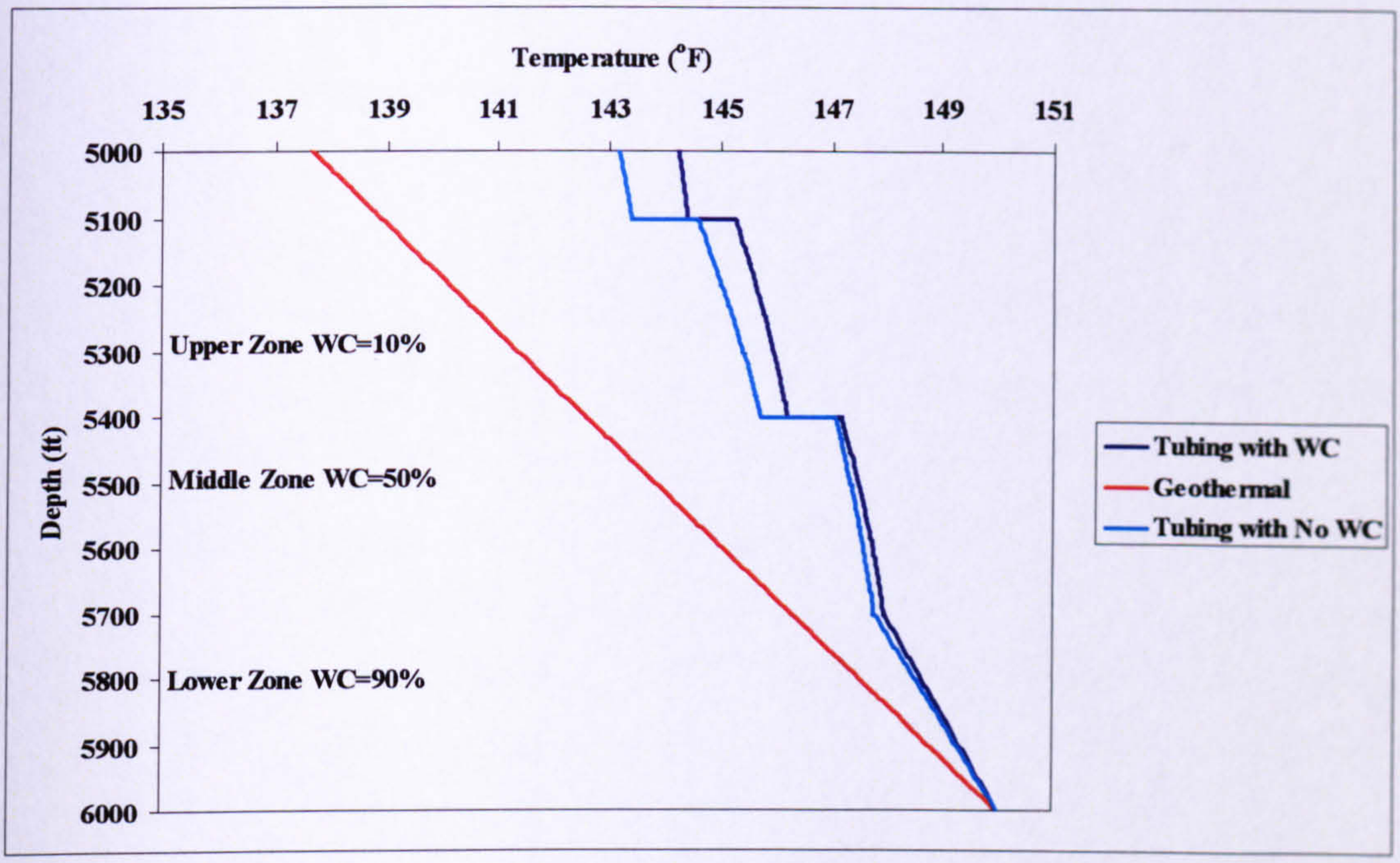

Figure 7-26. Effect of Variable Water Production from all Producing Zones (Water Cut Decreases from Bottom to Top Zone)

Table 7-12 shows the temperature difference for the water influx cases described in Figure 7-25 and Figure 7-26. The majority of these the temperature changes due to water influx are detectable with DTS (resolution= 0.18 °F).

Table 7-12. Temperature Changes Caused by Water Production from all the Zones

	Temperature Difference (T_{wc}-$T_{no,wc}$), °F		
	Lower ICV	Middle ICV	Upper ICV
Decreasing Water Cut from Lower zone (Figure 7-26)	0.17	0.47	1.00
Increasing Water Cut from Lower Zone (Figure 7-25)	0.03	-0.18	-1.69

7.7 Chapter Results Summary:

The modelling of the temperature behaviour in vertical wells completed with intelligent completions shows that:

1. The modelled annulus temperature profile for a zone which has been perforated along its full length will be closer to the geothermal temperature profile as the

segment length used in the model decreases (i.e. fluid inflow points placed at the bottom of each segment are closer together).

2. Smaller segment sizes may increase the running time of complex models (e.g. incorporation of rigorous pressure drop calculations for multiphase flow or horizontal wells. and when modelling changes in thermal properties). For simple cases, as the one studied here, 5 or 10ft segments are recommended since only small differences were observed between the two segment lengths.

3. The tubing-annulus overall heat transfer coefficient and the difference between the annulus and tubing inlet temperature are the drivers for the heat transfer from the tubing to the annulus. The low overall heat transfer coefficient values due to the low thermal conductivity of oil is balanced by an increasing difference between the annulus and tubing inlet temperatures.

4. Increasing the production rate will not change the temperature at the ICVs for each zone if the zones produce the same amount of oil and fully contribute to the inflow. Unless there is significant drawdown leading to Joule-Thompson heating.

5. In single-phase flow, the temperature profile can determine the general location of the major inflows. A higher temperature at the upper ICVs indicates a greater production rate from the bottom zones.

6. An increase in temperature at the ICVs, without a change in the surface flow rate, individual zonal flow rate and water cut, indicates that the upper part of the pay zone is not contributing to the zonal flow. A decrease in temperature indicates the opposite.

7. Temperature gauges placed at the ICV can detect changes in the flow rates if the zonal flow rates are different for *single-phase flow* in a vertical I-Well. Distributed Temperature Sensors (DTS) add extra benefits for single-phase oil production in the area flow assurance (e.g. wax formation) and completion integrity.

8. The location of the water-producing zones can be detected by the pattern of the temperature changes at the ICV:

a. Water breakthrough at the bottom zone will show an increase in the ICV mixing temperature for the middle and upper valve

b. Water breakthrough at the middle zone, will register a decrease in the ICV mixing temperature for the middle and upper valves.

c. Water breakthrough at the upper zone will show a decrease in the temperature at only the upper valve.

d. The magnitude of the temperature change will depend on the change in water cut as well as the zonal production rate.

e. A limited number of examples indicated that the water detection principles could be applied to wide ranges of water cut and production rates. The temperature changes caused by the lower water cuts production will be smaller; but remains detectable with current fibre optic sensing technologies in many cases.

9. Conclusions as to whether specific changes in the well production rate are detectable by DTS or fibre optic P/T sensor require that the model is run for the specific conditions.

7.8 Chapter Discussion:

This chapter presented a mathematical modelling approach that includes the complexities of intelligent wells in steady-state temperature models. This, or similar, new models is necessary if accurate prediction of temperature profiles in I-Wells is required. Such accurate prediction of the I-Well temperature improves the quality of the DTS profiles matching with prediction models for zonal flow rate allocation.

Full confirmation of the presented model in this chapter requires that both temperatures in the annulus and the tubing are simultaneously measured, a rare occurrence in well operations. The DTS cable is placed either in the annulus when it permanently installed, or in the tubing if wireline deployed.

The combination of pressure change trending [7.11] with temperature change trending could be used to extend this study. It will no doubt be a much more powerful tool for unambiguously determining the flow profiles and phase cuts than either temperature or pressure on its own.

7.9 References

7.1. Hasan, A.R. and C.S. Kabir, *Fluid Flow and Heat Transfer in Wellbores*: Published by Society of Petroleum Engineering in 2002.

7.2. Hasan, A.R. and C.S. Kabir, *A Mechanistic Model for Computing Fluid Temperature Profiles in Gas-Lift Wells.* SPE Production & Facilities, 1996: SPE26098 p. 179-185.

7.3. Hill, A.D., *Production Logging - Theoretical and Interpretive Elements*: Published by Society of Petroleum Engineers in 1990.

7.4. Romero, A., D. Zhu, and A.D. Hill. *Temperature Behaviour in Multilateral Wells: Application to Intelligent Wells.* Paper SPE94982 presented at SPE Latin American and Caribbean Petroleum Engineering Conference, Rio De Janiro, Brazil, 20-23 June 2005, Society of Petroleum Engineers.

7.5. Cengel, Y.A., *Heat Transfer - A Practical Approach.* Second ed: Published by McGraw-Hill Higher Education in 2003.

7.6. Spang, B., *Correlations for Convective Heat Transfer.* 2006, The Chemical Engineers' Resource Page www.cheresources.com.

7.7. Hasan, A.R. and C.S. Kabir. *Heat Transfer During Two-Phase Flow in Wellbores: Part I - Formation Temperature.* Paper SPE22866 presented at 66th Annual Technical Conference and Exhibition of the Society of Petroleum Engineers, Dallas, Texas, U.S.A., 6-9 October 1991, Society of Petroleum Engineers.

7.8. Dawkrajai, P., *Temperature Prediction Model for a Producing Horizontal Well,* in *Faculty of the Graduate School.* 2006, The University of Texas at Austin: Austin, Texas. p. 175.

7.9. Weatherford, *Optical Distributed Temperature-Sensing System* http://www.weatherford.com/weatherford/groups/public/documents/general/wft010195.pdf Accessed On:15-April-2007

7.10. Weatherford, *Optical Pressure-Temperature Gauge* http://www.weatherford.com/weatherford/groups/public/documents/general/wft010201.pdf Accessed On:15-April-2007

7.11. Aggrey, G.H., D.R. Davies, and L.T.Skarsholt. A Novel Approach of Detecting Water Influx Time in Multi-Zone and Multilateral Completions using Real-Time Downhole Pressure Data. Paper SPE105374 presented at 15th SPE Middle East Oil & Gas Show and Conference, Kingdom of Bahrain, 11–14 March 2007, Society of Petroleum Engineers.

Chapter 8 Conclusions and Areas of Future Research

8.1 Overall Summary:

This thesis study was initiated by examining the benefits of intelligent completions in developing two real field case studies. It revealed that optimum intelligent well operations required appropriate and reliable flow rates and phase cuts data. This realisation resulted in the decision to study in detail the information that could be derived from a detailed understanding of the changes in the well temperature.

The study discussed the application of fibre optic temperature sensors and the importance of the data they provide for the optimisation of intelligent well operations to maximize hydrocarbon production. A novel application of distributed temperature sensors in the area of flow assurance was presented. It was shown that the length and thickness of a scale layer could be determined by studying the temperature behaviour in a well during scale deposition inside the tubing. This approach can be used alongside

the established application of temperature monitoring for hydrate and wax formation during flowline cool-down.

Modelling of temperature behaviour in intelligent wells revealed that the temperature behaviour can indicate which part of the pay thickness is the major contributor to the zonal flow during periods of single-phase flow. Also the water influx can be detected by monitoring the temperature at the inflow control valves, in single phase flow.

8.2 Thesis Conclusions

This chapter summarizes the thesis conclusions that were detailed at the end of each chapter. The main conclusions from this thesis work are:

1. Comparison of intelligent completions with conventional completion to develop a multi-zone reservoir showed that the intelligent well is the best option for production acceleration.

2. The acceleration provided by intelligent completions can enhance the economical viability of the prospect. The benefit of acceleration is also coupled with the option of controlling unwanted fluid which has a:

    a. Technical Advantage: Maximizing the Production.

    b. Economical Advantage: Minimizing the processing cost of unwanted fluids.

3. Delaying the production of the unwanted fluid is a more effective production enhancement strategy in an I-Well completed in a thin oil column reservoir than controlling the fluid after breakthrough. In cases where the water and gas production is rapid and continuous changing of ICV position to control the fluid might not be practical.

4. Intelligent completions provide a good tool for mitigating reservoir uncertainty but can not replace good conventional reservoir engineering practices. Intelligent well completion optimisation must be preceded by conventional well design optimisation (well location and orientation, standoff point, etc).

5. Multilateral wells coupled with intelligent completions provide an additional opportunity for rate increase in thin oil column reservoir because of the reduced drawdown per lateral required to produce a target rate, as the rate is distributed between the laterals.

6. Temperature data can offer the engineers information about the downhole flow conditions in intelligent wells.

7. The area of temperature modelling and knowledge for oil and gas production wells is in its infancy, providing huge potential research area, particularly with the rapid deployment of temperature sensors.

8. Tubing scale deposition in a conventional well can detected with DTS data due to the low thermal conductivity of the scale. A decrease in the DTS temperature profile is observed if it is installed on the outside of the tubing. Earlier scale detection was shown to be possible in wells with low-to-moderate production rate, producing at lower water cut, with larger annulus area to promote heat transfer prior to the scale zone.

9. Temperature changes due to scale deposition are relatively low in high production rate wells; increasing the minimum scale thickness and the length of the scale deposits required before the deposition becomes detectable on DTS. Increased DTS resolution will increase the detectability of scale deposits in the tubing. It will also provide finer resolution to counter-balance the effect of rate fluctuations in the well.

10. The availability of the DTS temperature data eliminates the iterative solution procedure for determining the overall heat transfer coefficient. DTS profiles were shown to be able to determine the thickness of the scale layer as well as its length. The scale thickness is derived from the overall heat transfer coefficient for the scale deposited region, which is may be estimated using the DTS data.

11. Modification of existing temperature models is necessary to accurately model the temperature behaviour in intelligent well. The most important aspect is the addition of annulus temperature calculation routine together with inclusion of the distributed rather than point-source influx of the produced fluid into the annulus.

12. Modelling the temperature behaviour in an intelligent well shows that the water cut can be detected in two-phase flow by monitoring the mixing temperature at the ICV.

13. In single-phase flow, the temperature profile can determine the general location of the major inflows. A higher temperature at the upper ICVs indicates a greater

production rate from the bottom zones. This is particularly useful in the initial stages of the well production by identifying effective clean-up of the pay zone.

14. Flow rate allocation, one of the biggest prizes of DTS deployment, can be enhanced with accurate modelling of the downhole temperature, since the rate allocated through matching the downhole data with a prediction model. To achieve this more focus is needed on the wellbore modelling in conjunction with reservoir and sandface temperature prediction.

8.3 Areas of Future Research:

The complex nature of the heat transfer phenomenon in oil and gas wellbores require further study. A deeper understanding of the phenomenon will derive more applications for DTS and fibre optic temperature gauges. The work that was carried out on the scale detection and temperature modelling in I-Wells was based certain assumptions. Following are some of the future research areas that will enhance improve the work that was featured in this thesis.

Development of Heat Transfer Correlations for Oil and Gas Wellbore Environments:

Most correlations for convective heat transfer coefficient (natural or forced) are based on correlations that were developed under conditions very different from oil and gas production environments. Oil and gas wells extend into thousands of feets in with varying mixture of fluids and surrounding environments (different geologies and reservoir environments that can alter the heat transfer to the wells). Two options can be used to enhance this area:

1. Flow loop labs currently used to test completions equipments can be used to establish convective heat transfer correlations for conditions close to oil and gas wells. Such correlations will improve the accuracy of existing models and future temperature prediction models. Unfortunately this work will be expensive.
2. As more DTS systems are being deployed in the oil and gas wells, the temperature data can be used to derive heat transfer correlations that similar to field data based flow correlations (Hagedoorn and Brown, etc).

Study of Multiphase Flow Production Environments:

The work in Chapter 6 & 7 was carried out based on a Two-Phase (oil/water) flow assumption. Multiphase flow (oil/water/gas) occurs in the vast majority of production

wells. Modifications to accommodate complex completions can be incorporated with multiphase flow simulators (i.e. OLGA) to model the effect of added completions on the predicted temperature in a multi-phase production well.

Improved ICV mixing Temperature Modelling:

The work in Chapter 7 on modelling of intelligent wells assumed ideal mixing at the ICV, this is an ideal assumption and the constant and identical fluid properties for each zone, made this assumption viable for this study. Real situations can be more complex, e.g. mass transfer may also occur in addition to heat transfer at the ICV. This complex heat and mass transfer problem along with the kinetics involved can be investigated by using Multi-physics modelling packages (i.e. FEMLAB, Flow3D, etc). This is particularly important in multi-phase flow where compressible and incompressible fluid can mix in different concentrations from different zones, and the ideal mixing assumption might fail. One example is the mixing of a saturated oil and gas stream with under-saturated oil.

Deviated, Horizontal and Advanced Completions Temperature Modelling:

A vertical well was assumed for this study. Temperature modelling in open hole horizontal well is established and the concepts provided in Chapter 7 for intelligent completions can be applied to horizontal well and determine the effect of the intelligent completions equipments. In deviated wells, effect of pressure drop most be given a priority, in addition to the modelling of the geothermal temperature.

The increasing deployment of advanced completions such as Inflow Control Devices (ICDs) and AICD (Autonomous Inflow Control Devices), and the complex fluid dynamics behaviour in such completions require re-evaluation of the temperature prediction models and the modelling of such complexities. Advances in the temperature modelling for such devices can encourage service companies to invest in developing deployment techniques in such completions.

Use of Thermal Simulators:

The case studies presented in Chapters 2 & 3 can be simulated in thermal simulators to test the concepts of scale detection in conventional wells and water detection in intelligent completion wells. The wellbore temperature models may be required to be converted to transient model and coupled with thermal simulators. This is particularly important in modelling well start-up conditions.

Combination of Pressure and Temperature Data:

Examination of the pressure and temperature drop (DP and DT) trends between the ICVs can indicate the influx of water. Combination of both sets of data can provide a more accurate and reliable determination of the water influx point.

Appendix 1: Scale Thickness Expression Derivation

The overall heat transfer coefficient for scaled up region is:

$$\frac{1}{U_{to,scale}} = \frac{r_{to}\ln\left(r_{ti}/r_{si}\right)}{k_{scale}} + \frac{1}{(h_{nc}+h_r)} + \frac{r_{to}\ln\left(r_{wb}/r_{co}\right)}{k_{cem}} \qquad \textbf{Equation A1}$$

The overall heat transfer coefficient for the case where there is no scale deposited in the tubing is:

$$\frac{1}{U_{to,noscale}} = \frac{1}{(h_{nc}+h_r)} + \frac{r_{to}\ln\left(r_{wb}/r_{co}\right)}{k_{cem}} \qquad \textbf{Equation A2}$$

Substituting Equation A2 into Equation A1

$$\frac{1}{U_{to,scale}} = \frac{r_{to}\ln\left(r_{ti}/r_{si}\right)}{k_{scale}} + \frac{1}{U_{to,noscale}} \qquad \textbf{Equation A3}$$

Re-arranging Equation A3,

$$\frac{r_{to}\ln\left(r_{ti}/r_{si}\right)}{k_{scale}} = \frac{1}{U_{to,scale}} - \frac{1}{U_{to,noscale}}$$

$$\ln\left(r_{ti}/r_{si}\right) = \frac{k_{scale}}{r_{to}}\left(U^{-1}_{to,scale} - U^{-1}_{to,noscale}\right)$$

Finally,

$$\boxed{r_{si} = \frac{r_{ti}}{\exp\left(\frac{k_{scale}}{r_{to}}\left(U^{-1}_{to,scale} - U^{-1}_{to,noscale}\right)\right)}}$$

Appendix 2: Temperature Model with Scale Deposits

MATLAB Code

```
clear all
%for qt=0.1:0.1:0.9;
global L Teibh DevAng dti rti dto rto dci rci dco rco dwb rwb kcem kcas ke J
global DenF Cpe Tes g gc gG  TD Lr Phi wt Cpm
dti=4; %in
dti=dti*8.333*10^-2; %ft
rti=dti/2; %ft
dto=4.5; %in
dto=dto*8.333*10^-2; %ft
rto=dto/2; %ft
dci=6.46; %in
dci=dci*8.333*10^-2; %ft
rci=dci/2; %ft
dco=7; %in
dco=dco*8.333*10^-2; %ft
rco=dco/2; %ft
dwb=9; %in
dwb=dwb*8.333*10^-2; %ft
rwb=dwb/2; %ft
Roughness=0.0015;
emmissivity=0.9;
DevAng=(90*pi)/180;
L=6000;
%Cement Thermal Conductivity
kcem=4.024; %Btu/(hr-ft-F)
%Casing Thermal Conductivity
kcas=33; %Btu/(hr-ft-F)
%Formation Thermal Conductivity
ke=3.33; %Btu/(hr-ft-F)
%Formation Density
DenF=135; %lbm/ft3
%Formation Heat Capacity
Cpe=0.625; %Btu/(lbm-F)
%Production Time
t=158; %hr
%Dimensionless Time Calculations
td=(ke*t)/(DenF*Cpe*rwb^2);
%Dimensionless Temperature
TD=log10(exp(0.2*td)+(1.5-0.3719*exp(-td))*sqrt(td));
%Production DATA
%%%%%%%%%%%%%%%%%%%%%%
%Input Production Data
qt=1250; %BOPD
wc=0.2; %(fraction)
OilGravity=34.4; %Oil Gravity (oAPI)
DenW=63.68; %Water Density (lbm/ft3)
%Calculated Production Data
qw=qt*wc; %Water Production Rate (bbl/D)
qo=qt-qw; %Oil Production Rate (bbl/D)
DenO=(141.5/(131.5+OilGravity))*DenW; %Oil Density (lbm/ft3)
WatVF=qw/(qo+qw); %Water Volume Fraction
OilVF=qo/(qo+qw); %Oil Volume Faction
MixDen=WatVF*DenW+OilVF*DenO; %Mixture Density
%Calculation of Mass Flow rate for Tubing Flow Rate
```

```
%Conversion Factor (1 bbl/D = 0.2339 ft3/hr)
wt=(qt*0.2339)*MixDen; %Tubing Mass Flow Rate (lbm/hr)
%%%%%%%%%%%%%%%%%%%%%%%%%%%%%%%%%%
%Velocity Calculation (required for calculating Reynolds Number required to
%calculate the Convection Heat Transfer Coefficient
%%%%%%%%%%%%%%%%%%%%%%%%%%%%%%%%%%
vt=(qt*6.49836033951*10^-5)/(pi*rti^2); %Tubing Flow Velocity (ft/s)
%%%%%%%%%%%%%%%%%%%%%%%%%%%%%%%%%%%%%%%%%%%%%%%%%%%%%%%%%%%%%%%%%%%%%%%%%%%%%%%
%
Tes=76; %Formation Static Temperature at the surface
Teibh=150; %Bottom Hole Formation Temperature
gG=(Teibh-Tes)/L;
%%%%%%%%%%%%%%%%%%%%%%%%%%%%%%%%%%%%%%%%%%%%%%%%%%%%%%%%%%%%%%%%%%
%Production Fluid Thermal & Physical Properties
%%%%%%%%%%%%%%%%%%%%%%%%%%%%%%%%%%%%%%%%%%%%%%%%%%%%%%%%%%%%%%%%%%
%Heat Capacities
%%%%%%%%%%%%%%%%%%%%%%%%%%
Cpw=0.947; %Annular Fluid Heat Capacity (Btu/(lbm-F))
Cpo=0.507; %Tubular Fluid Heat Capacity (Btu/(lbm-F))
%Mixture Heat Capacity
Cpm=OilVF*Cpo+WatVF*Cpw;
%%%%%%%%%%%%%%%%%%%%%%%%
%Thermal Conductivities
%%%%%%%%%%%%%%%%%%%%%%%%
Kfo=0.081; %Tubular Fluid Thermal Conductivity (Btu/(hr-ft-F))
Kfw=0.383; %Annular Fluid Thermal Conductivity (Btu/(hr-ft-F))
%Mixture Thermal Conductivity
Kfm=OilVF*Kfo+WatVF*Kfw;
%%%%%%%%%%%%%%%%%%%%%%%%%%%%%%%%%%%%
%Viscosity Calculations:
%%%%%%%%%%%%%%%%%%%%%%%%%%%%%%%%%%%%
%Conversion Factor 1 cp = 6.712*10^-4 lbm/(ft.s)
visO=3; %Oil Fluid Viscosity (cp)
visW=1; %Water Fluid Viscosity (cp)
visM=visO*OilVF+visW*WatVF;
%%%%%%%%%%%%%%%%%%%%%%%%%%%%%%%%%%%%%%%%%%%%%%%%%%%%
%%Annular Fluid Properties
%%%%%%%%%%%%%%%%%%%%%%%%%%%%%%%%%%%%%%%%%%%%%%%%%%%%
Cpan= 0.949; %Btu/(lbm.F)
kan=0.368340283; %Btu/(hr-ft-F)
AnnVisc=0.52; %Annulus Static Fluid Viscosity (cp)
AnnDen=65.828; %lbm/ft3
Beta=0.00027; %1/F
emms=0.9;
%Constants
g=32.174; %Gravity Acceleration (ft/s2)
gc=32.17; %Conversion factor, 32.17 (lbm-ft)/(lbf-sec2)
J=778; %Mechanical Equivelant of Heat (ft-lbf)/Btu
StefBoltzConst=0.1714*10^-8; %Stefan-Boltzmann Constant Btu/(hr.ft2.R4)
%Scale Zone Properties
%for dsi=4:-1:1; %in
dsi=1;
dsit=dsi;
dsi=dsi*8.333*10^-2; %ft
rsi=dsi/2; %ft
ScaleRoughness=2.953e-4; %ft (0.045mm)
ScaleTop=4000; %ft
ScaleBottom=5000; %ft
kscale=2.081433537; %Scale Thermal Conductivity (Btu/(hr.ft.F))
%Indicate DZ (Segment Size)
DZ=10; %ft
% Calculate the number of segments for the well
```

```
Segs=L/DZ;
Segs=Segs+1;
Dca=(dci^2/dto^2)-1;
Title=['Scale Study Base Case NosDPDZ - DZ' int2str(DZ) ' qt=' int2str(qt) 'WC=' int2str(wc*100) '%' '
dsi=' int2str(dsit)]
for N=1:Segs
   zt(N)=L-(N-1)*DZ;
   Tei(N)=Teibh-(L-zt(N))*gG*sin(DevAng);
end
if dsi == dti;
   msg='No Scale is Present in The Tubing'
   NoScaleCalc4;
elseif dsi > dti;
   msg='Scale Diameter is larger than Tubing Diameter, Check Your Data'
elseif dsi==0
   msg='The Tubing is Blocked with Scale and Can not Flow'
else
   msg='Scale is Present in The Tubing'
   ScaleCalc4NOsDPDZ;
end;
DPDZ=DPDZ';
Gr=Gr';
Lr=Lr';
Nu=Nu';
Phi=Phi';
Pr=Pr';
hc=hc';
hr=hr';
Uto=Uto';
%Ttx=Ttx';
Tco=Tco';
Twb=Twb';
Tf=Tf';
zt=zt';
DPDZ2=DPDZ2';
Tei=Tei';
Ttx=Ttx';
xlswrite(Title,[zt,Tf,Tei,Gr,Pr,hc,hr,Uto,Lr,DPDZ,DPDZ2,Phi])
createfigure(Ttx, zt, Tei,Title)
CombinedUTempFigure2(Ttx, zt, Tei, Uto);
CombinedUTempFigureZoom(Ttx, zt, Tei, Uto);
PlotProfiles(Ttt,zt,Tat,Teit);
```

```
Subroutine to Calculate the temperature profile if there is Scale deposited in the well
err=1;
Tf(1)=Tei(1);
Ttx(1)=Tei(1);
for N=2:Segs;
   Uto(N)=10;
while err>0.01;
%   zt(N) = L - (N-1) * DZ;
   %Tei(N)=Teibh-(L-zt(N))*gG*sin(DevAng);
%   if zt(N) <= ScaleBottom && zt(N) >= ScaleTop;
%   DPDZ(N) = PDrop(dsi, qo, qw, MixDen, visM, ScaleRoughness, DevAng);
%   Phi(N)=3.995*10^-5*(1/(MixDen*Cpm))*DPDZ(N);
%   else
   DPDZ(N) = PDrop(dti, qo, qw, MixDen, visM, Roughness, DevAng);
   Phi(N)=3.995*10^-5*(1/(MixDen*Cpm))*DPDZ(N);
%   end;
   Lr(N)=((2*pi)/(Cpm*wt))*((rto*Uto(N)*ke)/(ke+rto*Uto(N)*TD));
   clear Tt;
   [z,Tt]=ode45('dTtdzG4',[zt(N-1) zt(N)],Tf(N-1),[],Lr(N),Phi(N));
```

```
    Tf(N)=mean(Tt);
% Calculating the wellbore to be used in calculating the casing inside temperature for Garshof Number
    Twb(N)=(rto*Uto(N)*Tf(N)+ke/TD*Tei(N))/(ke/TD+rto*Uto(N));
% Calculating the Casing inside temperature for Grashof number
    Tco(N)=Twb(N)+log(rwb/rco)/kcem*rto*Uto(N)*(Tf(N)-Twb(N));
% Calculating the radiation heat transfer coefficicent
    Ftci=(1/emmissivity+rto/rci*((1/emmissivity)-1))^-1;

hr(N)=StefBoltzConst*Ftci*((Tf(N)+459.67)^2+(Tco(N)+459.67)^2)*((Tf(N)+459.67)+(Tco(N)+459.67)
);
% Prandtl Number for packer fluid in the annulus
% 1cp = 2.419 lb/(ft.hr)
    Pr(N)=(Cpan*AnnVisc*2.419)/kan;
% Garshof Number for Packer fluid in the annulus
% 1cp = 0.000671969 lb/(ft.s)
    Gr(N)=abs(((rci-rto)^3*g*AnnDen^2*Beta*(Tf(N)-Tco(N)))/(AnnVisc*6.72e-4)^2);
% Steps to calculate the effective conductivity of the annulus fluid due to Natural Convection
% Lc = Characteristics Length for the annulus area (Cengel, 2002, p480)
    Lc=(dci-dto)/2;
% Fcyl is the Geometric Factor for Concentric Cylinders (Cengel, 2002,
% p481)
    Fcyl=(log(dci/dto))^4/(Lc^3*(dto^(-3/5)+dci^(-3/5))^5);
% RaL is Rayleigh Number (Cengel, 2002, p466)
    RaL = Gr(N) * Pr(N);
% keff is the effective thermal conductivity for the natural heat
% convection in the annulus of a concentric cylinders (Cengel, 2002,p481)
    keff=kan*(0.386*(Pr(N)/(0.861+Pr(N)))^0.25*(Fcyl*RaL)^0.25);
% Nusselt Number
    Nu(N)=keff/kan;
%   Nu(N) = (0.6 + (0.387 * RaL ^ (1 / 6)) / (1 + (0.559 / Pr(N)) ^ (9 /
%   16)) ^ (8 / 27)) ^ 2;
% Natural Heat Convection Coefficient (Btu/(hr.ft2.ft)
%   hc(N) = ((Nu(N) * kan) / Lc) * 0.25;
    hc(N) = ((Nu(N) * kan) / Lc);
    if zt(N) <= ScaleBottom && zt(N) >= ScaleTop;
       UTONew = ((rto*log(rti /rsi))/kscale+1/(hc(N)+hr(N))+(rto*log(rwb/rco)/kcem))^-1;
    else;
       UTONew = (1 /(hc(N)+hr(N))+(rto*log(rwb/rco)/kcem))^-1;
    end;
    err=abs((UTONew - Uto(N))/UTONew);
    Uto(N)=UTONew;
end
    clear Tt;
    Lr(N)=((2*pi)/(Cpm*wt))*((rto*Uto(N)*ke)/(ke+rto*Uto(N)*TD));
    [z,Tt]=ode45('dTtdzG4',[zt(N-1) zt(N)],Tf(N-1),[],Lr(N),Phi(N));
    Ttx(N)=mean(Tt);
    err=1;
end
```

Temperature Prediction Function

```
function dTtdzG4 = dTtdzG4(z,Tt,flag,Lra,Phia)
%Differential Equation for temperature profile in the tubing with natural
%convection in the annulus
global Teibh DevAng L gc g Cpm J gG
dTtdzG4=Lra*(Tt-(Teibh-gG*(L-z)*sin(DevAng)))+((g*sin(DevAng))/(gc*Cpm*J))-Phia;
```

Appendix 3: I-Well Temperature Model MATLAB Code

```
clear all
global Bdash L Teibh Angle g dti rti dto rto dci rci dco rco dwb rwb kcem kcas ke
global DenF Cpe Tes g gg Angle ke rco Uco TD rto Tm3 LRaa Phi wa1 qac1 qac2 qac3 Cpm1 Cpm2
Cpm3 CpV3 J gc
%%%%%%%%%%%%%%%%%%%%%%%%%%%%%
StefBoltzConst=0.1714*10^-8; %Stefan-Boltzmann Constant (Btu/(h.ft2.R4))
gg=32.174; %Gravitational Acceleration (ft/s2)
gc=32.17; %Conversion factor, 32.17 (lbm-ft)/(lbf-sec2)
J=778; %Mechanical Equivelant of Heat (ft-lbf)/Btu
%%%%%%%%%%%%%%%%%%%%%%%%%%%%%%%%%
dti=4; %in
rti=dti/2*8.333*10^-2; %ft
dto=4.5; %in
rto=dto/2*8.333*10^-2; %ft
dci=6.46; %in
rci=dci/2*8.333*10^-2; %ft
dco=7; %in
rco=dco/2*8.333*10^-2; %ft
dwb=9; %in
rwb=dwb/2*8.333*10^-2; %ft
Angle=(90*pi)/180;
Roughness=0.00015;
L=6000;
%Cement Thermal Conductivity
kcem=4.024; %Btu/(hr-ft-F)
%Casing Thermal Conductivity
kcas=33; %Btu/(hr-ft-F)
%Formation Thermal Conductivity
ke=3.33; %Btu/(hr-ft-F)
%Formation Density
DenF=135; %lbm/ft3
%Formation Heat Capacity
Cpe=0.625; %Btu/(lbm-F)
%Production Time
t=158; %hr
%Dimensionless Time Calculations
td=(ke*t)/(DenF*Cpe*rwb^2);
%Dimensionless Temperature
TD=log10(exp(0.2*td)+(1.5-0.3719*exp(-td))*sqrt(td));
%Production DATA
%%%%%%%%%%%%%%%%%%%%%
%Tubing Production (Zone1)
qt1=0; %BOPD
%Annulus Production (Zone1)
wc1=1; %(fraction)
qa1=500; %BOPD
qw1=qa1*wc1;
qo1=qa1-qw1;
DenW1=63.68; %Zone 2 Oil Density (lbm/ft3)
Z1OilGravity=34.4; %Oil Gravity (oAPI)
DenO1=(141.5/(131.5+Z1OilGravity))*DenW1; %Zone 1 Oil Density (lbm/ft3)
WatVF1=qw1/(qo1+qw1); %Water Volume Fraction
OilVF1=qo1/(qo1+qw1); %Oil Volume Faction
MixDen1=WatVF1*DenW1+OilVF1*DenO1;
%Calculation of Mass Flow rate for Tubing Flow Rate
```

```
%Conversion Factor (1 BOPD = 0.2339 ft3/hr)
wt1=(qt1*0.2339)*MixDen1; %Tubing Mass Flow Rate (lbm/hr)
%%%%%%%%%%%%%%%%%%%%%%%%%%%%%%%%%%%
%Annulus Production (Zone2)
%%%%%%%%%%%%%%%%%%%%%%%%%%%%%%%%%%%
wc2=1; %Water Cut for Zone 2 (fraction)
qa2=500; %Total Production BOPD
qw2=qa2*wc2; %Water Production BOPD
qo2=qa2-qw2; %Oil Production BOPD
DenW2=63.68; %Zone 2 Oil Density (lbm/ft3)
Z2OilGravity=34.4; %Oil Gravity (oAPI)
DenO2=(141.5/(131.5+Z2OilGravity))*DenW2; %Zone 1 Oil Density (lbm/ft3)
WatVF2=qw2/(qo2+qw2); %Water Volume Fraction
OilVF2=qo2/(qo2+qw2); %Oil Volume Faction
MixDen2=WatVF2*DenW2+OilVF2*DenO2;
%Tubing Production (Zone2)
qt2=qa1; %BOPD
%Calculation of Mass Flow rate for Tubing Flow Rate
%Conversion Factor (1 BOPD = 0.2339 ft3/hr)
wt2=(qt2*0.2339)*MixDen1; %Tubing Mass Flow Rate (lbm/hr)
%%%%%%%%%%%%%%%%%%%%%%%%%%%%%%%%%%%
%Annulus Production (Zone3)
%%%%%%%%%%%%%%%%%%%%%%%%%%%%%%%%%%%
wc3=1; %fraction
qa3=500; %BOPD
qw3=qa3*wc3;
qo3=qa3-qw3;
DenW3=63.68; %Zone 2 Oil Density (lbm/ft3)
Z3OilGravity=34.4; %Oil Gravity (oAPI)
DenO3=(141.5/(131.5+Z3OilGravity))*DenW3; %Zone 1 Oil Density (lbm/ft3)
WatVF3=qw3/(qo3+qw3); %Water Volume Fraction
OilVF3=qo3/(qo3+qw3); %Oil Volume Faction
MixDen3=WatVF3*DenW3+OilVF3*DenO3;
%Tubing Production (Zone3)
qt3=qt2+qa2; %BOPD
%Calculation of Mass Flow rate for Tubing Flow Rate
%Conversion Factor (1 BOPD = 0.2339 ft3/hr)
T3MixDen=(qt2/qt3)*MixDen1+(qa2/qt3)*MixDen2;
wt3=(qt3*0.2339)*T3MixDen; %Tubing Mass Flow Rate (lbm/hr)
%%%%%%%%%%%%%%%%%%%%%%%%%%%%%%%%%%%%%%%%%%
%%Final Rate of Production
%%%%%%%%%%%%%%%%%%%%%%%%%%%%%%%%%%%%%%%%%%%%%
qtF=qt3+qa3;
TFMixDen=(qt3/qtF)*T3MixDen+(qa3/qtF)*MixDen3;
wtF=(qtF*0.2339)*TFMixDen; %Tubing Mass Flow Rate (lbm/hr)
vtF=(qtF*6.49836033951*10^-5)/(pi*rti^2); %Tubing Flow Velocity (ft/s)
%%%%%%%%%%%%%%%%%%%%%%%%%%%%%%%%%%%
%Velocity Calculation (required for calculating Reynolds Number required to
%calculate the Convection Heat Transfer Coefficient
%%%%%%%%%%%%%%%%%%%%%%%%%%%%%%%%%%%
vt1=(qt1*6.49836033951*10^-5)/(pi*rti^2); %Tubing Flow Velocity (ft/s)
AnArea=pi*((2*rci)^2-(2*rto)^2)/4; %Annulus Area ft^2
va1=(qa1*6.49836033951*10^-5)/AnArea; %Annular Flow Velocity (ft/s)
%%%%%%%%%%%%%%%%%%%%%%%%%%%%%%%%%%
%%Second Zone Velocities
%%%%%%%%%%%%%%%%%%%%%%%%%%%%%%%%
%Velocity Calculation (required for calculating Reynolds Number for
%Convection Heat Transfer Coefficient Calculations
vt2=(qt2*6.49836033951*10^-5)/(pi*rti^2); %Tubing Flow Velocity (ft/s)
AnArea=pi*((2*rci)^2-(2*rto)^2)/4; %Annulus Area ft^2
va2=(qa2*6.49836033951*10^-5)/AnArea; %Annular Flow Velocity (ft/s)
%%%%%%%%%%%%%%%%%%%%%%%%%%%%%%%%%%%%%%%%%%%%%%%%%%%%%%%%%%%%%%%%%%%
```

```
%%%%%%%%%%%%%%%%%%%%%%%%%%
%%Third Zone Velocities
%%%%%%%%%%%%%%%%%%%%%%%%%%
%Velocity Calculation (required for calculating Reynolds Number for
%Convection Heat Transfer Coefficient Calculations
vt3=(qt3*6.49836033951*10^-5)/(pi*rti^2); %Tubing Flow Velocity (ft/s)
AnArea=pi*((2*rci)^2-(2*rto)^2)/4; %Annulus Area ft^2
va3=(qa3*6.49836033951*10^-5)/AnArea; %Annular Flow Velocity (ft/s)
%%%%%%%%%%%%%%%%%%%%%%%%%%%%%%%%%%%%%%%%%%%%%%%%%%%%%%%%%%%%%%%%%
Tes=76; %Formation Static Temperature at the surface
Teibh=150; %Bottom Hole Formation Temperature
g=(Teibh-Tes)/L;
%%%%%%%%%%%%%%%%%%%%%%%%%%%%%%%%%%%%%%%%%%%%%%%%%%%%%%%
%Production Fluid Thermal & Physical Properties
%%%%%%%%%%%%%%%%%%%%%%%%%%%%%%%%%%%%%%%%%%%%%%%%%%%%%%%
%Heat Capacities
%%%%%%%%%%%%%%%%%%%%
Cpw=0.947; %Annular Fluid Heat Capacity (Btu/(lbm-F))
Cpo=0.507; %Tubular Fluid Heat Capacity (Btu/(lbm-F))
%Zone 1 Mixture Heat Capacity
Cpm1=(qo1/(qo1+qw1))*Cpo+(1-(qo1/(qo1+qw1)))*Cpw;
%Zone 2 Mixture Heat Capacity
Cpm2=(qo2/(qo2+qw2))*Cpo+(1-(qo2/(qo2+qw2)))*Cpw;
%Zone 3 Mixture Heat Capacity
Cpm3=(qo3/(qo3+qw3))*Cpo+(1-(qo3/(qo3+qw3)))*Cpw;
%Heat Capacity for Mixed Fluid After Valve 2
qo2t=qo1+qo2;
qw2t=qw1+qw2;
CpV2=(qo2t/(qo2t+qw2t))*Cpo+(1-(qo2t/(qo2t+qw2t)))*Cpw;
%Heat Capacity for Mixed Fluid After Valve 3
qo3t=qo2t+qo3;
qw3t=qw2t+qw3;
CpV3=(qo3t/(qo3t+qw3t))*Cpo+(1-(qo3t/(qo3t+qw3t)))*Cpw;
%%%%%%%%%%%%%%%%%%%%%%
%Thermal Conductivities
%%%%%%%%%%%%%%%%%%%%%%
%Kfo=0.081; %Oil Fluid Thermal Conductivity (Btu/(hr-ft-F))
Kfo=0.081; %Oil Fluid Thermal Conductivity (Btu/(hr-ft-F))
Kfw=0.383; %Water Fluid Thermal Conductivity (Btu/(hr-ft-F))
%Zone 1 Mixture Heat Capacity
Kfm1=(qo1/(qo1+qw1))*Kfo+(1-(qo1/(qo1+qw1)))*Kfw;
%Zone 2 Mixture Heat Capacity
Kfm2=(qo2/(qo2+qw2))*Kfo+(1-(qo2/(qo2+qw2)))*Kfw;
%Zone 3 Mixture Heat Capacity
Kfm3=(qo3/(qo3+qw3))*Kfo+(1-(qo3/(qo3+qw3)))*Kfw;
%Heat Capacity for Mixed Fluid After Valve 2
qo2t=qo1+qo2;
qw2t=qw1+qw2;
KfV2=(qo2t/(qo2t+qw2t))*Kfo+(1-(qo2t/(qo2t+qw2t)))*Kfw;
%Heat Capacity for Mixed Fluid After Valve 3
qo3t=qo2t+qo3;
qw3t=qw2t+qw3;
KfV3=(qo3t/(qo3t+qw3t))*Kfo+(1-(qo3t/(qo3t+qw3t)))*Kfw;
%%%%%%%%%%%%%%%%%%%%%%%%%%%%%%%%
%Viscosity Calculations:
%%%%%%%%%%%%%%%%%%%%%%%%%%%%%%%%
%Conversion Factor 1 cp = 6.712*10^-4 lbm/(ft.s)
visO=(3*0.000671969); %Tubular Fluid Viscosity lbm/(ft.s)
visW=(1*0.000671969); %Annular Fluid Viscosity lbm/(ft.s)
visM1=visO*OilVF1+visW*WatVF1;
visM2=visO*OilVF2+visW*WatVF2;
visM3=visO*OilVF3+visW*WatVF3;
```

```
visV2=(qo2t/(qo2t+qw2t))*visO+(1-(qo2t/(qo2t+qw2t)))*visW;
visV3=(qo3t/(qo3t+qw3t))*visO+(1-(qo3t/(qo3t+qw3t)))*visW;
%%Annulus Overall Heat Transfer Coefficient (Between Annulus and Formation)
Uco=((rwb*log10(rco/rci))/kcas+(rwb*log10(rwb/rco))/kcem)^-1;
%%%%%%%%%%%%%%%%%%%%%%%%%%%%%%%%%%%%%%%
%%Annular Fluid Properties
%%%%%%%%%%%%%%%%%%%%%%%%%%%%%%%%%%%%%%%
Cpan= 0.949; %Btu/(lbm.F)
kan=0.368340283; %Btu/(hr-ft-F)
AnnVisc=0.52; %Annulus Static Fluid Viscosity (cp)
AnnDen=65.828; %lbm/ft3
Beta=0.000272222; %1/F
emms=0.9;
%Indicate DZ (Segment Size)
DZ=5; %ft
%Number of Zones
Zones=3;
%Zones Length
Z1L=300; %ft
Z2L=300; %ft
Z3L=300; %ft
%Calculate Zones Tops
ZT1=L-Z1L;
ZT2=ZT1-Z2L;
ZT3=ZT2-Z3L;
%Determine the inflow distribution for the zones
inflowdist2PhaseV8
Title=['I-Well Model V9a2 WC Sens qa1=' int2str(qa1) ' qa2=' int2str(qa2) ' qa3=' int2str(qa3) 'wc1='
int2str(wc1*100) ' wc2=' int2str(wc2*100) ' wc3=' int2str(wc3*100) ' DZ=' int2str(DZ)]
% Call The differential equation solver
for N=1:segs1+1;
   Tei1(N)=Teibh-(L-z1(N))*g*sin(Angle);
end;
Tei1=Tei1';
Ta1(1)=Tei1(1);
for N=2:segs1+1;
   XC1a=z1(N-1);
   XC1b=z1(N);
   if N==2
      InitT1(N-1)=Tei1(1);
   else
      InitT1(N-1)=(wac1(N-2)*Ta1(N-1)*Cpm1+wai1(N-1)*Tei1(N-1)*Cpm1)/(wac1(N-
2)*Cpm1+wai1(N-1)*Cpm1);
   end
   wa1=wac1(N-1);
   Daa1=Da1(N-1);
   [z,Ta]=ode15s('dTadz2PB82',[XC1a XC1b],InitT1(N-1),[],wa1,Cpm1,Daa1);
   Ta1(N)=mean(Ta);
end
Ta1=Ta1';
InitT1=InitT1';
Tt1=Ta1;
Tm1=Ta1(segs1+1);
%Zone2
Tt2(1)=Tm1;
for N=2:segs2+1;
   XC2a=z2(N-1);
   XC2b=z2(N);
   Utoi2a=Utoi2(N-1);
   wa2=wac2(N-1);
   Tti2=Tt2(N-1);
   [z,T]=ode15s('d2Tdz2D2P8',[XC2a XC2b],[Tti2;0],[],wa2,wt2,Utoi2a,Cpm2,Cpm1);
```

```
    FFF=size(T);
    XC2=FFF(1);
    T2=T(:,1);
    Ttd2=T(:,2);
    Tt2(N)=mean(T2);
end;
Tt2=Tt2';
for N=1:segs2+1;
    Tei2(N)=Teibh-(L-z2(N))*g*sin(Angle);
end;
Tei2=Tei2';
Ta2(1)=Tei2(1);
for N=2:segs2+1;
    XC2a=z2(N-1);
    XC2b=z2(N);
    if N==2
        InitT2(N-1)=Tei2(1);
    else
        InitT2(N-1)=(wac2(N-2)*Ta2(N-1)*Cpm2+wai2(N-1)*Tei2(N-1)*Cpm2)/(wac2(N-
2)*Cpm2+wai2(N-1)*Cpm2);
    end
    wa2=wac2(N-1);
    Utoi2a=Utoi2(N-1);
    Daa2=Da2(N-1);
    Ttv2=Tt2(N);
    [z,Ta]=ode15s('dTadz2P8',[XC2a XC2b],InitT2(N-1),[],wa2,Cpm2,Ttv2,Daa2,Utoi2a);
    Ta2(N)=mean(Ta);
end;
Ta2=Ta2';
InitT2=InitT2';
%Solving for tubing temperature using first order differential equation
Ttt2(1)=Tm1;
for N=2:segs2+1;
    XC2a=z2(N-1);
    XC2b=z2(N);
    Tti2=Ttt2(N-1)
    Taz2=Ta2(N);
    Utoi2a=Utoi2(N-1);
    Dt2=-Cpm1/(J*MixDen1*Cpm1)*PDropT(rto, qt2 , MixDen1, visM1, Roughness, Angle);
    Ttv2=Tt2(N);
    [z,Tt]=ode15s('dTtdz2P8',[XC2a XC2b],Tti2,[],wt2,Cpm1,Taz2,Dt2,Utoi2a);
    Ttt2(N)=mean(Tt);
end;
Ttt2=Ttt2';
%Redo annulus calculations based on new tubing temperatures
Taa2(1)=Tei2(1);
for N=2:segs2+1;
    XC2a=z2(N-1);
    XC2b=z2(N);
    if N==2
        InitT2(N-1)=Tei2(1);
    else
        InitT2(N-1)=(wac2(N-2)*Taa2(N-1)*Cpm2+wai2(N-1)*Tei2(N-1)*Cpm2)/(wac2(N-
2)*Cpm2+wai2(N-1)*Cpm2);
    end
    wa2=wac2(N-1);
    Utoi2a=Utoi2(N-1);
    Daa2=Da2(N-1);
    Ttv2=Ttt2(N);
    [z,Ta]=ode15s('dTadz2P8',[XC2a XC2b],InitT2(N-1),[],wa2,Cpm2,Ttv2,Daa2,Utoi2a);
    Taa2(N)=mean(Ta);
end;
```

```
Taa2=Taa2';
ErrTa2=((Ta2-Taa2)/Ta2)*100;
InitT2=InitT2';
%Calculations of the Temperatures in the Upper Zone
% Calculate the Mixed Temperature at the second valve (initial condition
% for Calculating the tubing temperature for third zone)
Tm2=(wa2*Taa2(segs2+1)*Cpm2+wt2*Cpm1*Tt2(segs2+1))/(wa2*Cpm2+wt2*Cpm1);
% Calculate temperature profile inside tubing for the third zone.
Tt3(1)=Tm2;
for N=2:segs3+1;
   XC3a=z3(N-1);
   XC3b=z3(N);
   Utoi3a=Utoi3(N-1);
   Tti3=Tt3(N-1);
   wa3=wac3(N-1);
   [z,T]=ode15s('d2Tdz2D2P8',[XC3a XC3b],[Tti3;0],[],wa3,wt3,Utoi3a,Cpm3,CpV2);
   FFF=size(T);
   XC3=FFF(1);
   T3=T(:,1);
   Ttd3=T(:,2);
   Tt3(N)=mean(T3);
end;
Tt3=Tt3';
for N=1:segs3+1;
   Tei3(N)=Teibh-(L-z3(N))*g*sin(Angle);
end;
Tei3=Tei3';
%Third Annulus Temperature Profile Calculations
Ta3(1)=Tei3(1);
for N=2:segs3+1;
   XC3a=z3(N-1);
   XC3b=z3(N);
   if N==2
      InitT3(N-1)=Tei3(1);
   else
      InitT3(N-1)=(wac3(N-2)*Ta3(N-1)*Cpm3+wai3(N1)*Tei3(N1)*Cpm3)/(wac3(N-
2)*Cpm3+wai3(N-1)*Cpm3);
   end
   wa3=wac3(N-1);
   Utoi3a=Utoi3(N-1);
   Daa3=Da3(N-1);
   Ttv3=Tt3(N);
   [z,Ta]=ode15s('dTadz2P8',[XC3a XC3b],InitT3(N1),[],wa3,Cpm3,Ttv3,Daa3,Utoi3a);
   Ta3(N)=mean(Ta);
end;
Ta3=Ta3';
InitT3=InitT3';
%Solving for tubing temperature using first order differential equation
Ttt3(1)=Tm2;
for N=2:segs2+1;
   XC2a=z3(N-1);
   XC2b=z3(N);
   Tti3=Ttt3(N-1);
   Taz3=Ta3(N);
   Utoi3a=Utoi3(N-1);
   Dt3=-Cpm1/(J*MixDen1*Cpm1)*PDropT(rto, qt3 , T3MixDen, visV2, Roughness, Angle);
   Ttv3=Tt3(N);
   [z,Tt]=ode15s('dTtdz2P8',[XC2a XC2b],Tti3,[],wt2,Cpm1,Taz3,Dt3,Utoi3a);
   Ttt3(N)=mean(Tt);
end;
Ttt3=Ttt3';
%Re-do Third Annulus Temperature Profile Calculations after new tubing
```

```
%calculations
Taa3(1)=Tei3(1);
for N=2:segs3+1;
   XC3a=z3(N-1);
   XC3b=z3(N);
   if N==2
      InitT3(N-1)=Tei3(1);
   else
      InitT3(N-1)=(wac3(N-2)*Taa3(N1)*Cpm3+wai3(N1)*Tei3(N1)*Cpm3)/(wac3(N-
2)*Cpm3+wai3(N-1)*Cpm3);
   end
   wa3=wac3(N-1);
   Utoi3a=Utoi3(N-1);
   Daa3=Da3(N-1);
   Ttv3=Ttt3(N);
   [z,Ta]=ode15s('dTadz2P8',[XC3a XC3b],InitT3(N1),[],wa3,Cpm3,Ttv3,Daa3,Utoi3a);
   Taa3(N)=mean(Ta);
end;
Taa3=Taa3';
ErrTa3=((Ta3-Taa3)/Ta3)*100;
InitT3=InitT3';
% Temperature For the tubing above the producing zones
Tm3=(wa3*Cpm3*Taa3(segs3+1)+wt3*CpV2*Ttt3(segs3+1))/(wa3*Cpm3+wt3*CpV2);
Segs4=(ZT3/DZ)+1;
err=1;
Tf(1)=Tm3;
for N=1:Segs4;
   zt4(N)=ZT3-(N-1)*DZ;
   Tei4(N)=Teibh-(L-zt4(N))*g*sin(Angle);
end
for N=1:Segs4;
   Uto(N)=10;
while err>0.01;
   DPDZ(N) = PDrop(dti, qo3t, qw3t, TFMixDen, visV3, Roughness, Angle);
%  Convert Phi Term (which includes Pressure Drop DP/DZ and Joule-Thompson
%  Effect for Incompressible Fluid to oF/ft
   Phi(N)=3.995*10^-5*(1/(TFMixDen*CpV3))*DPDZ(N);
   Lr(N)=((2*pi)/(CpV3*wtF))*((rto*Uto(N)*ke)/(ke+rto*Uto(N)*TD));
   clear Tt;
   if N==1
      Tf(N)=Tm3;
   else
      [z,Tt]=ode15s('dTtdzG2',[zt4(N-1) zt4(N)],Tf(N-1),[],Lr(N),Phi(N));
      Tf(N)=mean(Tt);
   end
%  Calculating the wellbore to be used in calculating the casing inside temperature for Garshof Number
   Twb(N)=(rto*Uto(N)*Tf(N)+ke/TD*Tei4(N))/(ke/TD+rto*Uto(N));
%  Calculating the Casing inside temperature for Grashof number
   Tco(N)=Twb(N)+log(rwb/rco)/kcem*rto*Uto(N)*(Tf(N)-Twb(N));
%  Calculating the radiation heat transfer coefficicent...*[[Checked]]*
    Ftci=(1/emms+rto/rci*((1/emms)-1))^-1;
hr(N)=StefBoltzConst*Ftci*((Tf(N)+459.67)^2+(Tco(N)+459.67)^2)*((Tf(N)+459.67)+(Tco(N)+459.67)
);
%  Prandtl Number for packer fluid in the annulus
%  1cp = 2.419 lb/(ft.hr).. *[[Checked]]*
   Pr(N)=(Cpan*AnnVisc*2.419)/kan;
%  Garshof Number for Packer fluid in the annulus
%  1cp = 0.000671969 lb/(ft.s)
   Gr(N)=((rci-rto)^3*gg*AnnDen^2*Beta*(Tf(N)-Tco(N)))/(AnnVisc*6.72e-4)^2; %%%Switched
casing and fluid temp.
   if Gr(N) < 0
      Gr(N)=abs(Gr(N));
```

```
   end
%  Steps to calculate the effective conductivity of the annulus fluid due to Natural Convection
%  Lc = Characteristics Length for the annulus area (Cengel, 2002, p480)
   Lc=((2*rci)-(2*rto))/2;
%  Fcyl is the Geometric Factor for Concentric Cylinders (Cengel, 2002,
%  p481)
   Fcyl=(log((2*rci)/(2*rto)))^4/(Lc^3*((2*rto)^(-3/5)+(2*rci)^(-3/5))^5);
%  RaL is Rayleigh Number (Cengel, 2002, p466)
   RaL = Gr(N) * Pr(N);
%  keff is the effective thermal conductivity for the natural heat
%  convection in the annulus of a concentric cylinders (Cengel, 2002,p481)
   keff=kan*(0.386*(Pr(N)/(0.861+Pr(N)))^0.25*(Fcyl*RaL)^0.25);
%  Nusselt Number
   Nu(N)=keff/kan;
%  Natural Heat Convection Coefficient (Btu/(hr.ft2.ft)
   hc(N) = ((Nu(N) * kan) / Lc);
   ht(N) = hcoefft(TFMixDen,vtF,rti,visV3,CpV3,KfV3,DZ);
   UTONew = (1 /(hc(N)+hr(N))+(rto*log(rwb/rco)/kcem))^-1;
   err=abs((UTONew - Uto(N))/UTONew);
   Uto(N)=UTONew;
end
   clear Tt;
   Lr(N)=((2*pi)/(CpV3*wtF))*((rto*Uto(N)*ke)/(ke+rto*Uto(N)*TD));
   err=1;
end
hc=hc';
ht=ht';
Uto=Uto';
zt4=zt4';
Tei4=Tei4';
Lr=Lr';
Phi=Phi';
Tt4(1)=Tf(1);
for N=2:Segs4
   XC2a=zt4(N-1);
   XC2b=zt4(N);
   INTt=Tt4(N-1);
   Lrv=Lr(N);
   Phiv=Phi(N);
   [z,Tt]=ode15s('dTtdzG2',[XC2a XC2b],INTt,[],Lrv,Phiv);
   Tt4(N)=mean(Tt);
end
Tt4=Tt4';
Ta4=Tt4;
% Compiling Results and Plotting the profiles
% Setting up the final composite profiles
hatot=[ha1;ha2,ha3;hc];
httot=[ht1;ht2,ht3;ht];
Utot=[Utoi1;Utoi2;Utoi3;Uto];
Ttt=[Tt1;Tt2;Tt3;Tt4];
Tttt=[Tt1;Ttt2;Ttt3;Tt4];
Tat=[Ta1;Ta2;Ta3;Ta4];
Taat=[Ta1;Taa2;Taa3;Ta4];
Teit=[Tei1;Tei2;Tei3;Tei4];
zt=[z1;z2;z3;zt4];
zts=[z1s;z2s;z3s;zt4];
xlswrite(Title,[zt,Ttt,Tat,Teit],'Temperature Profiles');
xlswrite(Title,[zt,Tttt,Taat,Teit],'Temperature Profiles 2');
xlswrite(Title,[zts hatot httot Utot],'Heat Transfer Profiles');
save(Title);
PlotProfilesa(Ttt,zt,Tat,Teit,Title);
PlotProfiles2a(Ttt,zt,Tat,Teit,L,ZT3,Title);
```